UNIVERSITÉ DU LUXEMBOURG

PhD-FSTM-2021-009
The Faculty of Sciences, Technology and Medicine

DISSERTATION

Defence held on 22/01/2021 in Luxembourg

to obtain the degree of

DOCTEUR DE L'UNIVERSITÉ DU LUXEMBOURG

EN PHYSIQUE

by

Thomas GALVANI
Born on 17 December 1991 in Metz, France

TIGHT-BINDING PERSPECTIVE ON EXCITONS IN HEXAGONAL BORON NITRIDE

Dissertation defence committee

Dr Ludger Wirtz, dissertation supervisor
Professor, Université du Luxembourg

Dr Hakim Amara
Maître de recherche, Office national d'études et de recherches aérospatiales

Dr Thomas Schmidt, Chairman
Professor, Université du Luxembourg

Dr Christophe Delerue
Directeur de recherche, Centre National de la Recherche Scientifique

Dr Gabriel Bester, Vice Chairman
Professor, Universität Hambourg

Tight-binding perspective on excitons in hexagonal Boron Nitride

Thomas Galvani

Abstract

Two dimensional materials, which are systems composed of one or several angstrom-thin layers of atoms, have recently received considerable attention for their novel electronic and optical properties. In such systems, the quasi two dimensional confinement of electrons as well as the reduced dielectric screening lead to a strong binding of electrons and holes. These bound electron-hole excitations, termed *excitons*, control many of the peculiar opto-electronic properties of 2D materials.

In this context we study hexagonal Boron Nitride (hBN) as a prototypical 2D system. hBN layers crystallize in a honeycomb lattice similar to graphene, with carbon atoms replaced by boron and nitrogen. Contrary to its carbon cousin, hBN is a wide band gap semiconductor, well know for its UV luminescence properties and its particularly strong excitons. We investigate theoretically the excitonic properties of single and multilayer hBN.

To describe excitons, we make use of the Bethe-Salpeter equation, which provides an effective hamiltonian for electron-hole pairs. We show that, owing to the relatively simple electronic structure of BN systems, it is possible there to construct a model that approximately maps the Bethe-Salpeter equation onto an effective tight-binding Hamiltonian with few parameters, which are in turn fitted to *ab initio* calculations.

Using this technique, we are able to study in detail the excitonic series in single layer hBN. We classify its excitons according to the symmetries of the point group of the crystal lattice, and thus provide precise optical selection rules. Because our model naturally preserves the crystal geometry, we are able to characterize the effects of the lattice, and show how their inclusion affects the excitonic and, in turn, optical properties of hBN compared to a continuum hydrogenoid model. Further, we can access exciton dispersion, which is a crucial component for the understanding of indirect processes. We thus examine the dispersion of the lowest bound state.

Having established the properties of the single layer, we turn our attention to multilayers. The interaction of several layers leads to a phenomenon known as Davydov splitting. Under this lens, we investigate how the number of layers affects the excitonic properties of hBN, with particular focus on the Davydov splitting of the lowest bound exciton, which is responsible for the main feature of the absorption spectra. We discuss the effects responsible for the splitting of excitons in multilayers, and construct a simple

one-dimensional model to provide a qualitative understanding of their absorption spectra as a function of the number of layers. In particular, we show that, from trilayers onwards, we can distinguish inner excitons, which are localized in the inner layers, and surface excitons, which are localized on the outer layers. Remarkably, the lowest bound bright state is found to be a surface exciton.

Finally, we briefly present a comparison of tight-binding calculations with *ab initio* calculations of the absorption spectrum of bulk hBN. We discuss its first peaks, and how they are related to the excitons of single-layer hBN.

Contents

Chapter 1

Introduction

1.1 Interactions of light with matter

One of the questions that drove the initial developments of quantum mechanics is the understanding of the absorption and emission spectra of atoms.[1, 2] Today, more generally, the question of understanding the structure of matter and, in turn, how it interacts with light remains at the forefront of research. The reason for this lasting interest is that light (more generally, electromagnetic radiation) is one of the most precise and efficient tools at our disposal to probe the structure and behavior of matter.

However, because this probe is not direct, one requires both a physical model of matter and of its interaction with light in order to make sense of any spectroscopy experiment. This situation is eminently common in science: starting from a model of matter and its interaction with light, we aim to predict the outcome of a particular experiment involving this interaction. Experimental evidence then validates or falsifies the model, allowing us to indirectly access information about the system under investigation. In turn, sufficiently predictive models can then predict the outcome of other experiments, and more generally the optical properties of matter systems.

The use of such models is manyfold: on the more applied side, a good theoretical understanding of a system's optical response opens the door to optical characterization techniques, which let us use spectroscopy to efficiently and non-destructively assess the nature, properties and/or quality of a sample. Predictive models also allow the direct computation of a system's optical properties without an experiment, or even without synthesizing the system of interest. This can guide research and save precious time and effort, especially in the current era where computational resources are becoming more and more abundant. Finally, since spectroscopy is such a precise probe, the

interplay of theory and experiment also drives fundamental understanding of the finer and more complex interactions between the constituents of matter and light itself.

The discipline of, starting from an elementary description of a matter system, seeking a theoretical understanding its behavior and its interaction with light, is known under the name of *theoretical spectroscopy*. Contributing to this discipline is the object of the current thesis.

1.2 *Ab initio* and second principles methods

Loosely speaking, one may distinguish two kinds of investigations in theoretical spectroscopy. *Ab initio* methods, as their name suggests, aim to simulate matter and light-matter interaction from first principles: given (only) a collection of atoms, the ultimate goal of *ab initio* techniques is to understand their collective behavior without introducing extraneous parameters that would have to be adjusted on experiments. The advantage of such methods is their high predicting power, and, in a sense, their generality: by design, they seek to include all possible effects, within the limit of tractability. These inestimable advantages, however, come with a certain complexity, and non negligible computational costs which in practice require computer implementations and time. This sometimes makes it hard to build intuition and understanding of a system from *ab initio* methods alone, and the more complex matter systems may be out of reach of such techniques because of the sheer computational resources their simulation would require.

On the other end of the spectrum lie analytical and semi-analytical methods. These methods, by design, work with simpler models, building approximations and simplifications which may differ from one system to another in order to keep the computational load light. Because of their simplicity and specificity, they are not as general as *ab initio* methods, and often require parameters which are specific to the system under study. These parameters, in turn, can be inferred from an experiment, or from an *ab initio* calculation. In this sense, such techniques are sometimes called *second principles* methods. The strength of such methods is their ability to treat more complex systems, and to, occasionally, allow for a more direct understanding of the main physical phenomena at play in a system or a class of systems by varying the material parameters or isolating the contributions of different effects.

The present work places itself at the level of these "second principles" techniques. It investigates a particular material, hexagonal Boron Nitride, which is prototypical for layered materials, through semi-analytical techniques. These investigations were led in close collaboration with *ab initio*

studies of the same system by the author's colleague, Fulvio Paleari.[3]

1.3 Hexagonal Boron Nitride

Hexagonal Boron Nitride (hBN) is a so-called two-dimensional system. It is a material made of atomically thin layers of boron and nitrogen arranged in a honeycomb lattice. It can exist either in a monolayer, in a multilayer, or in bulk form, with different possible stackings of the honeycomb layers.

Out of the family of two-dimensional materials, the most well known is probably graphene,[4, 5, 6] which shares the same honeycomb lattice structure as hBN, but is composed exclusively of carbon. Its exfoliation, through the celebrated "scotch tape" method, and its subsequent characterization, by Geim and Novoselov in 2004 has been rewarded by the 2010 Nobel prize in physics.[1][7] Since then, two dimensional materials have received considerable attention.

These systems span a wide range of properties,[8] from graphene as a semimetal, to hBN as a wide bandgap semiconductor, through moderate bandgap semiconductors such as the well-known transition metal dichalcogenides (TMDs), phosphorene,[9] germanene, silicene,[10] etc.[11]

As we have already noted, hBN differs from its carbon based cousin graphene, which is a semimetal, by the substitution of the carbon atoms by equal parts boron and nitrogen. Since boron has three valence electrons and nitrogen five, compared to carbon's four, and all three atoms are from the same row of the periodic table, it is not so surprising that hBN and graphene can adopt a very similar crystal structure and have similar atomic chemistry. Yet, the replacement of carbon atoms by two different kinds of atoms breaks the symmetry that gives rise to graphene's well known semimetal structure, leading to the opening of a gap. For this reason, the electronic properties of hBN are very different from that of graphene: it is a wide bandgap semiconductor (or, depending on one's sensibilities, an insulator), with a gap of about $5 - 8$ eV, depending on the particular structure.

Among two dimensional-semiconductors, hBN, in part because of this wide band gap, has been noted for its potential as an ultraviolet emitter.[12, 13] In addition, it has also attracted interest as an excellent substrate or encapsulating material for other two-dimensional systems, and for its applications in photonics.[14]

[1]The precise Nobel citation is: *"for groundbreaking experiments regarding the two-dimensional material graphene."*[7]

1.4 Excitons

One of the main differences between two-dimensional (2D) and three dimensional (3D) systems comes from their so-called *excitonic properties*. Let us consider a semiconductor in its ground state. At the level of independent particles, this ground state can be imagined as a Fermi sea of electrons. When one of them is excited, it leaves behind a hole in the Fermi sea, creating an electron-hole pair excitation. This situation is depicted in figure 1.1.

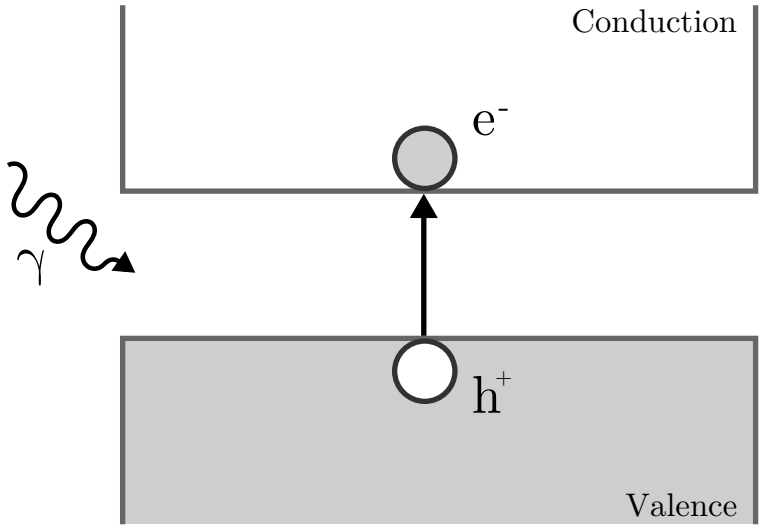

Figure 1.1: Excitation of an electron-hole pair: the incidence of a photon γ of appropriate energy has a certain probability to induce the transition of an electron e^- from the filled valence band to the empty conduction band. In doing so, it leaves behind a hole h^+.

However, the excited electron is a negative quasiparticle, while the hole it "left behind" is a positively charged quasiparticle. Therefore, both should interact. In fact, the attractive Coulomb interaction between them leads to the creation of bound states, called *excitons*.[15, 16] These electron-hole bound states are very much an analogue of a hydrogenoid system in the context of solid state physics. We illustrate this situation in figure 1.2.

In fact, in the limit where the hole and the electron are weakly bound, this analogy can be made precise. In certain approximations, which we shall discuss later, the problem of bound electron-hole pairs can indeed be reduced

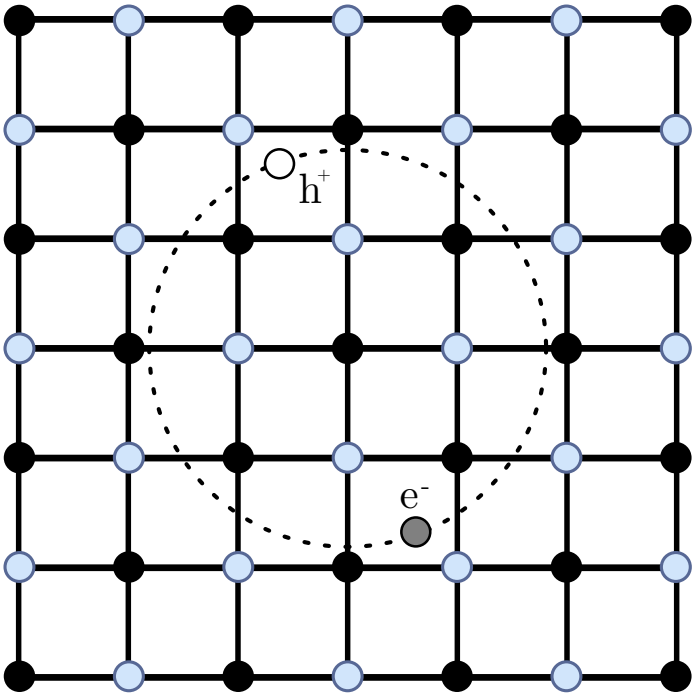

Figure 1.2: Schematic representation of an exciton in a crystal: the excited electron e^- and the hole h^+ interact together via an attractive Coulomb interaction to create a bound state: an exciton. Other dots and lines represent a crystal lattice.

to an effective Schrödinger equation in the relative coordinate $\mathbf{r} = \mathbf{r}_e - \mathbf{r}_h$:

$$-\frac{\hbar^2}{2\mu}\nabla^2 g(\mathbf{r}) + V(\mathbf{r})g(\mathbf{r}) = Eg(\mathbf{r}) \tag{1.1}$$

where $\mu = \frac{m_e m_h}{m_e + m_h}$ is the reduced mass of the pair, computed from the effective masses of the electron (m_e) and the hole (m_h), $V(\mathbf{r})$ is the so-called direct electron-hole potential, i.e. the Coulomb potential that binds them, g is an effective wavefunction for the pair,[2] and E is the pair's binding energy, which is negative. Equation 1.1 is the celebrated (hydrogenoid) Wannier model for excitons.[17] The central approximation here is clear: through the introduction of effective masses and, in general, of a macroscopic Coulomb potential for V (see below), the effects of the crystal lattice are averaged out, leading to a continuum description of the system.

[2]It is its so-called *envelope* wavefunction.

In typical three-dimensional bulk systems, the electron-hole interaction $V(\mathbf{r})$ is adequately modeled by a screened Coulomb potential $V(\mathbf{r}) = -\frac{e^2}{\epsilon r}$, where ϵ is the system's bulk dielectric constant, and so equation 1.1 yields the familar hydrogen series, with energy levels:

$$E_n^{3D} = -\frac{\mu \mathrm{Ry}}{m_0 \epsilon^2 n^2} \quad ; \quad n \in \mathbb{N}^*$$

where Ry ≈ 13.6 eV is the Rydberg energy, m_0 is the free electron mass, and the nonzero integer n is the principal quantum number. We therefore expect the appearance of "two-particle" bound states within the semiconductor's gap. For typical values of μ and ϵ, the binding energies are rather weak and the excitons have a large Bohr radius compared to the interatomic distances, so that the approximations leading to equation 1.1 make sense.

When moving to two-dimensional systems, such as hBN, the situation changes. Indeed, to a good approximation, in a $2D$ crystal, the electron and the hole are effectively confined in a two dimensional sheet, and so equation 1.1 becomes analogous to a *two*-dimensional hydrogen atom, which, famously, exhibits larger binding energies:[18]

$$E_n^{2D} = -\frac{\mu \mathrm{Ry}}{m_0 \epsilon^2 \left(n - \frac{1}{2}\right)^2} \quad ; \quad n \in \mathbb{N}^* \tag{1.2}$$

because of the modification of the Laplacian in two dimensions. In particular, the binding energy of the lowest bound state in $2D$, $E_{n=1}^{2D}$, is four times greater than its $3D$ equivalent, $E_{n=1}^{3D}$. Further, screening in a two dimensional sheet embedded in three dimensional space is not well described by a simple dielectric *constant*.[19, 20] Indeed, for a freestanding layer, the space around the sheet is mostly vacuum, which does not screen the electron-hole interaction. Not only does this modify the excitonic series for $2D$ systems, so that the Rydberg series of equation 1.2 is usually not observed,[21, 22] but this also favors a stronger electron-hole interaction. Therefore, both the confinement effect and the stronger binding potential "conspire" to create strongly bound excitons in two dimensional systems. In hBN, which has particularly strong excitons,[3][23, 24, 25] binding energies vary from about -2 eV in a single-layer to -0.6 eV in bulk.

These effects, in addition to other many-body effects which are enhanced due to the weaker screening of Coulomb interactions, therefore induce a very strong correction to the electronic structure of two-dimensional systems. This

[3]Note also that, since hBN systems have large gaps, the dielectric screening is further reduced.

has important consequences for their optical properties. In the simple hydrogenoid model, the oscillator strength of an excitonic state, which measures its coupling with light, is essentially given by $|g(\mathbf{0})|^2$. In other words, more concentrated excitons absorb more light, to the point where, in hBN, the strongly bound excitons "siphon" away most of the oscillator strength of the system. Because excitons are discrete bound states, these features manifest as discrete peaks in the absorption spsctrum, below the band gap energy.

In two-dimensional materials, therefore, excitons are not just a small perturbation to the optical properties of the system: they *control* the properties of the system. It is therefore crucial to get a physical understanding of these effects if we are to climb the Technology Readiness Level (TRL) ladder to reach the promising fruits that are the opto-electronic properties of two-dimensional materials. Furthering this understanding through semi-analytical, second principles models, which provide access to a more intuitive understanding of the phenomena at play, is the object of this work.

1.5 This work

Through the introductory remarks above, we have shown that excitonic effects play a central role in two-dimensional systems. We have also shown that excitons in two-dimensional systems are much more strongly bound than their three-dimensional equivalents. As a result, the continuum approximations of equation 1.1 are not always appropriate to describe them. Indeed, strongly bound excitons do feel the influence of the underlying crystal lattice. In particular, their kinetic energy is richer than that of an effective mass particle, and their symmetries, optical selection rules and activites, etc. are dictated by that of the underlying crystal lattice.

This "full" physics of excitons can be captured through the *Bethe-Salpeter equation*,[26, 27, 28] which can also be reduced to an effective hamiltonian for electron-hole pairs, but is considerably more complex than the simple weak interaction approximation of the hydrogenoid model. While it can be solved in the context of *ab initio* methods,[29, 30, 31, 32] it is not always straightforward to obtain an intuitive interpretation of the results. It is therefore of interest to develop second principles approximate models which take into account the crystal lattice while remaining semi-analytical and thus deliver complementary insight into such problems.

In this context, hBN has a role to play: it is a prototypical 2D system, which exhibits very strong excitonic effects, while at the same time having a simple electronic structure. This simple electronic structure will allow us to obtain and semi analytically solve a simple approximation of the Bethe-

Salpeter equation, in which, instead of effective masses, the kinetic energy of the electron-hole pair is described through an effective tight-binding hamiltonian. More precisely, we will show that, starting from a tight-binding description of hBN's electronic structure, it is possible to approximately map the Bethe-Salpeter equation onto the problem of a single particle moving on a lattice of electron-hole excitations, under the influence of an external field which represents the direct electron-hole interaction. In fact, the resulting equations are similar to the ones originally obtained by Wannier.[17] They take a particularly simple form in hBN because the relevant Wannier functions are actually well approximated by atomic orbitals: the hole states are well approximated by nitrogen orbitals, while the electron states are well approximated by boron orbitals.

This excitonic tight-binding model,[4] by construction, preserves the symmetries of the underlying crystal lattice. It will therefore allow us to intuitively explore the effects of the lattice on excitonic properties, classify the excitons with the symmetry group of the crystal instead of the hydrogenoid quantum numbers, and derive the appropriate optical selection rules. It will also provide us with a natural access to the dispersion of excitonic states, that is to say to the binding energies and excitonic eigenstates for excitons composed of indirect transitions. These are now of great interest to describe indirect absorption and emission processes, notably through coupling with phonons.[33, 34, 35, 36, 37]

Further, since this model is constructed from a tight-binding description of hBN's electronic structure, it can naturally describe multilayer systems. This will allow us to investigate the excitonic properties of coupled hBN layers. For illustration, in figure 1.3, we show the evolution of the absorption spectrum of hBN when increasing the number of layers, in the so-called AA' stacking (boron and nitrogen sites are inverted when going from one layer to the next). It is immediately apparent that the spectrum is dominated by discrete bound excitonic peaks. It can be seen that, in a single layer, the lowest bound exciton corresponds to the brightest peak. When moving to multilayers, this peak undergoes a non trivial splitting.

This splitting, and its peculiar fine structure, is intimately related to the number of layers in the system. We will provide a detailed study of bilayer hBN, treating on equal footing intra- and inter- layer excitons, and describe their evolution as well as that of the bilayer's optical properties as the coupling between the layers is varied. For higher multilayers, we will show that the splitting of the main peak can be qualitatively understood from a simple one-dimensional tight-binding model, where each layer is treated as a

[4] Or "tight-binding Wannier model".

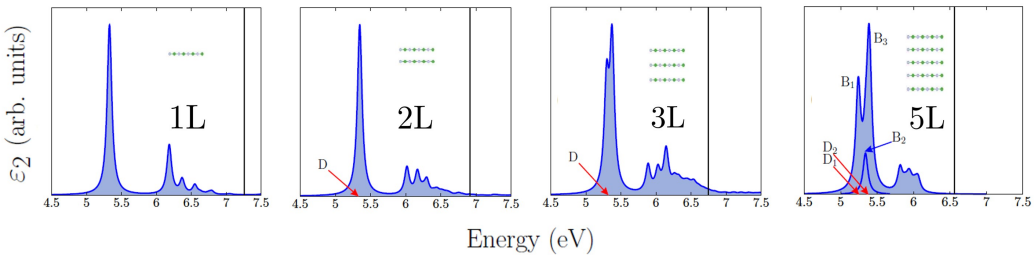

Figure 1.3: Panels adapted from [38]. *Ab initio* absorption spectrum of hBN for one, two, three and five layers in the AA' stacking (boron and nitrogen positions are inverted when going from one layer to the next).[38] Labels of "D" (resp. "B" for the pentalayer) indicate the energy position of dark (resp. bright) states. Vertical black lines indicate the band gap, i.e. the minimal (direct) hole-electron transition energy without excitonic effects. It is clear that the optical properties of the system are determined almost entirely by the discrete bound excitons below the gap.

site which can accomodate a "copy" of the lowest bound monolayer exciton. In doing so, we will display the mechanisms that drive this splitting, and highlight the roles of interlayer excitons, as well as variations in screening and atomic coordination numbers along the layers. We will see, in particular, that the lowest bound multilayer excitons are, in fact, localized on the surface layers, and that they can be optically active.

1.6 Organization

The contents of this thesis are organized as follows. Chapter 2 is devoted to general theoretical methods, and we describe tight-binding as a way to obtain the single particle electronic and optical properties of a system. We also present the Bethe-Salpeter equation and the hydrogenoid Wannier model, leading to equation 1.1. In chapter 3, we discuss the case of the linear boron nitride chain as a toy system, where we present the aforementionned excitonic tight-binding model, i.e. we realize the approximate mapping of the Bethe-Salpeter equation onto an effective tight-binding problem.

Chapter 4 is then concerned with the study of single-layer hBN. There, we briefly discuss single-particle properties, before moving on to excitonic problems. We present the direct excitonic series of single layer hBN at different levels of approximation: in the Wannier model, which can be seen as the limit of weak electron-hole interaction, in a limit of the excitonic tight-binding model which correspond to strong interactions, and finally in the

framework of the full model. We then briefly discuss its excitonic dispersion in the excitonic tight binding framework.

Chapter 5 deals with the direct excitons of hBN multilayers in the AA' stacking. We first establish the necessary generalization of the excitonic tight-binding model, before discussing the case of the bilayer in details. We then move on to general multilayers, for which we show that the main optical feature can be ascribed to the splitting of the first monolayer exciton, establish an effective model for this splitting and use it to discuss the appearence of surface excitons.

Chapter 6 concerns itself with bulk hBN in the AA' stacking. It is included for complenetess, and contains a brief descriptions of the releveant excitonic tight-binding model, which can be used to discuss the first excitons of its direct series as well and provides a way to access the dispersion of its lowest bound indirect excitons, both in real and reciprocal space.

Chapter 2

General theoretical methods: tight-binding, Bethe-Salpeter equation

The aim of this chapter is to provide an overview of the general theoretical methods that will be used in this work. We will introduce the tight-binding approximation, which will be central to our discussion. This approximation, which consists in writing the electronic states of a solid as appropriate linear combinations of localized atomic orbitals, provides a very tractable description of the electronic properties of solids. Because it is based on atomic orbitals, it intrinsically preserves the symmetries of the crystal and its lattice properties, therefore making it particularly suited to our goal. Within this approximation, we will further see how to compute the optical properties of solids (more specifically, their absorption spectrum).

Tight-binding is intrinsically a one-particle theory: it provides access to the electronic properties of a solid at the level of independent electrons. These independent electron states, in turn, will allow us to construct the two particle electron-hole / transition states that will serve as building blocks for our description of excitons. To this end, we will briefly introduce the general Bethe-Salpeter equation, which describes the coupling of these transition states, and gives rise to the excitonic states. We will further describe the hydrogenoid Wannier model, which is its weak coupling approximation, in which lattice effects are neglected. While this model precisely excludes some of the effects that most interest us in this work, it is a crucial basis to develop our understanding of excitons, and disentangle what stems from the lattice, and what is already present in a continuum description. The development and consequences of a more specific approximation of the Bethe-Salpeter equation that *does* include lattice effects for hBN systems will be the focus

of later chapters.

2.1 Electronic structure in the tight-binding approximation

2.1.1 Semi-empirical tight binding.

As stated above, we need a way to access the electronic structure of solids in order to compute the single electron states which will allow us to build electron-hole pair states. To this end, we will employ (orthogonal) semi-empirical tight-binding. We will give here only a simple overview, more detailed discussions may be found in [39, 40, 41].

We are mostly interested here in crystals, i.e. systems which are invariant under a set of lattice translations. What we mean by this is that there exists a *Bravais lattice*:

$$\mathcal{R} = \{\mathbf{R} = n_1\mathbf{a}_1 + n_2\mathbf{a}_2 + n_3\mathbf{a}_3 \ / \ n_1, n_2, n_3 \in \mathbb{Z}\} \tag{2.1}$$

such that translation by any $\mathbf{R} \in \mathcal{R}$ leaves the set of ionic cores invariant. In this case, the whole system may be constructed by periodic repetition of a unit cell. We suppose that the unit cell contains a certain number of ionic cores, indexed by some variable α. We denote their positions by $\mathbf{n}_\alpha^0$, and the corresponding sublattices:

$$\Lambda_\alpha = \mathbf{n}_\alpha^0 + \mathcal{R}$$

The central idea of tight-binding is then that we will try to write the eigenstates of the single electron hamiltonian for the system, $\hat{H}$, as linear combinations of the atomic orbitals associated to these ionic cores:

$$|\Psi\rangle = \sum_\alpha \sum_{n \in \Lambda_\alpha} \sum_j |\alpha_j, \mathbf{n}\rangle$$

where the sum over j runs over the one-electron orbitals associated to an ionic core of type α. This "basis" is, of course, overcomplete. The usual practice is to restrict oneself to only a certain set of atomic orbitals for each core type, based on the chemical makeup of the system and the properties under study. In the following, we will drop the sum on j and simply consider the α as multi-indices (or, without that, we can simply assume that we retain only one orbital per core, which will be the case most of the time in this work).

The atomic orbitals are by definition localized states, centered on their ionic core. In position representation, they are given by:

$$\langle \mathbf{r} | \alpha, \mathbf{n} \rangle = \phi_\alpha(\mathbf{r} - \mathbf{n})$$

which quickly (exponentially) decays away from their centers (here $\mathbf{n}$). Typically, in semi-empirical tight-binding, the exact form of the ϕ_α is not known. Indeed, the above properties will suffice for most of this work. We shall further assume (this is an additonal approximation) that these atomic orbitals are orthogonal:

$$\langle \alpha, \mathbf{m} | \beta, \mathbf{n} \rangle = \delta_{\alpha,\beta}\delta_{\mathbf{m},\mathbf{n}}$$

This is orthogonal tight-binding.

We are in a similar position with the matrix elements of the Hamiltonian in this basis. Because of the translational invariance of the system, we assume that matrix elements between two atomic orbitals depend only on their types and their *relative* positions, i.e. we have:

$$\langle \alpha, \mathbf{m} | \hat{H} | \beta, \mathbf{n} \rangle = t^{\alpha\beta}_{\mathbf{n}-\mathbf{m}}$$

The $t^{\alpha\beta}_{\mathbf{n}-\mathbf{m}}$ could be called the hopping elements of the system. The ones for which $\alpha = \beta$ and $\mathbf{m} = \mathbf{n}$ are usually given the name of onsite energies: they are essentially given by the atomic energies along with a correction for the crystal potential. All the other $t^{\alpha\beta}_{\mathbf{n}-\mathbf{m}}$ are more properly called hoppings: they describe an amplitude for an electron in the orbital $|\alpha, \mathbf{m}\rangle$ to "hop" to the orbital $|\beta, \mathbf{n}\rangle$. Just like the atomic orbitals themselves, the hopping elements are typically not known in semi-empirical tight-binding. Instead, they are taken as parameters. Because the atomic orbitals are strongly localized, the hopping elements are expected to decay quickly with the distance $\mathbf{n}-\mathbf{m}$, and therefore we typically only retain the hopping elements between sites within a few nearest neighbor distance from one another. In this way, the matrix elements of the Hamiltonian are detemined by a relatively small number of parameters.

In order to diagonalize $\hat{H}$, it is very convenient to introduce a particular type of Bloch function, which we call a tight-binding basis function. For each orbital type α, we define the associated tight-binding basis function as:

$$|\alpha, \mathbf{k}\rangle = \frac{1}{\sqrt{N}} \sum_{\mathbf{n} \in \Lambda_\alpha} e^{-i\mathbf{k}\cdot\mathbf{n}} |\alpha, \mathbf{n}\rangle$$

where N is the number of unit cells in the system and $\mathbf{k}$ is a wavevector / crystal momentum. These functions are useful because they "pre-diagonalize" $\hat{H}$, in the sense that:

$$\left\langle \alpha, \mathbf{k} \middle| \hat{H} \middle| \beta, \mathbf{k}' \right\rangle = \delta_{\mathbf{k},\mathbf{k}'} \sum_{\boldsymbol{\rho} \in \left(\Lambda_\beta - \mathbf{n}^0_\alpha\right)} t^{\alpha\beta}_{\mathbf{n}-\mathbf{m}} e^{-i\mathbf{k}\cdot\boldsymbol{\rho}}$$

where we have explicitly made use of the translation invariance of the system. It follows that the Hamiltonian preserves the crystal momentum $\mathbf{k}$, and is

block diagonal in it. This leads to the usual band picture: for each value of $\mathbf{k}$, the blocks of the Hamiltonian are given, in the basis of the tight binding functions $\{|\alpha, \mathbf{k}\rangle\}_\alpha$:

$$H_{\alpha,\beta}(\mathbf{k}) = \langle \alpha, \mathbf{k}|\hat{H}|\beta, \mathbf{k}\rangle$$

and the diagonalization of these matrices, which we call the *integral transfer matrices*,[39] thus provides the band energies and band states.[1] A typical way to estimate the hopping elements is then to fit the (parameter dependent) semi-empirical tight-binding band structure on the band structue obtained from another level of theory, or experiment. In this work, we will often do the former, and fit our hopping parameters in order to reproduce *ab initio* GW band structures.[2]

The matrix elements of the integral transfer matrices, the $H_{\alpha,\beta}(\mathbf{k}) = \sum_{\boldsymbol{\rho}\in\left(\Lambda_\beta - \mathbf{n}^0_\alpha\right)} t^{\alpha\beta}_{\mathbf{n}-\mathbf{m}} e^{-i\mathbf{k}\cdot\boldsymbol{\rho}}$, deserve a brief word. The set $\Lambda_\beta - \mathbf{n}^0_\alpha$ is nothing but the set of neighbors of β type of a given site of α type. It is a shifted copy of the system's Bravais lattice, $\mathcal{R}$. Overall, these matrix elements can be seen as Fourier transforms of the hopping elements on this lattice of neighbors. Retaining less nearest neighbors therefore amounts to truncating this series by removing high frequency terms. This point of view shows in which sense these functions retain information about the real space lattice geometry (and associated energetics). They are typically split in such a way that the different nearest neighbor "shells" (first, second, etc.) are separated and the common hoppings factorized. This is what we will do in the example below.

2.1.2 Example: the linear BN chain

As an example, let us consider a diatomic chain of boron and nitrogen. To fix notations, we define three cartesian axes x, y and z such that x is the direction of the chain, and let a be the nearest neighbor $B-N$ distance. Chemically, we can expect he optical properties of such a system to be mostly ascribed to the (hybridized) p orbitals which are perpendicular to the bonds, say here the p_y and p_z orbitals of the boron and nitrogen atoms. Since these orbitals have a different symmetry with respect to, say the xy mirror plane, the sets

[1] Here, we have made direct use of the orthogonal approximation that we mentionned above. In non-orthogonal tight-binding, we would instead have to solve a generalized eigenvalue problem involving an overlap matrix (which here reduces to the identity). It is for this reason that we reserve a "special" name for $H_{\alpha,\beta}(\mathbf{k})$. See e.g. [39].

[2] When we come to excitonic problems, we will also have the option to fit some hopping parameters directly on the exciton binding energies resulting from an *ab initio* solution of the Bethe-Salpeter equation. This will be discussed later.

of p_y and p_z orbitals do not interact with one another, and it is enough to discuss only the p_z orbitals (since the electronic problem for the p_y orbitals is exactly the same).[3]

The unit cell of the system contains two atoms: one boron, and one nitrogen. The system therefore has two sublattices, which we shall call Λ_B and Λ_N, the boron and nitrogen sublattices respectively. Let us therefore for each $n \in \Lambda_B$ denote by $|B, n\rangle$ the p_z orbital of the boron atom at position n, and likewise, for all $m \in \Lambda_N$, let $|N, m\rangle$ be the p_z orbital of the nitrogen atom at position m.

Let us now write the electronic hamiltonian $\hat{H}$ of this system in the basis of localized atomic orbitals defined above. Retaining only first nearest neighbors hoppings for simplicity, its matrix elements read:

$$\langle N, m|\hat{H}|N, m'\rangle = \begin{cases} -\Delta & \text{if } m = m' \\ 0 & \text{otherwise} \end{cases}$$

$$\langle B, m|\hat{H}|B, m'\rangle = \begin{cases} +\Delta & \text{if } m = m' \\ 0 & \text{otherwise} \end{cases}$$

$$\langle N, m|\hat{H}|B, n\rangle = \begin{cases} t & \text{if } n \text{ and } m \text{ are first nearest neighbors} \\ 0 & \text{otherwise} \end{cases}$$

where Δ and t are parameters. From there we can write the corresponding integral transfer matrix for each value of the wavenumber k:

$$H(k) = \begin{pmatrix} \Delta & tf(k) \\ tf(k) & -\Delta \end{pmatrix}$$

in the $\{|B, k\rangle, |N, k\rangle\}$ basis, and where $f(k) = e^{ika} + e^{-ika} = 2\cos(ka)$ is the geometric function associated to the B-N first nearest neighbor hoppings.[4] We can immediately check that $H(k)$ is $\frac{2\pi}{a}$-periodic, which, as expected, is

[3] More precisely, we may split the space of states $\mathcal{H}$ into $\mathcal{H}_{p_y}$ and $\mathcal{H}_{p_z}$, which are respectively spaned by the families of p_y and p_z orbitals, and such that $\mathcal{H} = \mathcal{H}_{p_y} \oplus \mathcal{H}_{p_z}$. Our symmetry considerations then allow us to write the hamiltonian of the system as a direct sum $\hat{H} = \hat{H}_{p_y} \oplus \hat{H}_{p_z}$, where $\hat{H}_{p_y}$ is formally the same hamiltonian as $\hat{H}_{p_z}$, except that it operates on the subspace spanned by the p_y orbitals. In the following, we shall simply write $\hat{H}$ for $\hat{H}_{p_z}$ and $\mathcal{H}$ for $\mathcal{H}_{p_z}$ in order to lighten notations.

[4] It may seem unnecessary to name this rather simple function. However, we do so because the structure of this integral transfer matrix is exactly the same as the one for the first nearest neighbor tight-binding for *hexagonal* single layer Boron Nitride, so we will be able to highlight similarities and re-use results later on. For the same reason, we may sometimes write $|f(k)|^2$ instead of $f(k)^2$ even though both are equal here (for hBN, the analogue of f is complex-valued).

the size of the system's first Brillouin zone. Diagonalization of $H(k)$ yields two eigenenergies per value of k, respectively the conduction and valence band energies:

$$E_c(k) = \sqrt{\Delta^2 + t^2|f(k)|^2}$$
$$E_v(k) = -\sqrt{\Delta^2 + t^2|f(k)|^2}$$

and, up to a phase, the corresponding eigenstates:

$$|\Psi_c(k)\rangle = \frac{1}{\mathcal{N}(k)}\Big[\,|B,k\rangle + a(k)\,|N,k\rangle\,\Big]$$
$$|\Psi_v(k)\rangle = \frac{1}{\mathcal{N}(k)}\Big[-a(k)\,|B,k\rangle + |N,k\rangle\,\Big]$$

where:

$$a(k) = \frac{tf(k)}{\Delta + \sqrt{\Delta^2 + t^2|f(k)|^2}}$$

and $\mathcal{N}$ is a normalization constant such that $|\mathcal{N}(k)|^2 = 1 + |a(k)|^2$.

It is very interesting to note that $f\left(\frac{\pi}{a}\right) = 0$, i.e. the coupling between the N and B sublattices vanishes at the high-symmetry point X, where the system's direct gap is found, with a value of $E_g = 2\Delta$. More precisely, we have:

$$f(X+q) = -2aq + \mathrm{o}\Big((aq)^2\Big)$$

Since most optical processes involve states near the gap, this suggests an approximation of the band energies in the vicinity of X points through an expansion in $\left|\frac{t}{\Delta}f(k)\right|^2$:

$$E_c(k) = -E_v(k) \approx \Delta + \frac{t^2}{2\Delta}|f(k)|^2 \tag{2.2}$$

which may be further approximated, near *a given* X point to:

$$E_c(X+q) = -E_v(X+q) \approx \Delta + 2\frac{t^2}{\Delta}(aq)^2 \tag{2.3}$$

Equation 2.3 yields parabolic bands: it is the effective mass approximation, which is no longer periodic and corresponds to a continuum approximation where lattice effects have been averaged out.

The behavior of the approximation given in equation 2.2, however, is very different: it remains periodic, and the geometric function f has been

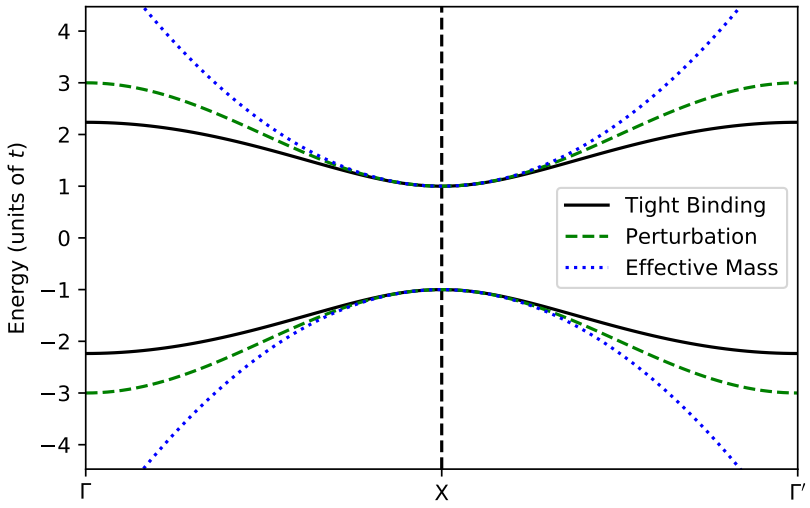

Figure 2.1: The tight binding bands of the BN linear chain (solid lines), with $\Delta = t$. Compare the approximation from the perturbation expansion in $\frac{t}{\Delta}|f(k)|$ (equation 2.2) and the effective mass approximation (equation 2.3).

preserved. As a result, the geometry (and symmetries) of the lattice is (are) preserved. This is *not* a continuum approximation.

Another important consequence of the fact that the coupling between the two sublattices vanishes near the gap is that the band states can be similarly approximated; indeed, we find that:

$$a(k) \approx \frac{t}{2\Delta} f(k)$$

in particular, this entails that, close to the gap, the conduction band is constituted almost purely of boron orbitals, while the valence band is constituted almost purely of nitrogen orbitals. This can be understood chemically by noting that nitrogen is more electronegative than boron, so that electrons in the ground state will tend to occupy nitrogen orbitals, whence the valence band states should indeed be mostly made of nitrogen orbitals. We will show later that this approximation, along with that of equation 2.2, in one form or another, underpins most of the models developed in this work. Both approximations are show in figure 2.1.

It is fruitful to note that, while this approximation was obtained here through a simple Taylor expansion, it can actually be obtained in a more general manner. Indeed, B-N systems usually exhibit a large gap, due to the electronegativity difference between nitrogen and boron. This translates into

the idea that Δ is larger than other, non onsite hopping parameters.[5] Added to the fact that, in the regions of interest, the coupling between boron and nitrogen sublattices is weak anyway, this suggests treating non onsite hopping elements as a perturbation, i.e. writing the electronic hamiltonian under the form:

$$\hat{H} = \hat{\Delta} + \hat{V}$$

where we define $\hat{\Delta}$ as $\hat{H}$ with all hoppings (all parameters apart from Δ) set to zero, while $\hat{V} = \hat{H} - \hat{\Delta}$ is likewise $\hat{H}$ with Δ set to zero. $\hat{\Delta}$ has two eigensubspaces: one at low energy, $-\Delta$, spanned by the all the nitrogen atomic orbitals, and one at high energy, $+\Delta$, spanned by all the boron atomic orbitals. Treating, then, $\hat{V}$ as a perturbation up to second order, we can recover the results discussed above. It turns out that this line of reasoning and its accompanying approximations are fruitful, and we will pursue it in later chapters, especially when we come to excitonic problems. In more "excitonic terms", we are essentially saying that the "hole" (valence) states are well approximated by linear combinations of nitrogen states, localized in the nitrogen sublattice Λ_N, while "electron" (conduction) states are well approximated by linear combinations of boron states, localized in the boron sublattice Λ_B. This geometric separation between sublatices, which, as we have seen, is very naturally expressed in tight-binding, will be extremely useful to us when dealing with excitonic problems.

2.2 Single particle optical properties

2.2.1 Absorption phenomena

Calculating the absorption spectrum of a crystal amounts to computing the imaginary part of its dielectric matrix, ϵ_i. At the independant particles level, in the limit of vanishing photon momentum, i.e. in the dipole approximation, it can be shown that:[16]

$$\epsilon_i(\omega) = \left(\frac{2\pi e}{m_e \omega}\right)^2 \sum_{\mathbf{k},v,c} |\langle c, \mathbf{k}|\mathbf{e}\cdot\hat{\mathbf{p}}|v, \mathbf{k}\rangle|^2 \delta(E_c(\mathbf{k}) - E_v(\mathbf{k}) - \hbar\omega) \qquad (2.4)$$

where:

- e is the elementary charge.

[5] This is not exactly true, since usually the first nearest neighbor hopping parameter, t, is of a magnitude comparable to Δ (although still smaller). However, we have shown already that the coupling mediated by t vanishes near the gap, i.e. for the regions from which most of the proprieties we want to study originate from.

- m_e is the mass of the electron.
- $\hbar\omega$ is the incoming photon energy.
- $\mathbf{e}$ is the incoming photon polarization vector.
- $\hat{\mathbf{p}}$ is the momentum operator.
- $\mathbf{k}$, v and c run over the first Brillouin zone, the valence band indices and the conduction band indices respectively.
- $|v, \mathbf{k}\rangle$, $|c, \mathbf{k}\rangle$ are the associated valence and conduction band states, respectively.
- $E_v(\mathbf{k})$ and $E_c(\mathbf{k})$ are the associated valence and conduction band energies, respectively.

To build intuition, we can comment a bit on this formula: it describes the absorption of a photon by a valence band electron, which is "promoted" to a conduction band state, through an electronic transition. Most of its terms can be traced back to Fermi's golden rule: in particular, the momentum matrix elements relate to the probability of optically exciting a transition from valence band v to conduction band c at a certain wavevector $\mathbf{k}$. Because we have assumed vanishing photon momentum, momentum conservation mandates that only transitions between electronic states of the same momentum / wavevector $\mathbf{k}$ can be optically excited.[6] This is usually a good approximation, since visible light is associated to momenta of the order of $\frac{2\pi}{\lambda}$, with the photon wavelength $\lambda \sim 500$ nm, while the typical length scale of the Brillouin zone is $\frac{2\pi}{a}$, with the crystal lattice parameter a is on the order of a few Å. Finally, the usual $\delta(E_c(\mathbf{k}) - E_v(\mathbf{k}) - \hbar\omega)$ factor expresses energy conservation: to excite a transition, the photon energy $\hbar\omega$ must match the direct[7] electronic *transition energy* $E_c(\mathbf{k}) - E_v(\mathbf{k})$. In particular, a consequence is that, within equation 2.4, absorption cannot occur at energies below the band gap.[8]

When it comes to direct single particle semiconductor absorption, these direct electronic transition energies, $E_c(\mathbf{k}) - E_v(\mathbf{k})$, are perhaps one of the most important quantity that can be read from the band structure. Indeed, note that the valence and conduction band energies only appear as

[6] For electronic states, we are more precisely speaking of crystal momentum, $\hbar\mathbf{k}$. We will usually drop the factor of $\hbar$ and speak in this context of momentum and wavenumber interchangeably, for brevity.

[7] The transition is said to be direct in the sense that it couples states with the same wavevector, $\mathbf{k}$.

[8] This is in strong contrast with what happens in the excitonic case, which we shall discuss later.

this difference, and not separately. Therefore, when it comes to direct optical phenomena, it is this difference that has to be captured when it comes to the system's energetics, rather than the valence and conduction energies separately. In fact, it is worth mentionning that in many semiconductors, the matrix elements $|\langle c, \mathbf{k}|\mathbf{e}\cdot\hat{\mathbf{p}}|v, \mathbf{k}\rangle|^2$ are not strongly dependant on $\mathbf{k}$, but in a first approximation, depend only on the band indices, v and c,[16] so that:

$$\epsilon_i(\omega) \approx \left(\frac{2\pi e}{m_e\omega}\right)^2 \sum_{v,c} |P_{v,c}|^2 \underbrace{\sum_{\mathbf{k}} \delta(E_c(\mathbf{k}) - E_v(\mathbf{k}) - \hbar\omega)}_{J_{v,c}(\hbar\omega)} \tag{2.5}$$

where $|P_{v,c}|^2$ is the aforementioned $\mathbf{k}$-independent approximation for the $|\langle c, \mathbf{k}|\mathbf{e}\cdot\hat{\mathbf{p}}|v, \mathbf{k}\rangle|^2$, and we have recognized the joint density of states $J_{v,c}$ at the photon energy $\hbar\omega$, which is in fact nothing more than the density of states for the "transition band" given by the direct electronic transition energy.

The approximation provided by equation 2.5 can be quite useful, especially in two-band systems such as the linear BN chain, or hexagonal Boron Nitride,[9] as it removes the need to compute momentum matrix elements since the sum on the band indices disappears and $|P_{v,c}|^2$ becomes a simple scaling factor, which can usually be discarded if we are interested in the absorption spectrum, since optical spectra are usually only determined up to a multiplicative constant anyway. It also provides qualitative insight on the spectrum, in particular asserting that absorption at a particular energy will be controlled by (and in fact roughly proportional to) the number (more accurately, the density) of available transitions with that transition energy.

2.2.2 Momentum matrix elements in tight-binding

Our tight-binding models give us access to the band energy differences $E_c(\mathbf{k}) - E_c(\mathbf{k})$, as well as to the expression of the band states $|c/v, \mathbf{k}\rangle$ in terms of atomic orbitals, but so far, we are missing a way to compute the matrix elements of the momentum operator $\hat{\mathbf{p}}$ in a meaningful basis. The purpose of this section is to display a way to obtain the sought-after matrix elements for atomic orbitals.

We shall follow the approach described in [40] and start by noting that momentum can be written in terms of the commutator between the system's

[9] Like graphene, the low energy optical properties of hBN are essentially deterlmied by its π and π^* bands, which are descended from the boron and nitrogen p_z orbitals.

hamiltonian and the position operator $\hat{\mathbf{r}}$:

$$\hat{\mathbf{p}} = \frac{m_e}{i\hbar}\left[\hat{\mathbf{r}}, \hat{H}\right]$$

The matrix elements of $\hat{\mathbf{p}}$ between two atomic orbitals $|\alpha, \mathbf{m}\rangle$ and $|\beta, \mathbf{n}\rangle$ then reads:

$$\langle \alpha, \mathbf{m}|\hat{\mathbf{p}}|\beta, \mathbf{n}\rangle = \frac{m_e}{i\hbar}\Big[\, \langle \alpha, \mathbf{m}|\hat{\mathbf{r}}\hat{H}|\beta, \mathbf{n}\rangle - \, \langle \alpha, \mathbf{m}|\hat{H}\hat{\mathbf{r}}|\beta, \mathbf{n}\rangle\Big] \tag{2.6}$$

Making now the approximation that the set of atomic orbitals for the system, $\{|\alpha, \mathbf{n}\rangle\}_{\alpha,\mathbf{n}}$ forms a basis of the system's space of states, we can resolve the identity and obtain:

$$\langle \alpha, \mathbf{m}|\hat{\mathbf{r}}\hat{H}|\beta, \mathbf{n}\rangle = \sum_{\gamma,\mathbf{l}} \langle \alpha, \mathbf{m}|\hat{\mathbf{r}}|\gamma, \mathbf{l}\rangle \, \langle \gamma, \mathbf{l}|\hat{H}|\beta, \mathbf{n}\rangle$$

We now introduce an approximation:

$$\langle \alpha, \mathbf{m}|\hat{\mathbf{r}}|\gamma, \mathbf{l}\rangle \approx \delta_{\alpha,\gamma}\delta_{\mathbf{m},\mathbf{l}} \, \langle \alpha, \mathbf{m}|\hat{\mathbf{r}}|\alpha, \mathbf{m}\rangle$$

which amounts to neglecting the intra-atomic polarizability of the atoms in the system. This is reasonable in semiconductors, where this intra-atomic polarizability only accounts for a small contribution to the system's total polarizability.[40]

We further assume that the expectation value of the position operator $\hat{\mathbf{r}}$ for the atomic orbital $|\alpha, \mathbf{m}\rangle$, which is centered on $\mathbf{m}$, is $\mathbf{m}$:[10]

$$\langle \alpha, \mathbf{m}|\hat{\mathbf{r}}|\alpha, \mathbf{m}\rangle = \mathbf{m}$$

Bringing now everything together, equation 2.6 yields:

$$\langle \alpha, \mathbf{m}|\hat{\mathbf{p}}|\beta, \mathbf{n}\rangle = -\frac{m_e}{i\hbar}(\mathbf{n} - \mathbf{m}) \, \langle \alpha, \mathbf{m}|\hat{H}|\beta, \mathbf{n}\rangle \tag{2.7}$$

which is the sought-after expression: indeed, recall now that the matrix elements $\langle \alpha, \mathbf{m}|\hat{H}|\beta, \mathbf{n}\rangle$ are nothing but the hopping elements of our electronic model. Therefore, this expression allows us to fully determine the matrix elements of $\hat{\mathbf{p}}$ in the basis of atomic orbitals without introducing any new free parameters to the model.

In single particle calculations for a periodic system, however, this basis is not the most convenient, since our band states will be expressed in terms

[10] In a periodic system, the position operator $\mathbf{r}$ is usually ill defined. Here, however, we will obtain an expression which depends on a *difference* of positions, which lets us avoid this issue.

of tight-binding basis functions. However, since these are, in turn, linear combinations of atomic orbitals, it is rather straightforward to obtain the matrix elements of $\hat{\mathbf{p}}$ in this basis, and we find:

$$\left\langle \alpha, \mathbf{k} \middle| \hat{\mathbf{p}} \middle| \beta, \mathbf{k}' \right\rangle = \delta_{\mathbf{k},\mathbf{k}'} \frac{i m_e}{\hbar} \sum_{\boldsymbol{\rho} \in \Lambda_{\alpha,\beta}} \langle \alpha, \mathbf{m}_\alpha | \hat{H} | \beta, \mathbf{m}_\alpha + \boldsymbol{\rho} \rangle \, \boldsymbol{\rho} e^{-i\mathbf{k}\cdot\boldsymbol{\rho}}$$

where $\mathbf{m}_\alpha$ is any element of Λ_α, and we have made use of the translational invariance of the system. Recognizing the gradient of the hamiltonian matrix elements $H_{\alpha,\beta}$ with respect to the wavevector $\mathbf{k}$, the above can be rewritten very compactly:

$$\left\langle \alpha, \mathbf{k} \middle| \hat{\mathbf{p}} \middle| \beta, \mathbf{k}' \right\rangle = -\frac{m_e}{i\hbar} \delta_{\mathbf{k},\mathbf{k}'} \boldsymbol{\nabla}_{\mathbf{k}} H_{\alpha,\beta}(\mathbf{k})$$

Note the Kronecker delta $\delta_{\mathbf{k},\mathbf{k}'}$: its presence shows that $\hat{\mathbf{p}}$ is block diagonal in the basis of the tight-binding basis functions, with one block for each value of the wavevector $\mathbf{k}$ as is the system's hamiltonian. This lets us define momentum matrices, in analogy to the integral transfer matrices:

$$p(\mathbf{k}) = -\frac{m_e}{i\hbar} \boldsymbol{\nabla}_{\mathbf{k}} H(\mathbf{k})$$

where the gradient is taken element-wise. The expressions above thus provide a practical way to evaluate momentum matrix elements, and, consequently, the absorption spectrum of a system described by a tight-binding hamiltonian through equation 2.4.[11]

2.3 Electron-hole interaction

Until now, we have remained at the level of independent electrons. The "reality" of a crystal is, of course, far more complex. One of the main difficulties is that electrons interact with each other, so that even with fixed nuclei, we are dealing with a (quantum) many body problem. There exist approximate methods to, nevertheless, study such problems. Their description is, for the most part, outside of the scope of this work. An overview can be found in [3] and references therein.

[11] Of course, this is not the only way to do so. Notably, other formulations of 2.4 will be discussed later, once we have introduced two-body formalism, in which they are more natural.

2.3.1 The Bethe-Salpeter Hamiltonian

One method that we will discuss is that of the Bethe-Salpeter equation, which provides a way to describe electron-hole pair excitations, and will form the basis upon which we study excitons.[29, 30, 31, 15, 32] It can be obtained in several ways, but under the usual approximations, reduces to an effective hamiltonian for electron-hole pairs, which is what we shall endeavor to succinctly present.

This hamiltonian is typically presented in the so-called transition basis, which is traditionally used for *ab initio* calculations. Such a basis can be seen as composed of tensor products of valence (hole) and conduction (electron) states:[12]

$$|v\mathbf{k}_v, c\mathbf{k}_c\rangle = |v, \mathbf{k}_v\rangle_h \otimes |c, \mathbf{k}_c\rangle_e$$

where the hole states, $|v, \mathbf{k}_v\rangle_h$ can be taken as the complex conjugates of the associated electronic valence (single electron) states, and the electron states $|c, \mathbf{k}_c\rangle_e$ as the electronic conduction states.[13] Here, v and c are respectively valence and conduction band indices, while $\mathbf{k}_v$ and $\mathbf{k}_c$ are wavevectors.

The Bethe-Salpeter hamiltonian, which we shall call $\hat{H}_X$, can be conveniently decomposed into three parts:[14]

$$\hat{H}_X = \hat{H}_0 + \hat{U} + \hat{J}$$

The first part, $\hat{H}_0$, describes the independent electron and hole pairs: it acts as a sort of kinetic energy, and we therefore call it the kinetic hamiltonian. Its expression in transition basis is given by:

$$\left\langle v\mathbf{k}_v, c\mathbf{k}_c \middle| \hat{H}_0 \middle| v'\mathbf{k}'_v, c'\mathbf{k}'_c \right\rangle = \delta_{(vc),(v'c')}\delta_{\mathbf{k}_v,\mathbf{k}'_v}\delta_{\mathbf{k}_c,\mathbf{k}'_c}(E_c(\mathbf{k}_c) - E_v(\mathbf{k}_v))$$

where $E_v(\mathbf{k}_v)$ and $E_c(\mathbf{k}_c)$ are the band energies respectively associated to the (electronic) band states $|v, \mathbf{k}_v\rangle$ and $|c, \mathbf{k}_c\rangle$. In other words, $\hat{H}_0$ is diagonal in the basis of transitions, and its diagonal matrix elements are the transition energies.

The other two terms describe the electron-hole interaction. They are *not* diagonal, and will therefore couple transitions from different wavevectors and valence-conduction pairs. Loosely speaking, this makes it so transitions are

[12] This is an effective basis, which from the many-body point of view can be taken to correspond to a singly excited Slater determinant.

[13] In the following, we shall mostly omit these indices, but keep in mind the necessary complex conjugation when going from electronic states to hole states.

[14] Since we will work with BN systems, and both Boron and Nitrogen are rather light atoms, we remain spin unpolarized. The matrix elements given below are for this case.

no longer eigenstates of the system, and breaks the single particle bands picture. The two coupling terms are the direct electron-hole interaction:

$$\left\langle v\mathbf{k}_v, c\mathbf{k}_c \middle| \hat{U} \middle| v'\mathbf{k}'_v, c'\mathbf{k}'_c \right\rangle = \delta_{\mathbf{k}_c-\mathbf{k}_v,\mathbf{k}'_c-\mathbf{k}'_v} \int \varphi^*_{c,\mathbf{k}_c}(\mathbf{r})\varphi_{c',\mathbf{k}'_c}(\mathbf{r})W(\mathbf{r},\mathbf{r}')\varphi_{v,\mathbf{k}_v}(\mathbf{r}')\varphi^*_{v',\mathbf{k}'_v}(\mathbf{r}')d\mathbf{r}d\mathbf{r}'$$

and the exchange electron-hole interaction:

$$\left\langle v\mathbf{k}_v, c\mathbf{k}_c \middle| \hat{J} \middle| v'\mathbf{k}'_v, c'\mathbf{k}'_c \right\rangle = 2\delta_{\mathbf{k}_c-\mathbf{k}_v,\mathbf{k}'_c-\mathbf{k}'_v} \int \varphi^*_{c,\mathbf{k}_c}(\mathbf{r})\varphi_{v,\mathbf{k}_v}(\mathbf{r})v(\mathbf{r},\mathbf{r}')\varphi_{c',\mathbf{k}'_c}(\mathbf{r}')\varphi^*_{v',\mathbf{k}'_v}(\mathbf{r}')d\mathbf{r}d\mathbf{r}'$$

where v is the *unscreened* (bare) Coulomb interaction:

$$v(\mathbf{r},\mathbf{r}') = \frac{e^2}{\|\mathbf{r}-\mathbf{r}'\|}$$

and W is the *screened* Coulomb interaction in its static limit, while the $\varphi_{\mu,\mathbf{k}}$ are the electronic band states $|\mu,\mathbf{k}\rangle$ in position representation.

2.3.2 Optical activity

In this framework, excitonic states are naturally written as linear superpositions of transition states:

$$|\Psi\rangle = \sum_{v\mathbf{k}_v,c\mathbf{k}_c} \Psi_{v\mathbf{k}_v,c\mathbf{k}_c} |v\mathbf{k}_v, c\mathbf{k}_c\rangle$$

and the excitons of the system are those which are solutions of the Bethe-Salpeter equation:

$$\hat{H}_X |\Psi\rangle = E_\Psi |\Psi\rangle$$

i.e. the eigenstates of the Bethe-Salpeter Hamiltonian $\hat{H}_X$, with the corresponding E_Ψ being the associated energies. It should be noted, from the matrix elements above, that $\mathbf{Q} = \mathbf{k}_c - \mathbf{k}_v$ is a good quantum number for $\hat{H}_X$. It corresponds to the center of mass momentum of an excitation of the form $|v\mathbf{k}_v, c\mathbf{k}_c\rangle$ or linear combination thereof, and $\hat{H}_X$ is therefore effectively block diagonal in $\mathbf{Q}$. We will come back to this point.

In this framework, the absorption spectrum of a system may be effectively computed as:

$$\epsilon_2(E) \propto \frac{1}{E^2} \sum_\Psi |\langle\emptyset|\mathbf{e}\cdot\hat{\mathbf{p}}|\Psi\rangle|^2 \delta(E - E_\Psi) \tag{2.8}$$

where the sum runs over an eigenbasis of $\hat{H}_X$, $|\emptyset\rangle$ is the (many body) vacuum state, i.e. the state where no electron-hole pairs are excited and E_Ψ, is the excitation energy for the exciton Ψ, i.e. the difference between its energy and the vacuum state energy (and so is reference independent), $E = \hbar\omega$ is the energy of the incoming photons and $\mathbf{e}$ is the corresponding polarization vector. The interpretation is essentially the same as the one of equation 2.4, except that instead of the momentum matrix element describing the probability for an electron to be excited from the valence to the conduction band, it now describes the probability of an exciton being excited from the vacuum state.

For an excitonic state of definitite center of mass momentum $\mathbf{Q}$, $|\Psi\rangle = \sum_{v,c,\mathbf{k}} \Psi_{v,c,\mathbf{k}} |v\mathbf{k}, c(\mathbf{k}+\mathbf{Q})\rangle$, the usual rules of calculation for two body operators provide the expression of these matrix elements:

$$\langle\emptyset|\mathbf{e}\cdot\hat{\mathbf{p}}|\Psi\rangle = \sum_{v,c,\mathbf{k}} \Psi_{v,c,\mathbf{k}} \langle c, \mathbf{k}+\mathbf{Q}|\mathbf{e}\cdot\hat{\mathbf{p}}|v,\mathbf{k}\rangle \tag{2.9}$$

Like in the single-particle case, there is no absorption due to $\mathbf{Q} \neq \mathbf{0}$ states in the limit of vanishing photon momentum.

We must note, at this point, that we will not work in the basis of transitions much: a significant portion of chapter 3 will be devoted to building up (an approximation of) the Bethe-Salpeter hamiltonian in another basis, starting from localized electron and hole wavefunctions instead of extended Bloch functions.

2.3.3 Wannier Model

In systems with parabolic bands and with some additional approximations which amount to forgetting the system's lattice structure, the Bethe-Salpeter hamiltonian can be greatly simplified.[42, 15, 16, 43] This is the so-called Wannier model, which results in an effective hydrogenoid equation 1.1.

One way to obtain this approximation consists in making use of Bloch's theorem and writing the band states as Bloch waves, ie.:

$$\varphi_{\mu,\mathbf{k}}(\mathbf{r}) = \frac{1}{\sqrt{\Omega}} e^{-i\mathbf{k}\cdot\mathbf{r}} u_{\mu,\mathbf{k}}(\mathbf{r})$$

where Ω is the system's volume,[15] and the $u_{\mu,\mathbf{k}}(\mathbf{r})$ are lattice periodic functions which consequently contain the information about the system's lattice

[15] Volume in the general sense: it would be the area in two dimensions. When we need it, we will let d stand for the dimension of the system.

structure. They are taken to be normalized over a unit cell of the system, i.e. $\frac{1}{\Omega_{u.c.}} \int_{u.c.} |u_{\mu,\mathbf{k}}(\mathbf{r})|^2 d\mathbf{r} = 1$, with $\Omega_{u.c.}$ the unit cell volume.

We restrict ourselves to working with direct excitons (which we can do, since $\hat{H}_X$ is block diagonal in $\mathbf{Q}$), both for simplicity and because they are the ones which are relevant for (direct) absorption. We therefore consider an excitonic state of the form:

$$|\Psi\rangle = \sum_{\mathbf{k},v,c} \Psi_{\mathbf{k},v,c} \, |v\mathbf{k}, c\mathbf{k}\rangle$$

and we will aim to show that we can obtain a simple effective equation for the Fourier transfom of $\Psi_{\mathbf{k},v,c}$.

Kinetic energy

We start with the kinetic hamiltonian. Its matrix elements read:

$$\left\langle v\mathbf{k}, c\mathbf{k} \middle| \hat{H}_0 \middle| v'\mathbf{k}', c'\mathbf{k}' \right\rangle = \delta_{(vc),(v'c')} \delta_{\mathbf{k},\mathbf{k}'} (E_c(\mathbf{k}) - E_v(\mathbf{k}))$$

Suppose now that the system has a direct gap, with valence band maximum and conduction band minimum at $\mathbf{k}_0$. We apply the effective mass approximation there, so that:

$$E_c(\mathbf{k}) \approx E_c(\mathbf{k}_0) + \frac{\hbar^2}{2m_c} (\mathbf{k} - \mathbf{k}_0)^2$$
$$E_v(\mathbf{k}) \approx E_v(\mathbf{k}_0) - \frac{\hbar^2}{2m_v} (\mathbf{k} - \mathbf{k}_0)^2$$

with m_c and m_v the electron and hole effective masses associated the the conduction and valence band c and v respectively. The direct transition energies, which are the matrix elements of the kinetic Hamiltonian then read:

$$E_c(\mathbf{k}) - E_v(\mathbf{k}) = \underbrace{E_c(\mathbf{k}_0) - E_v(\mathbf{k}_0)}_{E_g} + \frac{\hbar^2}{2\mu_{vc}} (\mathbf{k} - \mathbf{k}_0)^2$$

where $\mu_{vc} = \frac{m_v m_c}{m_v + m_c}$ is the two-body transition effective mass, and E_g is usually the gap energy. The action of $\hat{H}_0$ on our direct excitonic state then simply reads:

$$\langle v\mathbf{k}, c\mathbf{k} | \hat{H}_0 | \Psi \rangle = \delta_{(vc),(v'c')} \left[E_g + \frac{\hbar^2}{2\mu_{vc}} (\mathbf{k} - \mathbf{k}_0)^2 \right] \Psi_{\mathbf{k}}$$

Electron-hole interaction

If the band states are written in the prescribed Bloch form, the matrix elements of the direct interaction read:

$$\Big\langle v\mathbf{k}, c\mathbf{k}\Big|\hat{U}\Big|v'\mathbf{k}', c'\mathbf{k}'\Big\rangle = \frac{1}{\Omega^2}\int e^{-i\left(\mathbf{k}'-\mathbf{k}\right)\cdot\mathbf{r}}u^*_{c,\mathbf{k}}(\mathbf{r})u_{c',\mathbf{k}'}(\mathbf{r})W(\mathbf{r},\mathbf{r}')e^{i\left(\mathbf{k}'-\mathbf{k}\right)\cdot\mathbf{r}'}u_{v,\mathbf{k}}(\mathbf{r}')u^*_{v',\mathbf{k}'}(\mathbf{r}')d\mathbf{r}d\mathbf{r}'$$

The integral over, say, $\mathbf{r}'$, reads:

$$\int W(\mathbf{r},\mathbf{r}')e^{i\left(\mathbf{k}'-\mathbf{k}\right)\cdot\mathbf{r}'}\underbrace{u_{v,\mathbf{k}}(\mathbf{r}')u^*_{v',\mathbf{k}'}(\mathbf{r}')}_{\text{Lattice terms}}d\mathbf{r}'$$

where the integrand, as long as the potential is not too strong, is essentially the product of a slowly varying function (the potential and the plane wave) and the lattice terms. We replace the latter by their average over the unit cell:

$$\frac{1}{\Omega_{u.c.}}\int u_{v,\mathbf{k}_v}(\mathbf{r}')u^*_{v',\mathbf{k}'_v}(\mathbf{r}')d\mathbf{r}'$$

and if $\mathbf{k}$ and $\mathbf{k}'$ are not too different from each other, the above evaluates to $\delta_{v,v'}$. With this, the structure information about the lattice present in the bands has effectively been forgotten. We can do the same thing for the integration over $\mathbf{r}$. In the same spirit, we assume that the screened potential is macroscopic, and depends only on $\mathbf{r}'-\mathbf{r}$, i.e. that we have: $W(\mathbf{r}'-\mathbf{r}) = V(\mathbf{r}'-\mathbf{r})$. It follows that:

$$\Big\langle v\mathbf{k}, c\mathbf{k}\Big|\hat{U}\Big|v'\mathbf{k}', c'\mathbf{k}'\Big\rangle \approx \frac{\delta_{v,v'}\delta_{c,c'}}{\Omega^2}\int e^{i\left(\mathbf{k}'-\mathbf{k}\right)\cdot\left(\mathbf{r}'-\mathbf{r}\right)}V(\mathbf{r}'-\mathbf{r})d\mathbf{r}d\mathbf{r}'$$

so that within this approximation, the direct potential only couples transitions from the valence conduction pair. Introducing now the relative coordinate $\mathbf{R} = \mathbf{r}'-\mathbf{r}$, we have:

$$\begin{aligned}\Big\langle v\mathbf{k}, c\mathbf{k}\Big|\hat{U}\Big|v'\mathbf{k}', c'\mathbf{k}'\Big\rangle &\approx \frac{\delta_{v,v'}\delta_{c,c'}}{\Omega}\int e^{i\left(\mathbf{k}'-\mathbf{k}\right)\cdot\mathbf{R}}V(\mathbf{R})d\mathbf{R}\\ &\approx \frac{\delta_{v,v'}\delta_{c,c'}}{\Omega}\tilde{V}\Big(\mathbf{k}'-\mathbf{k}\Big)\end{aligned}$$

where we have recognized the Fourier transform $\tilde{V}$ of V. By way of consequence, we can evaluate the action of $\hat{U}$ on a direct excitonic state $|\Psi\rangle = \sum_{\mathbf{k}}\Psi_{\mathbf{k}}\,|v\mathbf{k}, c\mathbf{k}\rangle = \frac{\Omega}{(2\pi)^d}\int\Psi_{\mathbf{k}}\,|v\mathbf{k}, c\mathbf{k}\rangle\,d\mathbf{k}$ (we do not sum over band indices since transitions from different pairs are no longer coupled). We find:

$$\langle v\mathbf{k}, c\mathbf{k}|\hat{U}|\Psi\rangle = \frac{1}{(2\pi)^d}\int\tilde{V}\Big(\mathbf{k}'-\mathbf{k}\Big)\Psi_{\mathbf{k}'}d\mathbf{k}'$$

which is effectively a convolution product between the potential and the excitonic wavefunction in reciprocal space.

The same approximations can be performed for the exchange interaction, but there, the associated integrals over $\mathbf{r}$ and $\mathbf{r}'$ involve the overlap of valence and conduction bands, and therefore are negligible:

$$\left\langle v\mathbf{k}, c\mathbf{k}\middle|\hat{J}\middle|v'\mathbf{k}', c'\mathbf{k}'\right\rangle \approx 0$$

Fourier transform to coordinate space

At this point, the Bethe-Salpeter equation in component form reads:

$$-\frac{\hbar^2}{2m}(\mathbf{k}-\mathbf{k}_0)^2\Psi(\mathbf{k}) + \int \frac{\tilde{V}\left(\mathbf{k}'-\mathbf{k}\right)}{(2\pi)^d}\Psi\left(\mathbf{k}'\right)d\mathbf{k}' = (E-E_g)\Psi(\mathbf{k}) \tag{2.10}$$

where, on the left-hand side, the first term corresponds to the kinetic energy, and the second term to the direct potential, and we have introduced $\Psi(\mathbf{k}) = \sqrt{\frac{\Omega}{(2\pi)^d}}\Psi_{\mathbf{k}}$.

We now Fourier tansform the equation above. To this end, we introduce the sought after excitonic wavefunction in the relative coordinate:

$$\Psi(\mathbf{r}) \propto \int e^{-i\mathbf{k}\cdot\mathbf{r}}\Psi(\mathbf{k})d\mathbf{r}$$

and, because we expanded the band structure around the transition minima at $\mathbf{k}_0$, it is also useful to introduce:

$$g(\mathbf{r}) \propto \int e^{-i\mathbf{q}\cdot\mathbf{r}}\underbrace{\Psi(\mathbf{k}_0+\mathbf{q})}_{g(\mathbf{q})}d\mathbf{q}$$

so that $g(\mathbf{q})$ describes the excitonic wavefunction in reciprocal space with the origin at the expansion point $\mathbf{k}_0$. The two functions are related by a shift in reciprocal space, which becomes a phase factor in coordinate space:

$$\Psi(\mathbf{r}) = e^{-i\mathbf{k}_0\cdot\mathbf{r}}g(\mathbf{r})$$

With this, equation 2.10 is Fourier transformed into:

$$-\frac{\hbar^2}{2\mu}\nabla^2 g(\mathbf{r}) + V(\mathbf{r})g(\mathbf{r}) = E_b g(\mathbf{r}) \tag{2.11}$$

where $E_b = E - E_g$ denotes the exciton binding energy. This is an effective hydrogenoid Schrödinger equation for g, which can be solved to access both the excitonic eigenstates and their binding energies.

From the point of view of optical properties, we note that, if we further approximate that the optical matrix elements from the electronic transitions are $\mathbf{k}$-independant, $\langle c, \mathbf{k}|\hat{\mathbf{p}}|v, \mathbf{k}\rangle \approx \mathbf{p}_{v,c}$ then it follows from equation 2.3.3 that:[15, 16]

$$|\langle\emptyset|\mathbf{e}\cdot\hat{\mathbf{p}}|\Psi\rangle| \propto \left|\mathbf{e}\cdot\mathbf{p}_{v,c}\right|^2 \left|\int \Psi(\mathbf{k})d\mathbf{k}\right|^2 \propto |\Psi(\mathbf{0})|^2 \propto |g(\mathbf{0})|^2$$

as claimed in the introduction.

Conclusion

We have already discussed the consequences of this equation in the introduction, and we will discuss the Wannier model further in section 4.4.1. For now, let us comment on what is to follow. In the derivation of the Wannier equation, we have made several approximations that effectively amount to the neglect of the system's lattice structure, and in particular its geometry. Among them, the effective mass approximation amounts to disregarding this structure in the band energies, while our approximations regarding the lattice periodic components of the band states philosophically amount to its neglect in the band states. The next chapter aims to show that, in BN like systems, some of these approximations can be fruitfully relaxed without introducing too much complexity to the problem. As announced, we will not work in reciprocal space, but rather with localized electron and hole wavefunctions. However, it is worth noting that most of our manipulations have reciprocal space analogues, which do correspond closely to what we have described here. In essence, they will amount to replacing the band states by tight-binding basis functions or appropriate approximates to the tight-binding bands, and the effective mass approximation by an approximation to the tight-binding band energies. The approximations in question are essentially those described above for the BN chain. We should note, at this point, that the use of a tight-binding framework to compute excitonic (and more generally, many-body) properties in semiconductors and nanostructures is well known.[27, 44, 45] Our focus here will be on the aforementionned approximations and their consequences, in particular the fact that, in BN like systems, they allow the Bethe-Salpeter hamiltonian itself to be (approximately) rewritten as an effective tight-binding problem.

Chapter 3

Excitonic tight binding in the BN linear chain: a toy model

Through the previous chapter, we have come into possession of a way to describe single particle electron and hole states, via the tight-binding approximation, and of the Bethe-Salpeter equation, which describes the coupling of electron-hole transitions. Those are the theoretical ingredients that will let us describe excitonic properties in this work.

The object of this chapter is to show that, in hBN like systems, it is possible to approximately map the Bethe-Salpeter equation onto an effective tight-binding problem.[46, 47, 38, 48] We specialize here to the case of the linear BN chain for concreteness and simplicity. In particular, the fact that the chain is one dimensional will be helpful to build and illustrate some of the geometrical intuition behind the mapping procedure. Indeed, we will be naturally led to (intermediate, but interesting in their own right) tight-binding problems for electron-hole pairs, which are naturally expressed in a dimension that is twice that of the original crystal (so in a plane for the chain, but in four dimensions for hBN).

We should stress that our aim here is essentially pedagogical, and that we treat the linear BN chain as a toy problem, in such a way that it is a one-dimensional analogue to the two-dimensional hBN.[1] The physics of excitons in one-dimensional chains, and many-body effects there in general, is very rich, and we will not discuss its specificities. For an *ab initio* study of many-body effects including excitons in one-dimensional chains with a treatment of the linear BN chain, see for example [49].

[1] In fact, most of the equations presented here transfer directly to hBN with a change of geometric factors.

3.1 Electronic structure and relevant lattices

3.1.1 Notations

The description of the electronic structure of the linear BN chain was already discussed as an example in the previous chapter, within section 2.1.2. We will generalize here slighly by inclunding second nearest neighbors and more general notations, but overall, the spirit is very much the same, and so we will endeavour not to repat ourselves too much.

We consider a linear chain of BN. Its unit cell contains two atoms: one Nitrogen atom and one Boron atom. We call a the nearest neighbor $B-N$ distance. To fix notations, we let $\mathcal{R} = \{2na\mathbf{e}_x \ / \ n \in \mathbb{Z}\}$ be the underlying Bravais lattice of the system, with $\mathbf{e}_x$ a unit vector in the direction of the chain. We denote by $\mathbf{n}_\mu^0$ the position of the unit cell atoms, where μ runs over the atomic types ($\mu = B$ or N) and introduce the sublattices Λ_μ as:

$$\Lambda_\mu = \mathbf{n}_\mu^0 + \mathcal{R}$$

so that the sites in Λ_μ are exactly those which are translationnally equivalent to the unit cell site $\mathbf{n}_\mu^0$, and the set of sites of the full crystal lattice is given by $\cup_\mu \Lambda_\mu$.

It is enough to restrict ourselves to, say, the (hybridized) p_z orbitals, for the reasons discussed in section 2.1.2. We thus denote by $|B, \mathbf{n}\rangle$ and $|N, \mathbf{m}\rangle$ these localized boron and nitrogen p_z atomic orbitals, where $\mathbf{n} \in \Lambda_B$ and $\mathbf{m} \in \Lambda_N$ denote the atomic coordinates. From this basis of localized atomic orbitals, that we assume orthonormal, we define the associated tight-binding basis functions:

$$|\mu, \mathbf{k}\rangle = \frac{1}{\sqrt{N}} \sum_{\mathbf{n} \in \Lambda_{\mu,\alpha}} e^{-\mathbf{k}\cdot\mathbf{n}} \, |\mu, \mathbf{n}\rangle$$

where N is the number of unit cells in the system.

3.1.2 Electronic hamiltonian

We describe the electronic structure of the system using a tight-binding hamiltonian $\hat{H}_0^{(el)}$ constructed with second nearest neighbor hoppings, which,

in the basis of localized atomic orbitals, is given by:

$$\langle B,\mathbf{n}|\hat{H}_0^{(el)}|B,\mathbf{n}'\rangle = \begin{cases} \Delta & \text{if } \mathbf{n}=\mathbf{n}' \\ t_\perp^{BB} & \text{if } \mathbf{n} \text{ and } \mathbf{n}' \text{ are 2n.n.} \\ 0 & \text{else} \end{cases}$$

$$\langle N,\mathbf{m}|\hat{H}_0^{(el)}|N,\mathbf{m}'\rangle = \begin{cases} -\Delta & \text{if } \mathbf{m}=\mathbf{m}' \\ t_\perp^{NN} & \text{if } \mathbf{m} \text{ and } \mathbf{m}' \text{ are 2n.n.} \\ 0 & \text{else} \end{cases}$$

$$\langle B,\mathbf{n}|\hat{H}_0^{(el)}|N,\mathbf{m}\rangle = \begin{cases} t_\perp & \text{if } \mathbf{n} \text{ and } \mathbf{m} \text{ are 1n.n. in plane} \\ 0 & \text{else} \end{cases}$$

where Δ, $t_\perp$, $t_\perp^{NN}$ and $t_\perp^{BB}$ are parameters, which we shall call the "kinetic" parameters, in that they describe the system's band structure.

This hamiltonian is block diagonal in the basis of the tight-binding basis functions, and leads to the integral transfer matrix:

$$H(\mathbf{k}) = \begin{pmatrix} \Delta + t_\perp^{BB} f_2(\mathbf{k}) & t_\perp f_1(\mathbf{k}) \\ t_\perp f_1(\mathbf{k})^* & -\Delta + t_\perp^{NN} f_2(\mathbf{k}) \end{pmatrix}$$

in the basis $\{|B,\mathbf{k}\rangle, |N,\mathbf{k}\rangle\}$, where:

$$f_1(\mathbf{k}) = \sum_{\boldsymbol{\tau}} e^{i\mathbf{k}\cdot\boldsymbol{\tau}} = 2\cos(ka)$$
$$f_2(\mathbf{k}) = \sum_{\boldsymbol{\mu}} e^{i\mathbf{k}\cdot\boldsymbol{\mu}} = 2\cos(2ka)$$

where k is the wavenumber defined through $\mathbf{k} = k\mathbf{e}_x$, the $\boldsymbol{\tau}$ are the in-plane first nearest neighbors nitrogen to boron vectors, i.e. $\pm a\mathbf{e}_x$, and the μ are the second nearest neighbor vectors, i.e. the $\pm 2a\mathbf{e}_x$. Here, f_1 and f_2 correspond to the geometric terms for the first and second nearest neighbours respectively.

Let us now provide a reminder of an important discussion we had in the previous chapter, in section 2.1.2. As we have already noted, in our B-N systems, the electronic gap is quite large, which translates here to the idea that 2Δ is larger than the other parameters.[2] In other words, the difference in onsite energy between the nitrogen ($-\Delta$) and the boron ($+\Delta$) subspaces is large. Furthemore, the gap lies in the vicinity of the high-symmetry point **X**

[2] Actually, typically, $\Delta \sim |t_\perp|$ in magnitude. However, the electronic couplings mediated by $t_\perp$ are of less importance for excitations near the gap, because $f_1(\mathbf{X}) = 0$, as discussed below.

and $f_1(\mathbf{X}) = 0$, so that the coupling between these subspaces is even smaller near the gap. This suggests that the valence bands will be constituted mostly of nitrogen orbitals, while the conduction bands will be constituted mostly of boron orbitals.

This idea can be formalized by considering the following decomposition of the hamiltonian:

$$\hat{H}_0^{(el)} = \hat{\Delta} + \hat{V}$$

where we define $\hat{\Delta}$ as $\hat{H}_0^{(el)}$ with all hoppings (every parameter except Δ) set to 0, and, consequently, $\hat{V} = \hat{H}_0^{(el)} - \hat{\Delta}$ is likewise $\hat{H}_0^{(el)}$ with Δ set to 0. $\hat{\Delta}$ has two eigensubspaces: one at low energy, $-\Delta$, spanned by all the nitrogen atomic orbitals, and one at high energy, $+\Delta$, spanned by all the boron atomic orbitals. We can now treat $\hat{V}$ as a perturbation, and perform degenerate perturbation theory in both subspaces to obtain two separate effective hamiltonians for the low and high energy eigenstates of $\hat{H}_0^{(el)}$, which are by definition the valence and conduction bands.

Let us anticipate on excitonic problems by calling the low energy effective hamiltonian $\hat{H}_h$ (h for "holes") and the high energy one $\hat{H}_e$ (e for "electrons"). We shall compute them up to second order in $\hat{V}$. Two bases are of interest to express their matrix elements: the basis of localized atomic orbitals, and the basis of the tight-binding basis functions.

In the basis of localized atomic orbitals, we find:

$$\langle B, \mathbf{n}|\hat{H}_e|B, \mathbf{n}'\rangle = \begin{cases} \Delta + \eta\frac{t_\perp^2}{2\Delta} & \text{if } \mathbf{n} = \mathbf{n}' \\ \frac{t_\perp^2}{2\Delta} + t_\perp^{BB} & \text{if } \mathbf{n} \text{ and } \mathbf{n}' \text{ are 1n.n. in } \Lambda_B \\ 0 & \text{else} \end{cases}$$

$$-\langle N, \mathbf{m}|\hat{H}_h|N, \mathbf{m}'\rangle = \begin{cases} \Delta + \eta\frac{t_\perp^2}{2\Delta} & \text{if } \mathbf{m} = \mathbf{m}' \\ \frac{t_\perp^2}{2\Delta} - t_\perp^{NN} & \text{if } \mathbf{m} \text{ and } \mathbf{m}' \text{ are 1n.n. in } \Lambda_N \\ 0 & \text{else} \end{cases}$$

with $\eta = 2$ is a geometric factor.[3] Notice the "$-$" sign in front of $\langle N, \mathbf{m}|\hat{H}_h|N, \mathbf{m}'\rangle$. We can briefly comment on these effective hamiltonians. First, we note that both are effective first nearest neighbors tight-binding hamiltonians in their subspace. We may be surprised that we started with a second nearest neighbors hamiltonian, and now have only effective first nearest neighbors apart from these terms. This is because second nearest neighbors, by definition in

[3]We introduce this notation here because the corresponding effective hamiltonian for single-layer hBN will turn out to be exactly the same as the ones for the chain, except with $\eta = 3$. In fact, η is nothing more than the number of first nearest neighbors of a given site.

our lattice, connect atoms of the same type, and therefore are effectively first nearest neighbors within their subspaces. Note, however, that the second nearest neighbor interactions in the crystal break the electron-hole symmetry, even if $t_\perp^{NN} = t_\perp^{BB}$.

We can, likewise, express these effective hamiltonians in the basis of tight-binding basis functions where they are block-diagonal in $\mathbf{k}$, either by reconstructing them from the expression of the effective hamiltonians above, or by doing perturbation theory on the full integral transfer matrix above. Both ways are equivalent, and we find the following integral transfer matrices:

$$H_e(\mathbf{k}) = \left[\Delta + \frac{t_\perp^2}{2\Delta}|f_1(\mathbf{k})|^2 + t_\perp^{BB} f_2(\mathbf{k})\right] I_1$$

in the basis $\{|B_1, \mathbf{k}\rangle\}$ for the electron bands, and:

$$H_h(\mathbf{k}) = -\left[\Delta + \frac{t_\perp^2}{2\Delta}|f_1(\mathbf{k})|^2 - t_\perp^{NN} f_2(\mathbf{k})\right] I_1$$

in the basis $\{|N_1, \mathbf{k}\rangle\}$ for the hole bands. Here, I_1 stands for the identity matrix in dimension 1, so that this approximate hamiltonians are in fact diagonal in k. This results from the fact that there is only one "low energy" and one "high energy" state in the system's unit cell, and is a characteristic that is shared between the linear BN chain an the planar hBN. It ceases to be true for more complex systems, such as multilayers or certain bulk stackings (notably AA' and AB), in which cases the hamiltonian is "merely" block diagonal. Both blocks have a similar structure here, and, for a given value of k, differ essentially by the values of their parameters. Since both hamiltonians are diagonal, the band energies within this approximation are immediately given by:

$$E_c(\mathbf{k}) = \Delta + \frac{t_\perp^2}{2\Delta}|f_1(\mathbf{k})|^2 + t_\perp^{BB} f_2(\mathbf{k})$$
$$E_v(\mathbf{k}) = -\left[\Delta + \frac{t_\perp^2}{2\Delta}|f_1(\mathbf{k})|^2 + t_\perp^{NN} f_2(\mathbf{k})\right]$$

We have already discussed the band states for the chain at some length in section 2.1.2, in chapter 3. We kept then to a first nearets neighbor description, but the takaway remains essentially the same: to a good approximation, the conduction band is well approximated by the tight-biding basis function for Boron, and the valence band by the tight-binding basis function for Nitrogen:

$$|c, \mathbf{k}\rangle \approx |B, \mathbf{k}\rangle \quad ; \quad |v, \mathbf{k}\rangle \approx |N, \mathbf{k}\rangle$$

to zeroth-order.[4]

3.2 Excitonic hamiltonian

3.2.1 The basis of localized pairs

Kinetic hamiltonian

With the single particle band structure described by $\hat{H}_0^{(el)} \approx \hat{H}_h \oplus \hat{H}_e$, we now turn our attention to the description of excitonic states. We seek to describe transitions in a way which is compatible with our earlier approximations. A natural way to do this is to write transition space as a tensor product between the low (holes / nitrogen) and high (electrons / boron) energy spaces described earlier:

$$\mathcal{H} \approx \mathcal{H}_h \otimes \mathcal{H}_e$$

and to describe the non interacting electron-hole pairs by an "independent transitions hamiltonian", which we shall call the kinetic hamiltonian:

$$\hat{H}_0 \approx \hat{H}_h \otimes \mathbb{1}_e - \mathbb{1}_h \otimes \hat{H}_e$$

where $\mathbb{1}_h$ (resp. $\mathbb{1}_e$) is the identity on $\mathcal{H}_h$ (resp. $\mathcal{H}_e$). The space of transitions is therefore naturally spanned by states of the form:

$$|\mathbf{m}, \mathbf{n}\rangle = |N, \mathbf{m}\rangle \otimes |B, \mathbf{n}\rangle$$

each of which represents a localized electron-hole pair, where the hole and the electron are separated by the vector $\mathbf{R} = \mathbf{n} - \mathbf{m}$. These states play an important role for us, since our description of the system is naturally done in terms of localized states. In fact, the kinetic hamiltonian $\hat{H}_0$ is a $2d$-dimensional tight-binding hamiltonian for these states, where d is the dimension of the underlying crystal. In our case, the chain is $1D$, so $\hat{H}_0$ is the tight-binding hamiltonian of an effective $2D$ system. This system may be pictured geometrically by associating to each $|\mathbf{m}, \mathbf{n}\rangle$ a point of coordinates $(\mathbf{m}, \mathbf{n}) = \mathbf{m} \oplus \mathbf{n}$ in the space of dimension $2d$, i.e. here simply the point of coordinates (m, n) in the two-dimensional plane. Then, since the $\mathbf{m}$ and $\mathbf{n}$ are discrete (countable, in fact), these points form a discrete set, onto which the states $|\mathbf{m}, \mathbf{n}\rangle$ act as localized orbitals.

[4] We could correct the band states, as well as the localized electron and hole states, to first order in the non-onsite hoppings (since we went to second order in the energies). For simplicity, we do not do it explicitly here, and retain the zeroth-order notations. We will discuss the notion further in section 4.3.3, when we evaluate exchange matrix elements for the monolayer. See also footnote 7 and the associated main text in this chapter.

We can check this directly using the definition of $\hat{H}_0$ and the matrix elements derived for the effective hamiltonians $\hat{H}_h$ and $\hat{H}_e$ above to obtain the matrix elements of $\hat{H}_0$ in the basis of pairs. Leveraging the orthonormality of the basis of atomic orbitals, we find:

$$\langle \mathbf{m}, \mathbf{n} | \hat{H}_0 | \mathbf{m}', \mathbf{n}' \rangle = \begin{cases} 2\Delta + \eta \frac{t_\perp^2}{\Delta} & \text{if } \mathbf{m} = \mathbf{m}' \text{ and } \mathbf{n} = \mathbf{n}' \\ \frac{t_\perp^2}{2\Delta} + t_\perp^{BB} & \text{if } \mathbf{m} = \mathbf{m}' \text{ and } \mathbf{n}, \mathbf{n}' \text{ are 1n.n. in } \Lambda_B \\ \frac{t_\perp^2}{2\Delta} - t_\perp^{NN} & \text{if } \mathbf{m}, \mathbf{m}' \text{ are 1n.n. in } \Lambda_N \text{ and } \mathbf{n} = \mathbf{n}' \\ 0 & \text{otherwise} \end{cases}$$

We can recognize an effective hopping associated to the motion of the electron alone, $T_e' = \frac{t_\perp^2}{2\Delta} + t_\perp^{BB}$, and an effective hopping associated to the motion of the hole alone, $T_h' = \frac{t_\perp^2}{2\Delta} - t_\perp^{NN}$. Note that there is no hopping corresponding to a "simultaneous" motion of the electron and the hole. The resulting hopping structure on the lattice of pairs is depicted in figure 3.1.

As a consistency check, and to gather additional insight on the problem, we may diagonalize $\hat{H}_0$. Treating it as an effective tight-binding hamiltonian on a square lattice (with a single orbital in its unit cell), we introduce a basis of tight-binding basis functions:[5]

$$|\mathbf{k}_v, \mathbf{k}_c\rangle = \frac{1}{\sqrt{N^2}} \sum_{\substack{\mathbf{m} \in \Lambda_N \\ \mathbf{n} \in \Lambda_B}} e^{-i(-\mathbf{k}_v \cdot \mathbf{m} + \mathbf{k}_c \cdot \mathbf{n})} |\mathbf{m}, \mathbf{n}\rangle$$

Since there is only one "orbital" per unit cell of the lattice of pairs, this basis is automatically an eigenbasis of $\hat{H}_0$. These functions can be more tellingly rewritten as:

$$|\mathbf{k}_v, \mathbf{k}_c\rangle = \underbrace{\left(\frac{1}{\sqrt{N}} \sum_{\mathbf{m} \in \Lambda_N} e^{i\mathbf{k}_v \cdot \mathbf{m}} |N, \mathbf{m}\rangle \right)}_{|\Phi_v(\mathbf{k}_v)\rangle^*} \otimes \underbrace{\left(\frac{1}{\sqrt{N}} \sum_{\mathbf{n} \in \Lambda_B} e^{-i\mathbf{k}_c \cdot \mathbf{n}} |B, \mathbf{n}\rangle \right)}_{|\Phi_c(\mathbf{k}_c)\rangle} = |v\mathbf{k}_v, c\mathbf{k}_c\rangle$$

so that these tight-binding basis functions are in fact the transition states (within the approximations made above), which we thus naturally recover as

[5] One may wonder why we choose the unusual sign convention $e^{-i(-\mathbf{k}_v \cdot \mathbf{m} + \mathbf{k}_c \cdot \mathbf{n})}$ instead of the more standard $e^{-i(\mathbf{k}_v \cdot \mathbf{m} + \mathbf{k}_c \cdot \mathbf{n})}$. Let us first stress that this choice is only one of notation: it does not affect the physics of the system. The reason we make it here is that hole states are the conjugates of the corresponding electronic states: this sign convention anticipates on what follows, and will allow us to directly rewrite these basis functions as transition states with the "standard convention" for the hole and electron wavevectors.

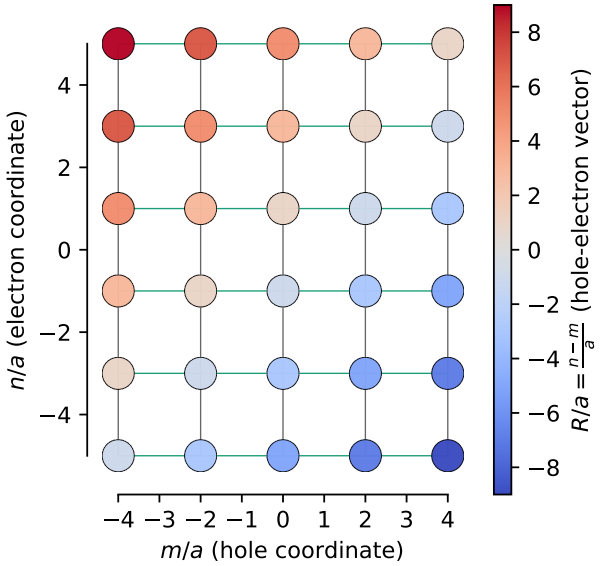

Figure 3.1: Effective tight-binding system associated to the hamiltonian $\hat{H}_0$ in the basis of pairs, in the $(\mathbf{m}, \mathbf{n})$ representation (partial view: the lattice is infinite in both directions). Each site is associated to a $|\mathbf{m}, \mathbf{n}\rangle$ pair state, which acts as an effective orbital for it. Connecting lines represent the effective hoppings, with vertical grey segments corresponding to electron hoppings $T'_e = \frac{t_\perp^2}{2\Delta} + t_\perp^{BB}$ and horizontal green segments corresponding to hole hoppings $T'_h = \frac{t_\perp^2}{2\Delta} - t_\perp^{NN}$. Color depicts the hole electron vector $\mathbf{R} = \mathbf{n} - \mathbf{m}$ for each pair: it will be shown that the direct electron hole interaction is (only) dependent on $\mathbf{R}$.

eigenstates of $\hat{H}_0$. Following through with the tight-binding analysis, we find that the associated eigenenergies are given by:

$$E_0(\mathbf{k}_v, \mathbf{k}_c) = 2\Delta + \eta\frac{t_\perp^2}{\Delta} + \left(\frac{t_\perp^2}{2\Delta} + t_\perp^{BB}\right) f_2(\mathbf{k}_c) + \left(\frac{t_\perp^2}{2\Delta} - t_\perp^{NN}\right) f_2(\mathbf{k}_v)$$

Noting now that $f_2(\mathbf{k}) = |f_1(\mathbf{k})|^2 - \eta$,[6] and recalling the approximate expressions for the band energies E_c (conduction) and E_v (valence) obtained from

[6]This can be shown either directly, through trigonometry, or geometrically, through the definition of these functions in terms of sums of exponentials. Indeed, noting that $|f_1(\mathbf{k})|^2 = \left|\sum_{\boldsymbol{\tau}} e^{i\mathbf{k}\cdot\boldsymbol{\tau}}\right|^2 = \sum_{\boldsymbol{\tau},\boldsymbol{\tau}'} e^{i\mathbf{k}(\boldsymbol{\tau}-\boldsymbol{\tau}')}$, it then suffices to remark that in our system, the difference of two first nearest neighbor vectors yields either a second nearest neighbor vector (yielding terms that contribute to f_2) or 0 when $\boldsymbol{\tau} = \boldsymbol{\tau}'$, yielding a constant term equal to the number of nearest neighbors of a site, η (here $\eta = 2$). For this reason, a similar relation exists between the analogues of f_1 and f_2 in two dimensional hBN.

the approximate hamiltonians $\hat{H}_e$ and $\hat{H}_h$ respectively, we can rearrange this expression into the more telling form:

$$E_0(\mathbf{k}_v, \mathbf{k}_c) = E_c(\mathbf{k}_c) - E_v(\mathbf{k}_v)$$

so that the eigenenergies of $\hat{H}_0$ are nothing but the transition energies (within our approximations), as expected.

Direct electron-hole interaction

A key interest of the basis of pairs is that the Coulomb interaction can be approximated in a relatively simple form in this basis. Indeed, if we let $\hat{U}$ stand for the direct Coulomb interaction, and $\phi_\mu(\mathbf{r} - \mathbf{n})$ stand for the position representation of the single particle state $|\mu, \mathbf{n}\rangle$, we have:

$$\langle \mathbf{m}, \mathbf{n}|\hat{U}|\mathbf{m}', \mathbf{n}'\rangle = \int \phi_N(\mathbf{r} - \mathbf{m})\phi_N(\mathbf{r} - \mathbf{m}')W(\mathbf{r}, \mathbf{r}')\phi_B(\mathbf{r}' - \mathbf{n})\phi_B(\mathbf{r}' - \mathbf{n}')d\mathbf{r}d\mathbf{r}'$$

where $W(\mathbf{r}, \mathbf{r}')$ is the screened Coulomb potential. We note now that, to zeroth-order,[7] the ϕ_μ are atomic orbitals, which therefore decay exponentially away from their centers (here taken to be $\mathbf{0}$). Therefore, only the terms of matching centers, i.e. those for which $\mathbf{m} = \mathbf{m}'$ and $\mathbf{n} = \mathbf{n}'$, contribute significantly to the integral. We are left with:

$$\langle \mathbf{m}, \mathbf{n}|\hat{U}|\mathbf{m}', \mathbf{n}'\rangle \approx \delta_{\mathbf{m},\mathbf{m}'}\delta_{\mathbf{n},\mathbf{n}'} \int |\phi_N(\mathbf{r} - \mathbf{m})|^2 W(\mathbf{r}, \mathbf{r}')|\phi_B(\mathbf{r}' - \mathbf{n})|^2 d\mathbf{r}d\mathbf{r}'$$

which is analogous to the semiclassical interaction between two charge densities. This approximation already provides us with an in interesting result. Indeed, it means that the Coulomb interaction has become diagonal in the basis of localized electron hole pairs. Evaluating such an integral, while less demanding than evaluating the four centers integral above, is still something which we would like to avoid, especially since the functions ϕ_μ are not known explicitly in semi-empirical tight-binding. Instead, we again note that the ϕ_μ are peaked around their centers, and therefore their densities may be approximated as delta functions, so that:

$$\langle \mathbf{m}, \mathbf{n}|\hat{U}|\mathbf{m}', \mathbf{n}'\rangle \approx \delta_{\mathbf{m},\mathbf{m}'}\delta_{\mathbf{n},\mathbf{n}'}W(\mathbf{m}, \mathbf{n})$$

[7] Note that this is an additional approximation. Indeed, since we have gone to second order in perturbation for the energies, we could also include in this calculation the first order contribution to the states. This would not modify results for the kinetic hamilonian, but would induce additional terms in the the direct and exchange electron hole interaction. We neglect these terms in the direct interaction, $\hat{U}$, but we will later show that they are needed for a good description of the exchange term.

Importantly, because of the translational invariance of the system, $W(\mathbf{m}, \mathbf{n})$ depends only on $\mathbf{R} = \mathbf{n} - \mathbf{m}$. In practice, we shall use a model potential $V(\mathbf{R})$ to approximate W.

Let us take a moment to review our situation. Neglecting exchange for the moment, the Bethe-Salpeter hamiltonian reads:

$$\hat{H}_X = \hat{H}_0 + \hat{U}$$

Within our approximations, $\hat{H}_0$ is a tight-binding hamiltonian in the basis of localized pairs, while $\hat{U}$ is diagonal, and so behaves as an effective external field which modifies the onsite energies. However, this hamiltonian is in $2d$ dimensions, which adds computational complexity, and further does not leverage the periodicity of the original crystal.

In the following sections, we will see that we can move to a hybrid representation, by treating the relative coordinate $\mathbf{R}$ in real space, and going to reciprocal space for the motion of the origin, which we shall fix on the hole. This hybrid representation will allow us to leverage both the fact that the center of mass momentum of the pair is a good quantum number because of the crystal periodicity, and the fact that $\hat{U}$ has simple matrix elements when expressed in relative coordinates.

Exchange interaction

The astute reader will have noted that we still have not discussed the exchange electron-hole interaction. Once again, we recall that our goal in these sections is not so much to provide a study of the physical system of the BN linear chain, but rather to discuss the implementation of the excitonic tight-binding model on a toy system.

It turns out that including exchange terms is delicate in one dimension: while relatively straightforward in the basis of pairs, difficulties emerge when moving to the hybrid representation, essentially because the Fourier transform of the Coulomb potential $\frac{1}{r}$ is ill-defined in 1D. These difficulties are removed in two dimensions, and so we delay our discussion of exchange terms until the treatemement of the physical system that is hBN. Therefore, we neglect this term in what follows, keeping in mind that such an approximation will in fact be reasonable in 2D at $\mathbf{Q} = 0$, and more generally in three dimensions. As a result, the hamiltonian $\hat{H}_X = \hat{H}_0 + \hat{U}$ will be, for us, the full Bethe-Salpeter hamiltonian for the moment.

3.2.2 The basis of elementary excitations

As announced above, the goal of this section is to establish a hybrid representation. To this end, we will describe a new basis and rewrite the excitonic hamiltonian in this new basis. We will do so in two complementary (and independent) ways. The first way proceeds by starting from the usual reciprocal space basis of transitions and introducing the new basis from there. This is, perhaps, the more direct way, and is well suited to more general problems (it generalizes more easily to problems in higher dimensions and more than two bands).

The other (equivalent) way leverages the fact that the excitonic hamiltonian describes an effective tight-binding problem in the basis of pairs, and shows that pursuing this line of reasoning naturally yields to the same results. This second approach is arguably more intuitive and visual than the first, and provides motivation for the definitions and choices made in the first procedure, as well as intuition for their results. However, it does not provide an immediate connection with the reciprocal space quantities, and becomes more cumbersome for more general problems.[8]

Elementary excitations as Fourier transforms of transition states

Let us start by noting that a given transition from valence band v at wavevector $\mathbf{k}$ to conduction band c at wavevector $\mathbf{k}+\mathbf{Q}$ can be written as:

$$\begin{aligned}|v\mathbf{k}, c(\mathbf{k}+\mathbf{Q})\rangle &= |v\mathbf{k}\rangle^* \otimes |c(\mathbf{k}+\mathbf{Q})\rangle \\ &\approx \frac{1}{\sqrt{N}} \sum_{\mathbf{m}\in\Lambda_N} e^{i\mathbf{k}\cdot\mathbf{m}} |N,\mathbf{m}\rangle \otimes \frac{1}{\sqrt{N}} \sum_{\mathbf{n}\in\Lambda_B} e^{-i(\mathbf{k}+\mathbf{Q})\cdot\mathbf{n}} |B,\mathbf{n}\rangle \\ &\approx \frac{1}{N} \sum_{\substack{\mathbf{m}\in\Lambda_N \\ \mathbf{n}\in\Lambda_B}} e^{-i\mathbf{Q}\cdot\mathbf{n}} e^{-i\mathbf{k}\cdot(\mathbf{n}-\mathbf{m})} |\mathbf{m},\mathbf{n}\rangle\end{aligned}$$

where we have written $|\mathbf{m},\mathbf{n}\rangle = |N,\mathbf{m}\rangle \otimes |B,\mathbf{n}\rangle$ for short, and noted that this state represents a localized electron-hole pair, where the hole and the electron are separated by the vector $\mathbf{R} = \mathbf{n} - \mathbf{m}$. Let us now change variables from $\mathbf{m},\mathbf{n}$ to $\mathbf{m},\mathbf{R}$. *A priori*, the set of $\mathbf{R}$ to be summed upon is $\Lambda(\mathbf{m}) = \Lambda_B - \mathbf{m}$. However, because the crystal is translationally invariant $\Lambda(\mathbf{m})$ is actually independant of $\mathbf{m}$. This lets us define the *lattice of excitations*:

$$\Lambda = \Lambda_B - \mathbf{m}_N^0 = \mathcal{R} + \left(\mathbf{n}_B^0 - \mathbf{m}_N^0\right)$$

[8] One notable difficulty comes from the fact that the effective tight-binding system in the basis of pairs is $2d$ dimensional, so already for a system like hBN where $d = 2$, we have to contend with a four-dimensional tight-binding problem. Still, the central ideas of the method remain valid.

which is therefore the set of all possible hole-electron vectors. With this, we can permute the sums above, and obtain:

$$|v\mathbf{k}, c(\mathbf{k}+\mathbf{Q})\rangle = \sum_{\mathbf{R}\in\Lambda} \frac{1}{\sqrt{N}} e^{-i(\mathbf{k}+\mathbf{Q})\cdot\mathbf{R}} \underbrace{\frac{1}{\sqrt{N}} \sum_{\mathbf{m}\in\Lambda_N} e^{-i\mathbf{Q}\cdot\mathbf{m}} |\mathbf{m}, \mathbf{m}+\mathbf{R}\rangle}_{|\mathbf{R},\mathbf{Q}\rangle}$$

where we have defined the states $|\mathbf{R}, \mathbf{Q}\rangle$, which can be recognized as tight-binding basis functions over the localized electron hole pairs.[9] We shall call such states "elementary excitations", and show that they are a convenient basis to solve the Bethe-Salpeter equation within our approximations. Let us now inject this expression in the transition basis expression of an indirect excitonic state with center of mass momentum $\mathbf{Q}$:

$$|\Psi_{\mathbf{Q}}\rangle = \sum_{v,c} \sum_{\mathbf{k}} \Psi_{v\mathbf{k},c(\mathbf{k}+\mathbf{Q})} |v\mathbf{k}, c(\mathbf{k}+\mathbf{Q})\rangle \tag{3.1}$$

In our case, there is only one valence band and one transition band, so we shall omit the corresponding summations. Permuting the sums on $\mathbf{R}$ and $\mathbf{k}$, we can rewrite the state as follows:

$$\begin{aligned} |\Psi_{\mathbf{Q}}\rangle &= \sum_{\mathbf{R}\in\Lambda} \underbrace{\frac{1}{\sqrt{N}} \sum_{\mathbf{k}} \Psi_{v\mathbf{k},c(\mathbf{k}+\mathbf{Q})} e^{-i(\mathbf{k}+\mathbf{Q})\cdot\mathbf{R}}}_{\Psi_{\mathbf{R},\mathbf{Q}}} |\mathbf{R}, \mathbf{Q}\rangle \\ &= \sum_{\mathbf{R}\in\Lambda} \Psi_{\mathbf{R},\mathbf{Q}} |\mathbf{R}, \mathbf{Q}\rangle \end{aligned}$$

We therefore see that the $|\mathbf{R}, \mathbf{Q}\rangle$ define a new basis for the excitonic states, which can directly be checked to be orthonormal:

$$\langle \mathbf{R}, \mathbf{Q} | \mathbf{R}', \mathbf{Q}' \rangle = \delta_{\mathbf{R},\mathbf{R}'} \delta_{\mathbf{Q},\mathbf{Q}'}$$

Importantly, this approach also provides us with conversion formulas between the excitonic weights in reciprocal / band space and their analogues in elementary excitation space:

$$\Psi_{\mathbf{R},\mathbf{Q}} = \frac{1}{\sqrt{N}} \sum_{\mathbf{k}} \Psi_{v\mathbf{k},c(\mathbf{k}+\mathbf{Q})} e^{-i(\mathbf{k}+\mathbf{Q})\cdot\mathbf{R}} \tag{3.2}$$

$$\Psi_{v\mathbf{k},c(\mathbf{k}+\mathbf{Q})} = \frac{1}{\sqrt{N}} \sum_{\mathbf{R}\in\Lambda} \Psi_{\mathbf{R},\mathbf{Q}} e^{i(\mathbf{k}+\mathbf{Q})\cdot\mathbf{R}} \tag{3.3}$$

[9] They are in fact exactly tight-binding basis functions for the localized electron hole pairs, leveraging the translation invariance on the hole coordinate, $\mathbf{m}$. This will be discussed in details in the following section.

Having now obtained the sought-after hybrid basis, where the relative coordinate is treated in direct space, while the center of mass motion is treated in reciprocal space, we proceed to rewrite the excitonic Hamiltonian $\hat{H}_X = \hat{H}_0 + \hat{U}$ in this new basis. The process in relatively straightforward, since we already know the matrix elements of $\hat{H}_0$ and $\hat{U}$ in the basis of localized pairs, and know the expressions of the $|\mathbf{R}, \mathbf{Q}\rangle$ in terms of the localized pairs. Performing the calculations, we find:

$$\langle \mathbf{R}, \mathbf{Q}|\hat{H}_0|\mathbf{R}', \mathbf{Q}'\rangle = \delta_{\mathbf{Q},\mathbf{Q}'} \begin{cases} 2\Delta + \eta\frac{t_\perp^2}{\Delta} & \text{if } \mathbf{R} = \mathbf{R}' \\ T'_e + T'_h e^{i\mathbf{Q}\cdot(\mathbf{R}'-\mathbf{R})} & \text{if } \mathbf{R}, \mathbf{R}' \text{ are 1n.n. in } \Lambda \\ 0 & \text{otherwise} \end{cases}$$

for the kinetic hamiltonian, and:

$$\langle \mathbf{R}, \mathbf{Q}|\hat{U}|\mathbf{R}', \mathbf{Q}'\rangle = \delta_{\mathbf{Q},\mathbf{Q}'}\delta_{\mathbf{R},\mathbf{R}'}V(\mathbf{R})$$

for the direct electron-hole interaction, which retains a very simple expression and remains diagonal in the new basis. Crucially, we verify that $\hat{H}_0$ and $\hat{U}$ preserve $\mathbf{Q}$, i.e. they do not couple elementary excitations of a different $\mathbf{Q}$. As a result, both $\hat{H}_0$ and $\hat{U}$ are block-diagonal in $\mathbf{Q}$. In this sense, we therefore have one effective hamiltonian, say $\hat{H}_X(\mathbf{Q})$, per value of $\mathbf{Q}$, which appears as a tight-binding hamiltonian on the lattice of excitations Λ.

Elementary excitations as tight-binding basis functions in the basis of pairs

Before dicussing this hamiltonian further, we will consider a complementary way to arrive at the results presented above, leveraging the perspective that our system reduces to a $2d$ dimensional tight-binding problem in the basis of localized pairs.

We start by changing coordinates from $\mathbf{m}, \mathbf{n}$ to $\mathbf{m}, \mathbf{R}$, with $\mathbf{R} = \mathbf{n} - \mathbf{m}$ the relative hole-electron vector, as above. In keeping with this, we re-index the pair states, by writing:

$$|\mathbf{m}, \mathbf{R}\rangle = |N, \mathbf{m}\rangle \otimes |B, \mathbf{m} + \mathbf{R}\rangle$$

It is then straightforwards to check that:

$$\langle \mathbf{m}, \mathbf{R}|\hat{U}|\mathbf{m}', \mathbf{R}'\rangle \approx \delta_{\mathbf{m},\mathbf{m}'}\delta_{\mathbf{R},\mathbf{R}'}W(\mathbf{m}, \mathbf{m} + \mathbf{R}) \approx \delta_{\mathbf{m},\mathbf{m}'}\delta_{\mathbf{R},\mathbf{R}'}V(\mathbf{R})$$

where we have recalled that, because of translation invariance, the direct electron-hole interaction depends only on $\mathbf{R}$. This is the main reason for the change of variables.

The matrix elements of the kinetic hamiltonian, $\hat{H}_0$, can likewise be expressed in the new coordinate system. We find:

$$\langle \mathbf{m}, \mathbf{R} | \hat{H}_0 | \mathbf{m}', \mathbf{R}' \rangle = \begin{cases} 2\Delta + \eta \frac{t_\perp^2}{\Delta} & \text{if } \mathbf{m} = \mathbf{m}' \text{ and } \mathbf{R} = \mathbf{R}' \\ \frac{t_\perp^2}{2\Delta} + t_\perp^{BB} & \text{if } \mathbf{m} = \mathbf{m}' \text{ and } \mathbf{R}, \mathbf{R}' \text{ are 1n.n. in } \Lambda \\ \frac{t_\perp^2}{2\Delta} - t_\perp^{NN} & \text{if } \mathbf{m}, \mathbf{m}' \text{ are 1n.n. in } \Lambda_N \text{ and } \mathbf{R}' - \mathbf{R} = \mathbf{m}' - \mathbf{m} \\ 0 & \text{otherwise} \end{cases}$$

The resulting tight-binding problem for the excitonic hamiltonian $\hat{H}_X = \hat{H}_0 + \hat{U}$ is depicted in figure 3.2.

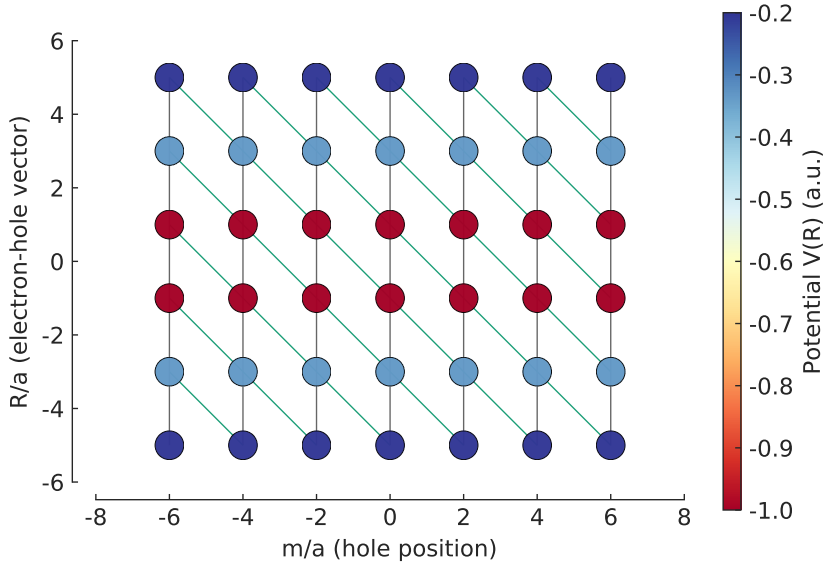

Figure 3.2: Effective tight-binding system associated to the hamiltonian $\hat{H}_X = \hat{H}_0 + \hat{U}$ in the basis of pairs, in the $(\mathbf{m}, \mathbf{R})$ representation (partial view: the lattice is infinite in both directions). Each site is associated to a $|\mathbf{m}, \mathbf{R}\rangle$ pair state, which acts as an effective orbital for it. Color depicts the direct electron-hole potential, which is diagonal within our approximations, and therefore acts as an onsite term (for clarity, the zero of energies has been set to $2\Delta + \eta \frac{t_\perp^2}{\Delta}$, the constant kinetic contribution to the onsite energies of all sites). Here a model potential of the form $V(R) \propto \frac{1}{R}$ is taken for illustration. Connecting lines represent the effective hoppings, with vertical grey segments corresponding to electron hoppings $T_e' = \frac{t_\perp^2}{2\Delta} + t_\perp^{BB}$ and oblique green segments corresponding to hole hoppings $T_h' = \frac{t_\perp^2}{2\Delta} - t_\perp^{NN}$.

This representation has the advantage of making the remaining periodicity of the system manifest. As can be seen in figure 3.2, the system remains

periodic in $\mathbf{m}$ *in the presence of the direct electron-hole interaction* $\hat{U}$. It can be seen that the lattice of excitations, Λ, constitutes a unit cell of the system. For a given $\mathbf{m}$, say $\mathbf{m} = \mathbf{0}$, each site $|\mathbf{m}, \mathbf{R}\rangle$ can be seen as a (unit cell) basis atomic orbital, in such a way that we can naturally construct, for each $\mathbf{R} \in \Lambda$, a tight-binding basis function:

$$|\mathbf{R}, \mathbf{Q}\rangle = \frac{1}{\sqrt{N}} \sum_{\mathbf{m} \in \Lambda_N} e^{-i\mathbf{Q}\cdot\mathbf{m}} |\mathbf{m}, \mathbf{R}\rangle$$

which we recognize as the elementary excitations introduced in the previous section, so that the wavevector $\mathbf{Q}$ that we have introduced has the interpretation of the state's center of mass momentum. The direct intrepretation of this state in terms of a tight-binding basis function, however, provides an immediate verification that $\mathbf{Q}$ is a good quantum number for $\hat{H}_X$ (similar arguments can be given to show that $\hat{H}_0$ and $\hat{U}$ also independently preserve $\mathbf{Q}$). We also obtain immediately that $\{|\mathbf{R}, \mathbf{Q}\rangle\}_{\mathbf{R},\mathbf{Q}}$ forms an orthonormal basis, since $\{|\mathbf{m}, \mathbf{R}\rangle\}_{\mathbf{m},\mathbf{R}}$ was one itself.

We can proceed further: as we have shown, $\hat{H}_X$ is block diagonal in $\mathbf{Q}$, and, leveraging the standard tight-binding formalism, these blocks are given by the associated integral transfer "matrices", which are in fact nothing but the $\hat{H}_X(\mathbf{Q})$ introduced in the previous section. Here, because Λ is infinite (but remains countable), so are these "matrices". For this reason, we present them as operators, the matrix elements of which can be computed in the usual way.[10] In other words, we have:

$$\hat{H}_X = \bigoplus_{\mathbf{Q}} \hat{H}_X(\mathbf{Q})$$

and the above procedure yields:

$$\langle \mathbf{R}, \mathbf{Q}|\hat{H}_X(\mathbf{Q})|\mathbf{R}', \mathbf{Q}\rangle = \begin{cases} 2\Delta + \eta\frac{t_\perp^2}{\Delta} + V(\mathbf{R}) & \text{if } \mathbf{R} = \mathbf{R}' \\ T_e' + T_h' e^{i\mathbf{Q}\cdot(\mathbf{R}'-\mathbf{R})} & \text{if } \mathbf{R}, \mathbf{R}' \text{ are 1n.n. in } \Lambda \\ 0 & \text{otherwise} \end{cases}$$

with the matrix elements of the full hamiltonian being then given by:

$$\langle \mathbf{R}, \mathbf{Q}|\hat{H}_X|\mathbf{R}', \mathbf{Q}'\rangle = \delta_{\mathbf{Q},\mathbf{Q}'} \langle \mathbf{R}, \mathbf{Q}|\hat{H}_X(\mathbf{Q})|\mathbf{R}', \mathbf{Q}\rangle$$

which, as expected, is the same result as the one found previously.

[10] For readers familiar with tight-binding calculations, they can be read directly from figure 3.2.

3.2.3 Discussion

Let us survey our situation. We have introduced a new basis, the basis of elementary excitations, $\{|\mathbf{R},\mathbf{Q}\rangle\}_{\mathbf{R},\mathbf{Q}}$, and rewritten the excitonic hamiltonian $\hat{H}_X$ in this new basis. We have shown that $\hat{H}_X$ does not couple elementary excitations of different center of mass momentum $\mathbf{Q}$, so that the resulting excitonic problem can be solved independently for each $\mathbf{Q}$, in analogy with the way the electronic problem can be solved independently for each value of the crystal momentum $\mathbf{k}$. For each value of $\mathbf{Q}$, we are reduced to studying a "transfer" hamiltonian, $\hat{H}_X(\mathbf{Q})$, in analogy with, say, the reduction of the electronic problem to the study of the integral transfer matrices in the tight-binding formalism.

These "transfer hamiltonians" can themselves be seen as tight-binding hamiltonians on the lattice of excitations Λ. In our case of the linear BN chain, for a given center of mass momentum $\mathbf{Q}$, the corresponding "transfer hamiltonian" is given by:

$$\hat{H}_X(\mathbf{Q}) = \sum_{\mathbf{R}\in\Lambda}\left(2\Delta + \eta\frac{t_\perp^2}{\Delta} + V(\mathbf{R})\right)|\mathbf{R},\mathbf{Q}\rangle\langle\mathbf{R},\mathbf{Q}| + \sum_{<\mathbf{R},\mathbf{R}'>} T_{\mathbf{R},\mathbf{R}'}(\mathbf{Q})\,|\mathbf{R},\mathbf{Q}\rangle\langle\mathbf{R}',\mathbf{Q}|$$

where $<\cdot,\cdot>$ denotes here summation over nearest neighbors (in Λ), and $T_{\mathbf{R},\mathbf{R}'}(\mathbf{Q}) = T'_e + T'_h e^{i\mathbf{Q}\cdot(\mathbf{R}'-\mathbf{R})}$ is the effective hopping between nearest neighbor excitations, which is complex in general. The associated tight-binding problem is depicted in figure 3.3. As we already pointed out, the reulsting equation are similar to the ones obtained by Wannier.[17] We also note a model of similar spirit obtained in [50] for single layer transition metal dichalcogenides.

Further breaking down this effective hamiltonian, we have seen that the kinetic hamiltonian $\hat{H}_0$ becomes a "standard" (periodic) tight-binding hamiltonian, describing the motion of a fictitious particle on the lattice Λ, while the direct electron-hole interaction $\hat{U}$ acts as a external potential, providing an $\mathbf{R}$ dependent contribution to the effective onsite energies that breaks the translation symmetry. In fact, the problem can be regarded as that of an impurity localized at the origin in the tight-binding lattice Λ.[16]

It is important to note that the potential, $V(\mathbf{R})$, which is in practice nothing but the real space screened electron-hole potential, is both attractive and decaying. This has an important computational consequence: to study $\hat{H}_X(\mathbf{Q})$ numerically, it is enough to include a finite number of elementary excitations $|\mathbf{R},\mathbf{Q}\rangle$, stopping after a certain cutoff R_{ctf} in electron hole

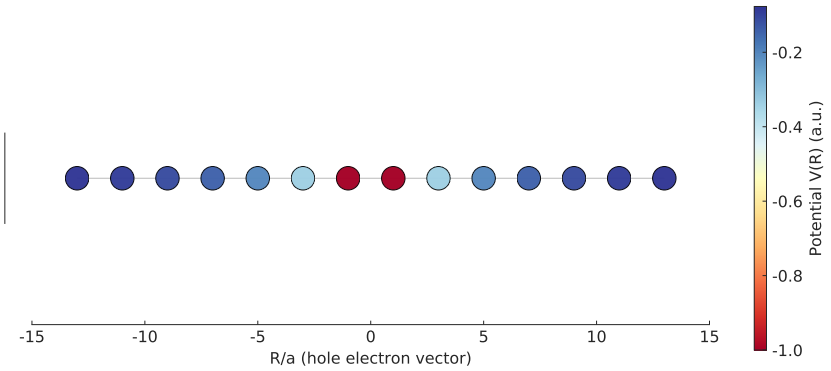

Figure 3.3: Effective tight-binding system associated to the "transfer" hamiltonian $\hat{H}_X(\mathbf{Q})$ in the basis of elementary excitations (partial view: the lattice is infinite). Each site of the lattice of excitations Λ is associated to a $|\mathbf{R}, \mathbf{Q}\rangle$ excitation state, which acts as an effective orbital for it. Color depicts the direct electron-hole potential, which is diagonal within our approximations, and therefore acts as an onsite term (for clarity, the zero of energies has been set to $2\Delta + \eta\frac{t_\perp^2}{\Delta}$, the constant kinetic contribution to the onsite energies of all sites). Here a model potential of the form $V(R) \propto \frac{1}{R}$ is taken for illustration. Connecting lines represent the effective hoppings $T_{\mathbf{R},\mathbf{R}'}(\mathbf{Q}) = T'_e + T'_h e^{i\mathbf{Q}\cdot(\mathbf{R}'-\mathbf{R})}$.

separation. This cutoff is then a numerical convergence parameter,[11] which should be much larger than the typical Bohr radius of the excitonic states under study. Since the Bohr radius of the states in a given excitonic series typically increases as one goes up in energy, studying higher energy states requires a higher cutoff.

Numerically, diagonalizing such a hamiltonian[12] can *a priori* be done with any computational tight-binding code (or even any diagonalization routine in the simplest cases). It should be noted that $\hat{H}_X(\mathbf{Q})$ is sparse, which is computationally advantageous. For this work, we have mainly used the *Hückel* code of Sylvain Latil, as well as the *pybinding* Python package.[52][13]

[11] Although it behaves differently, it is the analogue of the Brillouin zone sampling (finite number of "**k**-points") used in reciprocal space methods.

[12] More generally, since the problem is analogous to an impurity problem, exact diagonalization and Green's functions techniques are known to be very efficient. In this work, we will mostly use diagonalization techniques, but see e.g. [51] for the application of Green's function and recursion methods to the problem of computing one and two photon absorption in hBN with the same type of model hamiltonian.

[13] The *pybinding* package was also used to produce some of the figures of the effective tight-binding problems.

3.3 Excitonic properties

3.3.1 Model electron-hole potential

Before actually performing calculations, we require a model electron-hole potential, i.e. a functional form for $V(\mathbf{R})$. The simplest choice may be a screened Coulomb potential:

$$V(\mathbf{R}) = -\frac{e^2}{\epsilon R} \tag{3.4}$$

where $R = \|\mathbf{R}\|$ and ϵ would a a dielectric constant for the chain. However, such dielectric constants are only well defined for three-dimensional bulk systems: a peculiarity of the screened Coulomb potential in effective one and two-dimensional systems is that it does not take the simple form of equation 3.4, and thus no dielectric *constant* ϵ exists.[14] This has important consequences on the electron-hole interaction and the resulting excitons in one dimensional and layered (2D) materials. We will discuss these potentials and their consequences further when we come to the two-dimensional system hBN. For the time being, we simply give an overview of a common 1D model potential, which we shall use to proceed.

Let us thus consider one dimensional systems embedded in the physical three-dimensional space, such as atomic chains in vacuum. Among others, a possible model screened Coulomb potential for such systems is given by:[53, 54]

$$V(\mathbf{R}) = -\frac{e^2}{R + z_0} \tag{3.5}$$

where, again, $R = \|\mathbf{R}\|$ and $z_0 \geq 0$ can be thought of as a one-dimensional screening length:

$$V(\mathbf{R}) \approx \begin{cases} -\frac{e^2}{z_0}\left(1 - \frac{R}{z_0}\right) & \text{when } R \ll z_0 \\ -\frac{e^2}{R} & \text{when } R \gg z_0 \end{cases}$$

When $R \gg z_0$, the (3D) space between the electron an the hole is mostly free, so the screening from the one-dimensional system is negligible, and the effective potential $V(\mathbf{R})$, becomes an unscreened Coulomb potential. In contrast, when $R \ll z_0$, we find that the potential is affine in R. This may be pictured as follows: when $R \ll z_0$, the electron-hole distance is very small, and the electron-hole interaction can be thought of as "contained" within the one-dimensional chain, and therefore approximated by a "true" 1D system

[14] Although one can formally define a space dependent dielectric screening $\epsilon(\mathbf{R})$.

(by which we mean not embedded in the physical 3D space), in which the Coulomb potential of an unscreened point charge is known to be linear in R.[15][55]

Often, when this effective potential is used, the screening length z_0 is taken as a fitting parameter, and adjusted to reproduce the experimental results.[54]

3.3.2 Optical activity

Momentum and oscillator strength

Since our ultimate goal is to obtain the optical properties of the system, we would benefit from a convenient expression for the absorption spectra of a system whose excitonic eigenstates are described in the basis of elementary excitations. The relevant matrix elements are that of the (many body) momentum operator $\hat{\mathbf{p}}$: the strength of an optical transition from the ground state $|\emptyset\rangle$ to the excitonic state $|\Psi\rangle = \sum_{\mathbf{R}\in\Lambda} \Psi_{\mathbf{R},\mathbf{Q}} |\mathbf{R},\mathbf{Q}\rangle$ of center of mass momentum $\mathbf{Q}$ is governed by the matrix elements $\langle\emptyset|\hat{\mathbf{p}}|\Psi\rangle$, which we now shall endeavor to evaluate.

To this end, we shall briefly employ the formalism of second quantization. For every basis atomic orbital $|\mu,\mathbf{n}\rangle$ ($\mu \in \{B,N\}$), let $\hat{a}_{\mu,\mathbf{n}}$ denote the corresponding annihilation operator. The momentum operator then reads:

$$\hat{\mathbf{p}} = \sum_{\substack{\mu,\mathbf{n}\\ \mu',\mathbf{n}'}} \langle\mu,\mathbf{n}|\hat{\mathbf{p}}|\mu',\mathbf{n}'\rangle\, \hat{a}^\dagger_{\mu,\mathbf{n}}\hat{a}_{\mu',\mathbf{n}'}$$

Depending on the indices μ,μ', the operators $\hat{a}^\dagger_{\mu,\mathbf{n}}\hat{a}_{\mu',\mathbf{n}'}$ come in four types. Most importantly for us, the operator $\hat{a}^\dagger_{B,\mathbf{n}}\hat{a}_{N,\mathbf{m}}$ can be recognized as the operator that destroys an electron at $\mathbf{m}$, i.e. creates a hole there, and creates an electron at $\mathbf{n}$. In other words, it is the creation operator for the localized electron-hole pair $|\mathbf{m},\mathbf{n}\rangle$: $\hat{a}^\dagger_{B,\mathbf{n}}\hat{a}_{N,\mathbf{m}}|\emptyset\rangle = |\mathbf{m},\mathbf{n}\rangle$. We will now show that terms of this form are the only ones which contribute to $\hat{\mathbf{p}}|\emptyset\rangle$. We first note that their hermitian conjugates are the associated annihilation operators, which therefore return 0 when acting on the ground state (which has no excited pair to destroy). It then remains to discuss operators where $\mu = \mu'$. Operators of the form $\hat{a}^\dagger_{B,\mathbf{n}}\hat{a}_{B,\mathbf{n}'}$ also annihilate the ground state (since it

[15] This peculiar feature of "true" 1D systems can be seen by considering a point charge e in a 1D world, i.e. on the real line, at position $z = 0$. If we impose Gauss' law in this 1D world, then we may construct a 1D Gaussian surface, i.e. two points, which encloses the charge, at, say, $z = \pm r$. Then, Gauss' law yields for the electric field $E(r) + E(-r) = e$, whence by symmetry, $E(r) = e/2$ is a constant. The electric potential, whose derivative is the field, must therefore be affine (or, equivalently, linear up to a global energy shift).

has no excited electron to destroy). Finally, operators of the form $\hat{a}^{\dagger}_{N,\mathbf{n}}\hat{a}_{N,\mathbf{n}'}$ annihilate the ground state when $\mathbf{n} \neq \mathbf{n'}$ (by trying to create an electron in states which are already occupied), and when $\mathbf{n} = \mathbf{n'}$ the diagonal matrix elements $\langle \mu, \mathbf{n}|\hat{\mathbf{p}}|\mu, \mathbf{n}\rangle$ are zero, so these terms vanish as well.

Putting now everything together, recalling the expression of the momentum matrix elements in the basis of localized atomic orbitals, leveraging the translational symmetry of the system and recalling the definition of the elementary excitation states, we find:

$$\hat{\mathbf{p}}\,|\emptyset\rangle = -\sqrt{N}\frac{m_e}{i\hbar}\sum_{\mathbf{R}\in\Lambda} t_{\mathbf{R}}\mathbf{R}\,|\mathbf{R},\mathbf{0}\rangle$$

where $t_{\mathbf{R}} = \langle N, \mathbf{n}^0_N|\hat{H}^{(el)}_0|B, \mathbf{n}^0_N + \mathbf{R}\rangle$, the *electronic* hopping element from a nitrogen orbital to a boron orbital at $\mathbf{R}$ away. From there, $\langle\emptyset|\hat{\mathbf{p}}|\Psi\rangle$ can be obtained by scalar product:

$$\langle\emptyset|\hat{\mathbf{p}}|\Psi\rangle = -\frac{m_e\sqrt{N}}{i\hbar}\sum_{\mathbf{R}\in\Lambda} t_{\mathbf{R}}\Psi_{\mathbf{R},\mathbf{0}}\mathbf{R} \tag{3.6}$$

This formula is general, in the sense that it does not depend on our particular choices of hopping structure (number of nearest neighbors taken into account, etc.), nor on the specific geometry of the chain (it also holds for hBN).

Let us discuss this result. First, we note that only states with components at $\mathbf{Q} = 0$ can couple with light: we recover the usual result that only direct excitons contribute to absorption. This is not surprising, since already in the electronic case, we saw that the momentum operator only coupled valence and conduction states of the same wavevectors (of which $\mathbf{Q}$ is the difference), i.e. that only direct excitons could be excited optically (and a direct exciton is just that: an excitonic state made of direct transitions).

More specifically to our model, we note that, as electronic hoppings, the $t_{\mathbf{R}}$ are expected to decrease sharply with $R = \|\mathbf{R}\|$, so that only the components $\Psi_{\mathbf{R},\mathbf{0}}$ of short $\mathbf{R}$ contribute to the optical activity. In fact, in our description of the chain, only excitations corresponding to the nitrogen-boron nearest neighbor vectors $\boldsymbol{\tau} = \pm a\mathbf{e}_x$ contribute to the optical matrix elements. This result is the tight-binding analogue of the usual Elliott theory result that the oscillator strength of an exciton described in the hydrogenoid / Wannier model is proportional to the intensity of its envelope function at the origin:[56, 16] here, this oscillator strength is controlled by the probability amplitudes $\Psi_{\mathbf{R},\mathbf{0}}$ associated to the "local" electron-hole excitations.

Selection rules

When it comes to optical activity, the first question we may have about a state, is whether it is bright or dark, i.e. whether the associated excitonic transition is allowed or forbidden (respectively). In other words, we call dark a state which does not generate any signal in absorption, and bright a state which does, however faintly. In mathematical terms, the question is of knowing whether, for a given state $|\Psi\rangle$, $\langle\emptyset|\hat{\mathbf{p}}|\Psi\rangle = 0$ ($|\Psi\rangle$ is dark) or not ($|\Psi\rangle$ is bright). Often, symmetry considerations may already provide an answer to this question.

As an example, let us consider our linear BN chain. This one-dimensional system exhibits inversion symmetry, i.e. the system is left invariant under the transformation $\mathbf{r} \to -\mathbf{r}$. So is the excitonic hamiltonian at $\mathbf{Q} = 0$.[16] Barring accidental degeneracies, this entails that direct states are nondegenerate, and must be either odd or even with respect to the origin. In other words, if $|\Psi\rangle = \sum_{\mathbf{R}\in\Lambda} \Psi_{\mathbf{R}} |\mathbf{R}, \mathbf{0}\rangle$, then we must have either:

$$\forall\ \mathbf{R} \in \Lambda, \quad \Psi_{\mathbf{R}} = \Psi_{\mathbf{R}}$$

in which case $|\Psi\rangle$ is even, or:

$$\forall\ \mathbf{R} \in \Lambda, \quad \Psi_{\mathbf{R}} = -\Psi_{\mathbf{R}}$$

in which case $|\Psi\rangle$ is odd.

A well know result for the optical response of systems with inversion symmetry is that only odd states can be bright: states which are even cannot couple with light.[57] This can be formally checked by considering the parity operator, $\hat{I}$,[17] which implements inversion at the wavevector level. Its eigenfunctions are the even and the odd states, with eigenvalues 1 and -1 respectively. For any state $|\Phi\rangle$ of definite parity $s_\Phi = \pm 1$ under inversion, we have:

$$\langle\emptyset|\hat{\mathbf{p}}|\Phi\rangle = \underbrace{\langle\emptyset|\,\hat{I}^\dagger}_{=\langle\emptyset|}\ \underbrace{\hat{I}\hat{\mathbf{p}}\hat{I}^\dagger}_{=-\hat{\mathbf{p}}}\ \underbrace{\hat{I}\,|\Phi\rangle}_{=s_\Phi|\Phi\rangle} = -s_\Phi\,\langle\emptyset|\hat{\mathbf{p}}|\Phi\rangle$$

where we have used the fact that $\hat{I}$, as a symmetry operator, is unitary, that the ground state $|\emptyset\rangle$ is even under inversion, and that $\hat{\mathbf{p}}$ is odd under

[16] As long as the potential $V(\mathbf{R})$ is even, but this is physically mandated by the symmetries of the system.

[17] Some authors use the symbol $\hat{P}$, but we use here $\hat{I}$ for *inversion*, which is the more common group theoretical name and symbol, and to avoid a collision of notations with the momentum operator.

inversion.[18] We thus see that, if $|\Phi\rangle$ is even ($s_\Phi = 1$), $\langle\emptyset|\hat{\mathbf{p}}|\Phi\rangle = -\langle\emptyset|\hat{\mathbf{p}}|\Phi\rangle = 0$, and therefore $|\Phi\rangle$ is dark. This result is general, and does not directly depend on our specific model of the system, which is precious.

Such a result constitutes a *selection rule*: the symmetries of the system dictate which optical transitions are disallowed. Of course, this does not mean that a transition which is allowed by the selection rules (by which we mean that no selection rule *disallows* it) actually has $\langle\emptyset|\hat{\mathbf{p}}|\Phi\rangle \neq 0$, but this is often the case.

In particular, we must note the importance of the polarization of incoming light. If we denote the associated polarization vector by $\mathbf{e}$, then the optical activity of an excitonic eigenstate $|\Psi\rangle$ is controlled by $\mathbf{e} \cdot \langle\emptyset|\hat{\mathbf{p}}|\Phi\rangle$, so that having $\langle\emptyset|\hat{\mathbf{p}}|\Phi\rangle \neq 0$ is not enough to actually absorb light: it is also required that $\langle\emptyset|\hat{\mathbf{p}}|\Phi\rangle$ is not perpendicular to the polarization.

While it is often tremendously helpful to know which excitons are dark, this kind of symmetry analysis only tells us whether the oscillator strength of a particular excitonic transition is zero. For excitons which actually *do* contribute to the absorption, it does not yield information on the actual intensity of the transition. This is the object of the next section.

Wavefunction dipole

Since only direct states may be bright in absorption, let us consider a direct excitonic (eigen)state $|\Psi\rangle = \sum_{\mathbf{R}\in\Lambda} \Psi_{\mathbf{R}} |\mathbf{R}, \mathbf{0}\rangle$,[19]. Equation 3.6 behooves us to discuss the quantity:

$$\mathbf{d}_\Psi = \sum_{\mathbf{R}\in\Lambda} t_{\mathbf{R}} \Psi_{\mathbf{R}} \mathbf{R} \tag{3.7}$$

as $\langle\emptyset|\hat{\mathbf{p}}|\Psi\rangle \propto \mathbf{d}_\Psi$ with a proportionality constant that does not depend on $|\Psi\rangle$. $\mathbf{d}_\Psi$ therefore controls the optical activity of the state $|\Psi\rangle$, in the sense that, if incoming light of polarization vector $\mathbf{e}$ is shined at the system, the oscillator strength associated to the transition from the ground state $|\emptyset\rangle$ to $|\Psi\rangle$ verifies:

$$f_\Psi \propto |\mathbf{e} \cdot \mathbf{d}_\Psi|^2$$

We shall call $\mathbf{d}_\Psi$ the *wavefunction dipole*, or, for short, the dipole of the state $|\Psi\rangle$. Equation 3.7 shows its analogy with an electric dipole moment, with the quantities $t_{\mathbf{R}}\Psi_{\mathbf{R}}$ (which have the dimension of energies) taking the role the electric charges. We note that, while, in general, the $\Psi_{\mathbf{R}}$ may be complex,

[18] Intuition for this fact can be found by thinking of the momentum operator as a *first order* space derivative, and seeing that, upon reversal of the space coordinates, say $x' = -x$, we have $\frac{\partial}{\partial x'} = -\frac{\partial}{\partial x}$.

[19] We have dropped the $\mathbf{Q}$ index to lighten notations, with the understanding that we are considering only direct states, i.e. $\mathbf{Q} = \mathbf{0}$, as indirect states are dark in absorption.

the excitonic hamiltonian at $\mathbf{Q} = \mathbf{0}$ is real, so it does admit a basis of real eigenvectors.

In the specific geometry of the linear chain, with our choice of hopping structure, the wavefunction dipole is simply given by:

$$\mathbf{d}_\Psi = at_\perp(\Psi_{\mathbf{a}} - \Psi_{-\mathbf{a}})\mathbf{e}_x$$

so that for a state of definite parity under inversion $s_\Psi = \pm 1$:

$$\mathbf{d}_\Psi = at_\perp \Psi_{\mathbf{a}}(1 - s_\Psi)\mathbf{e}_x$$

we thus immediately recover the selection rules obtained previously: even states ($s_\Psi = 1$) are dark. In addition, the selection rules related to the polarization are immediately apparent, since the direction of $\mathbf{d}_\Psi$ is directly available.

The projection of $\mathbf{d}_\Psi$ on $\mathbf{e}$ also provides us directly (up to multiplicative factors) with the oscillator strength associated to $|\Psi\rangle$. Within our specific model of the chain, the intensity of bright states is proportional to $|\Psi_{\mathbf{a}}|^2$, or, more physically, to the intensity of the excitonic wavefunction corresponding to excitations where the hole and electron are nearest neighbors, as discussed earlier.

3.3.3 Excitonic states and dispersion

As announced previously, our goal in this chapter is not to produce a detailed study of the BN linear chain as a physical system, but rather to discuss it as a toy model through which the excitonic tight binding model can be displayed, and also as a point of comparison with two dimensional hBN. In this spirit, we will therefore briefly discuss the excitonic states of the model chain and their dispersion, but in order to avoid repeating ourselves, we postpone more detailed study of these phenomena to our study of hBN.

Numerical diagonalization

For illustration, let us start by diagonalizing $\hat{H}_X$ numerically. This is done, as usual, by diagonalizing $\hat{H}_X(\mathbf{Q})$ for all (in fact, a sufficiently dense grid of) values of $\mathbf{Q}$. While our model is not expected to remain precise at high energies, we nevertheless compute and show all states to provide a more complete qualitative overview. Using sample parameters, the resulting bands are shown in figure 3.4, while the densities of some of the lowest bound states are displayed in figure 3.5.

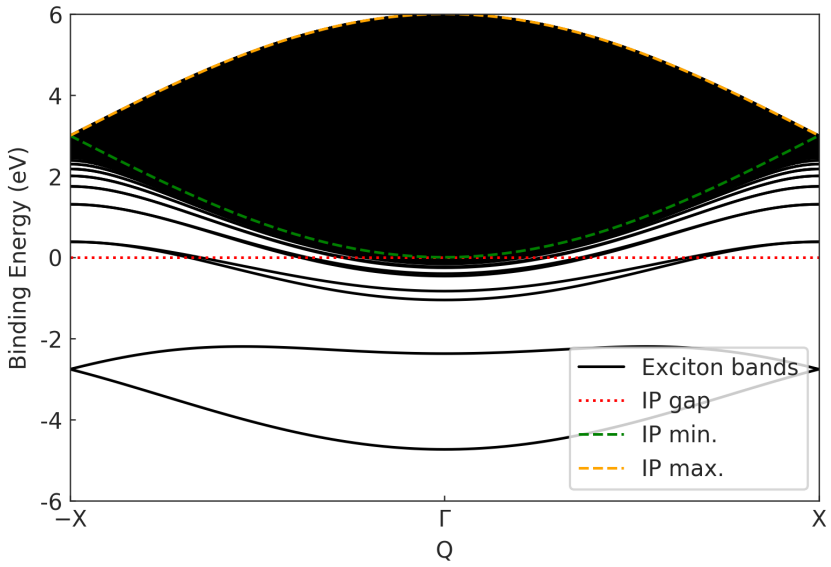

Figure 3.4: Example excitonic band structure for the BN linear chain (solid black lines), obtained by diagonalization of $\hat{H}_X(\mathbf{Q})$ on a grid of 101 $\mathbf{Q}$-points. Parameters used were $a = 1.5$ Å (C-C distance in the linear carbon chain), $T'_e = T'_h = 0.75$ eV (fitted hBN values for a first-nearest neighbor model), $V(R) = -\frac{e^2}{|R|+z_0}$, with 1D screening length $z_0 = 1$ Å (arbitrary value). To obtain the higher energy bands, a chain of 1500 $\mathbf{R}$-sites was used, with periodic boundary conditions. The electronic gap, 2Δ (red dotted line) was taken as the zero of the energy scale, so that we report binding energies. The green (resp. orange) dashed solid lines describe the transition energy envelope, i.e. the minimal (resp. maximal) independent particles transition energies $E_0(\mathbf{k}, \mathbf{Q}) = E_c(\mathbf{k} + \mathbf{Q}) - E_v(\mathbf{k})$ for each value of $\mathbf{Q}$.

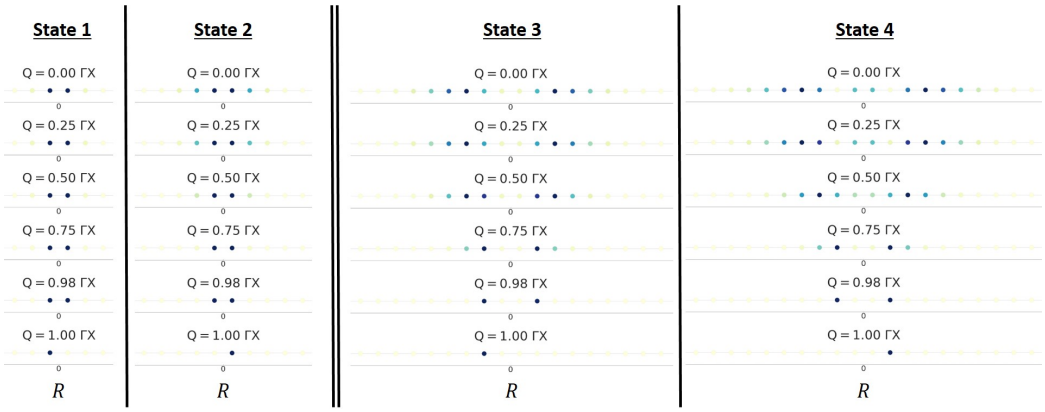

Figure 3.5: Evolution of the intensities (the $|\Psi_{\mathbf{R},\mathbf{Q}}|^2$) of the first four excitonic eigenstates as $\mathbf{Q}$ changes from $\mathbf{\Gamma}$ to $\mathbf{X}$, represented on Λ. Intensities are normalized separately for each state and each $\mathbf{Q}$ so that dark blue corresponds to the maximal intensity and white corresponds to an intensity of zero. The parameters are the same as in figure 3.4. Note that, at $\mathbf{Q} = \mathbf{X}$, states $(1, 2)$ and $(3, 4)$ form two pairs of degenerate states. It can be seen that, when $\mathbf{Q}$ approaches $\mathbf{X}$, the states "localize" on excitation sites of a single given $|R|$. This is due to the fact that hoppings between excitation sites vanish at $\mathbf{X}$ with a first nearest neighbors parametrization.

Let us first comment on figure 3.4: it depicts an example model excitonic band structure of the BN linear chain.[20] There, we have specifically taken a very large computation cell (i.e. included excitations of very large $|R|$ in order to also capture an approximation of states with positive binding energy $E_b = E - E_{gap} > 0$. More precisely, we have represented in figure 3.4, as a dashed green line, the minimal (single particle) transition energy $E_{min}(\mathbf{Q}) = \min_{\mathbf{k}}(E_c(\mathbf{k} + \mathbf{Q}) - E_v(\mathbf{k}))$ for each value of $\mathbf{Q}$. It corresponds to the lowest eigenenergy of the kinetic hamiltonian $\hat{H}_0$ at a given $\mathbf{Q}$: without electron-hole interaction, no state is expected below this limit. Here, of course, we do see such states: they are "bound" excitons, and appear as discrete bound states. Above this limit, we apear to have a continuum of states.[21] The energies of the excitonic bands is effectively bounded by the maximal transition energy at each $\mathbf{Q}$ (orange dashed line in figure 3.4), but this is a feature of the

[20] Periodic boundary conditions are usually not necessary, especially when studying bound excitons, which is what we usually do. Likewise, we usually do not require that many $\mathbf{R}$-points for the study of low-lying bound excitons.

[21] In the computation of figure 3.4, we have used a finite (but large) number of excitation sites, so we can only expect as many bands. The "solid" black region is therefore made of a dense concentration of bands.

model, which contain only π-bands. In "reality", other orbitals can give rise to higher energy states. In fact, the simple approximations of the excitonic tight-binding model typically start to fail when describing high energy states; we compute them here only for illustration purposes.

An interesting phenomenon shown in figure 3.4 deserves mention: at $\mathbf{X}$, all bands appear to become twice degenerate. This can be undestood through the hopping structure of $\hat{H}_X$. Indeed, the only coupling between excitation sites are the effective first nearest neighbor hoppings between them, which, within the first nearest neighbor approximation, is given by $T_{\mathbf{R},\mathbf{R}'}(\mathbf{Q}) = T'\Big(1 + e^{i\mathbf{Q}\cdot(\mathbf{R}'-\mathbf{R})}\Big)$. Note now that, for $\mathbf{R}, \mathbf{R}'$ first nearest neighbors in Λ, we always have $\mathbf{R}' - \mathbf{R} = \pm 2a\mathbf{e}_x$, so that at the excitonic $\mathbf{X}$ point, i.e. at $\mathbf{Q} = \frac{\pi}{2a}\mathbf{e}_x$, $T_{\mathbf{R},\mathbf{R}'}(\mathbf{Q}) = 0$. In other words, at $\mathbf{X}$, the hoppings between basis sites effectively vanish.

As a result, at $\mathbf{X}$, the excitonic hamiltonian becomes:[22]

$$\hat{H}_X(\mathbf{X}) = (2\Delta + 4T')\mathbb{1}_{\mathbf{X}} + \hat{U}_{\mathbf{X}}$$

which is diagonal in the $\{|\mathbf{R}, \mathbf{X}\rangle\}_{\mathbf{R}\in\Lambda}$ basis. More precisely, assuming the potential is symmetric and U_R is injective on $\{\mathbf{R} \in \Lambda \ / \ \mathbf{R}\cdot\mathbf{e}_x > 0\}$, its eigenvalues and eigensubspaces are given by:

$$\begin{aligned} E_z &= 2\Delta + 4T' + U_z \\ \mathcal{E}_{E_z} &= \mathrm{Span}\Big(\,|-\mathbf{z}, X\rangle\,, |\mathbf{z}, X\rangle\,\Big) \end{aligned}$$

for all $\mathbf{z} \in \Lambda$ with $\mathbf{z}\cdot\mathbf{e}_x > 0$.

This has interesting consequences: when following an excitonic band from $\mathbf{\Gamma}$ to $\mathbf{X}$, the corresponding state will tend to localize as $\mathbf{Q}$ nears $\mathbf{X}$, as can be seen in figure 3.5. The effect is particularly striking when considering states which are rather extended at $\mathbf{\Gamma}$. It also shows that, at $\mathbf{X}$, the excitonic bands become pairwise degenerate. The existence of a $\mathbf{Q}$ point where *all* kinetic nearest neighbour hoppings vanish appears to be a peculiarity of the chain: this does not happen in single layer hBN. However, the phenomenon *does* have a 2D analogue in the single layer: there, at the excitonic point $\mathbf{M}$, the excitonic hoppings in two out of three directions can be suppressed at once, turning the system into a set of uncoupled linear chains. This is discussed in section 4.5.3.

We should note, however, that this vanishing of the effective hoppings at $\mathbf{X}$ in the chain hinges on the precise compensation of the T'_h and T'_e. If this electron-hole symmetry is broken, for example by the addition of second

[22]Here, the symbols $\mathbb{1}_{\mathbf{X}}$ and $\hat{U}_{\mathbf{X}}$ stand for the restriction of the corresponding operators on the subspace corresponding to the wavevector $\mathbf{Q} = \mathbf{X}$.

nearest neighbors, an effective hopping will remain (of $t_\perp^{NN}+t_\perp^{BB}$ in the case of second nearest neighbors). Exchange interaction may also provide additional couplings. Further, in the case of a "real" chain transitions to (or from) non π bands may occur at $\mathbf{X}$ (see e.g. [49] for an *ab initio* computation of the BN chain band structure).

Strong potential approximation

In order to obtain analytical approximations in such tight-binding excitonic problems, a useful tool is to go to the "strong potential limit". We will develop this idea further in section 4.4.2, and so only provide the general idea now. If the direct interaction $\hat{U}$ is taken to be very strong, then in a first approximation, the two sites of lowest $|R|$ (corresponding to the excitations $|-\mathbf{a},\mathbf{Q}\rangle$ and $|+\mathbf{a},\mathbf{Q}\rangle$) effectively decouple from the rest of the excitonic lattice, and the excitonic hamiltonian reduces to:

$$H_X(\mathbf{Q}) = \begin{pmatrix} 2\Delta + 4T' + U_a & T'\left(1+e^{2i\mathbf{Q}\cdot\mathbf{a}}\right) \\ T'\left(1+e^{-2i\mathbf{Q}\cdot\mathbf{a}}\right) & 2\Delta + 4T' + U_a \end{pmatrix}$$

in the $\{|-\mathbf{a},\mathbf{Q}\rangle, |+\mathbf{a},\mathbf{Q}\rangle\}$ basis, where we have kept to first nearest neighbors for simplicity and thus wriiten $T' = T'_e = T'_h = \frac{t_\perp^2}{2\Delta} > 0$. The excitonic dispersion, in this limit, is then given by:

$$E_\pm(\mathbf{Q}) = 2\Delta + 4T' + U_a \pm 2T'\cos(\mathbf{Q}\cdot\mathbf{a})$$

When $\mathbf{Q} = \mathbf{X} + n\frac{\pi}{a}\mathbf{e}_x$ with $n \in \mathbb{Z}$, the two eigenstates are degenerate. Elsewhere, they are given up to a phase by:[23]

$$|\Psi_\pm(\mathbf{Q})\rangle = \frac{1}{\sqrt{2}}\left(e^{i\frac{\mathbf{Q}\cdot\mathbf{a}}{2}}|-\mathbf{a},\mathbf{Q}\rangle \pm e^{-i\frac{\mathbf{Q}\cdot\mathbf{a}}{2}}|+\mathbf{a},\mathbf{Q}\rangle\right)$$

At excitonic $\mathbf{\Gamma}$ ($\mathbf{Q}=\mathbf{0}$), we thus have a bonding and antibonding pair, the lowest bound of which is odd, while the other is even relative to the 1D inversion about $\mathbf{R}=\mathbf{0}$. The lowest bound state is therefore expected to be bright, while the following one should be dark.

This approximate dispersion is plotted on figure 3.6. While the lowest excitonic band is qualitatively reproduced, the upper one, associated to $|\Psi_+\rangle$, presents a qualitatively wrong dispersion at $\mathbf{\Gamma}$, where the curvature of the band is inverted (although the full state is indeed even, as expected). In a

[23] Note that, in this presentation, the band corresponding to $\pm = -$ is not always the lowest band outside of the first Brillouin zone.

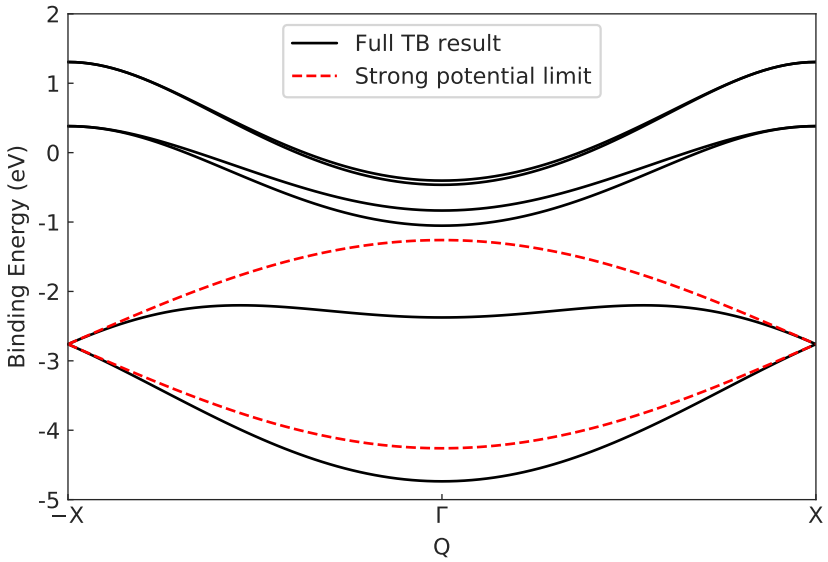

Figure 3.6: Example dispersion for the lowest bound states in the linear BN chain. Parameters are the same as figure 3.4, but only the six lowest bound states are depicted, and only 100 excitation sites were used. Solid black lines correspond to the full tight-binding result, and are virtually identical to the corresponding bands of figure 3.4. Dashed red lines correspond to the strong potential approximation for the two lowest bound states.

sense, this is to be expected, since figure 3.5 shows that this state has non-negligible intensity on excitations other than $|-\mathbf{a}, \mathbf{Q}\rangle$ and $|+\mathbf{a}, \mathbf{Q}\rangle$. Higher energy states, in general, tend to be more extended, so that the strong potential approximation is mostly useful for the lowest bound states. Strikingly, however, the approximation appears very good for both bands in the neighborhood of the excitonic $\mathbf{X}$ point: this is due to the fact that, at $\mathbf{X}$, hoppings between excitation sites vanish, and so the two excitation sites of lowest $|R|$ *do* decouple from the rest of the lattice, making the strong potential limit exact.

Chapter 4

Excitonic tight binding in single layer hBN

We now come to single layer hBN.

4.1 Introduction

The contents of this chapter are mostly derived from [47], as well as [48] for the discussion of excitons dispersion.

4.2 Electronic structure and relevant lattices

We start this section with good news: almost everything we have done to establish the electronic and excitonic hamiltonians in the case of the linear BN chain can be directly applied to the case of single-layer hBN up to a change in geometry and the corresponding substitutions. The key similarity between the two systems is the fact that both systems have only one "hole" (Nitrogen) orbital and one "electron" (Boron) orbital in their unit cell.

4.2.1 Lattices and notations

We consider a freestanding sheet of single layer hexagonal Boron Nitride (hBN). Its unit cell contains two atoms: one Nitrogen atom and one Boron atom. We call τ the nearest neighbor $B-N$ distance. Apart from the replacement of carbon atoms by boron and nitrogen, our system is therefore identical to graphene from the point of view of its lattice. See e.g. [39] for an introductory presentation of the geometry and tight-binding description of graphene.

Let us denote by $\mathbf{e}_x$ and $\mathbf{e}_y$ two cartesian unit vectors in-plane. The underlying Bravais lattice of the system is triangular, and given by $\mathcal{R} = \{n\mathbf{a}_1 + m\mathbf{a}_2 \ / \ n, m \in \mathbb{Z}\}$, where the direct lattice vectors are conventionally given as:

$$\mathbf{a}_1 = a\cos(\pi/3)\mathbf{e}_x + a\sin(\pi/3)\mathbf{e}_y$$
$$\mathbf{a}_2 = a\cos(\pi/3)\mathbf{e}_x - a\sin(\pi/3)\mathbf{e}_y$$

where $a = \sqrt{3}\tau$ is the lattice parameter. Again, we denote by $\mathbf{n}_\mu^0$ the position of the unit cell atoms,[1] where μ runs over the atomic types ($\mu = B$ or N):

$$\mathbf{n}_B^0 = \frac{2}{3}\mathbf{a}_1 + \frac{1}{3}\mathbf{a}_2$$
$$\mathbf{n}_N^0 = \frac{1}{3}\mathbf{a}_1 + \frac{2}{3}\mathbf{a}_2$$

and we introduce the sublattices Λ_μ as:

$$\Lambda_\mu = \mathbf{n}_\mu^0 + \mathcal{R}$$

so that the sites in Λ_μ are exactly those which are translationnally equivalent to the unit cell site $\mathbf{n}_\mu^0$, and the set of sites of the full crystal lattice is given by $\cup_\mu \Lambda_\mu$. This lattice structure is depicted in figure 4.1.

The associated reciprocal lattice is also triangular, and is given by $\mathcal{G} = \{u\mathbf{b}_1 + v\mathbf{b}_2 \ / \ u, v \in \mathbb{Z}\}$, where:

$$\mathbf{b}_1 = b\cos(\pi/6)\mathbf{e}_x + b\sin(\pi/6)\mathbf{e}_y$$
$$\mathbf{b}_2 = b\cos(\pi/6)\mathbf{e}_x - b\sin(\pi/6)\mathbf{e}_y$$

with where $b = \|\mathbf{b}_1\| = \|\mathbf{b}_2\| = \frac{4\pi}{\sqrt{3}a}$ are the reciprocal lattice basis vectors. This reciprocal lattice is represented in figure 4.2. The two basis vectors, $\mathbf{b}_1$ and $\mathbf{b}_2$, subtend a parallelogram $\mathcal{U}_\mathcal{G}$ that is a possible choice of primitive unit cell for reciprocal space. Here, we prefer working with the first Brillouin zone, which is an hexagon obtained from the Wigner-Seitz construction, and depicted in figure 4.3. The advantage of this representation is that it is geometrically invariant under the symmetries of the system, and it is therefore more convenient to use when discussing wavefunction symmetries.

[1] Occasionally, we will write $\mathbf{m}_N^0$ for the position of the unit cell Nitrogen site, for consistency with our practice of using the letter $\mathbf{m}$ for the positions of hole type sites (i.e. Nitrogen sites) and $\mathbf{n}$ for electron type sites (i.e. Boron sites) when discussing excitonic problems. We keep the notation $\mathbf{n}_\mu^0$ to avoid having to repeat general definitions twice.

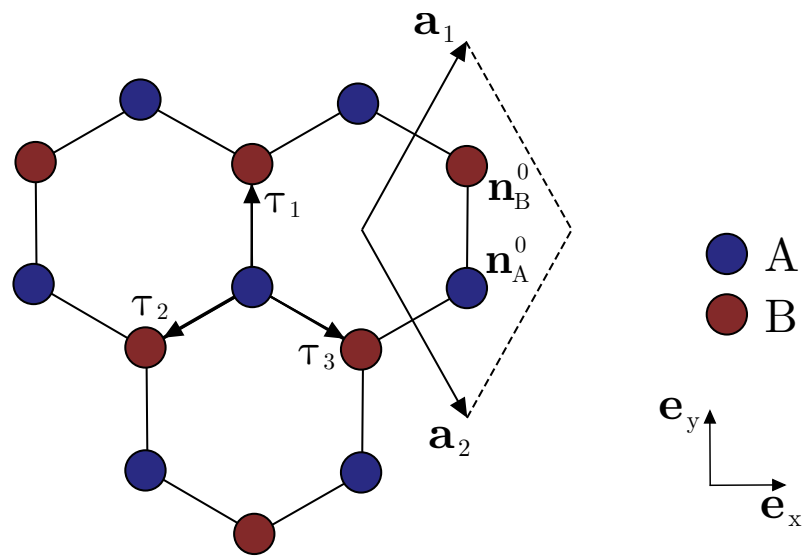

Figure 4.1: Direct lattice structure of single layer hBN: A sites are occupied by Nitrogen atoms while B sites are occupied by Boron atoms. The parallelogram subtended by the basis lattice vectors $\mathbf{a}_1$ and $\mathbf{a}_2$ is the real space unit cell. $\boldsymbol{\tau}_1$, $\boldsymbol{\tau}_2$ and $\boldsymbol{\tau}_3$ are the nearest neighbor Nitrogen-Boron vectors, which will play an imporant role in our tight-binding description of the system. The scale of the cartesian basis vectors $\mathbf{e}_x$ and $\mathbf{e}_y$ is arbitrary.

The conventional high symmetry points are given by:

$$\begin{aligned}\boldsymbol{\Gamma} &= \mathbf{0} \\ \mathbf{M} &= \frac{1}{2}\mathbf{b}_1 \\ \mathbf{K} &= \frac{1}{3}\mathbf{b}_1 + \frac{1}{3}\mathbf{b}_2\end{aligned}$$

and when representing quantities on a path in reciprocal space, we will use the path $\boldsymbol{\Gamma} \to \mathbf{M} \to \mathbf{K} \to \boldsymbol{\Gamma}$, as can be seen in figure 4.3. The so-called $\mathbf{K}$ points will be important later, and deserve a bit of our time now. There are six corners of the hexagonal first Brillouin zone, but not all of them are equivalent, because they are not all linked together by a reciprocal lattice vector. In fact, they come in two equivalence classes: the $\mathbf{K}$ and $\mathbf{K}'$ points. This can be more easily seen in the primitive cell $\mathcal{U}_{\mathcal{G}}$: it contains exactly one $\mathbf{K}$ and one $\mathbf{K}'$ point (figure 4.2). The situation is the same in the first Brillouin zone: the hexagon has six corners, which alternate between $\mathbf{K}$ and $\mathbf{K}'$ points as one rotates around the hexagon. There are thus three corners

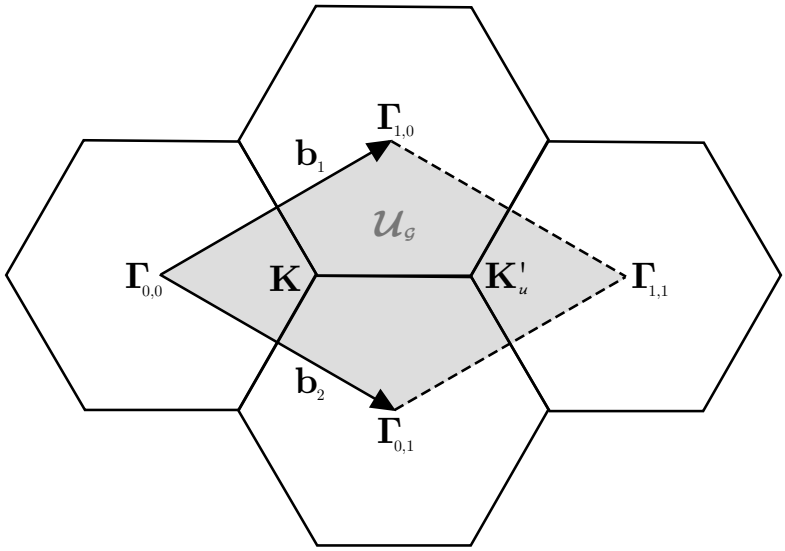

Figure 4.2: Reciprocal lattice structure of single layer hBN. The shaded region is the primitive unit cell $\mathcal{U}_\mathcal{G}$. The $\mathbf{\Gamma}_{u,v} = u\mathbf{b}_1 + v\mathbf{b}_2$ are the points of the reciprocal lattice $\mathcal{G}$; their surrounding hexagons are the corresponding Voronoi tessellation, so that the hexagon centered on $\mathbf{\Gamma}_{0,0}$ is the first Brillouin zone. The latter is depicted in more details in figure 4.3.

of each kind, and since each corner is shared between three hexagons, we recover the fact that our first Brillouin zone contains effectively one $\mathbf{K}$ and one $\mathbf{K}'$ point. It is immediately apparent, in the first Brillouin zone, that for each $\mathbf{K}$ point, the opposite point, $-\mathbf{K}$, is a $\mathbf{K}'$ point. These $(\mathbf{K}, \mathbf{K}')$ pairs are therefore images of one another by time reversal symmetry.

Let us finally specify the space of states of interest: we shall restrict ourselves to the p_z orbitals of Boron of Nitrogen, which are responsible for most of the low energy optical properties of the system, as the ones of carbon are in graphene.[39] We thus denote by $|B, \mathbf{n}\rangle$ and $|N, \mathbf{m}\rangle$ these localized boron and nitrogen p_z atomic orbitals, where $\mathbf{n} \in \Lambda_B$ and $\mathbf{m} \in \Lambda_N$ denote the atomic positions. From this basis of localized atomic orbitals, that we assume orthonormal, we define the associated tight-binding basis functions:

$$|\mu, \mathbf{k}\rangle = \frac{1}{\sqrt{N}} \sum_{\mathbf{n} \in \Lambda_\mu} e^{-\mathbf{k}\cdot\mathbf{n}} |\mu, \mathbf{n}\rangle$$

where N is the number of unit cells in the system and $\mathbf{k}$ is the wavevector.

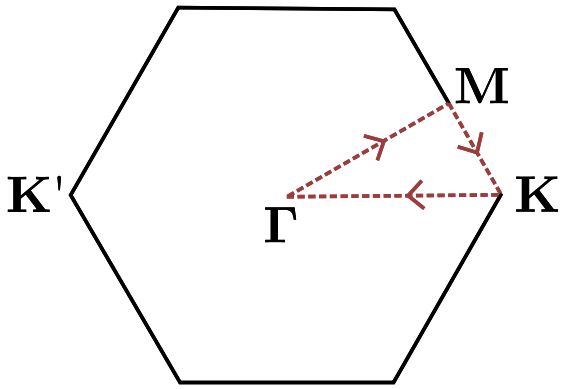

Figure 4.3: First Brillouin zone of single layer hBN and remarkable high-symmetry points. The $\mathbf{\Gamma}$ point corresponds to the origin of the reciprocal lattice ($\mathbf{\Gamma}_{0,0}$ in figure 4.2). The dashed path is the high symmetry path, which encloses the so-called irreducible wedge. Arrows on the path indicate the chosen orientation for the representation of reciprocal space quantities (band structures, etc.).

4.2.2 Electronic hamiltonian

We describe again the electronic structure of the system using a tight-binding hamiltonian $\hat{H}_0^{(el)}$ in second nearest neighbors, which, in the basis of localized atomic orbitals, is given by:

$$\langle B, \mathbf{n}|\hat{H}_0^{(el)}|B, \mathbf{n}'\rangle = \begin{cases} \Delta & \text{if } \mathbf{n} = \mathbf{n}' \\ t_\perp^{BB} & \text{if } \mathbf{n} \text{ and } \mathbf{n}' \text{ are 2n.n.} \\ 0 & \text{else} \end{cases}$$

$$\langle N, \mathbf{m}|\hat{H}_0^{(el)}|N, \mathbf{m}'\rangle = \begin{cases} -\Delta & \text{if } \mathbf{m} = \mathbf{m}' \\ t_\perp^{NN} & \text{if } \mathbf{m} \text{ and } \mathbf{m}' \text{ are 2n.n.} \\ 0 & \text{else} \end{cases}$$

$$\langle B, \mathbf{n}|\hat{H}_0^{(el)}|N, \mathbf{m}\rangle = \begin{cases} t_\perp & \text{if } \mathbf{n} \text{ and } \mathbf{m} \text{ are 1n.n.} \\ 0 & \text{else} \end{cases}$$

where Δ, $t_\perp$, $t_\perp^{NN}$ and $t_\perp^{BB}$ are the "kinetic" parameters. As claimed, this hamiltonian is exactly the same as the one for the chain, up to the change in underlying lattice. Note as well that it reduces to the familiar tight-binding hamiltonian for graphene[39] in the limit $\Delta \to 0$ and $t_\perp^{NN} = t_\perp^{BB}$. Moving to the basis of the tight-binding basis functions, we obtain the integral transfer

matrices (similar to the ones reported in [58] with a different tight-binding convention):

$$H(\mathbf{k}) = \begin{pmatrix} \Delta + t_\perp^{BB}\gamma_2(\mathbf{k}) & t_\perp\gamma_1(\mathbf{k}) \\ t_\perp\gamma_1(\mathbf{k})^* & -\Delta + t_\perp^{NN}\gamma_2(\mathbf{k}) \end{pmatrix}$$

in the basis $\{|B,\mathbf{k}\rangle, |N,\mathbf{k}\rangle\}$, with:

$$\gamma_1(\mathbf{k}) = \sum_{\boldsymbol{\tau}} e^{i\mathbf{k}\cdot\boldsymbol{\tau}}$$
$$\gamma_2(\mathbf{k}) = \sum_{\boldsymbol{\mu}} e^{i\mathbf{k}\cdot\boldsymbol{\mu}} = |\gamma_1(\mathbf{k})|^2 - 3$$

where the $\boldsymbol{\tau}$ are the in-plane first nearest neighbors nitrogen to boron vectors:[2]

$$\boldsymbol{\tau}_1 = \tau\mathbf{e}_y$$
$$\boldsymbol{\tau}_2 = \tau\left(-\frac{1}{2}\mathbf{e}_x - \frac{\sqrt{3}}{2}\mathbf{e}_y\right)$$
$$\boldsymbol{\tau}_3 = \tau\left(\frac{1}{2}\mathbf{e}_x - \frac{\sqrt{3}}{2}\mathbf{e}_y\right)$$

and the μ are the second nearest neighbor vectors, which are conveniently given by:

$$\boldsymbol{\mu}_{i,j} = \boldsymbol{\tau}_j - \boldsymbol{\tau}_i$$

for $i \neq j$. Here, γ_1 and γ_2 correspond respectively to the geometric terms for the first and second nearest neighbours,[3] and we see that we have obtained the same integral transfer matrices as in the linear chain case, up to the substitutions:

$$f_1 \to \gamma_1$$
$$f_2 \to \gamma_2$$

and the change of first Brillouin zone. Note, in passing, that γ_1 can take complex values, while its chain analogue, f_1, was fully real: this is because the set of nearest N-B neighbor vectors (the τs) in hBN is not invariant under inversion, whereas it is in the chain. *A contrario*, γ_2 takes real values because the sets of N-N and B-B nearest neighbor vectors (in both cases, the μs) *are* invariant under inversion.

[2]The labels are chosen such that $\boldsymbol{\tau}_1 = \tau\mathbf{e}_y$ and $\boldsymbol{\tau}_{\alpha+1} = C_3\boldsymbol{\tau}_\alpha$ where C_3 is the (in plane, anticlockwise) vector rotation of angle $2\pi/3$.

[3]Expectedly, they are exactly the same as their analogues in graphene, see [39].

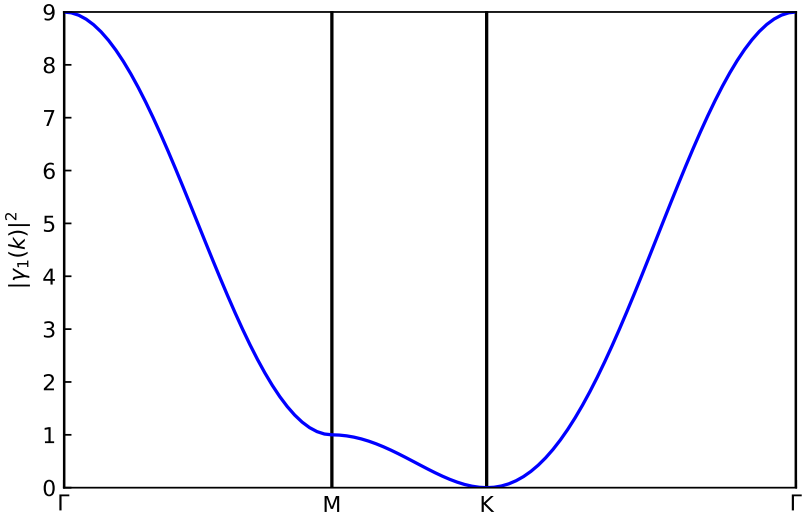

Figure 4.4: Plot of $|\gamma_1|^2$ (solid blue line). Values at the high-symmetry points are given in equation 4.1. Note how $|\gamma_1|$, which characterizes the coupling between the Boron and Nitrogen sublattices, remains small in the neighborhood of $\mathbf{K}$ (where, in particular, it vanishes).

In analogy with f_1, γ_1 describes, in reciprocal space, the coupling between the two sublattices (up to a factor of $t_\perp$). It is therefore useful to analyse its variations. Because it is complex, we study instead $|\gamma_1|^2$ which we represent in figure 4.4. Conveniently, this doubles as a study of $\gamma_2(\mathbf{k}) = |\gamma_1(\mathbf{k})|^2 - 3$. Its values at the high symmetry points are given by:

$$|\gamma_1(\mathbf{\Gamma})|^2 = 9 \quad ; \quad |\gamma_1(\mathbf{M})|^2 = 1 \quad ; \quad |\gamma_1(\mathbf{K})|^2 = 0 \tag{4.1}$$

so that the couplings between the the sublattices vanish at the $\mathbf{K}/\mathbf{K}'$ points, in analogy with the situation at $\mathbf{X}$ in the chain.

The band energies are obtained by diagonalization of $H(\mathbf{k})$:

$$E_\pm(\mathbf{k}) = \frac{t_\perp^{BB} + t_\perp^{NN}}{2}\gamma_2(\mathbf{k}) \pm \sqrt{\left(\Delta + \frac{t_\perp^{BB} - t_\perp^{NN}}{2}\gamma_2(\mathbf{k})\right)^2 + t_\perp^2 |\gamma_1(\mathbf{k})|^2} \tag{4.2}$$

where the plus sign corresponds to the conduction band and the minus sign to the valence band. The direct transition energies, in turn, are given by:

$$\delta E(\mathbf{k}) = E_+(\mathbf{k}) - E_-(\mathbf{k}) = 2\sqrt{\left(\Delta + \frac{t_\perp^{BB} - t_\perp^{NN}}{2}\gamma_2(\mathbf{k})\right)^2 + t_\perp^2 |\gamma_1(\mathbf{k})|^2} \tag{4.3}$$

and so we note that the direct transition energies (which are the quantities that will actually enter the Bethe-Salpeter equation at $\mathbf{Q} = \mathbf{0}$ with our approximations and essentially govern absorption on the kinetic side) only depend on $t_\perp^{BB} - t_\perp^{NN}$, and reduce to the first nearest neighbors ($t_\perp^{BB} = t_\perp^{NN} = 0$) expression if this difference vanishes. Since $t_\perp^{BB}$ and $t_\perp^{NN}$ are expected to be close anyway, this means that remaining at the level of first nearest neighbors will often be a good approximation as long as we are interested only in direct excitations:[4] in this chapter, we will thus often keep to this approximation as it favorably reduces the number of free parameters of the model at little cost in accuracy.

We note in particular that, within the first nearest neighbors approximation, the transition energy is bounded from below by 2Δ, and this bound is reached whenever $\gamma_1(\mathbf{k}) = 0$, i.e. exactly at the high symmetry $\mathbf{K}$ and $\mathbf{K}'$ points: we recover the known *ab initio* result that the system's gap is direct, and realized at the $\mathbf{K}$ and $\mathbf{K}'$ points.

Within the first nearest neighbors approximation, the band states are likewise given by:

$$\begin{aligned} |c,(\mathbf{k})\rangle &= \frac{1}{\mathcal{N}(\mathbf{k})}\Big[\,|B,\mathbf{k}\rangle + a(\mathbf{k})\,|N,\mathbf{k}\rangle\,\Big] \\ |v,(\mathbf{k})\rangle &= \frac{1}{\mathcal{N}(\mathbf{k})}\Big[-a(\mathbf{k})\,|B,\mathbf{k}\rangle + |N,\mathbf{k}\rangle\,\Big] \end{aligned} \tag{4.4}$$

where:

$$a(\mathbf{k}) = \frac{t\gamma_1(\mathbf{k})}{\Delta + \sqrt{\Delta^2 + t_\perp^2 |\gamma_1(\mathbf{k})|^2}}$$

and $\mathcal{N}$ is a normalization constant such that $|\mathcal{N}(\mathbf{k})|^2 = 1 + |a(\mathbf{k})|^2$. This is the chain result, with $f_1 \leftarrow \gamma_1$, and the same commentary applies. In particular, close to $\mathbf{K}$, where γ_1 vanishes, $a(\mathbf{k}) \approx \frac{t_\perp}{2\Delta}\gamma_1(\mathbf{k})$ and there the conduction (resp. valence) bands are expected to be well approximation by Boron (resp. Nitrogen) tight-binding basis functions to zeroth order.[5]

Again, we note that the band states depend on the second nearest neighbor hoppings $t_\perp^{BB}$ and $t_\perp^{NN}$ only through their difference $t_\perp^{BB} - t_\perp^{NN}$, so that the first nearest neighbors result is recovered if $t_\perp^{BB} = t_\perp^{NN}$. Indeed, if $t_\perp^{BB} = t_\perp^{NN}$, the integral transfer matrix can be rewritten:

$$H(\mathbf{k}) = t_\perp^{BB}\gamma_2(\mathbf{k})I_2 + \begin{pmatrix} \Delta & t_\perp\gamma_1(\mathbf{k}) \\ t_\perp\gamma_1(\mathbf{k})^* & -\Delta \end{pmatrix}$$

[4] But this ceases to be the case when considering indirect excitations, as we will see later.

[5] The given approximation for a being the first order correction to the states when the non-onsite hoppings are re-introduced as a perturbation.

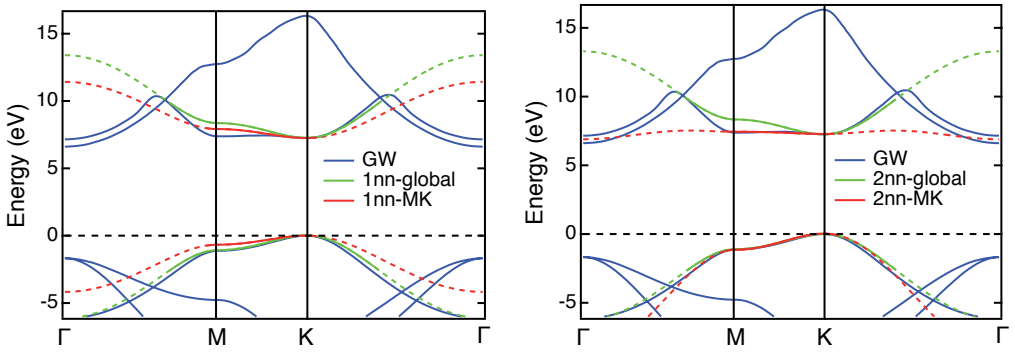

Figure 4.5: Figure reproduced from [47]. *Ab initio* band structure for single layer hBN, along with the various tight-binding fits reported in table 4.1. Left: first nearest-neighbor fits. Right: second-nearest neighbors fit. Solid lines correspond to the regons which were included in the fitting procedure, dashed-lines are their continuation on the rst of the high-symmetry wedge.

where I_2 is the 2×2 identity matrix: the action of second nearest neighbors is therefore only a global (but $\mathbf{k}$ dependent) energy shift, which therefore has no influence on the *direct* transition energies or the eigenstates.

4.2.3 Electronic band structure

To estimate the value of the kinetic parameters, we can fit the band energies provided by equation 4.2 to the *ab initio* band structure of a free floating hBN single-layer. We do so on a band structure computed within the G_0W_0 approximation by F. Paleari:[47] a number of relevant fits are depicted in figure 4.5. The corresponding parameters are reported in table 4.1.

The quality of the fit is better for the valence band than for the conduction band, which is a common feature of tight-binding models. This can usually be ascribed to the fact that conduction states are more delocalized. Two further difficulties are present here. First, we notice that the conduction band is particularly flat in the optically active **MK** region, at variance with the behavior of the valence band. Such an asymmetry is difficult to reproduce in tight-binding, because two-bands (orthogonal) first nearest neighbor tight binding models typically have symmetric bands.[6] In our case, if we keep a

[6] In $2D$, two bands $E_c(\mathbf{k})$ and $E_v(\mathbf{k})$ are symmetric (with respect to a plane of constant energy) if there exists a constant σ such that $E_c(\mathbf{k}) - \sigma = \sigma - E_v(\mathbf{k})$, i.e. if and only if $E_c(\mathbf{k}) + E_v(\mathbf{k}) = C^{st}$. However, the band energies are the eigenvalues of the integral transfer matrix $H(\mathbf{k})$, and thus in the 2×2 case, $E_c(\mathbf{k}) + E_v(\mathbf{k}) = \mathrm{Tr}(H(\mathbf{k}))$. Therefore, as long as there are no hoppings between atoms of the same species (which would yield $\mathbf{k}$-dependent diagonal elements in $H(\mathbf{k})$), the bands are symmetric.

Fit	Δ	$t_\perp$	$t_\perp^{BB}$	$t_\perp^{NN}$
1nn global	3.625	-3.0	0	0
1nn local	3.625	-2.30	0	0
2nn global	3.625	-3.0	-0.1	-0.1
2nn local	3.625	-2.30	-0.1	-0.1

Table 4.1: Kinetic parameters found through various direct fits of the hBN band structure by equation 4.2. Energies are given in electron-Volts (eV). The value of Δ has been fixed to reproduce the band gap. "Global" fits correspond to a fit of the full π bands, disregarding the nearly free electron states which occur near $\mathbf{\Gamma}$, while "local" fits are performed along the **MK** line, from the region of which most of the contributions to the excitonic wavefunctions orginate. Second nearest neighbor (2nn) fits have been performed with the simplifying constraint $t_\perp^{BB} = t_\perp^{NN}$.

first nearest neighbor description, our system displays electron-hole symmetry, which is not prestent in the *ab initio* band structure. This difficulty can be somewhat mitigated by the inclusion of second nearest neighbors, which breaks this symmetry. This asymmetry will play an important role when discussing indirect excitonic effects, but as we have seen above, its effects are relatively minor as long as we restrict ourselves to $\mathbf{Q} = \mathbf{0}$.

A further issue comes from the parabolic conduction bands near Γ, which are not at all captured by the tight-binding description. The states responsible for these are known as nearly free electron-states, highly delocalized states extending above and below the two-dimensional layer.[59] Consequently, they are very difficult to describe through linear combinations of atomic orbitals, and projections of the *ab initio* states confirm that they have a very small overlap with the atomic p_z orbitals, and therefore cannot be captured in our model. However, due to their extremely delocalized nature, these states are expected to couple only very weakly to the localized σ or π valence states, and should therefore not contribute significantly to absorption.

We have claimed several times that BN systems, because of their large gaps, tend to have conduction bands made almost purely of Boron orbitals, and valence bands made almost purely of Nitrogen orbitals. Since we now have explicit values for the kinetic parameters for a realistic system, we are in a position to quantify that claim. To this end, we depict in figure 4.6 the (modulus squared of the) projections of the band states onto the tight-binding basis functions for Nitrogen and Boron, which can be read from equation 4.4. It can be seen that, in the vicinity of the optically active **MK** region, the valence (resp. conduction) band is composed at more than 90%

of Nitrogen (resp. Boron) orbitals, up to a maximum of 100% at the gap, in $\mathbf{K}/\mathbf{K}'$, where the states are pure because the coupling between the two lattices, $t_\perp \gamma_1(\mathbf{k})$ vanishes. The approximation is therefore very good in the **MK** region. It may in fact even be argued that it remains reasonable in the rest of the Brillouin zone, but care must be taken that the structure of the conduction band depicted by *ab initio* calculations there is more complex than the tight-binding one.

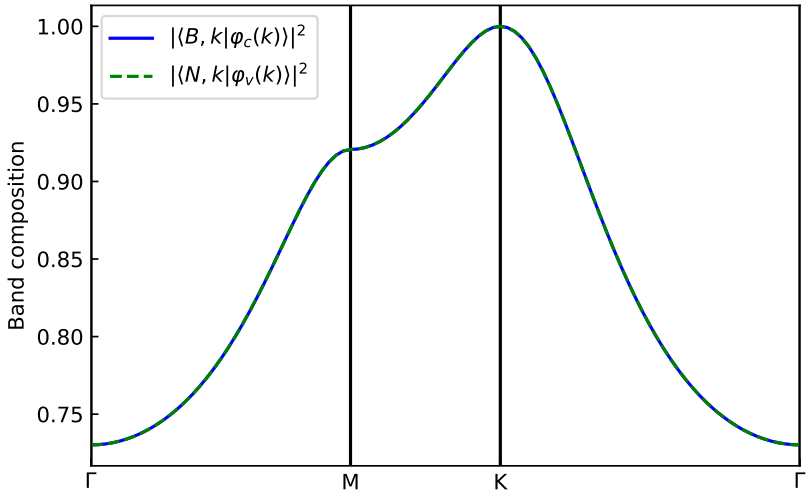

Figure 4.6: Compositions of the conduction and valence bands of single layer hBN in terms of Boron and Nitrogen tight-binding functions (respectively). Since the band wavefunctions are two-component vectors for a given $\mathbf{k}$, we have only plotted one component for each, the other being obtained by its complement to one, e.g. $|\langle N,\mathbf{k}|\varphi_c(\mathbf{k})\rangle|^2 = 1 - |\langle B,\mathbf{k}|\varphi_c(\mathbf{k})\rangle|^2$. Kinetic parameters were taken from the first nearest neighbors "local 1nn" fit (but note that the result depends only on the second nearest neighbor hoppings if $t_\parallel^{BB} \neq t_\parallel^{NN}$).

4.2.4 Optical response

As we have noted in previous chapters, the absorption spectrum of the system at the independent-particle level is given by:

$$\epsilon_i(E) = \left(\frac{2\pi\hbar e}{m_e E}\right)^2 \sum_{\mathbf{k},v,c} |\langle c,\mathbf{k}|\mathbf{e}\cdot\hat{\mathbf{p}}|v,\mathbf{k}\rangle|^2 \delta(E_c(\mathbf{k}) - E_v(\mathbf{k}) - E) \tag{4.5}$$

where the variable $E = \hbar\omega$ describes the energy of the incoming photons and $\mathbf{e}$ is their polarization vector. Armed with the tight-binding band states and

the expressions for the momentum matrix elements derived in the previous chapters, we can compute this quantity numerically.

Two approximations of interest are also available. The first is to assume that momentum matrix elements are approximately constant over the Brillouin zone, which leads to the approximation that the absorption spectrum is proportional to the joint density of states divided by the squared photon energy.

The other approximation is the one discussed earlier, in which we assume that the valence (resp. conduction) states are well approximated by Nitrogen (resp. Boron) tight-binding basis functions. We will discuss this approximation in the case of hBN in details in 4.3.1, but for now, it is enough to know that it amounts here to:

$$\begin{aligned} |c,\mathbf{k}\rangle &\approx |B,\mathbf{k}\rangle \\ |v,\mathbf{k}\rangle &\approx |N,\mathbf{k}\rangle \\ E_c(\mathbf{k}) - E_v(\mathbf{k}) \approx E_0(\mathbf{k}) &= 2\Delta + 3\frac{t_\perp^2}{\Delta} + \left(\frac{t_\perp^2}{\Delta} + t_\perp^{BB} - t_\perp^{NN}\right)\gamma_2(\mathbf{k}) \end{aligned}$$

from which follows the simple result:

$$\langle c,\mathbf{k}|\hat{\mathbf{p}}|v,\mathbf{k}\rangle \approx -\frac{m_e}{\hbar} t_\perp \boldsymbol{\nabla}_{\mathbf{k}}\gamma_1(\mathbf{k})$$

The resulting spectra are plotted in figure 4.7, where for simplicity and considering the arguments given above, we have restricted ourselves to first nearest neighbors. The most salient feature of these spectra is a van-Hove singularity, situated approximately at $E_{vH} = 2\Delta + \frac{t_\perp^2}{\Delta}$, which is the approximate transition energy at point $\mathbf{M}$, $E_0(\mathbf{M})$, and comes about because γ_2 has a critical point at $\mathbf{M}$.

We should note, of course, that this single particle spectrum cannot, by itself, present an accurate representation of the optical properties of the system. Excitonic effects significantly modify the optical response of hBN.[60]

4.3 Excitonic Hamiltonian

Once again, we start this section with the good news that, apart from a change of lattice and Brillouin zone, everything proceeds as in the case of the linear chain, up to a few substitutions which we will outline. We shall therefore remain brief whenever going through procedures that were already treated in details in the case of the chain.

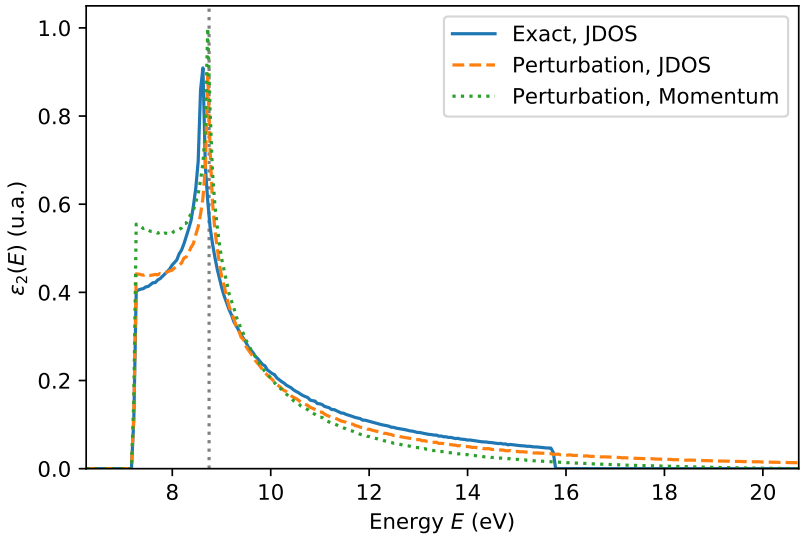

Figure 4.7: Single particle absorption spectra of single layer hBN within various tight-binding approximations. Solid blue line: spectrum computed using the joint density of states approximation with the "exact" tight-binding band energies. Dashed orange line: same, but with the approximated band energies. Dotted green line: sepctrum computed by calculating explicitely the momentum matrix elements, as indicated in the text. Vertical dashed line: approximate position of the van-Hove singularity at $E_{vH} = 2\Delta + \frac{t_\perp^2}{\Delta}$. The presented spectra are normalized so that they enclose the same area. Parameters used: $\Delta = 3.625$ eV, $t_\perp = -2.33eV$, $t_\perp^{NN} = t_\perp^{BB} = 0$.

4.3.1 Kinetic hamiltonian

Our first task will be to obtain effective hamiltonians for the electrons and the holes. This is done by treating the (non-onsite) hoppings as perturbation of the onsite terms, and, up to second order, we obtain, in the basis of atomic orbitals:

$$\langle B,\mathbf{n}|\hat{H}_e|B,\mathbf{n}'\rangle = \begin{cases} \Delta + \eta\frac{t_\perp^2}{2\Delta} & \text{if } \mathbf{n}=\mathbf{n}' \\ \frac{t_\perp^2}{2\Delta} + t_\perp^{BB} & \text{if } \mathbf{n} \text{ and } \mathbf{n}' \text{ are 1n.n. in } \Lambda_B \\ 0 & \text{else} \end{cases}$$

$$-\langle N,\mathbf{m}|\hat{H}_h|N,\mathbf{m}'\rangle = \begin{cases} \Delta + \eta\frac{t_\perp^2}{2\Delta} & \text{if } \mathbf{m}=\mathbf{m}' \\ \frac{t_\perp^2}{2\Delta} - t_\perp^{NN} & \text{if } \mathbf{m} \text{ and } \mathbf{m}' \text{ are 1n.n. in } \Lambda_N \\ 0 & \text{else} \end{cases}$$

with $\eta = 3$. This is the same result as in the chain case, up to a change of underlying lattices and the geometric factor η, which counts the number of first nearest neighbors of an N or B atom, changing from 2 in the linear chain to 3 in the hexagonal single layer. It is convenient at this point to introduce the notations $T = \frac{t_\perp^2}{\Delta}$ as shorthand, and $T'_h = \frac{T}{2} - t_\perp^{NN}$ and $T'_e = \frac{T}{2} + t_\perp^{BB}$ for the effective hole and electron hoppings (respectively). These hamiltonians can be expressed in the basis of tight-binding basis functions, in which they are diagonal, and yield the approximate band energies:

$$E_c(\mathbf{k}) = \Delta + \frac{t_\perp^2}{2\Delta}|\gamma_1(\mathbf{k})|^2 + t_\perp^{BB}\gamma_2(\mathbf{k})$$
$$E_v(\mathbf{k}) = -\left[\Delta + \frac{t_\perp^2}{2\Delta}|\gamma_1(\mathbf{k})|^2 + t_\perp^{NN}\gamma_2(\mathbf{k})\right]$$

By their difference, we can likewise construct the direct transition energies:

$$E_0(\mathbf{k}) = 2\Delta + 3T + (T'_h + T'_e)\gamma_2(\mathbf{k}) \tag{4.6}$$

which, as stated above, is the crucial kinetic quantity that will enter the direct Bethe-Salpeter equation. They are plotted and compared in figure 4.8 with reference *ab initio* and "exact" tight-binding results, as well as the transition energies computed from applying the effective mass approximation to both (tight-binding) bands, which would enter a hydrogenoïd model. Even remaining at the level of first nearest neighbors, the quality of the perturbation expansion can be seen to be very good. In the neighborhood of the optically active **MK** region, it matches closely the "exact" tight-binding result, which itself is in good agreement with the G_0W_0 calculation. *A contrario*, the effective mass approximation, while expectedly very good near the

gap at **K**, quickly decays in accuracy and fails to reproduce the transition energies on the **MK** segment.

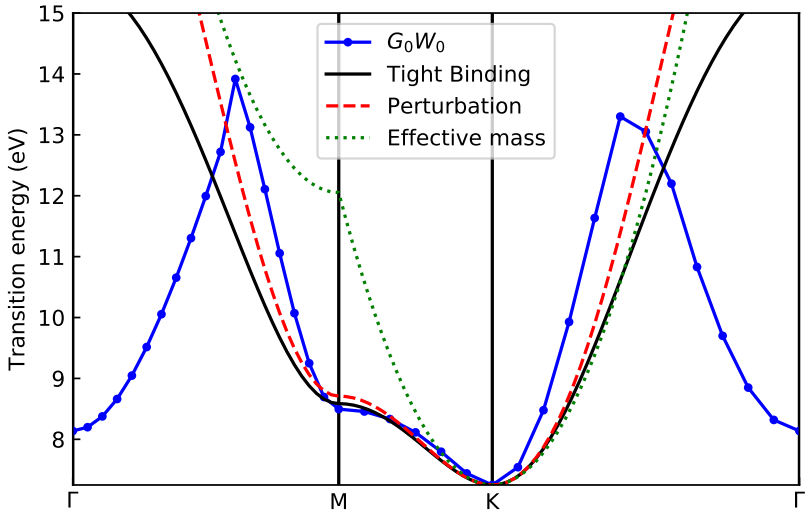

Figure 4.8: Direct transition energies for single-layer hBN, at various levels of approximation: *ab initio* G_0W_0 calculation by F. Paleari (solid line with markers), tight-binding (solid line), second order perturbation expansion of the TB result (dashed line), and effective mass approximation (dotted line). Kinetic parameters were taken from the first nearest neighbors "local 1nn" fit (but note that the result depends only on the second nearest neighbor hoppings if $t_{\parallel}^{BB} \neq t_{\parallel}^{NN}$). Note the low energy transitions near $\mathbf{\Gamma}$ in the G_0W_0 results: they are transitions from the σ valence sates to the (conduction) nearly free electron states, which are not included in the tight-binding model (see main text).

The expressions of $\hat{H}_e$ and $\hat{H}_h$ found above allow us to proceed to the kinetic hamiltonian $\hat{H}_0 = \hat{H}_h \otimes \mathbb{1}_e - \mathbb{1}_h \otimes \hat{H}_e$ in the basis of elementary excitations $|\mathbf{R}, \mathbf{Q}\rangle$ by means of direct calculation, i.e. by directly introducing the elementary excitation states as:[7]

$$|\mathbf{R}, \mathbf{Q}\rangle = \frac{1}{\sqrt{N}} \sum_{\mathbf{m} \in \Lambda_N} e^{-i\mathbf{Q}\cdot\mathbf{m}} |\mathbf{m}, \mathbf{R}\rangle \tag{4.7}$$

where the pair state $|\mathbf{m}, \mathbf{R}\rangle$ is defined through:

$$|\mathbf{m}, \mathbf{R}\rangle = |N, \mathbf{m}\rangle \otimes |B, \mathbf{m} + \mathbf{R}\rangle$$

[7]It is not particularly illuminating here to explicitly go through the lattice of pairs in the case of hBN, because its dimension is twice that of the underlying crystal lattice, i.e. four. It therefore does not quite fit on the page.

and where the $\mathbf{R}$ are the vectors of the lattice of excitations, defined as usual through:

$$\Lambda = \Lambda_B - \mathbf{m}_N^0 = \mathcal{R} + \underbrace{\left(\mathbf{n}_B^0 - \mathbf{m}_N^0\right)}_{\boldsymbol{\tau}}$$

which is here nothing but a triangular lattice ($\mathcal{R}$) offset by a nearest neighbor $N - B$ vector ($\boldsymbol{\tau}$). Again, the result is that of the chain, with $\eta = 3$:

$$\langle \mathbf{R}, \mathbf{Q}|\hat{H}_0|\mathbf{R}', \mathbf{Q}'\rangle = \delta_{\mathbf{Q},\mathbf{Q}'} \begin{cases} 2\Delta + 3T & \text{if } \mathbf{R} = \mathbf{R}' \\ T_e' + T_h' e^{i\mathbf{Q}\cdot(\mathbf{R}'-\mathbf{R})} & \text{if } \mathbf{R}, \mathbf{R}' \text{ are 1n.n. in } \Lambda \\ 0 & \text{otherwise} \end{cases} \tag{4.8}$$

We depict the associated tight-binding problem on the lattice of excitations in figure 4.9.

4.3.2 Direct electron-hole potential: Rytova-Keldysh potential

By the same reasoning as in the chain case, we obtain that the direct electron-hole potential is, to a first approximation, diagonal in the basis of pairs, and depends only on the relative coordinate $\mathbf{R}$:

$$\langle \mathbf{m}, \mathbf{R}|\hat{U}|\mathbf{m}', \mathbf{R}'\rangle = \delta_{\mathbf{m},\mathbf{m}'}\delta_{\mathbf{R},\mathbf{R}'}U_{\mathbf{R}}$$

from which it follows that it is also diagonal in the basis of elementary excitations:

$$\langle \mathbf{R}, \mathbf{Q}|\hat{U}|\mathbf{R}', \mathbf{Q}'\rangle = \delta_{\mathbf{Q},\mathbf{Q}'}\delta_{\mathbf{R},\mathbf{R}'}U_{\mathbf{R}}$$

The main difficulty here is therefore not so much to perform the change of basis, but to actually determine the matrix elements $U_{\mathbf{R}}$, themselves given by the semiclassical expression:

$$U_{\mathbf{R}} \approx W\left(\mathbf{n}_N^0, \mathbf{n}_N^0 + \mathbf{R}\right) = V(\mathbf{R})$$

We therefore need to evaluate the *screened* Coulomb interaction W in our system, or, rather, provide a model $V(\mathbf{R})$ for it. Once again, an expression of the form:

$$V(R) \propto \frac{1}{\epsilon_f R}$$

is not adequate for a low-dimensional (1 or 2 D) materials. To see why in the two-dimensional case, let us introduce a model system. Consider a thin slab of thickness d and of (bulk) dielectric constant ϵ, representing the monolayer

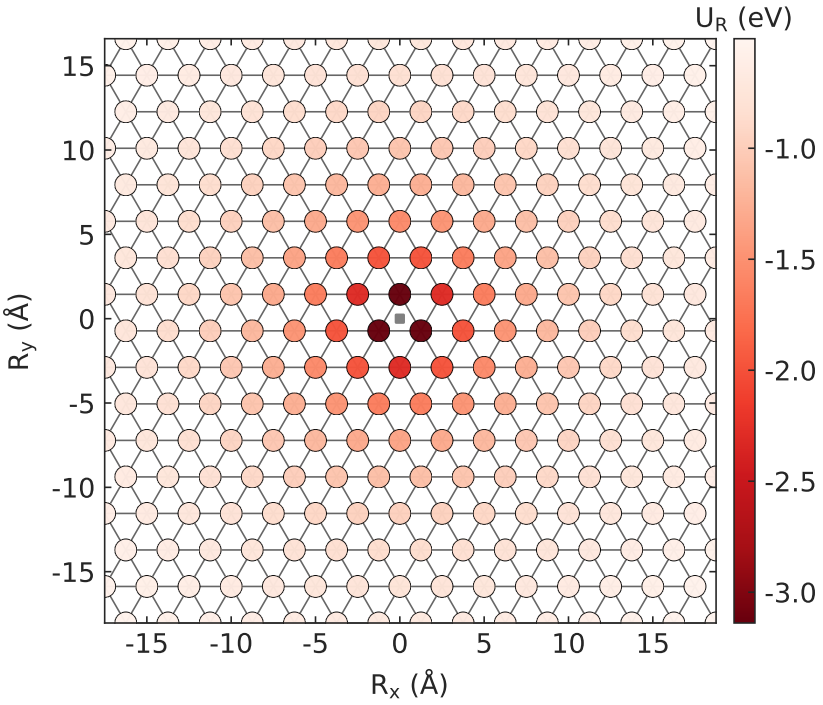

Figure 4.9: Lattice of excitations and associated excitonic tight-binding problem for single layer hBN at $\mathbf{Q} = \mathbf{0}$. At $\mathbf{Q} \neq \mathbf{0}$, hoppings become direction dependent, as per equation 4.8. The color scale denotes the onsites energies, with the zero of energies being set to the constant $2\Delta+3T$ (so that the onsite energies are just the potential, $V(R)$, taken here to be the Rytova-Keldysh potential with polarizability radius $r_0 = 10$ Å - see section 4.3.2). The gray square denotes the origin (for the relative coordinate $\mathbf{R}$).

$2D$ material. We "sandwitch" this slab between two semi-infinite dielectric media of lower dielectric constants ϵ_1 and ϵ_2, representing the environment (a substrate, vacuum, etc.). If the thickness of the slab is vanishingly small ($d \to 0$), i.e. in the strict $2D$ limit, then the (electrostatic) interaction potential between two charges q_1 and q_2 within the slab and separated by a distance R is given by:[19, 20]

$$V_{RK}(R) = -\frac{\pi q_1 q_2}{2r_0}\left[H_0\left(\frac{\kappa R}{r_0}\right) - Y_0\left(\frac{\kappa R}{r_0}\right)\right]$$

where $\kappa = \frac{\epsilon_1+\epsilon_2}{2}$ and $r_0 = \frac{\epsilon d}{2}$ with an effective layer thickness d is a material parameter which describes the polarizability of the two dimensional slab,[61] Y_0 is the Bessel function of the second kind of order zero, and H_0 is the Struve function of order zero. This is the celebrated Rytova-Keldysh potential,[19,

20] which has yielded great success in reproducing the typically non Rydberg excitonic series of two dimensional materials.[21, 22] For a freestanding layer, the surrounding media is vacuum, and $\epsilon_1 = \epsilon_2 = 1$, so that $\kappa = 1$. In that case, an elegant and purely two-dimensional derivation of the above potential has been provided in [61], along with a remarkably precise approximation in terms of elementary functions.

The asymptotic behaviors of this potential are revealing. It displays a natural length scale, $\rho_0 = \frac{r_0}{\kappa}$, which we call *effective* polarizability radius (we reserve the expression "polarizability radius" for r_0, which *a priori* depends only on the $2D$ material, and not its surroundings). It can be shown that:[61]

- If $R \ll \rho_0$, then the potential has a logarithmic behavior typical of purely two dimensional systems:

$$V_{RK}(R) \approx -\frac{q_1 q_2}{\kappa \rho_0}\left[\ln\left(\frac{R}{2\rho_0}\right) + \gamma\right]$$

  where $\gamma \approx 0.577$ is the Euler-Mascheroni constant.

- If $R \gg \rho_0$, then the screening of the two dimensional layer is inefficient, and the potential behaves as a Coulomb potential screened by an effective dielectric constant κ associated with the surrounding media:

$$V_{RK}(R) \approx \frac{q_1 q_2}{\kappa R}$$

  In particular, for a freestanding layer, $\kappa = 1$ and there is thus no screening at long distances.

An intuitive understanding of the situation, at least for the case of a freestanding layer, can be developed as follows:[22] if the two point charges are close together, most of the field lines associated to the interaction are contained within the layer, and so the screening is effectively two-dimensional, and therefore logarithmic. However, in the limit where the two charges are far apart, most of the field lines are outside of the layer, in vacuum, and therefore the associated dielectric screening becomes negligible so that the potential behaves as an unscreened Coulomb potential.

Considering the above, we therefore turn to the Rytova-Keldysh potential to model the direct electron-hole interaction in our system of freestanding hBN, i.e. we set:

$$U_{\mathbf{R}} = V_{RK}(\|\mathbf{R}\|)$$

for each $\mathbf{R} \in \Lambda$. For reference, we present in figure 4.10 a plot of the Rytova-Keldysh potential for a freestanding layer ($\kappa = 1$) with $r_0 = 10$ Å. While we

could have chosen to use ρ_0 as a unit of length, we chose here this particular value of r_0 because it will turn out to provide the best fit to the direct *ab initio* binding energies using the present excitonic tight-binding model (see below).

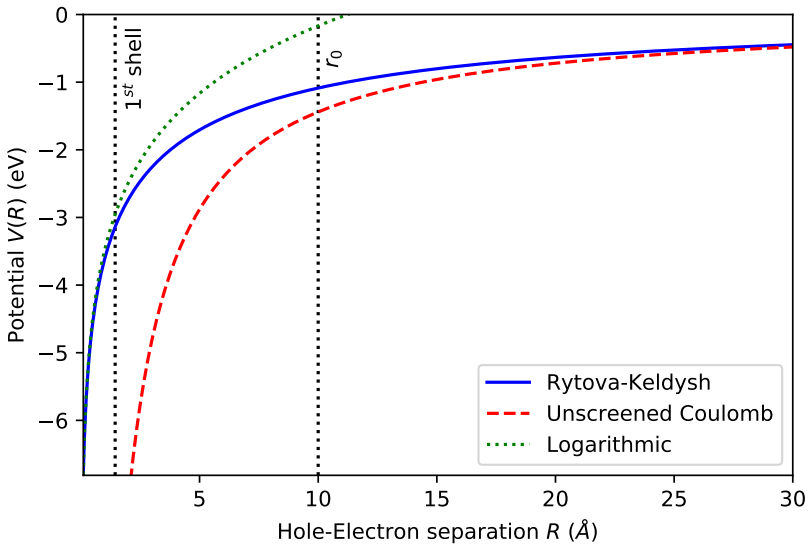

Figure 4.10: The Rytova-Keldysh potential and its asymptotic regimes, for $r_0 = 10$ Å. The 1^{st} shell corresponds to the shortest possible value for R in Λ, i.e. the first nearest neighbor $B - N$ distance, $\tau \approx 1.73$ Å.

4.3.3 Exchange interaction

We now move to the computation of the exchange part of the electron-hole interaction $\hat{J}$. We will follow a route essentially similar to the one discussed in [48] (see also references therein). As a remark, the approximate expression for the exchange interaction developed in this section will vanish for direct ($\mathbf{Q} = \mathbf{0}$) states, which will be the focus of section 4.4, but it will be crucial in reproducing the correct dispersion for some indirect ($\mathbf{Q} \neq \mathbf{0}$) states, as discussed in section 4.5.

Basis of pairs

We start from the basis of pairs, i.e. the $\{|\mathbf{m}, \mathbf{R}\rangle\}_{\mathbf{m}\in\Lambda_N, \mathbf{R}\in\Lambda}$, for which our usual definition is:

$$|\mathbf{m}, \mathbf{R}\rangle = |N, \mathbf{m}\rangle \otimes |B, \mathbf{m} + \mathbf{R}\rangle$$

The exchange interaction can then be computed directly, noting that:

$$\langle \mathbf{m}_1, \mathbf{R}_1 | \hat{J} | \mathbf{m}_2, \mathbf{R}_2 \rangle = 2 \int \varphi_c^*(\mathbf{r}' - (\mathbf{m}_1 + \mathbf{R}_1)) \varphi_c(\mathbf{r} - (\mathbf{m}_2 + \mathbf{R}_2)) \\ v(\mathbf{r} - \mathbf{r}') \varphi_v(\mathbf{r} - \mathbf{m}_1) \varphi_v^*(\mathbf{r}' - \mathbf{m}_2) d\mathbf{r} d\mathbf{r}'$$

where $v(\mathbf{r} - \mathbf{r}') = \frac{e^2}{|\mathbf{r} - \mathbf{r}'|}$ is the bare Coulomb potential, and the φ_c (resp. φ_v) are the localized electron (resp. hole) wavefunctions in position representation. It now appears that, if we keep our zeroth-order approximation of these functions as Boron (resp. Nitrogen) atomic orbitals, and proceed by retaining only terms of matching center (i.e. the same approximations we used to obtain the direct part of the electron-hole interaction), we will have a problem. Indeed, because the hole sublattice Λ_N and the electron sublattice Λ_B are disjoint, the integral above contains, at zeroth-order, no terms of matching centers in the same integration variable, and therefore applying the usual approximation of retaining only these terms, evaluates to zero.

This issue is lifted by taking into account the first order corrections to the localized electron and hole states, which effectively amounts to computing approximate Wannier functions. For all $\mathbf{n} \in \Lambda_B$ and $\mathbf{m} \in \Lambda_N$, they are given to first order in $\frac{t_\perp}{2\Delta}$ by:[47][8]

$$\varphi_c(\mathbf{r} - \mathbf{n}) \approx \varphi_B(\mathbf{r} - \mathbf{n}) + \frac{t_\perp}{2\Delta} \sum_{\boldsymbol{\tau}} \varphi_N(\mathbf{r} - (\mathbf{n} - \boldsymbol{\tau}))$$

$$\varphi_v(\mathbf{r} - \mathbf{m}) \approx \varphi_N(\mathbf{r} - \mathbf{m}) - \frac{t_\perp}{2\Delta} \sum_{\boldsymbol{\tau}} \varphi_B(\mathbf{r} - (\mathbf{m} + \boldsymbol{\tau}))$$

in position representation, where the sum over $\boldsymbol{\tau}$ runs over the Nitrogen to Boron first nearest neighbor vectors, the φ_B (resp. φ_N) are Boron (resp. Nitrogen) *atomic* orbitals (i.e. the aforementionned zeroth-order localized electron and hole states). In effect, instead of atomic orbitals, we now have localized electron (resp. hole) wavefunctions, which are still centered on the Boron (resp. Nitrogen) lattice sites, but also have a significant amplitude on their nearest neighbor sites in the Nitrogen (resp. Boron) sublattice.

With this, the calculation can proceed. Retaining only terms with *atomic orbitals* of matching centers and keeping to second order in $\frac{t_\perp}{2\Delta}$ (the zeroth and first order terms vanish), we find:

$$\langle \mathbf{m}_1, \mathbf{R}_1 | \hat{J} | \mathbf{m}_2, \mathbf{R}_2 \rangle = \left(\frac{t_\perp}{2\Delta} \right)^2 \sum_{\boldsymbol{\tau}_1, \boldsymbol{\tau}_2} \delta_{\mathbf{R}_1, \boldsymbol{\tau}_1} \delta_{\mathbf{R}_2, \boldsymbol{\tau}_2} \\ [I_{vv}(\mathbf{m}_1, \mathbf{m}_2) + I_{cc}(\mathbf{n}_1, \mathbf{n}_2) - I_{vc}(\mathbf{n}_1, \mathbf{n}_2) - I_{vc}(\mathbf{m}_2, \mathbf{n}_1)] \quad (4.9)$$

[8] Note that in [47], the Nitrogen-Boron hopping was denoted by $-t$, where here we have $t_\perp$ instead, leading to a sign change compared to this reference.

where we have introduced the notation $\mathbf{n}_i = \mathbf{p}_i + \mathbf{R}_i$ for the electron coordinate, the sums on $\boldsymbol{\tau}_1$ and $\boldsymbol{\tau}_2$ run over the Nitrogen to Boron first nearest neighbor vectors, and:

$$I_{\mu\nu}(\mathbf{n}, \mathbf{m}) = \int \left|\varphi_\mu^{at}(\mathbf{r} - \mathbf{n})\right|^2 v(\mathbf{r} - \mathbf{r}') \left|\varphi_\nu^{at}(\mathbf{r}' - \mathbf{m})\right|^2 d\mathbf{r} d\mathbf{r}'$$

where $\mu, \nu = v$ or c and the φ_c^{at} (resp. φ_v^{at}) are the Boron (resp. Nitrogen) atomic orbitals (respectively φ_B and φ_N from above, relabeled for notational convenience). It is worth noting that in equation 4.9, the sum $\sum_{\boldsymbol{\tau}_1, \boldsymbol{\tau}_2} \delta_{\mathbf{R}_1, \boldsymbol{\tau}_1} \delta_{\mathbf{R}_2, \boldsymbol{\tau}_2} [\ldots]$ has nine terms in general, but that, if $\mathbf{R}_1$ and $\mathbf{R}_2$ are Nitrogen-Boron first nearest neighbor vectors (i.e. one of the three $\boldsymbol{\tau}$), only one of these terms is nonzero, and the expression vanishes otherwise.

Equation 4.9 has an immediate physical meaning: the terms $I_{vv}(\mathbf{m}_1, \mathbf{m}_2)$ and $I_{cc}(\mathbf{n}_1, \mathbf{n}_2)$, which are repulsive, correspond respectively to the hole-hole and the electron-electron Coulomb interactions between the two pairs, while the attractive terms $-I_{vc}(\mathbf{m}_1, \mathbf{n}_2)$ and $-I_{vc}(\mathbf{m}_2, \mathbf{n}_1)$ correspond to a part the electron-hole interaction between the two pairs (loosely speaking, the electron-hole interactions "inside" each pair is "contained" in the direct interaction term). We note that, within our approximations, exchange is only important between the "shortest" electron-hole pairs, i.e. the pairs such that the electron and the hole are first nearest neighbors. We present a schematic depiction of these exchange electron-hole interactions alongside the direct interaction in the basis of pairs in figure 4.11.

Since the atomic wavefunctions φ_μ^{at} are strongly localized, one may naively approximate the $I_{\mu\nu}(\mathbf{n}, \mathbf{m})$ as:

$$I_{\mu\nu}(\mathbf{n}, \mathbf{m}) \approx v(\mathbf{n} - \mathbf{m}) \approx \frac{2e^2}{|\mathbf{n} - \mathbf{m}|} \tag{4.10}$$

in analogy with what we have done for the direct interaction. However, this expression diverges when $\mathbf{n} = \mathbf{m}$, which can happen for the repulsive terms.

Basis of elementary excitations

Nevertheless, the simple expression above (equations 4.9 and 4.10) can lead us to the matrix elements in the basis of elementary excitations as they are given in [48]. To see this, we proceed as usual by making use of the definition of the elementary excitations in terms of the localized pair states (equation

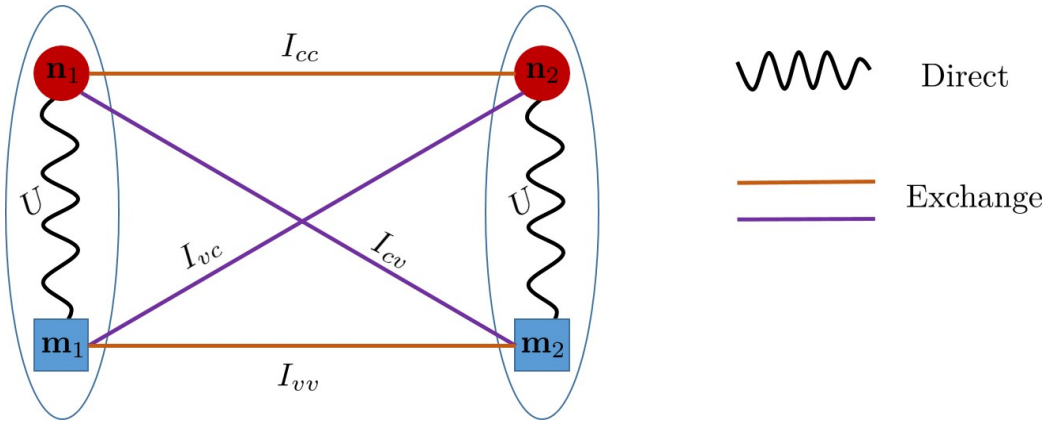

Figure 4.11: Schematic depiction of the electron-hole interaction(s) in the basis of pairs, between a pair $|\mathbf{m}_1, \mathbf{n}_1\rangle$ and a pair $|\mathbf{m}_2, \mathbf{n}_2\rangle$ (blue squares figure holes while red disks figure electrons). Straight lines represent the $I_{\mu\nu}(\mathbf{n}, \mathbf{m})$ components of the exchange interaction ($\hat{J}$), which are attractive when $\mu \neq \nu$ (purple lines) and repulsive otherwise (orange lines). Wiggly lines represent the direct electron-hole interaction ($\hat{U}$). These terms are not always nonzero: in our approximations, exchange is only important between the "shortest" electron hole pairs, i.e. when $\mathbf{R}_1$ and $\mathbf{R}_2$ are $N - B$ first nearest neighbors, while the direct interaction is diagonal, so that it is only important when $\mathbf{m}_1 = \mathbf{m}_2$ *and* $\mathbf{n}_1 = \mathbf{n}_2$, but it has long range in the hole-electron separation, $\mathbf{R}$.

4.7), and note that:[9]

$$\begin{aligned}\langle \mathbf{R}_1, \mathbf{Q}|\hat{J}|\mathbf{R}_2, \mathbf{Q}'\rangle &= \frac{1}{N}\sum_{\mathbf{m},\mathbf{m}'\in\Lambda_N} e^{-i\mathbf{Q}'\cdot\mathbf{m}'} e^{i\mathbf{Q}\cdot\mathbf{m}} \langle \mathbf{m}, \mathbf{R}_1|\hat{J}|\mathbf{m}', \mathbf{R}_2\rangle \\ &= 2e^2\left(\frac{t_\perp}{2\Delta}\right)^2 \delta_{\mathbf{Q},\mathbf{Q}'} \sum_{\boldsymbol{\tau}_1,\boldsymbol{\tau}_2} \delta_{\mathbf{R}_1,\boldsymbol{\tau}_1}\delta_{\mathbf{R}_2,\boldsymbol{\tau}_2}[\sigma(\mathbf{0}) + \sigma(\mathbf{R}_2 - \mathbf{R}_1) \\ &\qquad - \sigma(\mathbf{R}_2) - \sigma(-\mathbf{R}_1)]\end{aligned}$$

where we used the fact that $\langle \mathbf{m}, \mathbf{R}_1|\hat{J}|\mathbf{m}', \mathbf{R}_2\rangle$ depends only on $\mathbf{m}$ and $\mathbf{m}'$ through $\boldsymbol{\rho} = \mathbf{m}' - \mathbf{m}$ (from which we also obtained that $\hat{J}$ conserves $\mathbf{Q}$) and we have defined:

$$\sigma(\mathbf{z}) = \sum_{\boldsymbol{\rho}\in\mathcal{R}} \frac{e^{-i\mathbf{Q}\cdot\boldsymbol{\rho}}}{|\boldsymbol{\rho} + \mathbf{z}|}$$

[9] One may be worried that the sum below contains infinite terms (e.g. when $\mathbf{n} = \mathbf{n}'$). A possible way to avoid this difficulty is by replacing the approximation of equation 4.10 by, e.g., $I_{\mu\nu}(\mathbf{n}, \mathbf{m}) \approx \frac{2e^2}{|\mathbf{n}-\mathbf{m}|+\alpha}$ for some $\alpha > 0$ and let $\alpha \to 0$ at the end of the calculation. Here we proceed formally.

Noting that the $\boldsymbol{\rho}$ describe the system's Bravais lattice, $\mathcal{R}$, we can compute the above in the two dimensional case using the $(2D)$ Poisson summation formula:[10]

$$\sigma(\mathbf{z}) = \frac{2\pi}{A} \sum_{\mathbf{G}\in\mathcal{G}} \frac{e^{i(\mathbf{Q}-\mathbf{G})\cdot\mathbf{z}}}{|\mathbf{Q}-\mathbf{G}|}$$

where A is the area of the unit cell of Λ_N, and the sum over $\mathbf{G}$ is over the reciprocal lattice $\mathcal{G}$ of $\mathcal{R}$ (see section 4.2.1), so that:

$$\begin{aligned}\langle \mathbf{R}_1, \mathbf{Q}|\hat{J}|\mathbf{R}_2, \mathbf{Q}'\rangle &= 2e^2 \frac{2\pi}{A}\left(\frac{t_\perp}{2\Delta}\right)^2 \delta_{\mathbf{Q},\mathbf{Q}'} \sum_{\mathbf{G}\in\mathcal{G}} \frac{e^{i(\mathbf{Q}-\mathbf{G})\cdot(\mathbf{R}_2-\mathbf{R}_1)} - e^{i(\mathbf{Q}-\mathbf{G})\cdot\mathbf{R}_2} - e^{-i(\mathbf{Q}-\mathbf{G})\cdot\mathbf{R}_1} + 1}{|\mathbf{Q}-\mathbf{G}|} \\ &= 2e^2 \frac{2\pi}{A}\left(\frac{t_\perp}{2\Delta}\right)^2 \delta_{\mathbf{Q},\mathbf{Q}'} \sum_{\mathbf{G}\in\mathcal{G}} \frac{\left(e^{i(\mathbf{Q}-\mathbf{G})\cdot\mathbf{R}_2} - 1\right)\left(e^{-i(\mathbf{Q}-\mathbf{G})\cdot\mathbf{R}_1} - 1\right)}{|\mathbf{Q}-\mathbf{G}|}\end{aligned}$$

for $\mathbf{R}_1$ and $\mathbf{R}_2$ Nitrogen to Boron first nearest neighbor vectors, and zero otherwise, which is the result found in [48]. Following the approximation made there, we can note that only the $\mathbf{G} = 0$ term is singular, and neglect all others to obtain the final result:

$$\begin{aligned}\langle \mathbf{R}_1, \mathbf{Q}|\hat{J}|\mathbf{R}_2, \mathbf{Q}'\rangle \approx 2e^2 \frac{2\pi}{A}\left(\frac{t_\perp}{2\Delta}\right)^2 &\delta_{\mathbf{Q},\mathbf{Q}'} \\ &\sum_{\tau_1,\tau_2} \delta_{\mathbf{R}_1,\boldsymbol{\tau}_1}\delta_{\mathbf{R}_2,\boldsymbol{\tau}_2} \frac{\left(e^{i\mathbf{Q}\cdot\mathbf{R}_2} - 1\right)\left(e^{-i\mathbf{Q}\cdot\mathbf{R}_1} - 1\right)}{|\mathbf{Q}|}\end{aligned} \quad (4.11)$$

In effect, keeping only the $\mathbf{G} = 0$ term amounts to making a long range / small $\mathbf{Q}$ approximation, so that the expression above is expected to be reasonable close to the center of the Brillouin zone, but not necessarily so much away from it. Each of the four terms of the expansion of $\frac{\left(e^{i\mathbf{Q}\cdot\mathbf{R}_2}-1\right)\left(e^{-i\mathbf{Q}\cdot\mathbf{R}_1}-1\right)}{|\mathbf{Q}|}$ can be tracked to their respective origins in equation 4.9: $\frac{e^{i\mathbf{Q}\cdot(\mathbf{R}_2-\mathbf{R}_1)}}{|\mathbf{Q}|}$ and $\frac{1}{|\mathbf{Q}|}$ correspond respectively to the electron-electron and the hole-hole repulsions, while $\frac{e^{i\mathbf{Q}\cdot\mathbf{R}_2}}{|\mathbf{Q}|}$ and $\frac{e^{-i\mathbf{Q}\cdot\mathbf{R}_1}}{|\mathbf{Q}|}$ are the electron-hole (attractive) interactions.

We can remark now that the approximation of exchange given in equation 4.11 vanishes at $\mathbf{Q} = \mathbf{0}$. As a result, it will not affect the direct excitonic series. It is worth noting that, in a more complete treatment, the exchange interaction *would* affect $\mathbf{Q} = \mathbf{0}$ excitons. We will briefly discuss this point in section 4.4.2; in that same section, see also table 4.4 which presents *ab initio*

[10] For any suitable function f and Bravais lattice $\mathcal{R}$, $\sum_{\rho\in\mathcal{R}} f(\rho)e^{-iq\rho} = \frac{1}{A_{uc}}\sum_{g\in\tilde{\mathcal{R}}} \tilde{f}(q-g)$, where A_{uc} is the area of the unit cell of $\mathcal{R}$, $\tilde{\mathcal{R}}$ is the reciprocal lattice of $\mathcal{R}$ and $\tilde{f}(q) = \int e^{-irq} f(r)dr$ is the Fourier transform of f. The result below then follows from the 2D Fourier transform of $\frac{1}{|\rho|}$ and the shift property of the Fourier transform.

results for exitonic binding energies in hBN with and without exchange. We will discuss exchange and the consequences of equation 4.11 further when we come to the study of exciton dispersion in section 4.5, where it is crucial in reproducing the linear dispersion of some branches of the exciton band structure at small $|\mathbf{Q}|$.[62, 63] Even though we have an "exact" expression for it, we will then write the prefactor $2e^2\frac{2\pi}{A}\left(\frac{t_\perp}{2\Delta}\right)^2$ of equation 4.11 as $\frac{J}{4\tau}$ and take J as a fitting parameter, in consistence with [48].

4.4 Direct excitonic series

Because they are responsible for the system's absorption, we will start by studying direct ($\mathbf{Q} = \mathbf{0}$) excitons in details. In this section, we thus restrict ourselves to first nearest neighbor parametrizations, for the reasons discussed above. Since we will only study direct states here, we introduce the shorthand $|\mathbf{R}\rangle = |\mathbf{R}, \mathbf{Q} = \mathbf{0}\rangle$.

4.4.1 Wannier limit

It is instructive to study what happens in the Wannier limit, which corresponds essentially to a continuum / effective mass limit, where lattice effects are consequently averaged out and interactions between the $\mathbf{K}$ and $\mathbf{K}'$ points are neglected. Related work in similar limits[21, 22] or using more advanced $\mathbf{k}\cdot\mathbf{p}$ models, and, notably, massive Dirac models[64] has been published by several authors (for hBN see eg. [65, 66]). It is nevertheless interesting to carry out a study using the simple hydrogneoid model in some detail here. Indeed, this will allow us to intuitively appreciate the importance of lattice effects and of the interactions between the $\mathbf{K}$ and $\mathbf{K}'$ valleys, which are captured by the TB model proposed above, but not by the usual hydrogenoid Wannier model relying on the effective mass approximation around one of the $\mathbf{K}$ or $\mathbf{K}'$ points.

Wannier model as an approximation of the excitonic TB model

Before discussing the hydrogenoid model proper, we start this section by showing that it can be recovered as an approximation of our TB model, precisely by moving to the effective mass picture.[11] We do so by applying the

[11] Of course, the hydrogenoïd model is more general than our tight-binding model: it can be obtained in the usual manner for hBN. Our goal in this section is only to show more explicitly that this can also be done here *from* the tight-binding model by "forgetting" about the existence of the lattice.

effective mass approximation directly to the effective excitonic hamiltonian $\hat{H}_X$ in its interpretation as a particle moving on a triangular lattice with kinetic energy $\hat{H}_0$ under the influence of an external potential $\hat{U}$. To obtain the effective mass of this fictitious particle, we compute the band energies associated to the kinetic hamiltonian $\hat{H}_0$, which correspond to the unique band of a one-orbital triangular lattice, i.e.:

$$E_0(\mathbf{k}) = 2\Delta + 3T + T\gamma_2(\mathbf{k}) = 2\Delta + T|\gamma_1(\mathbf{k})|^2.$$

We thus recover the independent particle transition energies, as expected by construction of the model, and the minima of $E_0(\mathbf{k})$ are therefore found at the $\mathbf{K}/\mathbf{K}'$ points. To obtain the corresponding effective masses, we compute the Hessian of $E_0(\mathbf{k})$ at these points, with respect to, say, k_x and k_y. We find:

$$H_{E_0}(\mathbf{K}) = H_{E_0}(\mathbf{K}') = \frac{3a^2T}{2} I_2$$

which are scalar, and independent of whether the minima under consideration is the one at $\mathbf{K}$ or at $\mathbf{K}'$.[12] The sought-after effective mass is therefore scalar as well (i.e. it is isotropic) and likewise the same for both considered minima. We thus have:

$$\mu = \frac{2\hbar^2}{3a^2T}$$

the effective mass of *transitions* at the $\mathbf{K}/\mathbf{K}'$ points, or, equivalently, the effective mass of the fictitious particle involved in our excitonic TB model. Within our usual approximations, the result is the same as the usual procedure of first calculating the effective hole and electron masses, resp. m_h^* and m_e^*, and then forming the corresponding two body mass $\mu = \frac{m_e^* m_h^*}{m_e^* + m_h^*}$.

Intuitively, we see now that if we replace the kinetic energy operator $\hat{H}_0$ with the corresponding effective mass expression, we will recover the usual hydrogenoïd equation. Formally, we proceed by writing down the (direct) Bethe-Salpeter equation in components:

$$\forall \mathbf{R} \in \Lambda \; ; \quad \sum_{\mathbf{R}' \in \Lambda} h_0(\mathbf{R}' - \mathbf{R}) \Psi_{\mathbf{R}'} + U_{\mathbf{R}} \Psi_{\mathbf{R}} = E \Psi_{\mathbf{R}}$$

where $h_0(\mathbf{R}' - \mathbf{R}) = \langle \mathbf{R} | \hat{H}_0 | \mathbf{R}' \rangle$.[13] In contrast with the reciprocal space situation, it is the kinetic energy that is expressed as a convolution, while

[12] This last fact is expected, and is a direct consequence of the system's time-reversal invariance.

[13] The fact that these matrix elements only depend on a difference is ensured by the transnational invariance of the kinetic energy hamiltonian.

the potential is a simple product. We now "forget" about the lattice by introducing a continuous excitonic wavefuncton and turning the sum into an integral:[14]

$$\Psi_{\mathbf{R}} \to \Psi(\mathbf{R})$$
$$\sum_{\mathbf{R}' \in \Lambda} \to \int d\mathbf{R}'$$

The direct electron-hole interaction $\hat{U}$ converts straightforwardly to the continuous picture through the electrostatic model $V(R)$. The kinetic energy can be given a meaning in the continuous setting by noting that the convolution can be rewritten as a product in Fourier space, applying the effective mass approximation, and going back to direct space. This is the analogue of the treatment given to the potential in the usual derivation of the Wannier model. We thus obtain the continuum approximation:

$$-\frac{\hbar^2}{2\mu}\nabla^2 g(\mathbf{R}) + V(\mathbf{R})g(\mathbf{R}) = E_B g(\mathbf{R}) \tag{4.12}$$

for both minima $\mathbf{k}_0 = \mathbf{K}$ or $\mathbf{K}'$, where the eigenvalues E_B are the binding energies and the exciton wavefunctions are given by $\Psi(\mathbf{r}) = e^{-i\mathbf{k}_0\cdot\mathbf{r}} g(\mathbf{r})$. As claimed, this continuum approximation is exactly the Wannier limit: we have recovered the usual hydrogenoid model by taking the continuum / effective mass approximation for the fictitious particle involved in our TB model.

Energy levels, states and degeneracies

Equation 4.12 is a typical 2D hydrogenoïd equation. It is fruitfully nondimensionalized by introducing the excitonic equivalent of atomic units, which we may call "excitonic units":

- Mass: reduced effective mass of the pair: μ.
- Length: exciton Bohr radius: $a = \frac{m_0}{\mu} a_0$.
- Energy: exciton Hartree: $\varepsilon = \frac{\mu}{m_0}$Ha.

where $m_0 \approx 9.11 \times 10^{-31}$ kg and $a_0 \approx 0.529$ Å are respectively the electron mass and the Bohr radius and Ha ≈ 27.2 eV is the Hartree energy. For hBN, using the parameters of our 1nn excitonic fit,[15] these take the values:

[14] Up to suitable normalization factors that will cancel out in the final result.

[15] By which we mean a fit of T and r_0 to reproduce *ab initio* binding energies though the diagonalization of $\hat{H}_X$. More details in section 4.4.2; fit parameters are reported in equation 4.20.

- Mass: $\mu = 0.54 m_0$.
- Length: $a = 0.98$ Å.
- Energy: $\varepsilon = 14.69$ eV.

Performing this change of units, equation 4.12 becomes:

$$-\frac{1}{2}\nabla^2 g(\mathbf{R}) + V(\mathbf{R}) g(\mathbf{R}) = E g(\mathbf{R}) \tag{4.13}$$

Moving to polar coordinates, since $V(\mathbf{R})$ depends only on $R = \|\mathbf{R}\|$, the problem has cylinder symmetry, and so the equation is separable, and admits a basis of solutions of the form $g(R, \theta) = e^{im\theta}\Phi(R)$, where the radial wavefunction Φ satisfies the following radial equation:

$$\left[-\frac{1}{2}\left(\frac{1}{R}\frac{\mathrm{d}}{\mathrm{d}R} R \frac{\mathrm{d}}{\mathrm{d}R} - \frac{m^2}{R^2}\right) + V(R)\right]\Phi(R) = E\Phi(R) \tag{4.14}$$

and m corresponds to the angular momentum quantum number. This equation may then be solved numerically with the relevant potentials to obtain the binding energies and wavefunctions of the excitonic states by imposing relevant boundary conditions.[16] It can be noted that equation 4.14 can be recast in the form of a Sturm-Liouville equation with appropriate boundary conditions, so that standard results (number of nodes of the solutions, etc.) apply.[17]

If the direct electron-hole potential $V(R)$ is a Coulomb potential, i.e. if there exists ϵ such that $V(R) = -\frac{1}{\epsilon R}$, this is exactly the problem of the two dimensional hydrogen atom, whose solutions are known analytically:[18]

$$E = -\frac{1}{2}\frac{1}{\epsilon^2\left[n' + |m| - \frac{1}{2}\right]^2} \quad ; \quad n' \in \mathbb{N}^*$$

Famously, states sharing the same principal quantum number $n = n' + m$ are degenerate, leading to, e.g. the degeneracy of the $2s$ and the $2p$ states.[67] This is a particular property of the Coulomb problem, and ceases to hold when $V(R)$ is replaced by a more realistic potential. We are, of course, interested in the case of the Rytova-Keldysh potential.

[16] The physical requirement is that of finite norm, but it is typically enough numerically to ask that the wavefunctions vanish at infinity.

[17] This is typically done through the change of unknown function $u(R) = \sqrt{R}\Phi(R)$, but this is not very suitable for numerical calculations, because u may behave badly near the origin for s states, for which $\Phi(0)$ is finite.

Level	1	2	3	4	5	6
Character	$1s$	$2p$	$2s$	$3d$	$3p$	$3s$
Energy	-1.92	-1.00	-0.80	-0.62	-0.54	-0.46
Degen.	$\times 2$	$\times 4$	$\times 2$	$\times 4$	$\times 4$	$\times 2$
Strength	1	0	0.14	0	0	0.05

Table 4.2: First few bound states for hBN in the Wannier model. Binding energies are given in eV, and degeneracies take into account the $\mathbf{K}/\mathbf{K}'$ valley degeneracy. The "Strength" value is proportional to the oscillator strength of the state, normalized so that the value 1 is given to the highest bright state (the $1s$ state). A value of 0 indicates that the state is dark.

We therefore aim to solve equation 4.14 with the Rytova-Keldysh potential:

$$V(R) = \frac{\pi e^2}{2r_0}\Big[H_0\Big(\frac{R}{r_0}\Big) - Y_0\Big(\frac{R}{r_0}\Big)\Big]$$

Equation 4.14 therefore effectively depends on one material parameter, the polarizability radius r_0. For hBN, we estimate it to be $r_0 \approx 10$ Å,[18] i.e. $r_0 = 10.19$ in excitonic units. To our knowledge, no simple analytical solutions for equation 4.14 are known in this case, although there exist approximations based on the calculation of an effective dielectric constant,[68], lowest bound state variational approximations[21, 69] and semi-classical approximations.[66] Here, we solve equation 4.14 numerically[19] in the case of hBN, and report the eigenenergies of the first few bound states in table 4.2, while the states are depicted in figures 4.12 ($m = 0$, i.e. s states) and 4.13 ($m = \pm 1$, i.e. p states).

It is worth taking a moment to discuss the degeneracies of excitonic states in the Wannier model with the Rytova-Keldysh potential. It can be directly seen that equation 4.14 is invariant under the transformation $m \to -m$, which means that all states with $m \neq 0$ are (at least) twice degenerate. The only exceptions are s states, wich correspond to $m = 0$. Further, we must recall that equation 4.14 results from an effective mass approximation in the vicinity of the $\mathbf{K}/\mathbf{K}'$ points, which are inequivalent: each of the two points yields its own hydrogenoid equation, and thus its own excitonic series. However, the effective mass is the same at both points, so the effective hydrogenoïd equation attached to both points is exaclty the same: it is therefore enough to treat only one hydrogenoid equation (which is what we have

[18] Again, this estimate comes from the 1n.n. excitonic fit, see section 4.4.2 and in particular equation 4.20.

[19] We made use of *Mathematica*. Notes on the topic can be found in [70].

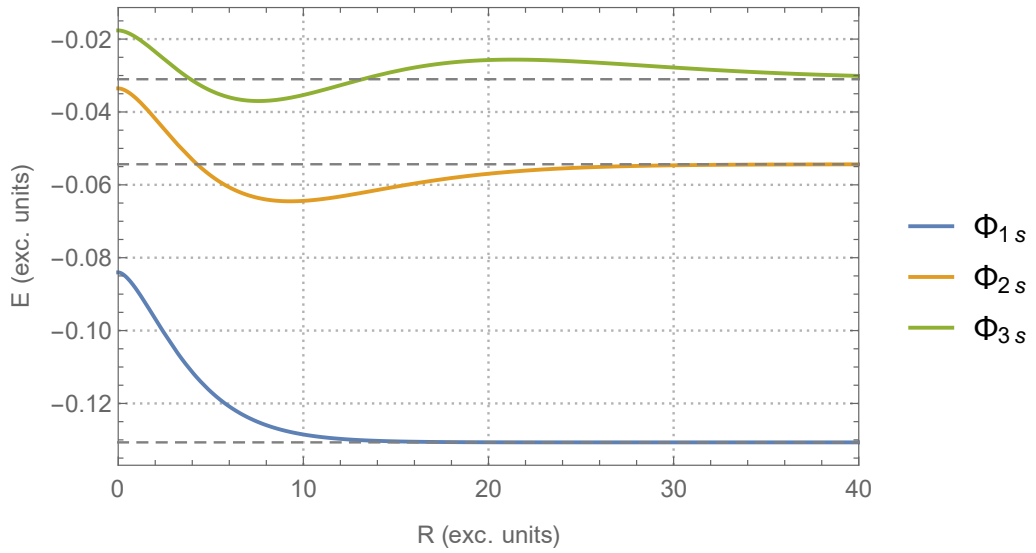

Figure 4.12: Radial wavefunctions for the first three s excitonic states of hBN within the Wannier model. These correspond to the $m = 0$ solutions of equation 4.14. Dashed lines correspond to the binding energies E of each state, and are also the zero for their respective eigenfunctions. The radial wavefunctions are represented to scale with one another; note in particular how the intensity at the origin decreases for higher energy levels, leading to a decrease in optical activity.

done until now), and multiply all degeneracies by two.[20] Barring accidental degeneracies, of which it seems there are none, these are all the degeneracies we expect: s ($m = 0$) states are twice degenerate, while all others are four times degenerate.

Optical activities and selection rules

Let us now turn our attention to the optical properties of our system. Within the approximations of the Wannier model, it can be shown that the oscillator strength of a given excitonic eigenstate $\Psi(\mathbf{R})$ is proportional to the intensity of its envelope function at the origin, $|g(\mathbf{0})|^2$.[21] More precisely, within the

[20] Recall, as we have discussed in section 4.2.1, that the system's first Brillouin zone contains exactly one $\mathbf{K}$ and one $\mathbf{K}'$ point. The linear independence of the solutions arising from both valleys can be seen from the expression of the excitonic wavefunctions: $\Psi_{\mathbf{k}_0}(\mathbf{R}) = e^{-i\mathbf{k}_0\cdot\mathbf{R}} g(\mathbf{R})$, for $\mathbf{k}_0 = \mathbf{K}$ or $\mathbf{K}'$. Thus, even if the enveloppe functions g are the same, the excitonic states are not.

[21] This result is usually found by assuming that the modulus squared of the interband optical matrix elements, $|\langle c, \mathbf{k}|\mathbf{e}\cdot\hat{\mathbf{p}}|v, \mathbf{k}\rangle|^2$, are constant. In the tight-binding framework,

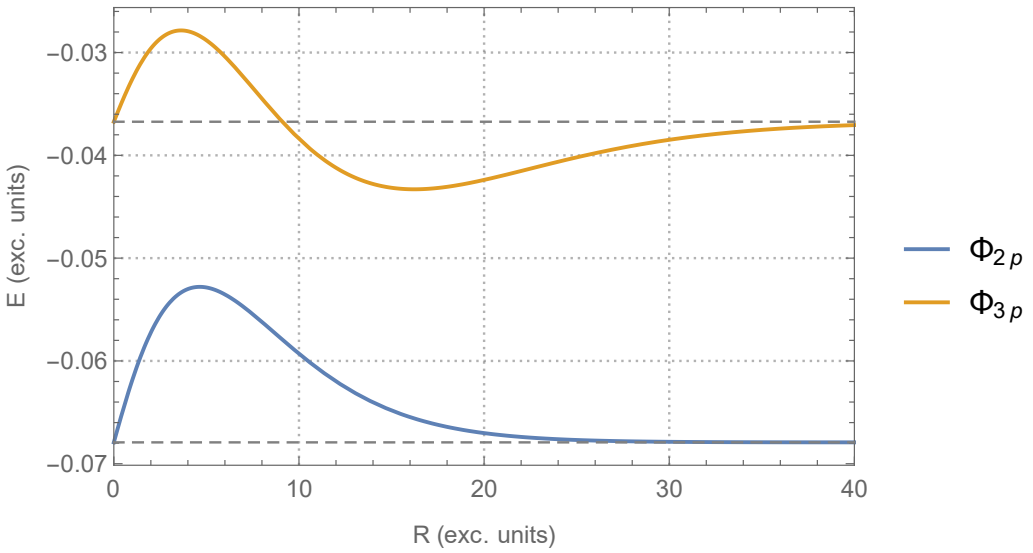

Figure 4.13: Radial wavefunctions for the first two p excitonic states of hBN within the Wannier model. The states plotted here correspond to the $m = 1$ solutions of equation 4.14, $m = -1$ solutions being indentical. Dashed lines correspond to the binding energies E of each state, and are also the zero for their respective eigenfunctions. The radial wavefunctions are represented to scale with one another. Note that the intensity at the origin always vanishes for p states, leading them to be optically dark.

Wannier model, the absorption spectrum is given by:[15, 16]

$$\epsilon_2(E) \propto \frac{1}{E^2} \sum_{\Psi} |\Psi(\mathbf{0})|^2 \delta(E_\Psi - E)$$

where the sum runs over a basis of (eigen)solutions of 4.13, and E_Ψ is the total excitation energy for the state Ψ (not just its binding energy): $E_\Psi = E_{gap} + E_{binding}(\Psi)$. This important result, which is a cornerstone of Elliott theory for excitons, provides an immediate selection rule: only states which have non-vanishing intensity at the orgin can be bright. This is only possible for rotationally symmetric states, i.e. states with $m = 0$ / s states. Indeed, with our (conventional) choice of basis, hydrogenoid states are of the form:

$$g(R, \theta) = e^{im\theta}\Phi(R)$$

with our approximations for the bands and exciton wavefunctions obtained from the continuum / hydrogenoïd approximation, this optical selection rule is recovered when $\tau \to 0$, which is indeed in the spirit of our continuum approximation.

so that, at the origin, the wavefunction must satisfy $\Phi(0) = e^{im\theta}\Phi(0)$ for all θ. This is only possible if either $m = 0$, in which case this condition is trivial, or if $\Phi(0) = 0$ for all other values of m. It can be immediately checked that our numerical solutions, presented in figures 4.12 and 4.13, satisfy this condition.

If the binding potential is strong enough, most of the oscillator strength of the system is taken by its bound states, and the part of the spectrum due to the scattering states is minimal. The problem thus becomes essentially that of computing the intensities at the origin for s states. In two dimensions, if the potential is of the Coulomb form, these values are known analytically:[18]

$$|g_{ns}(\mathbf{0})|^2 \propto \frac{1}{\left(n - \frac{1}{2}\right)^3} \propto |E_n|^{\frac{3}{2}} \tag{4.15}$$

where n is the principal quantum number: the intensity at the origin becomes lower for larger values of n, which can be intuitively understood as the wavefunction becoming more delocalized for higher excited states. Therefore, the oscillator strength of bound states is expected to drop rather sharply as we move up in energy in the excitonic series.

In the case of the Rytova-Keldysh potential, the same qualitative behavior can be observed,[22] as can be seen in figure 4.12, where we have taken care to normalize the s state wavefunctions and represent them to scale with one another. To provide a more quantitative picture, we display in figure 4.14 the intensities at the origin of the first few s states for hBN within the Wannier model, with respect to their binding energy, in log-log scale. In turn, we can use these values to construct the absorption spectrum of hBN within the Wannier model. This is done in figure 4.15, using $E_g = 2\Delta = 7.25$ eV as the value of the electronic gap.

A striking feature, or lack thereof, in these calculations, should retain our attention. We note that, in the *ab initio* calculations, the second absorption peak is visible with a binding energy of about -1 eV, but this peak appears missing in figure 4.15. Suspiciously, however, the $2p$ states have exactly this binding energy, but, as p states, they are dark within our approximations. It turns out that these states are indeed responsible for the peak under consideration, as we will show later. For the moment, we will close our analysis of hBN under the lens of the Wannier model with the following remark: the selection rules that we have enunciated above, in the context of the hydrogenoïd model, rely implicitly on the circular symmetry of the model. However, crystals in general, and hBN in particular, do not enjoy circular symmetry. It

[22] But recall that the repartition of binding energies are different between the two functional forms for the potential, so that the expected spectrum is, in turn, also different.

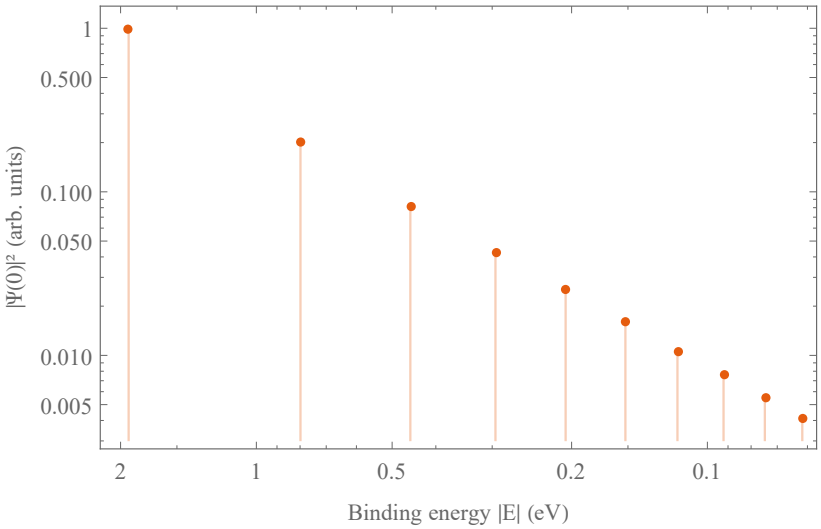

Figure 4.14: Intensities at the origin of the first ten s hydrogenoïd wavefunctions for hBN in the Wannier model (Rytova-Keldysh potential), log-log scale. The choice of the log-log scale is suggested by the known power law relationship between the binding energies and the intensities at the origin of s states in the case of the Coulomb potential (equation 4.15).

is only approximately realized when the underlying crystal structure can be averaged out and seen as a continuum, i.e. in situations where the typical exciton radii are significantly larger the the lattice parameters. Outside of this situation, we expect lattice effects to become important, and a satisfactory model should therefore respect the symmetries of the crystal lattice. In particular, even though we have obtained satisfactory binding energies from the above calculations, we will show that, when it comes to the optical response, selection rules have to be modified to account for the discrete C_{3v} symmetry of hBN.

4.4.2 Excitonic tight-binding

Let us now move back to the "full" excitonic tight-binding model, as presented in section 4.3. In the sense discussed in section 4.4.1 , this amounts to relaxing the continuum approximation compared to the Wannier limit. In other words, the lattice structure of the hBN crystal is now explicitely taken into account. We will start this section with a discussion of the symmetries of our system, and from there, we will obtain the appropriate optical selection rules.

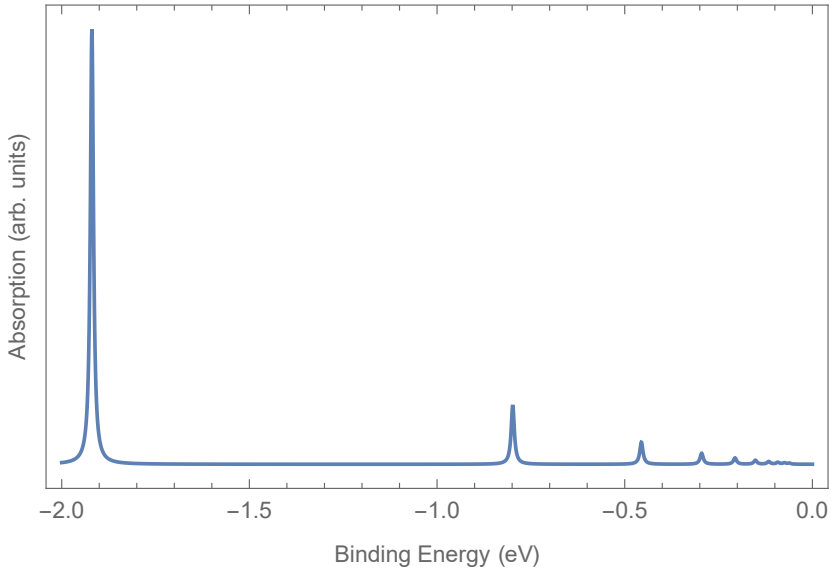

Figure 4.15: Absorption spectrum of hBN below the electronic gap, computed within the usual approximations of the Wannier model, using the intensities at the origin of the first ten s states, with a lorentzian broadening of 5 meV. Note that, compared to the *ab initio* results, the second peak at a binding energy of about -1 eV is missing: this is because it originates from a state of p character, which is dark in the Wannier model, but needs not be in a crystal without circular symmetry.

Symmetries and selection rules

The excitonic tight-binding model, by construction, has the symmetries of the underlying crystal lattice. The "true" point group of single layer hBN is the dihedral group D_{3h}: hBN has the planar symmetries of the triangle, as well as a horizontal mirror plane, which coincides with the plane of the layer.

However, this last symmetry is trivial in our case where we are restricted to fixed atomic positions and p_z orbitals. This is especially flagrant when considering the effective tight-binding hamiltonian (electronic or excitonic), which is purely planar, so that all representations that are odd under the horizontal mirror symmetry[23] are frustrated (only the zero vector transforms according to them, i.e. there are no corresponding eigenstates).

It is therefore very convenient to disregard this horizontal mirror, i.e. to

[23]There is a matter of convention here that we should clarify: when we say that we move to the tight-binding picture, and that the problem is planar, we mean that the $|\Psi\rangle$ are effectively a collection of scalars $\{\Psi_{\mathbf{R}}\}$ attached to the $\mathbf{R}$-points of Λ, which is planar. In this context, all states that transform oddly under the σ_h mirror must be zero.

$\mathbf{C_{3v}}$	E	$2C_3(z)$	$3\sigma_v$
A_1	1	1	1
A_2	1	1	-1
E	2	-1	0

Table 4.3: Character table of the point group C_{3v},[71] the "effective" point group of single layer hBN (see text).

work only with the planar symmetries of the system. The corresponding point group is then the subgroup C_{3v} of D_{3h}, i.e. the point group of the triangle. As it will be useful to our discussion, we partially reproduce the character table of C_{3v} in table 4.3.

Within the C_{3v} point group description, group theoretical arguments mandate that only E states can be bright. We will recover this result through a direct calculation of the matrix elements of momentum in the excitonic tight-binding formalism, which will also yield the associated oscillator strength.

Let us recall the expression of optical matrix elements within the excitonic tight-binding model. In analogy with the chain case, we have, for a direct eigenstate $|\Psi\rangle = \sum_{\mathbf{R}\in\Lambda} \Psi_{\mathbf{R}} |R\rangle$:

$$\langle\emptyset|\hat{\mathbf{p}}|\Psi\rangle = -\frac{m_e\sqrt{N}}{i\hbar} \underbrace{\sum_{\mathbf{R}\in\Lambda} t_{\mathbf{R}}\Psi_{\mathbf{R}}\mathbf{R}}_{\mathbf{d}_\Psi} \tag{4.16}$$

once again proportional to the wavefunction dipole $\mathbf{d}_\Psi$, which here reads simply:

$$\mathbf{d}_\Psi = t_\perp \sum_{\boldsymbol{\tau}} \Psi_{\boldsymbol{\tau}}\boldsymbol{\tau}$$

It is at once clear that, within our approximations, the system cannot respond to light polarized out of plane: because Λ is planar, so is $\mathbf{d}_\Psi$. *Ab initio* calculations appear to confirm this:[72] when computing the spectrum for hBN computedlight polarized perpendicular to the plane, the system responds only at very high energies,[24] and there is no absorption at the energies we are probing.

More precise selection rules can be extracted from equation 4.16 through the possible symmetries of the eigenstates, as summarized in table 4.3. The case of the one dimensional representations is particularly simple. We note

[24]This response, in addition to being difficult to measure in practice, is expected be weak compared to the response from light polarized in-plane, precisely because of the quasi two-dimensional geometry of the real system.

immediately that, if Ψ transforms as A_1, then the state is fully symmetric and $\Psi_{\boldsymbol{\tau}}$ is independent of $\boldsymbol{\tau}$, and so, by symmetry, $\mathbf{d}_\Psi = \mathbf{0}$. The same happens for A_2 states, which are odd with respect to the σ_v mirrors: since each $\boldsymbol{\tau}$ is left invariant by one mirror, all $\Psi_{\boldsymbol{\tau}}$ are zero, and so $\mathbf{d}_\Psi = \mathbf{0}$. Thus, all states transforming according to one of the one dimensional representations are dark.

The case of the E states is more interesting: they are the only ones that can be optically bright. Because the representation E is of dimension two, states transforming according to it come within eigensubspaces of dimension two. To compute the optical matrix element for a given state, it is therefore useful to give ourselves a basis.[25] A convenient choice is to remark that, since the rotation C_3 commutes with the hamiltonian, we can always find a basis whose elements are also eigenstates of C_3. We will discuss this problem further in section 4.4.2, but for now it is enough to note that we can always find a basis $\{\Psi^+, \Psi^-\}$ of an E subspace such that:

$$\forall \mathbf{R} \in \Lambda, \quad \hat{C}_3 \Psi^\pm_{\mathbf{R}} = \omega_\mp \Psi^\pm_{(C_3\mathbf{R})}$$

where $\omega_\pm = e^{\pm\frac{2i\pi}{3}}$. It follows that we can choose $\{\Psi^+, \Psi^-\}$ in such a way that there exists a common amplitude C_Ψ such that $\Psi^\pm_{\boldsymbol{\tau}_\alpha} = \omega_\pm^{\alpha-1} C_\Psi$, and therefore the corresponding dipoles are given by:

$$\mathbf{d}_\Psi = \mp\frac{3}{2} i\tau t_\perp C_\Psi (\mathbf{e}_x \pm i\mathbf{e}_y) \tag{4.17}$$

we see therefore that the components of this basis respond to circularly polarized light, in analogy with the situation in single layer transition metal dichalcogenides, which have a similar C_3 symmetry.[64] Indeed, if the in-plane polarization of the incoming light is decomposed in a circular basis:

$$\mathbf{e} = \frac{e_+}{\sqrt{2}} \begin{pmatrix} 1 \\ i \end{pmatrix} + \frac{e_-}{\sqrt{2}} \begin{pmatrix} 1 \\ -i \end{pmatrix}$$

then we have:

$$\mathbf{e} \cdot \mathbf{d}_{\Psi_\pm} = \mp\frac{3}{2} i\tau t_\perp C_\Psi e_\pm$$

and the oscillator strength associated to the E subspace under consideration is such that:

$$f \propto \left|\mathbf{e} \cdot \mathbf{d}_{\Psi_+}\right|^2 + \left|\mathbf{e} \cdot \mathbf{d}_{\Psi_-}\right|^2 \propto \|\mathbf{e}\|^2 |C_\Psi|^2 \tag{4.18}$$

[25] Note that the optical matrix element for a single state within a degenerate subspace is *a priori* not a meaningful quantity, since it depends on our choice of basis for that subspace: what *is* basis independent is the sum of the oscillator strengths of the basis states. However, it is still useful to choose a basis in order to perform calculations.

which is independent of the direction of in-plane polarization, a well known property of hexagonal systems. As in the case of the chain, we recover our result that the oscillator strength of a bright exciton is proportional to its intensity on the nearest neighbor excitations. Note that this statement now has a precise, basis independent meaning: $|C_\Psi|^2$ is a characteristic of the eigensubspace (informally, of the "exciton"), not of a single eigenstate. If one constructs the (normalized) density associated to the eigensubspace, which by Born's rule is $\left(|\Psi_a|^2 + |\Psi_b|^2\right)/2$ for *any* basis $\{\Psi_a, \Psi_b\}$, then the density on each τ will be $|C_\Psi|^2$.[26]

Strong potential approximation, lowest bound state

Before diagonalizing the full excitonic hamiltonian, it is interesting to examine a simple approximation, in order to develop some intuition about the behavior of the model. Noting that the direct potential is essentially a decreasing (in absolute value) function of $R = \|\mathbf{R}\|$, we may imagine that, if the potential is particularly strong, this monotonous decay will be sharp enough that the excitations corresponding to the shortest Rs will be essentially decoupled from the rest of the lattice of excitations.[27] These excitations are precisely those where $\mathbf{R}$ is a nitrogen to boron nearest neighbor vector (one of the $\boldsymbol{\tau}$s), and can then be treated independently from the rest of the system to obtain an approximation to the lowest bound state.

We may also picture this approximation as considering the direct potential as being so strong that the electron and the hole *must* remain nearest neighbors for the lowest bound excitons: then, the lattice of excitations reduces to the states such that $\mathbf{R} \in \{\boldsymbol{\tau}_1, \boldsymbol{\tau}_2, \boldsymbol{\tau}_3\}$. Another way to describe this approximation formally is by writing:

$$U_{\mathbf{R}} \approx \begin{cases} U & \text{if } \|\mathbf{R}\| = \tau \\ +\infty & \text{otherwise} \end{cases}$$

For the reasons outlined above, we call this approximation the "strong potential approximation". It is arguably the simplest possible approximation for our problem that retains the symmetries of the system, and the opposite of the Wannier limit discussed in section 4.4.1 (which could be thought of as

[26] Taking a step back, f could not physically depend on a choice of basis, since it is (indirectly) observable through the absorption spectrum.

[27] In more precise terms, this amounts to the condition that $|V(\tau) - V(\mu)| \gg T$ (where τ is the B-N 1n.n. distance and $\mu = a = \sqrt{3}\tau$ is the 2n.n. distance): the difference in onsites between the first shell of constant R and the other excitations is so large that the kinetic couplings between them are negligible.

the "weak potential approximation"). Under these conditions, the excitonic hamiltonian reduces to:

$$\hat{H}_X = (2\Delta + 3T + U)\mathbb{1} + T \sum_{\boldsymbol{\tau} \neq \boldsymbol{\tau}'} |\boldsymbol{\tau}\rangle\langle\boldsymbol{\tau}'|$$

Which is in fact just a simple LCAO hamiltonian for a triangular molecule. Pleasantly, this Hamiltonian has almost no "true" dependence on its parameters: we do not need to know the model for the potential, or even its value U on the first shell, nor do we need to know the exact value of T, as all of these only result in shifts and rescalings of the energy scale. It is only useful to know the sign of T, and by definition in first nearest neighbors, $T = \frac{t_1^2}{\Delta} > 0$. In matrix form, it reads:

$$H_X = (2\Delta + 3T + U)I_3 + T \begin{pmatrix} 0 & 1 & 1 \\ 1 & 0 & 1 \\ 1 & 1 & 0 \end{pmatrix}$$

in the $\{|\boldsymbol{\tau}_1\rangle, |\boldsymbol{\tau}_2\rangle, |\boldsymbol{\tau}_3\rangle\}$ basis. It has two eigenvalues:

$$E_{A_1} = 2\Delta + 3T + U + 2T$$
$$E_E = 2\Delta + 3T + U - T$$

The latter of which is twice degenerate. Let us briefly comment about the first eigensubspace. It is of dimension one, and spanned by:

$$\Psi_{A_1} = \frac{1}{\sqrt{3}} \begin{pmatrix} 1 \\ 1 \\ 1 \end{pmatrix}$$

which clearly transforms according to the fully symmetric A_1 representation, and thus is dark. Being $3T$ in energy higher than the other eigensubspace, we don't expect it to provide a particularly accurate picture of a state of the full system, except as a qualitative prototype of an A_1 state.[28]

The second eigensubspace, which we shall call $\mathcal{E}$, is much more interesting. It is the lowest energy eigensubspace in this low-energy approximation, and so we expect it to be a qualitative model for the lowest bound exciton. It is of dimension two,[29] from which it immediately follows[30] that it transforms

[28] What is remarkable, however is that this state is non degenerate: in the hydrogenoïd limit, this could not occur. The discussion of why this happens here is delicate within the confines of this simple approximation, so we leave it for later.

[29] More precisely, here, it is the (hyper)plane of equation $\Psi_{\boldsymbol{\tau}_1} + \Psi_{\boldsymbol{\tau}_2} + \Psi_{\boldsymbol{\tau}_3} = 0$.

[30] Barring a possible accidental degeneracy, which the following will show is not the case.

according to the E representation, and therefore is bright. As a doubly degenerate lowest lying bright state, it appears as an analogue of the $1s$ state found in the Wannier limit. We will show later that this analogy can be made more precise.

We thus expect the lowest lying exciton of our system to be twice degenerate and bright (which it indeed is). This degeneracy, which will be shared by all bright states, since they must transform according to the E representation, leaves us with the following question: is there a natural way to choose a basis for an eigensubspace associated to the E representation (and therefore of dimension two)?

Of course, since the subspace is of dimension two, there are infinitely many possible choices of basis. However, two classes of basis stand out as "natural". Indeed, our system has the C_{3v} symmetry, and therefore commutes with the symmetry operators associated to the three vertical mirrors, σ_v, and with the rotation of angle $\frac{2\pi}{3}$, C_3. The usual results on simultaneous diagonalization therefore ensure that any E eigensubspace admits a basis composed of eigenstates of one of the system's symmetry operators.[31] Let us now examine these two choices.

Let us start with the mirrors. Without loss of generality, we work with σ_1, the mirror which lets $\boldsymbol{\tau}_1$ invariant. It has two eigenvalues, $+1$ and -1, and we will therefore obtain a basis with definite parity with respect to σ_1. Up to a global multiplicative factor, we find the following basis vectors for $\mathcal{E}$:

$$\Psi_+ = \sqrt{\frac{2}{3}} \begin{pmatrix} 1 \\ -\frac{1}{2} \\ -\frac{1}{2} \end{pmatrix} \qquad ; \qquad \Psi_- = \frac{1}{\sqrt{2}} \begin{pmatrix} 0 \\ 1 \\ -1 \end{pmatrix}$$

with $\hat{\sigma}_1 \Psi_\pm = \pm \Psi_\pm$. This choice has the advantage of resulting in a real basis. However, it is somewhat tainted by the choice one has to make of a given mirror, and the densities of the basis states do not have the symmetry of the crystal.[32]

Let us now consider the rotations. A first fact should retain our attention: rotations of angle $\frac{2\pi}{3}$ are not diagonalizable in $\mathbb{R}$. We will therefore have to move to $\mathbb{C}$. This is not a fundamental problem, however, and a basis of $\mathcal{E}$

[31] But not all at the same time: this is not possible for E eigensubspaces, essentially because C_{3v} is not abelian. All other eigensubspaces, which are nondegenerate, do however enjoy this property.

[32] Which they certainly *need* not have.

which is also an eigenbasis of C_3 is given by:[33]

$$\Psi_+ = \frac{1}{\sqrt{3}} \begin{pmatrix} 1 \\ \omega \\ \omega^2 \end{pmatrix} \qquad ; \qquad \Psi_- = {\Psi_+}^* = \frac{1}{\sqrt{3}} \begin{pmatrix} 1 \\ \omega^* \\ \omega^{*2} \end{pmatrix}$$

where $\omega = e^{\frac{2i\pi}{3}}$[34] and $\hat{C}_3 \Psi_\pm = e^{\mp \frac{2i\pi}{3}} \Psi_\pm$. This is the basis we used in section 4.4.2 to analyse oscillator strengths. The obvious disadvantage of such a choice is that is leads to a complex basis. On the other hand, it enjoys several advantages, the first of which being that it does not set a preferred direction. Further, since $\Psi_- = {\Psi_+}^*$, the two states are in fact connected by time-reversal symmetry.

An important property of this basis, related to the above, appears when moving to reciprocal space. This is done through the change of basis formula:

$$\Psi(\mathbf{k}) = \frac{1}{\sqrt{N}} \sum_{\boldsymbol{\tau}} e^{i\mathbf{k}\cdot\boldsymbol{\tau}} \Psi_{\boldsymbol{\tau}}$$

which yields the remarkable result:

$$\Psi_\pm(\mathbf{k}) = \frac{1}{\sqrt{3N}} \gamma_1(\pm\mathbf{K} - \mathbf{k})$$

or, since $-\mathbf{K}$ is a $\mathbf{K}'$ point:

$$\Psi_+(\mathbf{k}) \propto \gamma_1(\mathbf{K} - \mathbf{k}) \qquad ; \qquad \Psi_-(\mathbf{k}) \propto \gamma_1(\mathbf{K}' - \mathbf{k})$$

and so this choice of basis effectively filters the contributions from the $\mathbf{K}$ and $\mathbf{K}'$ valleys.[35] This also means, by equation 4.17, that polarized light excites selectively one of the two valleys, a fact that has been used to great effect in transition metal dichalcogenides.[64] Because of its properties, we call a basis of this kind a *chiral* basis. We depict these reciprocal space wavefunctions in figure 4.16. To represent the complex amplitudes, we have chosen a representation such that color indicates phase, while the transparency of each pixel is a function of the density ($|\Psi(\mathbf{k})|^2$) at this point. This representation allows us to convey information about the phase of the wavefunction, which we will see carries useful information both in direct and in reciprocal space when it comes to understanding the symmetries of a given state.

[33] Note that here, we do not have to choose one of the two rotations: they commute.

[34] We could have chosen any third root of unity different from one ($\omega = 1$ results in Ψ_{A_1}), but note that these are 1, ω and $\omega^2 = \omega^*$, so this would only exchange Ψ_+ and Ψ_-.

[35] Indeed, recall that $|\gamma_1(\mathbf{k})|$ is maximal in $\mathbf{\Gamma}$, and vanishes at $\mathbf{K}$ and $\mathbf{K}'$. Then, by geometry of the first Brillouin zone, note that for any pair of $\mathbf{K}$, $\mathbf{K}'$ points, their difference is a $\mathbf{K}$ or $\mathbf{K}'$ point, while the difference of two $\mathbf{K}$ (resp. $\mathbf{K}'$) points yields a $\mathbf{\Gamma}$ point (possibly outside of the first Brillouin zone).

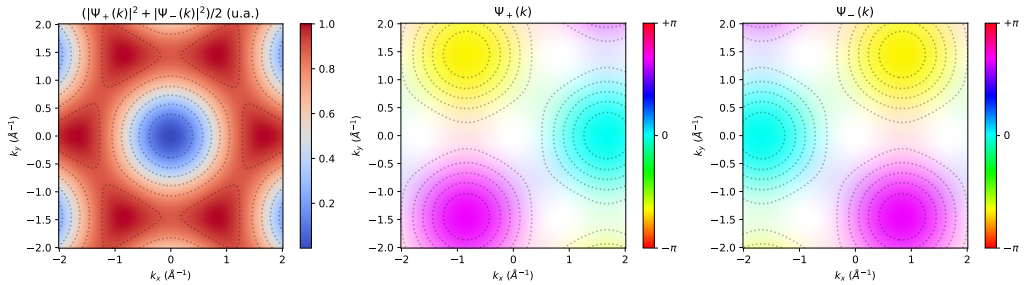

Figure 4.16: Reciprocal space wavefunctions for the lowest bound state in the strong potential approximation. Left panel: total exciton density. Middle and right panels: chiral basis wavefunctions $\Psi_+(\mathbf{k})$ and $\Psi_-(\mathbf{k})$ (resp.) in the density-phase representation (density controls transparency, while color indicates phase). Dotted lines are contour levels for the density, which have been added for lisibility.

In general, i.e. even away from the strong potential approximation, there is a simple link between the two bases:

$$\begin{pmatrix} \Psi_+^{C_3} \\ \Psi_-^{C_3} \end{pmatrix} = \frac{1}{\sqrt{2}} \begin{pmatrix} 1 & i \\ 1 & -i \end{pmatrix} \begin{pmatrix} \Psi_+^{\sigma_1} \\ \Psi_-^{\sigma_1} \end{pmatrix}$$

which is useful because the σ_1 basis, being real, is easier to construct from an arbitrary basis (as is typically obtained from a numerical diagonalization). This therefore provides a simple way to construct a polarized basis from a numerical diagonalization of $\hat{H}_X$.

We end this section with a note about the A_2 representation: we found no eigenvector transforming according to it in the strong potential approximation. This is because, there, this representation is frustrated: states transforming as A_2 must be odd relative to the σ_v mirrors, but since each $\boldsymbol{\tau}$ is left invariant by at least one mirror the only possible "A_2 state" is zero.

Higher excited states

Having now an idea of what to expect from our excitonic TB model, and a model for the lowest bound state, we are in position to diagonalize the full hamiltonian $\hat{H}_X$ numerically.[36] For direct states, in first nearest neighbors,

[36] Of course, we could have done it directly without passing through the limiting cases, but the analytical insights that we gathered go hand in hand with the numerical calculation.

this hamiltonian reads:

$$\langle \mathbf{R}|\hat{H}_X|\mathbf{R}'\rangle = \begin{cases} 2\Delta + 3T + V(R) & \text{if } \mathbf{R} = \mathbf{R}' \\ T & \text{if } \mathbf{R}, \mathbf{R}' \text{ are 1n.n. in } \Lambda \\ 0 & \text{otherwise} \end{cases} \tag{4.19}$$

where $T = \frac{t_\perp^2}{\Delta}$. *A priori*, it depends on three parameters: two kinetic parameters, which we can choose to be either $(\Delta, t_\perp)$ or (Δ, T), and one potential parameter, the polarizability radius r_0.[37] However, 2Δ is the value of the direct gap, and only a global energy shift, so we can redefine the energy scale by choosing 2Δ as its zero: the eigenenergies of $\hat{H}_X$ will the be the excitonic binding energies: $E_b = E - E_{gap}$. In this case, we only have two effective parameters: the effective hopping between excitations, T, which controls the kinetic energy scale, and the polarizability radius, r_0, which controls V, and therefore the electron-hole binding potential. In this context, we note that we could non-dimensionalize the problem: we could choose T as an energy scale, τ or a as a unit of length, and, the functional form of the potential being fixed, the problem would depend only one one dimensionless parameter, say $\upsilon = U_{\boldsymbol{\tau}}/T$. Since we discuss here the specific case of hBN and intend to fit on *ab initio* data, we instead remain in "conventional" units.

The question at hand is therefore that of determining these parameters. The kinetic parameters can be naturally estimated from a fit of the band structure. If we fix Δ to reproduce the correct value of the gap, we can fit $t_\perp$ to reproduce the band energies (or the transition energies) as well as possible in the regions of the Brillouin zone which will contribute the most to the excitons we want to study, i.e. the **MK** region. This is the spirit of the "1n.n. local fit" displayed in table 4.1. Using these parameters, we estimate $2\Delta = 7.25$ eV (the gap) and $T = 1.46$ eV.

It remains to estimate r_0, which amounts to estimating the screening of our crystal. In theory, this can be done through a DFT calculation using a generalized Clausius-Mossotti relation, as demonstrated in [61]. It is also possible to directly compute the (macroscopic) static dielectric function $\epsilon(q)$ *ab initio* and fit its small q (long range) part with the corresponding Rytova-Keldysh expression, $\epsilon_{RK}(q) = 1 + r_0 q$.[74, 75] Such estimates in the literature place r_0 for hBN at approximately $6 - 7$ Å.[74, 76]

[37] Technically, the evaluation of the potential $V(R)$ also depends on the lattice constant, a through the coordinates of the elementary excitation sites, and requiring compatibility with r_0 (whose fitted value therefore depends on our value for a) and $e^2 \approx 14.4$ eV.Å (which has dimension of energy times length in our unit system). Working here in Angstrom for concreteness, we have, in consistency with the *ab initio* calculations, set a to the optimized bulk value $a = 2.5$ Å.[73] On the other hand, distances do not appear explicitly in the kinetic part of $\hat{H}_X$.

Here, we take a different approach: since we can write and diagonalize $\hat{H}_X$ without actually knowing the band structure of the system, we can fit our two parameters, T and r_0, directly on the *ab initio* binding energies, without intermediaries. We do so by fitting the first four *ab initio* binding energies,[38] and obtain best fit parameters of:

$$T = 1.5 \text{ eV} \quad ; \quad r_0 = 10 \text{ Å} \tag{4.20}$$

from which the values of the electronic kinetic parameters can be extracted through the knowledge of the *ab initio* gap, $2\Delta = 7.25$ eV, whence $t_\perp = 2.33$ eV. We therefore obtain excellent agreement with the kinetic parameters estimated from the band structure. While the agreement with estimated values for the polarizability radius is less satisfying, we must keep in mind that we are fitting a model continuous potential on a discrete system where we expect lattice effects to be relevant. In this light, and considering the approximations we have made in deriving our expression for the potential, the order of magnitude agreement that we obtain remains acceptable. In any event, since our model is constrained by the correct crystal symmetries, we do not expect exact values of the parameters to qualitatively influence our results for the lowest bound states overmuch.

We will use the parameters of equation 4.20 from now on. The binding energies obtained by the diagonalization of $\hat{H}_X$ with this set of parameters are reported in table 4.4, along with the corresponding *ab initio* binding energies, with and without exchange interaction. We find excellent agreement of the model values with the reference *ab initio* data, although we do not exactly reproduce the *ab initio* order of states, essentially due to an overbinding of the fourth state (A_1), which will be discussed later. To avoid confusion, we shall use the *ab initio* state order when labeling the eigensubspaces.

The excitonic wavefunctions are represented in figure 4.17. Again, we obtain a satisfying agreement between *ab initio* and tight-binding. In particular, in tight-binding, we have represented both the intensities and the amplitudes of the excitonic wavefunctions. This lets us easily classify the different states according to the symmetries of the system's point group. First, all doubly degenerate states, i.e. excitons 1, 2 and 5, are likely[39] E states, which the tight-binding amplitudes confirm. Excitons 3 and 4 then belong to representations of dimension one: we need only find which. Since A_2 states transform oddly under the σ_v mirrors, this strongly hints at the

[38] Not counting degeneracies: the target values for the fitting were the first four columns of the "*Ab initio*" line of table 4.4.

[39] Only "likely" at this point because we cannot *a priori* exclude an accidental degeneracy.

Exciton	1 (×2)	2 (×2)	3	4	5 (×2)
Ab initio	−1.932	−1.076	−1.045	−0.980	−0.892
Ab initio (no exchange)	−2.018	−1.095	−1.045	−1.358	−0.898
Tight binding	−1.932	−1.053	−0.999	−1.0944	−0.830
Symmetry	E	E	A_2	A_1	E

Table 4.4: Binding energies and symmetries for the first five excitons for hBN, in the order fixed by the full *ab initio* calculation (first line). Binding energies are given in eV, and degeneracies are reported in parenthesis. Symmetries are given in terms of the irreducible representations of the C_{3v} point group, and are extracted from the *ab initio* and tight binding wave functions. *Ab initio* calculations by F. Paleari.[47] The tight-binding calculations used a box of $\sim 10^3$ sites, whuth the potential cut off after the 28^{th} R-shell.

fact that the state 3 transforms like A_2, as it displays zero intensity on the sites along the σ_v planes. Again, this is confirmed by the tight-binding amplitudes. State 4, which does display intensity along these mirror planes, can then only be A_1, which the tight-binding amplitudes also confirm.

Having identified and matched the *ab initio* and tight-binding states, let us proceed with a global analysis. We can identify three bright subspaces: excitons 1, 2 and 5. It is tempting, and, indeed, interesting, to compare the results of the tight binding model, in table 4.4, with the results of the Wannier model, in table 4.2. A naive comparison of binding energies[40] hints at the fact that excitons 1 and 5 are respectively the $1s$ and $2s$ Wannier excitons. Both are twice degenerate and bright, as is expected from s-like states. This leaves states 2, 3 and 4. All three are clustered around a binding energy of about -1 eV, which hints that they are descended from the $2p$ Wannier subspace, whose fourfold degeneracy was thus lifted into $2 \oplus 1 \oplus 1$ by the now accounted for lattice effects.[41] Interestingly, state 2 belongs to the E representation, and thus is bright, even though it comes from a p subspace whose brightness was forbidden in the hydrogenoïd model. This directly illustrates the importance of the change of selection rules when lowering the symmetry of the system through the inclusion of lattice effects.

Exciton 4 still appears to stand out: in tight-binding, it is found below states 2 and 3, while it is above *ab initio*. This fact is illuminated when considering the effects of the exchange interaction. When it is removed from

[40] The following sections will show that this energy comparison, while naive, does in fact provide the right picture.

[41] It is, in fact, possible to make a more precise analysis of the splitting of the $2p$ subspace. Details can be found in [47].

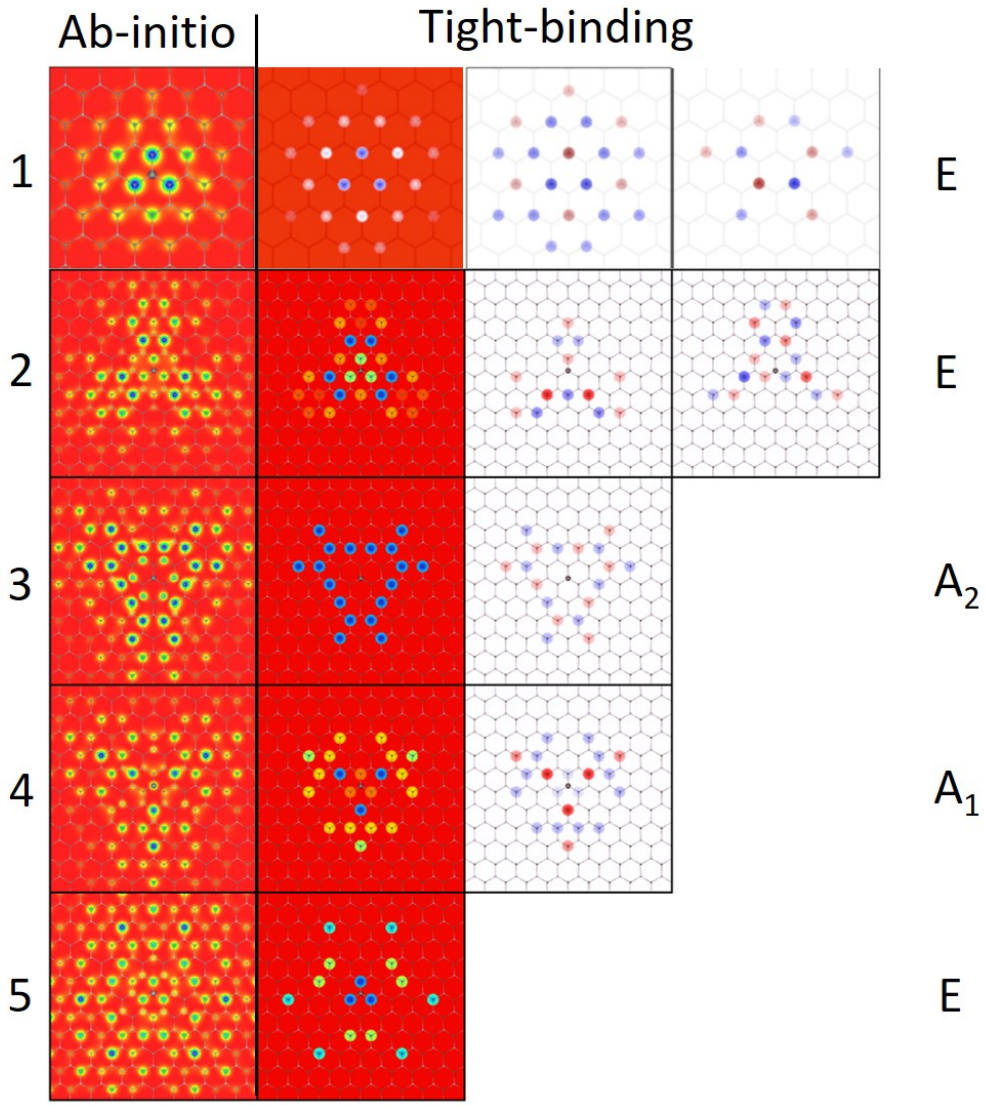

Figure 4.17: Figure adapted from [47]. Direct space excitonic wavefunctions for single layer hBN. Left: *ab initio* densities. Right: tight-binding densities (red background) and amplitudes in the density-phase representation (transparency is proportional to the density while color depicts the phases: red is opposite to blue). The dark grey dot materializes the position of the hole. A real basis has been chosen to depict the tight-binding amplitudes; in particular, we have chosen a basis of definite parity with respect to the σ_1 miror plane (in-plane, the vertical line passing through the hole) for the twice degenerate E subspaces (see section 4.4.2).

the *ab initio* calculation, the binding energy of state 4 is strongly increased, and it falls below states 2 and 3, as can be seen in table 4.4. The effects of exchange on other states is much less important. This peculiarity can be explained by the symmetry of state 4: of the states under investigation, it is the only one which transforms under the fully-symmetric A_1 representation. This means in particular that it is not forbidden for it to have electronic intensity at the "origin", i.e. at the "position of the hole", which indeed it does. Recalling now the expression of the exchange integrals, we note that they are maximized when the electron and the hole wavefunctions overlap, i.e. precisely at the origin of the relative coordinates. The effect of the exchange interaction is therefore maximal for A_1 states, as we observe. Since this interaction is overall repulsive, it shifts exciton 4 up in energy above exciton 2 and 3. The different ordering of states between *ab initio* and tight-binding then stems at least in part from the fact the tight-binding model neglects the exchange interaction. The fact that the error in energy is not so great compared to the *ab initio* results with exchange can be traced back to the fact that the tight-binding model also neglects the effects of electron-hole wavefunctions overlap for the *direct* interaction, which is attractive. This is discussed in more details in appendix C of [47].

The splitting scheme discussed above is summarized in figure 4.18. We started with two (one for $\mathbf{K}$, one for $\mathbf{K}'$) uncoupled systems of cylinder symmetry. At the Coulomb level, an additional symmetry caused the degeneracy of all states with the same principal quantum number. This symmetry was then broken by moving to the more realistic Rytova-Keldysh potential, which physically corresponds to the inclusion of a realistic $2D$ screening. This caused the splitting of the s and p states. The inclusion of lattice effects then transitioned us to one single system of triangular symmetry: they have effectively coupled the two hydrogenoïd equations, and in lowering the symmetry, have generated further splittings.

4.4.3 Momentum space representation and link with the hydrogenoid classification

General remarks

In this section, we will move back to reciprocal space. This will allow us to make our discussion of splittings more precise by linking our tight-binding states to the Wannier model states computed earlier. In addition, this will let us verify that the composition of our excitons in terms of electronic transitions is indeed essentially from the **MK** region.

For the tight-binding states, the transition from **R**-space to **k**-space is

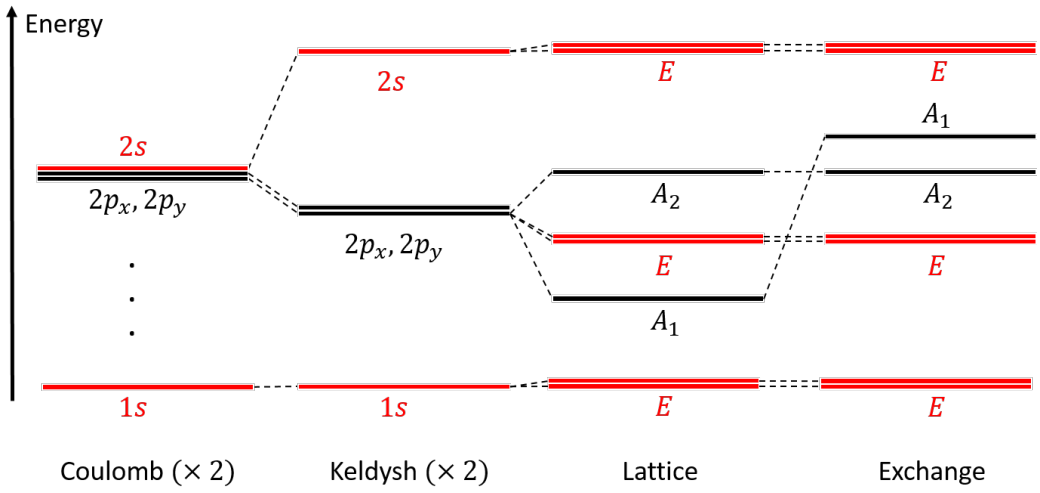

Figure 4.18: Schematic splitting of excitonic states from the hydrogenoïd model with Coulomb and Rytova-Keldysh potential to the tight-binding and *ab initio* descriptions, which include lattice effects (energies are not to scale). States from the "Coulomb" and "Rytova-Keldysh" columns are to be doubled: as explained in the text, there is one hydrogenoïd equation for $\mathbf{K}$ and one for $\mathbf{K}'$. Bright states according the the current model are in red, while dark states are in black.

done through the usual change of basis formula:

$$\Psi(\mathbf{k}) \propto \Psi_{\mathbf{k}} = \frac{1}{\sqrt{N}} \sum_{\mathbf{R}\in\Lambda} e^{i\mathbf{k}\cdot\mathbf{R}} \Psi_{\mathbf{R}} \tag{4.21}$$

while the *ab initio* states are naturally computed in reciprocal space. The results of this calculation are presented in figure 4.19. Again, we are representing the tight-binding densities and amplitudes, using the density-phase representation introduced earlier. For E states, we have used a chiral basis, for reasons that shall become clear later.

It is at once clear that excitons 1 and 5 are of the same nature, while excitons 2, 3, 4 belong to a different group. This can already be seen from the densities alone, by the fact that excitons 1 and 5 have their maxima at $\mathbf{K}/\mathbf{K}'$, while excitons 2, 3, 4 instead have vanishing (or low in the case of 2) intensity there. The corresponding phases reinforce this notion: the states we have labeled as s-type have constant phases around given $\mathbf{K}/\mathbf{K}'$ points, while in the case of the supposed p-type states, the phase rotates by 2π while going around a given $\mathbf{K}/\mathbf{K}'$ point.

It can be checked as well that, for E states, the use of a chiral basis indeed filters the contribution of the $\mathbf{K}$ and $\mathbf{K}'$ points, although this filtering is only clear in the case of the two s states: while some remarkable separation of the contributions is also achieved there, the E state of p type shows a more complex behavior that we will discuss later. Non-degenerate states, as expected from (time reversal) symmetry, display contributions from both $\mathbf{K}$ and $\mathbf{K}'$. Overall exciton intensities (so, the summed intensities of the basis states of a subspace) appear to display a hexagonal symmetry. This is a consequence of the C_3 symmetry of the lattice along with the time reversal symmetry which maps $\mathbf{k}$ onto $-\mathbf{k}$ and thus creates this *apparent* sixfold symmetry.

Analysis of these intensities confirms that the lowest bound excitonic states are indeed composed mostly of transitions in the neighborhood of $\mathbf{K}/\mathbf{K}'$, although contributions from the $\mathbf{MK}$ lines are also notable. This confirms that the these are indeed the regions of interest, which support the system's "main" optical activity. Trigonal warping is very noticeable, both in tight-binding and *ab initio*, although even moreso in the latter. This shows indirectly the importance of the actual triangular geometry of the system.

Finally, we can check quite clearly on the s-type states that as we go higher in energy in a series of excitons of same character, and the direct space wavefunctions become more spread in the relative coordinate $\mathbf{R}$, the corresponding reciprocal-space wavefunctions become more localized in $\mathbf{k}$.

This is a good time to remark that, for the lowest bound state, the results of the "full calculations" actually display features from both the Wannier (low

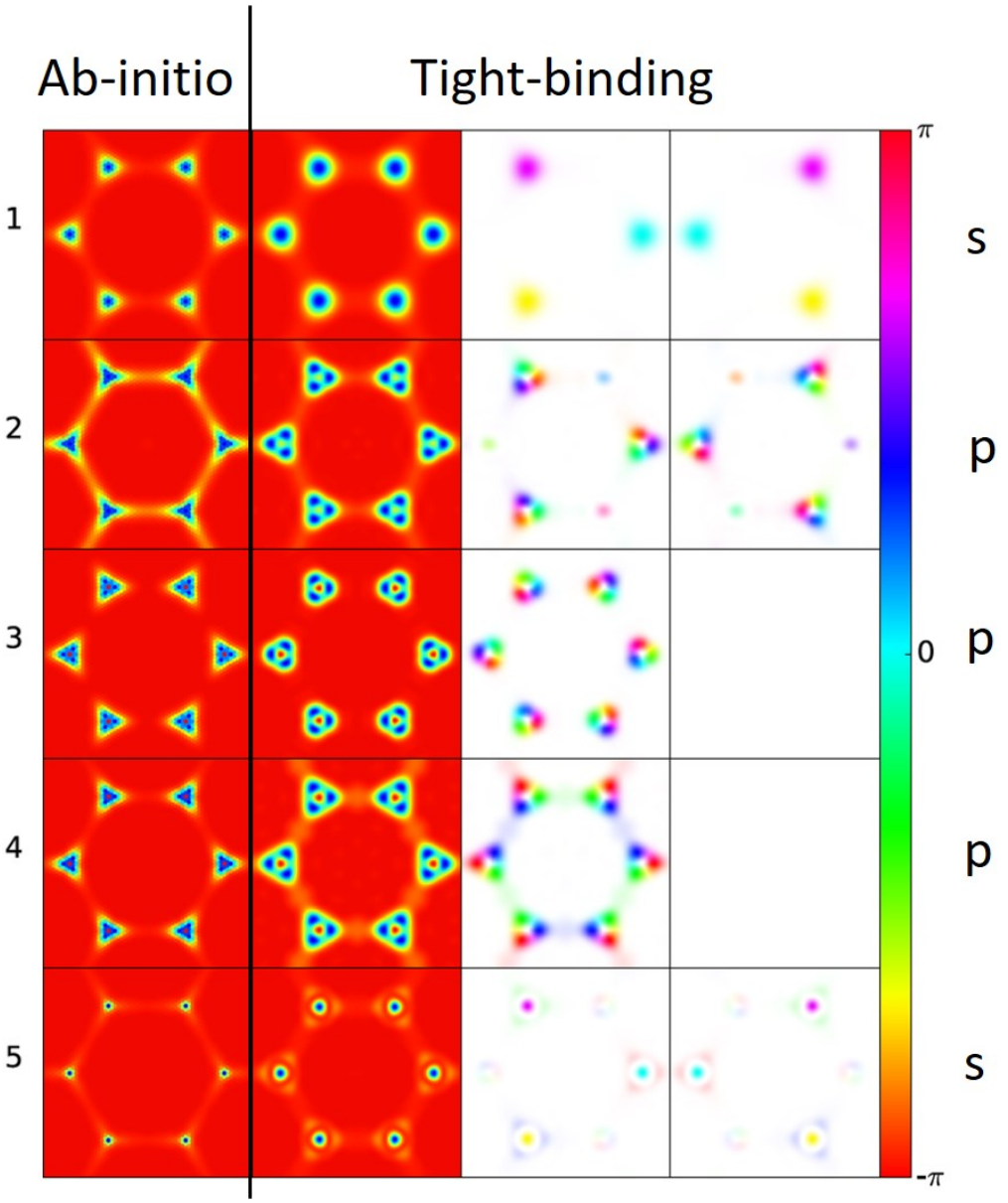

Figure 4.19: Figure adapted from [47]. Reciprocal space excitonic wavefunctions for single layer hBN. Left: *ab initio* densities. Right: tight-binding densities (red background) and amplitudes in the density-phase representation (color depicts the phases while transparency is proportional to the density $|\Psi(\mathbf{k})|^2$).

potential) limit, which will be discussed further below, and from the strong potential limit. In particular, the reciprocal space intensities in the strong potential limit display strong intensities along **MK**, i.e. extreme trigonal warping, which is by nature absent in the effective mass approximation. This can be understood from the fact that in the strong potential limit, the system is just a triangle: lattice effects are therefore at their strongest, and so is trigonal warping. In the real system, the excitonic wavefunctions are more extended, but not so much that lattice effects are washed out and vanish.

Connection with the Wannier formalism

Many of the behaviors discussed above can be rationalized if we recall the construction of excitonic wavefunctions in the Wannier model.[42] For a given transition energy minmum at a point, $\mathbf{k}_0$, the excitonic wavefunction $\Psi(\mathbf{k})$ is Fourier transformed into a "real-space" wavefunction in the relative coordinate:

$$\Psi(\mathbf{r}) = e^{-i\mathbf{k}_0\cdot\mathbf{r}} g(\mathbf{r}) \tag{4.22}$$

this function $g(\mathbf{r})$ is then the one which is found as the solution of the hydrogenoïd equation (equation 4.12). The s, p, ... nomenclature thus describes the symmetries of g. The function g itself, owing to the polar symmetry of the system can be decomposed into an angular and a radial part:

$$g(\mathbf{r}) = e^{im\theta}\Phi(r)$$

where $\Phi(r)$ is radial and m is the angular momentum quantum number, which is then the one containing the s, p, ... symmetry information.

We thus see that the full symmetry of the excitonic state is obtained as the product of the one of the phase factor $e^{-i\mathbf{k}_0\cdot\mathbf{r}}$, and the one of the *envelope*[43] function $g(\mathbf{r})$. For example, let us consider the $1s$ state from the hydrogenoïd equation at **K**: g_{1s} is radial, i.e. fully symmetric, while the phase factor $e^{-i\mathbf{K}\cdot\mathbf{r}}$ is chiral: the full excitonic state $\Psi_{\mathbf{K},1s}(\mathbf{r}) = e^{-i\mathbf{K}\cdot\mathbf{r}} g_{1s}(\mathbf{r})$ is therefore chiral, and transforms by multiplication by ω_- under the C_3 rotation. The corresponding $1s$ state from the $\mathbf{K}'$ valley is then $\Psi_{\mathbf{K}',1s}(\mathbf{r}) = e^{-i\mathbf{K}'\cdot\mathbf{r}} g_{1s}(\mathbf{r}) = e^{+i\mathbf{K}\cdot\mathbf{r}} g_{1s}(\mathbf{r})$, which is also chiral, but with the opposite chirality. Note that under this form, it is clear that $\Psi_{\mathbf{K},1s}$ and $\Psi_{\mathbf{K}',1s}$ are time reversal images of one another. These two degenerate chiral states combine in the full system to form an E subspace, in the C_{3v} nomenclature.

[42] The interpretation that we follow and adapt here was originally given by F. Ducastelle.

[43] Some authors call $\Psi(\mathbf{k})$ the envelope function, on account of the fact that the full excitonic state $|\Psi\rangle$ is written as $|\Psi\rangle = \sum_{\mathbf{k}} \Psi(\mathbf{k}) |\mathbf{k}, v, c\rangle$, where the $|\mathbf{k}, v, c\rangle$ are the transition states. Here, we prefer calling Ψ the excitonic wavefunction, and g the envelope wavefunction.

This analysis can be fruitfully extended to reciprocal space: to obtain the reciprocal-space excitonic wavefunction $\Psi(\mathbf{k})$ at the Wannier level, i.e. in the neighborhood of a given $\mathbf{k}_0$ point associated to the hydrogenoïd equation,[44] one simply needs - by definition - to Fourier transform $\Psi(\mathbf{r})$:[45]

$$\Psi(\mathbf{k}) \propto \int e^{i\mathbf{k}\cdot r}\Psi(\mathbf{r})d\mathbf{r} \propto \int e^{-i(\mathbf{k}_0-\mathbf{k})\cdot\mathbf{r}}g(\mathbf{r})d\mathbf{r}$$

the real-space phase factor $e^{i\mathbf{k}\cdot r}$ is nothing but a shift by $\mathbf{k}_0$ in reciprocal space; writing $\mathbf{k} = \mathbf{k_0} + \mathbf{q}$ we find:

$$\Psi(\mathbf{k}_0 + \mathbf{q}) \propto \int e^{i\mathbf{q}\cdot\mathbf{r}}g(\mathbf{r})d\mathbf{r} \tag{4.23}$$

which incidentally reasserts that g is actually the Fourier transform of $\Psi(\mathbf{k}_0 + \mathbf{q})$.

Suppose now that Ψ has an s type enveloppe, i.e. g is radial. Then, $\Psi(\mathbf{k}_0 + \mathbf{q})$ is radial in $\mathbf{q}$: its phase is constant around point $\mathbf{k}_0$, which is indeed what we observe for the states of excitons 1 and 5. We can go a bit further: since g is radial, $\Psi(\mathbf{k}_0 + \mathbf{q}) \propto \int_0^{+\infty} J_0(qr)g(r)dr$ with J_0 the Bessel function of the first kind of order zero and $q = \|\mathbf{q}\|$. Then, if the envelope is peaked at a certain radius r_c, we find that, approximately, $\Psi(\mathbf{k}_0 + \mathbf{q}) \propto J_0(r_c q)$: it is maximal at $q = 0$, i.e. at $\mathbf{k} = \mathbf{k}_0$, and decays isotropically in intensity away from it with a characteristic peak width of $1/r_c$. In the pure hydrogenoïd model, the s envelopes are not peaked (away from the origin), but if we consider the tight-binding or *ab initio* wavefunctions, then, owing to the system's geometry, it is sensible to expect r_c is at least on the order of the nearest neighbor distance, τ.

We can in fact perform a similar analysis for envelope functions of arbitrary angular quantum number m. Let indeed $g(\mathbf{r}) = e^{im\theta}\Phi(r)$; then the angular part of the integral of equation 4.23 can be computed analytically, using e.g. the Jacobi-Anger expansion.[77] We find:

$$\Psi(\mathbf{k}_0 + \mathbf{q}) \propto e^{im\theta_\mathbf{q}} \int_0^{+\infty} \Phi(r)J_m(qr)dr$$

where $\theta_\mathbf{q}$ is the angle between $\mathbf{e}_x$ and $\mathbf{q}$, and the J_m are the Bessel functions of the first kind of order m. This has two consequences: first, if $m \neq 0$, $J_m(0)$=0, so that $\Psi(\mathbf{k}_0) = 0$. In other words, for non s states, $\Psi(\mathbf{k})$ actually vanishes at the $\mathbf{K}/\mathbf{K}'$ points. This is indeed what we observe for excitons

[44] For us, $\mathbf{k}_0$ is a $\mathbf{K}$ or $\mathbf{K}'$ point.

[45] We have in fact taken the convention $\Psi(\mathbf{k}) \propto \int e^{+i\mathbf{k}\cdot r}\Psi(\mathbf{r})d\mathbf{r}$ (note the sign in the exponential) to ensure compatibility with the discrete tight-binding change of basis formula, equation 4.21, so that the latter appropriately reduces to the former in the continuum limit.

2 (very approximately), 3 and 4, both in the tight-binding and *ab initio* densities, although in the case case of exciton 2, we only have what appears to be local minimas instead. We will come back to this peculiarity later. The phase of the wavefunctions contains more information: another consequence of the above equation is that the phase of $\Psi(\mathbf{k}_0 + \mathbf{q})$ rotates by $2m\pi$ as one describes a circle of constant q in the neighborhood of $\mathbf{k}_0$. This provides a very efficient way to identify the s, p, ... character of a given state, and confirms now that excitons 1 and 5 are essentially of s character, while 2, 3 and 4 are essentially of p character. Again, if $\Phi(r)$ is peaked at a certain radius r_c, we find that, roughly, $\Psi(\mathbf{k}_0 + \mathbf{q}) \propto e^{im\theta_{\mathbf{q}}} J_m(r_c q)$.

We can push the above discussion a bit further. In figure 4.19, we can see that when moving between two equivalent $\mathbf{K}$ points, the "local" structure of the reciprocal wavefunction remains the same, up to a rotation of $\pm 2\pi/3$ of its phase, i.e. multiplication by $\omega_\pm$. Overall, this is not surprising: we have chosen chiral bases for the E states, and excitons of other symmetries are singly degenerate, so all of the states are eigenfunctions of the C_3 rotation operators, and therefore transform under rotation by multiplication by $\omega_\pm$. On the other hand, until now, our predictions based on the Wannier envelopes have remained at the level of a single $\mathbf{k}_0$ point. This is expected, since these expressions are obtained through the effective mass approximation at the vicinity of a given $\mathbf{k}_0$ point, and therefore the periodicity of the system is lost. Note that it is preserved in tight-binding: this is a consequence of the fact that our approximation for the transition energies preserves the periodicity of the system. Still, the above suggests investigating how $\Psi(\mathbf{k}_0 + \mathbf{q})$ is modified when moving from $\mathbf{k}_0$ point to an equivalent point, i.e. a point $\mathbf{k}_0 + \mathbf{G}$ where $\mathbf{G} \in \mathcal{G}$ is a reciprocal lattice vector. We will show that we can naturally recover the remark above about rotations.

To this end, let us recall the change of basis formula 4.21. After the discussion above, it is natural to inquire about the correspondance:

$$\Psi_{\mathbf{R}} \leftrightarrow \Psi(\mathbf{r})$$

where the left side is in the discrete tight-binding picture while the right side is in a continuous picture, e.g. Wannier. Assuming the Wannier form, i.e. $\Psi(\mathbf{r}) = e^{-i\mathbf{k}_0\cdot\mathbf{r}} g(\mathbf{r})$, yields:

$$\begin{aligned}\Psi_{\mathbf{k}} &\propto \sum_{\mathbf{R}\in\Lambda} e^{-i(\mathbf{k}-\mathbf{k}_0)\cdot\mathbf{R}} g(\mathbf{R}) \\ &\propto \int \underbrace{\sum_{\mathbf{R}\in\Lambda} \delta(\mathbf{r}-\mathbf{R})}_{n(\mathbf{r})} e^{-i(\mathbf{k}-\mathbf{k}_0)\cdot\mathbf{r}} g(\mathbf{r}) d\mathbf{r}\end{aligned}$$

where we have introduced the site density of the lattice of excitations, $n(\mathbf{r})$. Making use of the Poisson summation formula, and noting that $\Lambda = \mathcal{R} + \boldsymbol{\tau}$, i.e. that the lattice of excitations is just the triangular Bravais lattice of hBN shifted by a nearest neighbor vector, we have $n(\mathbf{r}) \propto \sum_{\mathbf{G}\in\mathcal{G}} e^{i\mathbf{G}\cdot(\mathbf{r}-\boldsymbol{\tau})}$, and therefore:[46]

$$\Psi_{\mathbf{k}} \propto \sum_{\mathbf{G}\in\mathcal{G}} e^{-i\mathbf{G}\cdot\boldsymbol{\tau}} \underbrace{\int e^{-i(\mathbf{k}_0-\mathbf{G}-\mathbf{k})\cdot\mathbf{r}} g(\mathbf{r}) d\mathbf{r}}_{I_{\mathbf{G}}(\mathbf{k})}$$

where the inner integrals all reduce to the one of equation 4.23 with the substitution $\mathbf{k}_0 \leftarrow \mathbf{k}_0 - \mathbf{G}$. In particular, if $\mathbf{k} \approx \mathbf{k}_0 - \mathbf{G}_0$ for a certain $\mathbf{G}_0$, i.e. we are in the neighborhood of a point equivalent to $\mathbf{k}_0$, we can perform a macroscopic approximation and neglect all $I_{\mathbf{G}}(\mathbf{k})$ for which $\mathbf{G} \neq \mathbf{G}_0$,[47] and we find:

$$\Psi_{\mathbf{k}_0-\mathbf{G}_0+\mathbf{q}} \propto e^{-i\mathbf{G}_0\cdot\boldsymbol{\tau}} \int e^{-i\mathbf{q}\cdot\mathbf{r}} g(\mathbf{r}) d\mathbf{r}$$

where the integral is nothing but the local structure near $\mathbf{k}_0$ that we have already discussed above, and the phase factor $e^{-i\mathbf{G}_0\cdot\boldsymbol{\tau}}$, which can evaluate to 1, ω_+ or $\omega_- = \omega_+^2$, describes its evolution when moving between equivalent $\mathbf{K}/\mathbf{K}'$ points, which recovers and, in a sense, generalizes the symmetry result given above.

4.4.4 Absorption spectrum

We now have all elements in hand to produce and interpret the excitonic absorption spectrum for single layer hBN. Using the states computed in section 4.4.2 to evaluate the formulas of section 4.4.2, we obtain the sought-after spectrum, which is depicted in figure 4.20, to be compared with the *ab initio* spectrum shown in figure 4.21.

Overall, both in tight-binding and *ab initio*, the spectrum is dominated by the first bright peak, coming from the lowest bound exciton. This can be understood from the fact that, as per equation 4.18, the oscillator strength of bright states is directly proportional to the intensity on the nearest neighbor excitations. The lowest bound exciton, as expected, is by far the most concentrated one in direct space, and, therefore dominates absorption.

One notable difference between the *ab initio* and tight-binding descriptions lies in the second peak, corresponding to exciton number two, the "$2p$"

[46] Which particular $\boldsymbol{\tau}$ is chosen does not matter here, since they are all connected by direct lattice vectors.

[47] We are essentially making use of the Borel-Lebesgue lemma: the integrands of the $I_{\mathbf{G}}(\mathbf{k})$ for which $\mathbf{G} \neq \mathbf{G}_0$ oscillate rapidly, and therefore do not contribute much to the sum.

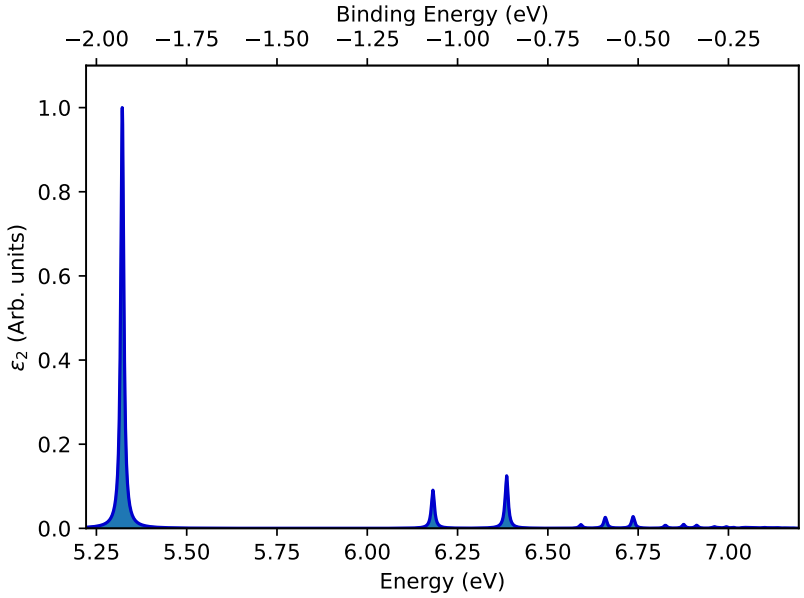

Figure 4.20: Tight-binding absorption spectrum for single layer hBN, with a lorentzian broadening of 5 meV, computed in the excitonic tight-binding framework. The G_0W_0 band gap is at an energy of 7.25 eV, or, equivalently, at 0 eV on the binding energy scale.

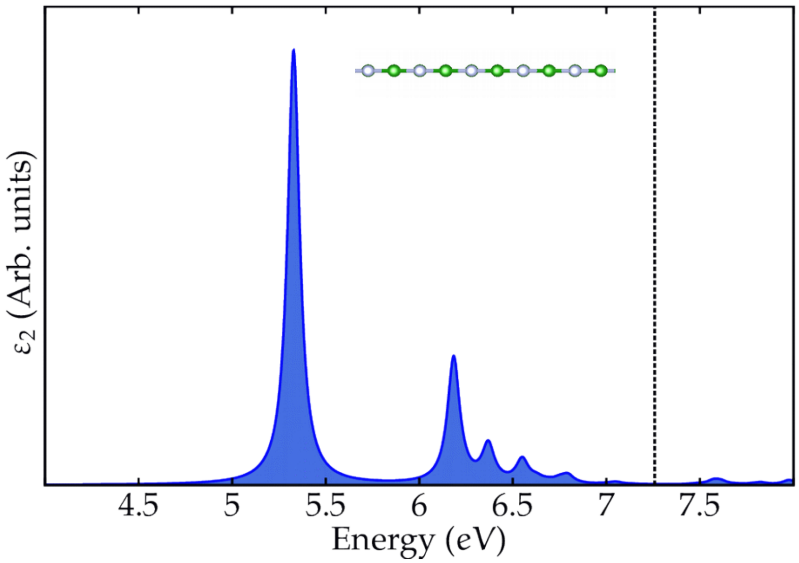

Figure 4.21: *Ab initio* absorption spectrum for single layer hBN (the band gap is materialized by a vertical dotted line); calculation by F. Paleari.

state. This exciton is significantly brighter *ab initio*, where it is brighter than the $2s$ state, while in tight-binding the opposite appears true. We should note, at this point, that the predictions of the tight-binding model are already an improvement on the hydrognoïd limit, where this state is completely dark: the fully circular symmetry in this case forbids its coupling with light. These couplings can therefore be traced back to the lattice symmetries.

This sets the stage for a more detailed analysis of exciton 2, which we have deferred until now. The envelope wavefunction-based discussions of section 4.4.3, while not in complete disagreement with the numerical results on the reciprocal space amplitudes, both *ab initio* and in tight-binding, are not fully satisfactory either. Indeed, figure 4.19 clearly shows that the exciton (subspace) intensity for this state does not vanish at the $\mathbf{K}/\mathbf{K}'$ points, as expected from a p-type state. This is the case both in tight-binding, where the intensity appears locally minimal, but nonvanishing, and *ab initio*, to a much greater extent: there, the intensity is even close to maximal at $\mathbf{K}/\mathbf{K}'$. Once again, the amplitdes reveal more information through a careful analysis of the chiral basis states for exciton E. Focusing one one of the states, we can see that the phase-rotating components characteristic of p states originate from point, say, $\mathbf{K}$, while the $\mathbf{K}'$ points house the constant phase contributions typical of s-type states. For the other basis state, the roles of $\mathbf{K}$ and $\mathbf{K}'$ are reversed.

This shows rather clearly that exciton 2 is not fully of p character. Indeed, this observation strongly suggests that it results from the mixing of the hydrogenoid p states from one valley with the hydrogenoid s states of the other valley. In a triangular system, this is allowed: the circular symmetry that gave rise to the s, p, ... states is broken; in other words, m as defined before is no longer a good quantum number, and states of different m can mix, as can states of different valleys. This is, of course, not a peculiarity of exciton 2: all states are affected by the lowering of the symmetry, but exciton 2, perhaps, displays it in the most spectacular fashion. In fact, exciton 5 also shows, at least in tight-binding, faint contributions evocative of p character.

The analysis above illustrates once again the interest of studying the phases of the excitonic wavefunctions. Such a study is more difficult, however, without a semi analytical model. This is due to the fact that the overall phases of transition states is arbitrary: in a model, one can - as we did here - make a cogent choice that will make later analysis tractable. If the transition states are determined numerically, however, their overall phases are essentially random, hampering further study.

If one only looks at the exciton densities, which do not carry phase information, the most prominent signal of this mixing is the intensity at $\mathbf{K}/\mathbf{K}'$ for supposedly non s-type states. While indirect, it still provides interesting

information, especially in the *ab initio* case where we have no direct access to the phases. From this indicator, we can see that the s/p mixing for exciton 2 is significantly higher *ab initio* than in tight-binding, in the sense that it has a higher s component in the former than in the latter. This resonates with our earlier remark about its oscillator strength: exciton 2 is brighter *ab initio* than in tight-binding.

We can pursue this idea further: since we expect lattice effects to be at the orgin of the brightness of exciton 2, it would be interesting to somehow "vary" the influence of the lattice, and see how this affects the states and absorption spectrum of the system. Intuitively, we expect that, for "weak" lattice effects, we should tend towards the predictions of a continuous hydrognoid description, with states well described by the s, p, ... classification, with only s states being bright. On the other hand, for "strong" lattice effects, we should instead tend towards a situation where this description is poor and hydrogenoid states are mixed and additional peaks appear in the absorption spectrum, like what happens with exciton 2. Of course, we do not have a direct "lattice effects" parameter to tune. However, we should recall that the Wannier limit is essentially that of low electron-hole coupling: if the potential is weak compared to the kinetic energy, the excitons are dilute in the sense that their Bohr radii are (much) larger than the lattice spacing, and consequently, lattice effects become negligible. Conversely, if we make the potential stronger, excitons will become more concentrated, and therefore more sensitive to lattice effects. The natural "lattice effects" parameter is therefore the strength of the potential compared to the kinetic hoppings (here T). In a dimensionless version of the problem, it could be the parameter v introduced before. Here, if we keep T constant, it thus makes sense to examine the effects of varying the polarizability radius r_0: the shorter r_0, the stronger the potential. With this in mind, we compute the absorption spectrum of hBN within the excitonic tight-binding model for various values of r_0 and report the results in figure 4.22. For $r_0 = 30$ Å, which is more typical of transition metal dichalcogenides,[75] the peak associated to exciton 2 has become negligible compared to the third peak, itself associated to the $2s$ state. The hydrogneoïd selection rules seem to be validated. The case $r_0 = 10$ Å corresponds to the fitted value: the second peak no longer has a neglibible intensity compared to the third one. Conversely, when r_0 is reduced to 5 Å, the second peak becomes more intense than the third (as in the *ab initio* results).

4.5 Exciton dispersion

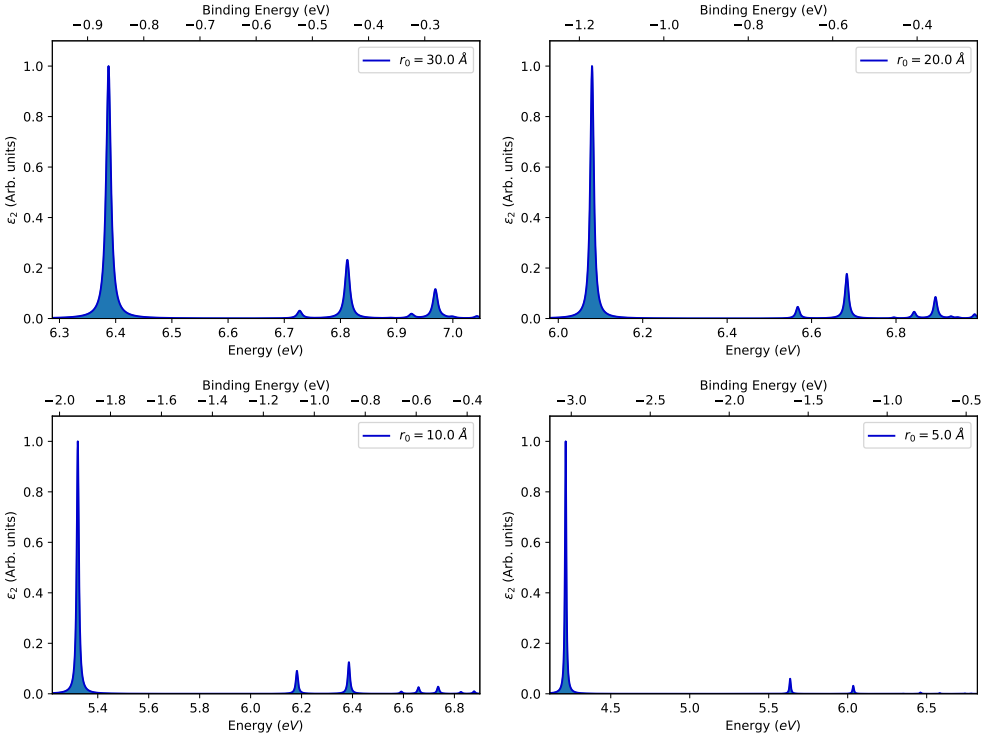

Figure 4.22: Evolution of the absorption spectrum of hBN in the excitonic tight binding model as the polarizability radius of the potential is varied (kinetic parameters are kept fixed to the fitted values $2\Delta = 7.25$ eV and $T = 1.5$ eV). In each case, the spectrum is computed from the lowest bound 30 excitonic states, with a lorentzian boradening of 5 meV. As r_0 decreases, the binding potential becomes stronger and so the excitons become more localized, and therefore more sensitive to lattice effects. The intensity ratio between the second ("$2p$") and the third ("$2s$") peaks is an optical manifestation of this. For dilute excitons (large r_0), the lattice effects can be averaged out, and we are closer to the predictions of the Wannier model, which makes the $2p$ states dark. *A contrario*, for strongly bound excitons, the second peak becomes more intense than the third. At the same time, because the potential is increased, the much more strongly bound first peak ($1s$) further dominates the spectrum.

4.5.1 Introduction

Until now, we have focused only on direct excitonic states, i.e. states with center of mass momentum $\mathbf{Q} = \mathbf{0}$. Our reasons for this were that only these states could be bright in absorption: in the limit of vanishing photon momentum, conservation of momentum requires indirect states to be dark.

However, the above ceases to hold if another interaction can supply momentum. In solid state, this interaction typically comes in the form of phonons. This leads to indirect absorption and, more crucially, indirect emission processes, which are now known to be important in bulk hexagonal Boron Nitride. This is because, as was demonstrated experimentally[33, 34, 35] and theoretically[37, 36] these materials have indirect excitonic gaps: their lowest bound excitons are indirect. Their emission spectrum is therefore dominated by (phonon assisted) indirect effects.

The description of such effects naturally requires the knowledge of indirect excitonic states. There is thus, at present, a need for simple methods which can provide access to these states and lend themselves to analysis. We should mention, of course, that such states can also be obtained *ab initio*, but as in the case of direct states, this does not obviate the need for second principles methods. This is especially true because recently proposed diagrammatic methods[3, 78] for indirect absorption, in opposition to static finite difference[37, 36] methods, may require knowledge of the exciton dispersion and states over a very fine mesh of $\mathbf{Q}$ points close to the excitonic gap. This is an area where second principles methods, properly adjusted on a coarser *ab initio* grid, could even be called upon to play an important computational role.

Our objective in this section is therefore not to develop a theory of indirect / phonon-assisted absorption and emission, but rather, since our excitonic tight-binding model naturally extends to the case $\mathbf{Q} \neq \mathbf{0}$, to investigate the excitonic dispersion of single layer hBN. The study of dispersion in bulk in the AA', AB and ABC stackings, is possible within the same model, and, along with the monolayer is the object of [48]. However, apart from chapter 6 which introduces the general theory in the AA' case, it falls mostly outside of the scope of the present work and so that for detailed results on bulk hBN, we instead refer the interested reader to [48].

4.5.2 Analytical estimates

Before going to the numerical diagonalization of the excitonic hamiltonian at finite $\mathbf{Q}$, we first try to obtain analytical estimate of the system's behavior. In this section, we remain in first nearest neighbors for simplicity.

Strong potential approximation for the lowest bound states

As per our usual strategy, we start with the strong potential approximation, in order to obtain a first idea of what can be expected from the model. In this case, the problem reduces to:

$$H_X(\mathbf{Q}) = 2\Delta + 3T + U + \frac{T}{2}\begin{pmatrix} 0 & h_{1,2} & h_{1,3} \\ h_{2,1} & 0 & h_{2,3} \\ h_{3,1} & h_{3,2} & 0 \end{pmatrix} + \frac{J}{4Q\tau}\begin{pmatrix} j_{1,1} & j_{1,2} & j_{1,3} \\ j_{2,1} & j_{2,2} & j_{2,3} \\ j_{3,1} & j_{3,2} & j_{3,3} \end{pmatrix}$$

where we have kept to first nearest neighbors in order to obtain a minimal model, and introduced the notation $Q = \|\mathbf{Q}\|$, and $h_{i,j}(\mathbf{Q}) = 1 + e^{i\mathbf{Q}\cdot(\boldsymbol{\tau}_i - \boldsymbol{\tau}_j)}$.

In the absence of exchange ($J = 0$), the lowest two eigenergies read:[48]

$$\begin{aligned} E_1(\mathbf{Q}) &= 2\Delta + 3T + U - T \\ E_2(\mathbf{Q}) &= 2\Delta + 3T + U - \frac{T}{2}(1 - |\gamma_1(\mathbf{Q})|) \end{aligned}$$

So that the lowest bound exciton, which is doubly degenerate at the excitonic $\mathbf{\Gamma}$ point, splits in two distinct branches when $\mathbf{Q} \neq \mathbf{0}$. The lowest branch,[49] remarkably, is non dispersing. This last behavior, while interesting in its own right,[79] only occurs here exactly in the strong potential limit where the electron and the hole are constrained to remain nearest neighbors. The second branch, however, exhibits a parabolic dispersion close to $\mathbf{\Gamma}$:

$$E_2(\mathbf{Q}) \approx E_2(\mathbf{\Gamma}) + \frac{3}{8}T(Q\tau)^2$$

which corresponds to an *exciton* effective mass of $\mu_X = \frac{4\hbar^2}{3T\tau^2}$.

Perturbation

Our interest lies mostly in the behavior of the lowest bound exciton. It turns out that estimates can be obtained, at the price of some approximations. To this end, we will follow the perturbation methods discussed in appendix D of [48]. We work in the subspace corresponding to the lowest bound exciton.

[48] The third eigenergie is $E_3(\mathbf{Q}) = 2\Delta + 3T + U + \frac{T}{2}(1 - |\gamma_1(\mathbf{Q})|)$, but, like at $\mathbf{Q} = \mathbf{0}$, it is unphysical.

[49] Recall that $|\gamma_1(\mathbf{Q})|$ is maximal at $\mathbf{Q} = \mathbf{\Gamma}$, so $E_2(\mathbf{Q})$ actually increases when moving away from $\mathbf{\Gamma}$.

For this, it is convenient to chose a chiral basis $\mathcal{C} = \{|\Psi^-\rangle, |\Psi^+\rangle\}$ such that:[50]

$$\left\langle \boldsymbol{\tau}, \mathbf{Q} \middle| \Psi^{\pm} \right\rangle = \Psi_\tau e^{\pm i\mathbf{K}\cdot\boldsymbol{\tau}}$$

for the shortest excitations, which, at $\mathbf{Q} = \mathbf{0}$, reduces to the usual chiral states. In the strong potential approximation, $|\Psi_\tau| = \frac{1}{\sqrt{3}}$, while in general, the excitonic states have other components on excitations with $R \gg \tau$.

Exchange interaction

Treating the exchange interaction as a perturbation, the associated matrix elements in the basis $\mathcal{C}$ are found to be:

$$J_\Psi(\mathbf{Q}) = \frac{J|\Psi_\tau|^2}{4\tau Q} \begin{pmatrix} |\gamma_1(\mathbf{K}+\mathbf{Q})|^2 & \gamma_1(\mathbf{K}+\mathbf{Q})\gamma_1(\mathbf{K}-\mathbf{Q}) \\ \gamma_1^*(\mathbf{K}+\mathbf{Q})\gamma_1^*(\mathbf{K}-\mathbf{Q}) & |\gamma_1(\mathbf{K}-\mathbf{Q})|^2 \end{pmatrix} \tag{4.24}$$

It is convenient, at this point, to perform a small $\mathbf{Q}$ approximation ($|Q\tau| \ll 1$). In this case, we can expand $\gamma_1(\mathbf{K} \pm \mathbf{Q})$ to first order in $\mathbf{Q}$ around $\mathbf{K}$, and we find:

$$\begin{aligned} \gamma_1(\mathbf{K} \pm \mathbf{Q}) &\approx \mathbf{Q} \cdot \boldsymbol{\nabla}_{\mathbf{k}=\mathbf{K}} \gamma_1(\mathbf{k}) \\ &\approx \mathbf{Q} \cdot \sum_{\boldsymbol{\tau}} \boldsymbol{\tau} \underbrace{e^{i\mathbf{K}\cdot\boldsymbol{\tau}}}_{\frac{1}{\Psi_\tau}\langle\boldsymbol{\tau}|\Psi^+\rangle} \end{aligned}$$

and we recognize, up to a factor of $t_\perp$, the wavefunction dipole for state $|\Psi^+\rangle$: $\mathbf{d}_{\Psi^+} = t_\perp \sum_{\boldsymbol{\tau}} \langle\boldsymbol{\tau}|\Psi^+\rangle \boldsymbol{\tau}$. In analogy, we thus define $\mathbf{d}_+ = \frac{1}{t_\perp \Psi_\tau} \mathbf{d}_{\Psi^+}$, which is proportional to it, and so we have $\gamma_1(\mathbf{K} \pm \mathbf{Q}) = \mathbf{Q} \cdot \mathbf{d}_+$. It follows that:

$$J_\Psi(\mathbf{Q}) \approx \frac{J|\Psi_\tau|^2}{4\tau} \frac{|\mathbf{Q}\cdot\mathbf{d}_+|^2}{Q} \underbrace{\begin{pmatrix} 1 & -e^{2i\theta} \\ -e^{-2i\theta} & 1 \end{pmatrix}}_{M(\mathbf{Q})} \tag{4.25}$$

where $e^{i\theta} = \frac{\mathbf{Q}\cdot\mathbf{d}_+}{|\mathbf{Q}\cdot\mathbf{d}_+|}$ is a $\mathbf{Q}$-dependent phase. Drawing on equation 4.17, we have $|\mathbf{Q}\cdot\mathbf{d}_+|^2 = \frac{9}{4}(Q\tau)^2$, so that the prefactor is linear in Q.

The matrix $M(\mathbf{Q})$ has 0 and 2 as eigenvalues, so that we expect one non-dispersing and one linearly dispersing branch, the latter of which is typical of exchange in two dimensions.[62, 63]

[50] Recall that the $e^{\pm i\mathbf{K}\cdot\boldsymbol{\tau}}$ are third roots of unity, i.e. as $\boldsymbol{\tau}$ runs over the first nearest neighbor Nitrogen to Boron vectors, they run over $\{1, \omega, \omega^2\}$, so the states defined below are indeed our usual chiral states. This form makes the following calculations (which we do not detail) much more straightforward, however. The amplitude Ψ_τ is, possibly up to a phase, the analogue of the quantity C_Ψ introduced earlier.

Kinetic dispersion

A similar treatment can be given to the dispersion originating from the kinetic terms. We can define the perturbing operator $\hat{h}(\mathbf{Q}) = \hat{H}_0(\mathbf{Q}) - \hat{H}_0(\mathbf{Q}=\mathbf{0})$. In that case, we have:

$$\langle \mathbf{R}|\hat{h}(\mathbf{Q})|\mathbf{R}'\rangle = \begin{cases} \frac{T}{2}\left(e^{i\mathbf{Q}\cdot(\mathbf{R}'-\mathbf{R})}-1\right) & \text{if } \mathbf{R} \text{ and } \mathbf{R}' \text{ are 1n.n. in } \Lambda \\ 0 & \text{otherwise} \end{cases}$$

The situation is therefore *a priori* more complex, because the kinetic "perturbation" is not localised on the shortest excitations, so that the result is expected to depend on the specifics of the excitonic states in $\mathcal{C}$, and not just their symmetries. Still, we can adapt the treatment above by assuming that the states of $\mathcal{C}$ have most of their intensity on these excitations and neglect the rest, i.e. by taking $|\Psi_\tau|^2 \approx \frac{1}{3}$. This essentially corresponds to the strong potential approximation, so we expect results similar to those obtained previously. It is nevertheless interesting to perform this calculation in the perturbative framework.

By the same methodology as in the exchange case, we compute the matrix elements of $\hat{h}$ and obtain likewise:

$$h(\mathbf{Q}) \approx \frac{T}{2}|\Psi_\tau|^2 \begin{pmatrix} |\gamma_1(\mathbf{K}+\mathbf{Q})|^2 & \gamma_1(\mathbf{K}+\mathbf{Q})\gamma_1(\mathbf{K}-\mathbf{Q}) \\ \gamma_1^*(\mathbf{K}+\mathbf{Q})\gamma_1^*(\mathbf{K}-\mathbf{Q}) & |\gamma_1(\mathbf{K}-\mathbf{Q})|^2 \end{pmatrix} \tag{4.26}$$

in the basis $\mathcal{C}$, and performing likewise a small $\mathbf{Q}$ approximation, we find:

$$h(\mathbf{Q}) \approx \frac{T}{2}|\Psi_\tau|^2|\mathbf{Q}\cdot\mathbf{d}_+|^2 \underbrace{\begin{pmatrix} 1 & -e^{2i\theta} \\ -e^{-2i\theta} & 1 \end{pmatrix}}_{M(\mathbf{Q})}$$

with the same definitions as above. We obtain the same matrix, up to the prefactor, although crucially the prefactor is here quadratic in Q, while it was linear in the case of exchange.

Once again, because the eigenvalues of $M(\mathbf{Q})$ are 0 and 2, we have one non-dispersing branch, and one which disperses quadratically in Q. Keeping to the strong potential approximation, we have $|\Psi_\tau|^2|\mathbf{Q}\cdot\mathbf{d}_+|^2 = \frac{3}{4}(Q\tau)^2$, so that we recover the same effective mass for the dispersing branch as we found by direct calculation.

Discussion

Overall, the perturbing elements for the "kinetic" terms are quadratic, while those of exchange are linear. For small values of Q, we thus expect dispersion

due to exchange to dominate along branches which are sensitive to exchange. Such branches will therefore show a linear dispersion. As we have shown above, some branches are not affected by exchange at the perturbation level. For such branches, only the kinetic dispersion then remains, and so we expect a quadratic dispersion.

The estimates above show that, within the strong potential approximation, we expect the lowest bound exciton to split into one non-dispersing branch, and one branch whose dispersion is affected by both exchange and kinetic effects, although exchange is expected to dominate. Outside of the strong potential approximation (but still remaining in the perturbation regime), we have no reason to expect the non dispersing branch not to be affected by kinetic effects, and indeed, numerical diagonalization of $\hat{H}_X(\mathbf{Q})$ shows that it does display a parabolic dispersion. Such splitting of doubly degenerate states into a parabolic and a linear branch has also been predicted in MoS_2.[64, 62]

Lastly, because exchange matrix elements affect only the shortest elementary excitations (the $|\boldsymbol{\tau}, \mathbf{Q}\rangle$), we intuitively expect that the slope of linearly dispersing branches will be higher for states that are more concentrated, i.e. for the lowest bound states. This is reinforced by the appearance of $|\Psi_\tau|^2$ in the prefactors of equation 4.25, showing that this is the case at least for the linear branch associated to the splitting of direct exciton 1. Indeed, in the limit of a weak direct electron-hole interaction ($\hat{U}$), which leads to dilute states, this prefactor decays and consequently reduces the linear slope of the dispersion.

4.5.3 Numerical results

Exciton band structure

Let us first present the numerical exciton band structure in first nearest neighbors. This is done in figure 4.23, both with and without exchange. The qualitative features of this numerical dispersion within the tight-binding model are in reasonable agreement with the analytical expectations of section 4.5.2 and the resulting discussion above. We do note that, while the lowest excitonic branch is indeed almost unaffected by exchange, it is not flat, but instead displays a parabolic dispersion originating from the kinetic terms. As discussed above, we expect this branch to flatten (only) in the strong potential limit: here, it is the fact that the state is extended which allows for dispersion.

A comparison with *ab initio* calculations by L. Sponza is provided in [48]. It is shown in figure 4.24. Satisfying agreement is found for the dispersion of

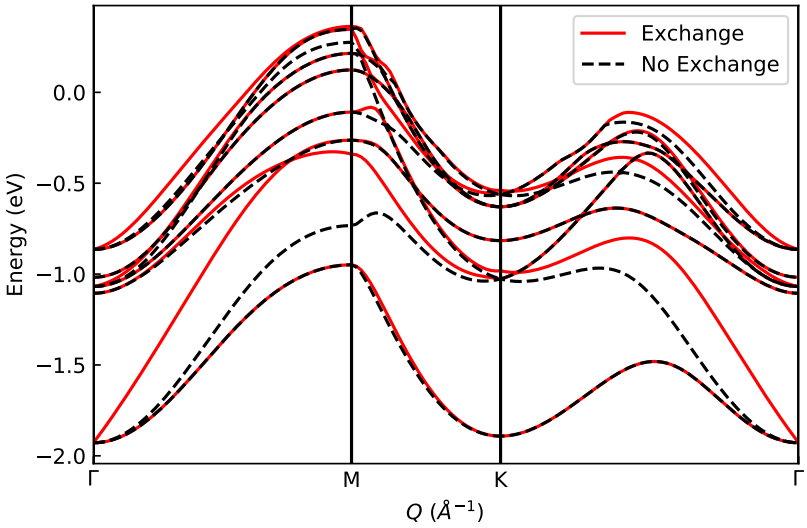

Figure 4.23: Exciton dispersion for single-layer hBN computed by numerical diagonalization of the excitonic tight binding hamiltonian $\hat{H}_X$, in first nearest neighbors. We used the same parameters as in the direct case, with the addition of $J = 5$ eV to reproduce exchange. At each value of $\mathbf{Q}$, only the 8 lowest energy states were retained (so that, at excitonic $\mathbf{\Gamma}$, only states of table 4.4 are shown). Dashed black lines: dispersion without exchange ($J = 0$). Solid red lines: full dispersion.

.

the lowest two branches, although the quality of this agreement quickly worsens for higher energy states. This can be traced back to two reasons. First, at higher energies, the simple approximations of the tight-binding model begin to fail. Secondly, *ab initio* calculations reveal that these excitons contain significant components from the nearly free electron states, which cannot be captured at all in the π-bands based tight-binding model. To reproduce the observed linear dispersions in the *ab initio* bands, a value of $J \approx 5$ eV was found. The "exact" value of the prefactor in equation 4.11 is therefore an overestimate (at least for our values of the other parameters and current approximations), although the associated functional form appears satisfying.

Figure 4.24 also displays the effect of adding second nearest neighbors, by taking $t_\perp^{NN} = t_\perp^{BB} = -0.1$ eV. While we have seen that such an addition yields almost no correction to the excitonic hamiltonian at $\mathbf{Q} = \mathbf{0}$, it clearly affects the excitonic dispersion. The origin of this distinction can be seen in equation 4.8: at $\mathbf{Q} = \mathbf{0}$, the effective hoppings between nearest neighbor excitations reads as $T'_e + T'_h$, where $T'_h = \frac{t_\perp^2}{2\Delta} - t_\perp^{NN}$ and $T'_e = \frac{t_\perp^2}{2\Delta} + t_\perp^{BB}$, so the effects of second nearest neighbors hoppings compensate each other. Pictorially, if $t_\perp^{BB} = t_\perp^{NN} < 0$, the fact that the effective hopping for electrons becomes weaker (ie. that the conduction band becomes flatter, or from an effective mass point of view, electrons becomes heavier) is compensated by the fact the effective hopping for holes becomes stronger (likewise, the valence band increases in curvature, i.e. the holes become lighter). When $\mathbf{Q} \neq \mathbf{0}$, however, the effective hoppings become $T'_e + T'_h e^{i\mathbf{Q}\cdot(\mathbf{R}'-\mathbf{R})}$, and the phase factor associated to the effective hole hopping breaks this compensation effect. From the electronic point of view, the situation is that we do not just have to accurately reproduce the transition band at $\mathbf{Q} = \mathbf{0}$, a task which can be accomplished satisfactorily even if the bands are not reproduced faithfully, but for *all* values of $\mathbf{Q}$, which is practically equivalent to a correct reproduction of the bands.

Evolution of the states and remarkable Q-points

The evolution of the wavefunctions of the lowest bound states is discussed in [48], and depicted in the lower panels of figure 4.24. In this section, we focus on the situation at the excitonic high-symmetry points $\mathbf{M}$ and $\mathbf{K}$. The situation at $\mathbf{\Gamma}$ corresponds to the direct excitonic series, which has been been discussed at length in section 4.4.

Let us start with the lowest bound state at $\mathbf{K}$. It can be seen that its binding energy is practically equal to the energy of the doubly degenerate $1s$ subspace at $\mathbf{\Gamma}$, and likewise its density is almost the same, even though its is singly degenerate. The coincidence in binding energy is expected on

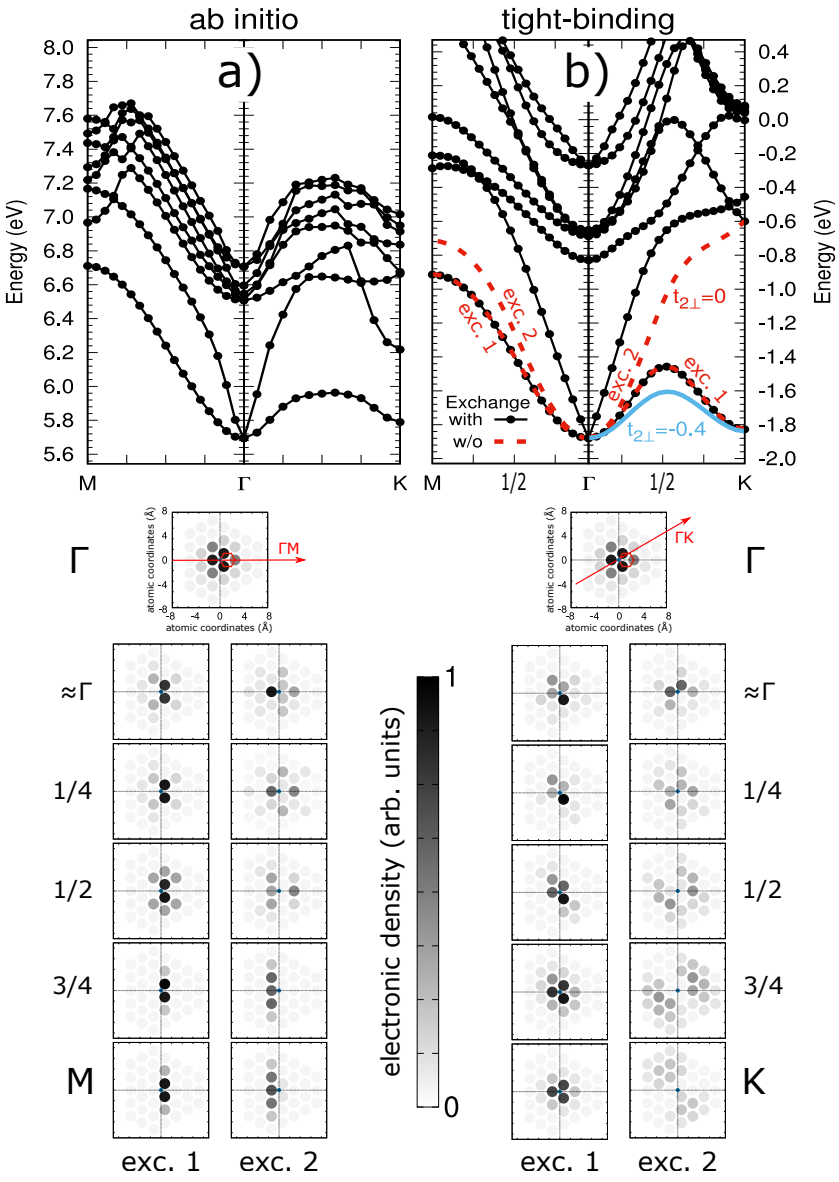

Figure 4.24: Figure reproduced from [48]. Top panel: exciton dispersion for single layer hBN along **ΓM** and **ΓK**. *a*): *ab initio* dispersion by L. Sponza. *b*): tight-binding dispersion (same parameters as figure 4.23 excpet for second nearest neighbors). The solid black line corresponds to first nearest neighbor hoppings with exchange, while the dashed red line corresponds to $J = 0$ (no exchange). The solid blue line corresponds to $t_\perp^{NN} = t_\perp^{BB} = -0.4$ eV (both denoted as $t_{2\perp}$ in [48]). Bottom panel: tight-binding excitonic densities for the lowest bound pair, along **ΓM** (left) and **ΓK** (right). At **Γ**, where the statates are degenerate, the direction of **Q** is shown as well as a direct space unit cell (red hexagon).

electronic grounds. Indeed, the vector $\mathbf{\Gamma K}$ connects neighboring $\mathbf{K}$ and $\mathbf{K'}$ points, i.e. two valleys, and by time reversal symmetry, the transition energy between, say, the valence band at $\mathbf{K}$ and the conduction band at $\mathbf{K'}$ is the same as the direct transition energy at, say, $\mathbf{K}$.

The correspondance of their densities is straightforwardly understood within the strong potential approximation, directly or from the perturbative treatment. The latter provides a straighter route: we are not at "small $\mathbf{Q}$", so we turn our attention to the matrices of equations 4.26 and 4.24. At $\mathbf{Q} = \mathbf{K}$, we have $\gamma_1(\mathbf{K} + \mathbf{Q}) = 0$, while $\gamma_1(\mathbf{K} - \mathbf{Q}) = \gamma_1(\mathbf{\Gamma}) = 3$, and so both are of the form:

$$\begin{pmatrix} 0 & 0 \\ 0 & 1 \end{pmatrix}$$

in the basis $\mathcal{C} = \{|\Psi^-\rangle, |\Psi^+\rangle\}$. As a result, the lowest energy state is just the chiral state, $|\Psi^-(\mathbf{K})\rangle = \sum_{\boldsymbol{\tau}} e^{-i\mathbf{K}\cdot\boldsymbol{\tau}} |\boldsymbol{\tau}, \mathbf{K}\rangle$, which indeed has the same density as the "$1s$" direct state.

The situation at $\mathbf{M}$ may also appear peculiar: there, the system's eigenfunctions become "elongated". This can be easily understood by noting that the effective kinetic hoppings between neighboring excitations are of the form, in first nearest neighbors:

$$\langle \mathbf{R}, \mathbf{M} | \hat{H}_0 | \mathbf{R}', \mathbf{M} \rangle = \frac{T}{2}\Big(1 + e^{i\mathbf{M}\cdot(\mathbf{R}'-\mathbf{R})}\Big)$$

so that there are effectively six different values of the hoppings, one for each nearest neighbor direction in Λ, or, more preicsely, three values and their three complex conjugates. What happens at $\mathbf{M}$ points is that two of the aforementioned three kinetic hoppings vanish: this is the $2D$ analogue of what happened in one dimension in the chain at $\mathbf{Q} = \mathbf{X}$. As a result, the effective tight-binding system becomes, in the absence of exchange, a collection of parallel, uncoupled linear chains. The "elongated" wavefunctions are therefore nothing but the eigenfunctions of these chains. In a more realistic treatment, exchange interaction, as well as second nearest neighbors breaking the exact compensation of electron and hole hoppings, are expected to couple the chains, but the signs of the phenomenon are still apparent.

Chapter 5

Multilayers

The contents of this chapter are based on [38].

Having now a better understanding of single-layer Boron Nitride, we turn our attention to multilayers, i.e. coupled hBN layers. It is indeed relevant to study their excitonic and optical properties, since experimental results have been obtained in the synthesis and characterization of few layer BN systems.[80, 81, 82, 35] We must note that other studies on this topic have already appeared in the litterature for hBN (see notably [83]) although a majority of these works has focused on single layer or bulk-like systems.

Our aim in this chapter is therefore to investigate the excitonic and optical properties of few layer hBN systems, with a particular attention to the surface effects that arise due to their lack of translational invariance in the stacking direction. We will notably focus on the splitting of the first monolayer peak and its evolution as the number of layer is increased, since it is the most prominent feature of the system's absorption spectrum.

By way of introduction to the phenomena at play in this chapter, let us consider N identical systems, $\mathcal{S}_1 \dots \mathcal{S}_N$. If we keep them sufficiently distant so that they do not interact, then all of them have the same eigenstates and eigenenergies: if we consider an energetically well separated, nondegenerate eigenstate of $\mathcal{S}_1$, then the full system will have a degenerate eigensubspace of dimension N. As the individual systems are brought together, they will start to interact, and this degenerate subspace will split in up to N eigenstates of the full system. An example of the case $N = 2$ is what happens when two hydrogen atoms are brought together: when they are far from each other, they each exhibit a $1s$ orbital (disregarding spin) at the same energy, and as they are brought together, these orbitals combine into a bonding and antibonding pair, which are energetically split.

This is a simplified description of the notion of Davydov splitting, which was first introduced to describe the splittings of energy levels in clusters

of identical molecules,[84] and was also applied to molecular crystals.[85] Likewise, one can consider a stack of identical layers of two dimensional materials, and Davydov splitting of phonons has indeed been reported in few-layer systems of transition metal dichalcogenides.[86, 87, 88]

Here, our identical systems are naturally the hBN monolayers, and we are interested in the Davydov splitting of excitons. Our goal is to identify the interactions between the layers and their consequences.

5.1 General tight-binding model

5.1.1 Crystal lattice

For both concreteness and simplicity, we will focus here on the AA' stacking of multilayer hBN, which appears to be the most common. We must note, however, that other stackings, notably AB (Bernal)[89] and ABC (rhombohedric)[90] are also observed in experiment and are therefore also of interest. In fact, the tight-binding model can be straightforwardly adapted to other stackings, and, as we have already mentioned, this is done for bulk systems in [48].

AA' hBN can be described as follows: consider a set of N parallel single layers of hBN, stacked onto one another such that two consecutive layers are heads to tails, i.e. the Boron sites of layer $n+1$ are on top of Nitrogen sites of layer n, and the Nitrogen sites of layers $n+1$ are are on top of boron sites of layer n. Technically, the interlayer distance does not need to be a fixed quantity,[1] but within this chapter, we consider it fixed.[2] To set notations, we therefore let τ and d be the nearest neighbor B-N distance and interlayer spacing, respectively. We depict the AA' bilayer in figure 5.1 for illustration.

Formally, the multilayer system has a triangular Bravais lattice, $\mathcal{R}$, which apart from its parameters can be taken to be identical to that of the monolayer. The difference is that it has a basis of $2N$ sites in its unit cell: one

[1] Not only does it *a priori* depend on N, couple of consecutive layers since there is no translation periodicity in the stacking direction.

[2] This is done for a number of reasons. First, it is not necessarily trivial to accurately relax the geometry of large multilayers *ab initio*. Second, taking such a phenomenon into account would require distance dependent hoppings in the semi-empirical electronic tight-binding models, which adds significant complexity whose benefits may be dwarfed by the other sources of error (single particle band structures, finite range hoppings, etc.). Lastly, we will anyway only treat the AA' bilayer explicitly before introducing a qualitative $1D$ model for $N > 2$, and so we would not benefit from such complications. On the *ab-initio* side, the in-plane lattice constant was fixed to the optimized bulk value $a = \sqrt{3}\tau = 2.496$ Å,[73] while the interlayer distance was set to the experimental bulk value $d = 3.305$ Å.

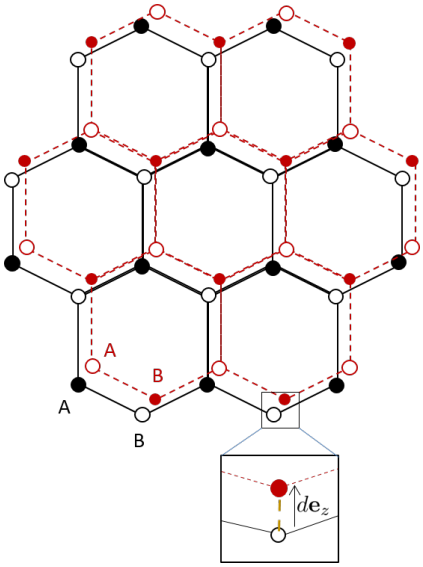

Figure 5.1: Schematic crystal structure of hBN bilayer in the AA' stacking. Filled circles represent Nitrogen sites (A), while hollow circles represent Boron sites (B). Lines (dashed and solid) connect in-plane $B-N$ nearest neighbors. The bottom layer is schematized in black, while the top layer is schematized in red. In a top view Boron sites of the top layer would be right above the Nitrogen sites of the bottom layer, and vice versa. Inset: partial side view; $\mathbf{e}_z$ is the stacking direction and the dashed orange line connects an interlayer first nearest neighbor $B-N$ pair.

Boron and one Nitrogen atom per layer. We denote their positions by $\mathbf{m}^0_{N,\alpha}$ for the Nitrogen (hole type) sites and $\mathbf{n}^0_{B,\beta}$ for the Boron (electron type) sites, where $\alpha, \beta \in [\![1, N]\!]$ are layer indices.[3] They may naturally be taken such that:[4]

$$\forall n \in [\![1, N-1]\!], \quad \mathbf{m}^0_{N,n+1} = \mathbf{n}^0_{B,n} + \mathbf{d} \quad ; \quad \mathbf{n}^0_{B,n+1} = \mathbf{m}^0_{N,n} + \mathbf{d}$$

with $\mathbf{m}^0_{N,1}$ and $\mathbf{n}^0_{B,1}$ lying in an (xy) plane and $\mathbf{d} = d\mathbf{e}_z$. To fix notations, we will thus consider that the layers are parallel to the (Oxy) plane, and thus that $\mathbf{e}_z$ is the stacking direction. This lets us define the Nitrogen (hole) and Boron (electron) sublattices:

$$\Lambda_{A,\alpha} = \mathcal{R} + \mathbf{m}^0_{N,\alpha}$$
$$\Lambda_{B,\beta} = \mathcal{R} + \mathbf{n}^0_{B,\beta}$$

From a symmetry point of view, the point groups of multilayers depend on the parity of the number of layers, N. If N is even, the system has inversion symmetry, and has the D_{3d} point group, while if N is odd, it has a mirror symmetry about the central layer, and therefore has the D_{3h} point group. We will later see that this inversion / mirror symmetry plays a central role in the determination of selection rules for multilayers, which consequently also depend on the parity of N.

Finally, let us spare a word for the situation in reciprocal space. The Bravais lattice $\mathcal{R}$ of multilayers is still triangular, exactly like the one of a single monolayer. The only difference is the unit cell basis. Therefore the reciprocal lattice and the Brillouin zone geometry remain the same as in the monolayer case. In particular, both the real (Bravais) and reciprocal lattices remain two dimensional.

5.1.2 Electronic Hamiltonian

Having described their geometry, we are now positioned to give a general description of the electronic structure of hBN multilayers. Since we will restrict ourselves to direct states in this chapter, and in the interest of simplicity, we shall restrict ourselves to a first-nearest neighbor tight-binding model, although it is straightforward to extend the following to include second nearest neighbors.

For the same reasons as previously, we consider a basis of nitrogen (A) and boron (B) p_z orbitals, $\{|A_\alpha, \mathbf{m}\rangle, |B_\beta, \mathbf{n}\rangle\}_{\alpha,\beta\in[\![1,N]\!]}$, where $\alpha, \beta \in [\![1, N]\!]$

[3] The double bracket notation $[\![1, N]\!]$ is used to denote the set of *integers* from 1 to N (both included).

[4] But of course, this is by no means the only possible choice.

are layer indices, N is the number of layers, and $\mathbf{m}$ and $\mathbf{n}$ run over the associated nitrogen and boron sublattices (respectively). In this basis, the general form of the tight-binding Hamiltonian $\hat{H}_0^{(el)}$ for hBN multilayers is as follows:

$$\begin{aligned}
\langle A_\alpha, \mathbf{m}|\hat{H}_0^{(el)}|A_\alpha, \mathbf{m}\rangle &= -\Delta \\
\langle B_\beta, \mathbf{n}|\hat{H}_0^{(el)}|B_\beta, \mathbf{n}\rangle &= +\Delta \\
\langle A_\alpha, \mathbf{m}|\hat{H}_0^{(el)}|B_\beta, \mathbf{n}\rangle &= \begin{cases} t_\perp & \text{if } \mathbf{m}, \mathbf{n} \text{ are in-plane 1n.n.} \\ t_\parallel & \text{if } \mathbf{m}, \mathbf{n} \text{ are out-of-plane 1n.n.} \\ 0 & \text{else} \end{cases}
\end{aligned} \tag{5.1}$$

where $\Delta, t_\perp$ and $t_\parallel$ are the kinetic parameters.[5] As usual, we assume our basis of atomic orbitals to be orthonormal.

We can define the corresponding tight-binding basis functions:

$$\begin{aligned}
|A_\alpha, \mathbf{k}\rangle &= \frac{1}{\sqrt{M}} \sum_{\mathbf{m}\in\Lambda_{A,\alpha}} e^{-i\mathbf{k}\cdot\mathbf{m}} |A_\alpha, \mathbf{m}\rangle \\
|B_\beta, \mathbf{k}\rangle &= \frac{1}{\sqrt{M}} \sum_{\mathbf{n}\in\Lambda_{B,\beta}} e^{-i\mathbf{k}\cdot\mathbf{n}} |B_\alpha, \mathbf{n}\rangle
\end{aligned}$$

where M is the number of unit cells (equivalently, the number of Boron *or* Nitrogen atoms in a given layer), so that $|\mu_\alpha, \mathbf{k}\rangle$ is the tight-binding basis function corresponding to the atoms of type $\mu = A$ or B in layer α. It is then possible to construct the integral transfer matrices, whose diagonalization yields the band structure of the system. While instructive, this step is not directly needed: we can formulate the excitonic Hamiltonian through second order perturbation theory starting from the direct space matrix elements given in equation 5.1. This is particularly useful here, since the integral transfer matrices are of dimension $2N$, and quickly become unwieldy.

5.1.3 Excitonic Hamiltonian

As per our previous strategy, we wish to define a basis of elementary excitations in which we can recast the Bethe-Salpeter Hamiltonian (neglecting exchange):

$$\hat{H}_X = \hat{H}_0 + \hat{U}$$

[5] We have used the symbol $\perp$ to denote in-plane quantities, because they are associated to vectors perpendicular to the stacking axis, while the symbol $\parallel$ has been chosen for out-of-plane quantities, which, in the case of the out-of-plane first nearest neighbor hoppings in most stackings, corresponds to vectors which are parallel to the stacking axis. This is the opposite of the notation chosen in [38], but follows the one of [48].

We proceed, as usual, by approximating the electronic Hamiltonian $\hat{H}_0^{(el)}$ by separating it into an effective low energy (hole) Hamiltonian $\hat{H}_h$ and an effective high energy (electron) Hamiltonian $\hat{H}_e$, so that:

$$\hat{H}_0 = \mathbb{1}_h \otimes \hat{H}_e - \hat{H}_h \otimes \mathbb{1}_e \tag{5.2}$$

which, as mentioned above, are obtained from second order perturbation theory by considering the hopping elements $t_\perp$ and $t_\parallel$ as perturbation, so that:[6]

$$\begin{aligned}\hat{H}_h \approx &- \sum_{\mathbf{m}\in\Lambda_h} \left(\Delta + \frac{{t_\perp}^2}{2\Delta}\mathcal{N}_\perp(\mathbf{m}) + \frac{{t_\parallel}^2}{2\Delta}\mathcal{N}_\parallel(\mathbf{m})\right) |\alpha,\mathbf{m}\rangle\langle\alpha,\mathbf{m}| \\ &- \sum_{<\mathbf{m},\mathbf{m'}>_\perp} \frac{{t_\perp}^2}{2\Delta} |\alpha,\mathbf{m}\rangle\langle\alpha,\mathbf{m'}| - \sum_{<\mathbf{m},\mathbf{m'}>_\parallel} \frac{t_\perp t_\parallel}{2\Delta} |\alpha,\mathbf{m}\rangle\langle\alpha',\mathbf{m'}| \\ &- \sum_{[\mathbf{m},\mathbf{m'}]_\parallel} \frac{t_\parallel^2}{2\Delta} |\alpha,\mathbf{m}\rangle\langle\alpha',\mathbf{m'}|\end{aligned} \tag{5.3}$$

$$\begin{aligned}\hat{H}_e \approx &\sum_{\mathbf{n}\in\Lambda_e} \left(\Delta + \frac{{t_\perp}^2}{2\Delta}\mathcal{N}_\perp(\mathbf{n}) + \frac{{t_\parallel}^2}{2\Delta}\mathcal{N}_\parallel(\mathbf{n})\right) |\beta,\mathbf{n}\rangle\langle\beta,\mathbf{n}| \\ &+ \sum_{<\mathbf{n},\mathbf{n'}>_\perp} \frac{{t_\perp}^2}{2\Delta} |\beta,\mathbf{n}\rangle\langle\beta,\mathbf{n'}| + \sum_{<\mathbf{n},\mathbf{n'}>_\parallel} \frac{t_\perp t_\parallel}{2\Delta} |\beta,\mathbf{n}\rangle\langle\beta',\mathbf{n'}| \\ &+ \sum_{[\mathbf{n},\mathbf{n'}]_\parallel} \frac{t_\parallel^2}{2\Delta} |\beta,\mathbf{n}\rangle\langle\beta',\mathbf{n'}|\end{aligned} \tag{5.4}$$

where $<\cdot,\cdot>_\perp$ (resp. $<\cdot,\cdot>_\parallel$) denotes summation over in plane (resp. out of plane) nearest neighbors of the same species, and $[\cdot,\cdot]_\parallel$ denotes summation over vertical neighbors of the same species between second nearest layers.[7] $\mathcal{N}_\perp(\cdot)$ (resp. $\mathcal{N}_\parallel(\cdot)$) denotes the number of in plane (resp. out of plane) nearest neighbors of the opposite species (boron for nitrogen and nitrogen for boron).

The quantities $\mathcal{N}_\perp(\cdot)$ and $\mathcal{N}_\parallel(\cdot)$ depend on the geometry of the system, and thus on the stacking of the layers. In the case of the AA' stacking, we

[6] In the equations below, we omit the A and B sublattice indices and write $|\alpha,\mathbf{m}\rangle$ for the hole state associated to $|A_\alpha,\mathbf{m}\rangle$, and $|\beta,\mathbf{m}\rangle$ for the electron state associated to $|B_\beta,\mathbf{m}\rangle$. In any event, $\hat{H}_h$ operates only on the hole subspace and $\hat{H}_e$ only on the electron subspace.

[7] For simplicity, we will often neglect these terms, given that they are off-diagonal elements in the *a priori* weakest hopping $t_\parallel^2$.

get:

$$\mathcal{N}_\perp(\mathbf{n}) = 3$$

$$\mathcal{N}_\parallel(\mathbf{n}) = \begin{cases} 2 & \text{if } \mathbf{n} \text{ belongs to the inner (2 to } N-1\text{) layers} \\ 1 & \text{if } \mathbf{n} \text{ belongs to the outer (1 and } N\text{) layers} \end{cases}$$

$\mathcal{N}_\perp(\mathbf{n})$ and $\mathcal{N}_\parallel(\mathbf{n})$ are, in fact, the in-plane and out-of-plane (respectively) coordination numbers for the site $\mathbf{n}$, or, in other words, its number of in-plane or out-of plane nearest neighbors. This is why $\mathcal{N}_\perp(\cdot)$ is constant, as it is fixed by the monolayer structure (it is, in fact, the quantity η from the previous chapters). On the other hand, $\mathcal{N}_\parallel(\cdot)$ is variable: sites in the surface layers only have one out-of-plane nearest neighbor (one above *or* one below), while atoms in the inner layers have two (one above *and* one below). Each in-plane nearest neighbor of an electron sites (resp. hole) contributes $t_\perp^2/(2\Delta)$ (resp. $-t_\perp^2/(2\Delta)$) to its effective kinetic onsite energy, while each out-of-plane nearest neighbor contributes $t_\parallel^2/(2\Delta)$ (resp $-t_\parallel^2/(2\Delta)$). Note that, in the AA' stacking, these coordination numbers of a site depend only on its layer index. It follows from equation 5.2 that the pair states $|A_\alpha, \mathbf{m}\rangle \otimes |B_\beta, \mathbf{n}\rangle$ involving a site on the surface layer will have a lower kinetic onsite energy than states which do not. In particular, the difference in effective kinetic onsite energy between a state for which both the electron and the hole are in the surface layers ($\alpha, \beta \in \{1, N\}$) compared to one where both the electron and the hole are in the inner layers ($\alpha, \beta \in [\![2, N-1]\!]$) is $t_\parallel^2/\Delta$, which we will see has an order of magnitude of about 0.1 eV. This effect is therefore quite significant, and will have important consequences on the splitting of excitonic states.

To proceed, let us recall the interpretation of states of the form $|A_\alpha, \mathbf{m}\rangle \otimes |B_\beta, \mathbf{n}\rangle$: they are localized electron hole-pairs, with the hole in layer α and the electron in layer β, separated by a hole-electron vector $\mathbf{R} = \mathbf{n} - \mathbf{m}$. To move to the representation of elementary excitations, our strategy is to construct tight-binding basis functions of translationally equivalent pairs. In the chain and in the single layer case, this meant grouping the pairs of common $\mathbf{R}$, as they shared the same matrix elements for the direct interaction and were translationally equivalent from the point of view of the kinetic Hamiltonian. In a multilayer system, however, this is no longer the case, because not all layers are translationally equivalent. The simplest way to generalize this strategy is to keep track of the layer indices. For all pairs $(\alpha, \beta) \in [\![1, N]\!]^2$, we can construct excitation sublattices:

$$\Lambda_{\alpha,\beta} = \Lambda_{B,\beta} - \mathbf{m}^0_{N,\alpha}$$

and for all $\mathbf{R} \in \Lambda_{\alpha,\beta}$, naturally build the tight-binding basis functions:

$$|\mathbf{R}_{\alpha,\beta}, \mathbf{Q}\rangle = \frac{1}{\sqrt{M}} \sum_{\mathbf{m}\in\Lambda_{A,\alpha}} e^{-i\mathbf{Q}\cdot\mathbf{m}} \, |A_\alpha, \mathbf{m}\rangle \otimes |B_\beta, \mathbf{m}+\mathbf{R}\rangle \tag{5.5}$$

which are the (generalization of the) elementary excitations for multilayer systems: note how such a state is indeed composed of translationally equivalent pairs from the excitation sublattice $\Lambda_{\alpha,\beta}$. The lattice of excitations is then the union of all the excitation sublattices:

$$\Lambda = \bigcup_{\alpha,\beta\in[\![1,N]\!]} \{\mathbf{R}_{\alpha,\beta} \quad / \quad \mathbf{R} \in \Lambda_{\alpha,\beta}\}$$

where we have purposefully introduced indices because the $\Lambda_{\alpha,\beta}$ are not necessarily disjoint. Since we will work mostly with direct states here, we set the notation $|\mathbf{R}_{\alpha,\beta}\rangle = |\mathbf{R}_{\alpha,\beta}, \mathbf{Q} = \mathbf{0}\rangle$. Likewise, when there is no ambiguity, we will write $|\alpha, \mathbf{m}\rangle$ for a hole state localized in layer α, and $|\beta, \mathbf{n}\rangle$ for an electron state localized in layer β.

Using the matrix elements of equations 5.3 and 5.4 as well as definition 5.5, it is then straightforward to express the matrix elements of the Bethe-Salpeter Hamiltonian (neglecting exchange):

$$\hat{H}_X = \hat{H}_0 + \hat{U}$$

in the basis of elementary excitations. We find, for the kinetic Hamiltonian (respectively for the diagonal and off-diagonal elements):

$$\langle \mathbf{R}_{\alpha,\beta} | \hat{H}_0 | \mathbf{R}_{\alpha,\beta} \rangle = 2\Delta + 3\frac{t_\perp^2}{\Delta} + \frac{\mathcal{B}(\alpha,\beta)}{2}\frac{t_\parallel^2}{\Delta}$$

$$\left\langle \mathbf{R}_{\alpha,\beta} \middle| \hat{H}_0 \middle| \mathbf{R}'_{\alpha',\beta'} \right\rangle = \begin{cases} \frac{t_\perp^2}{\Delta} & \text{if } \mathbf{R} \text{ and } \mathbf{R}' \text{ are } 1n.n. \text{ with } \alpha = \alpha' \text{ and } \beta = \beta' \\ \frac{t_\perp t_\parallel}{\Delta} & \text{if } \mathbf{R} \text{ and } \mathbf{R}' \text{ are } 1n.n. \text{ with } (|\alpha' - \alpha| = 1) \veebar (|\beta' - \beta| = 1) \\ \frac{t_\parallel^2}{\Delta} & \text{if } \mathbf{R}' - \mathbf{R} = \pm\mathbf{c} \text{ with } (|\alpha' - \alpha| = 2) \veebar (|\beta' - \beta| = 2) \\ 0 & \text{otherwise} \end{cases} \tag{5.6}$$

where $\veebar$ is the "exclusive or" logical symbol,[8] and the notion of first nearest neighbors ("1n.n.") is to be understood in the lattice of excitations, Λ. The

[8] Which is to say that, if p and q are propositions, $p \veebar q$ is true in two cases: p is true and q is false; p is false and q is true. It is false in all other cases: both p and q are false; both p and q are true. Physically, we are expressing here the fact that the hoppings of $\hat{H}_0$ only contains terms where either the hole or the electron "moves", but not both at the same time. *A fortiori*, only one of them can thus "change layers", so that a hopping can happen between excitations which differ either in α or in β, but not in both.

potential remains diagonal in the basis of elementary excitations:

$$\left\langle \mathbf{R}_{\alpha,\beta} \middle| \hat{U} \middle| \mathbf{R}'_{\alpha',\beta'} \right\rangle = \delta_{\mathbf{R},\mathbf{R}'} \delta_{\alpha,\alpha'} \delta_{\beta,\beta'} V_{\alpha,\beta}(\mathbf{R}) \tag{5.7}$$

Here, the $V_{\alpha,\beta}$ are model potentials to be specified, and $\mathcal{B}(\alpha,\beta)$ is a geometrical factor, given in the AA' stacking by:

$$\mathcal{B}(\alpha,\beta) = \begin{cases} 2 & \text{if } \alpha,\beta \in \{1,N\} \\ 3 & \text{if } \alpha \in \{1,N\} \text{ and } \beta \in [\![2,N-1]\!] \\ 3 & \text{if } \beta \in \{1,N\} \text{ and } \alpha \in [\![2,N-1]\!] \\ 4 & \text{if } \alpha \in [\![2,N-1]\!] \text{ and } \beta \in [\![2,N-1]\!] \end{cases} \tag{5.8}$$

This term relates to the out-of-plane coordination numbers of the hole and electron sites of the layers α and β respectively. In fact, we have:

$$\mathcal{B}(\alpha,\beta) = \mathcal{N}_{\parallel}\left(\mathbf{m}^0_{N,\alpha}\right) + \mathcal{N}_{\parallel}\left(\mathbf{n}^0_{B,\beta}\right)$$

so that $\mathcal{B}(\alpha,\beta)$ counts the total out-of-plane coordination numbers of a pair involved in an excitation of the type $|\mathbf{R}_{\alpha,\beta}\rangle$.

5.1.4 Discussion

The direct excitonic Hamiltonian, given in the basis of elementary excitations by equations 5.6 and 5.7 is *a priori* more complex in the multilayer case than in the single-layer case, and therefore requires some discussion.

Lattice of excitations

Let us first examine the lattice of excitations Λ. In the single layer case, the set of hole-electron vectors in Λ is a triangular lattice with the origin chosen at the center of one triangle, and then attaching to each excitation site the corresponding amplitude $\langle \mathbf{R}_{\alpha,\beta}|\Psi\rangle$ of the excitonic state yields (to zeroth order) the usual fixed hole representation of excitonic states in direct space. This is because, in the monolayer, all lattice positions of the hole (that is to say, all nitrogen centers) are equivalent. In other words, the lattice of exciations is just $\Lambda_{SL} = \Lambda_B - \mathbf{n}^0_N$, where Λ_B is the (triangular) lattice of Boron sites $\mathbf{n}^0_N$ is *any* Nitrogen / hole site position.

In multilayers, this is no longer the case: while it is still true that all positions of the hole within a given layer are equivalent, the layers are translationally inequivalent, and as a result one has to sweep the position of the hole over all layers in order to reconstruct the full symmetry of the wavefunction. We may picture the situation as follows: for each couple of layers

(α, β), select one hole position, say $\mathbf{m}^0_{N,\alpha}$ in layer α (the exact position chosen does not matter, as all hole positions *within that layer* are equivalent), and then consider all the electron hole vectors from this position of the hole to the possible electron positions (that is to say, all the boron centers) of layer β, $\Lambda_{B,\beta} = \mathcal{R} + \mathbf{n}^0_{B,\alpha}$. The set of hole-electron vectors associated to the couple (α, β) is then simply the shifted triangular lattice $\mathcal{R} + \mathbf{n}^0_{B,\beta} - \mathbf{m}^0_{N,\alpha}$, which is by definition the excitation sublattice $\Lambda_{\alpha,\beta}$: the set of all possible vectors from a hole site in layer α to an electron in layer β. It is important to note, at this point, that the geometrical sets $\Lambda_{\alpha,\beta}$ are not necessarily disjoint: a given hole-electron vector can be realized in several pairs of layers, and so different excitation sites might have the same position in the lattice.[9] This is the reason why the points of the lattice of excitations, Λ, must be labeled by the indices (α, β).[10]

The existence of these several excitation sublattices, or, more directly, the inequivalence of the different hole positions, points at a possible problem in the practice of fixing the hole at one given position when representing real space excitonic wavefunctions. Indeed, by setting the position of the hole in a given layer, this amounts to fixing α to a certain α_0, and "projecting out" all excitations outside of the sublattices $\Lambda_{\alpha_0,\beta}$. This may be extremely problematic, because there is no *a priori* guarantee that the amplitudes $\langle \mathbf{R}_{\alpha_0,\beta} | \Psi \rangle$ alone are representative of the full state $|\Psi\rangle$, and often they are not (we will present examples). An accurate direct space representation of an excitonic state therefore requires sweeping over all possible values of α (and, implicitly, β).

5.2 Bilayer

To make things concrete, and also because it already displays effects which are important for the general case, we start by discussing the $N = 2$ case.

5.2.1 Electronic structure

As we already stated, we do not strictly *need* the electronic bands, but we include them here for completeness. The integral transfer matrices are obtained by the usual procedure, and, in the $\{|B_1, \mathbf{k}\rangle, |A_1, \mathbf{k}\rangle, |B_2, \mathbf{k}\rangle, |A_2, \mathbf{k}\rangle\}$,

[9] In an AA' trilayer, for example, the geometrical excitation sublattices $\Lambda_{1,1}$ and $\Lambda_{3,3}$ contain the same vectors. The situation thus appears as soon as $N \geq 3$.

[10] The situation is formally similar to that of a multi-orbital tight-binding model, with the layer indices (α, β) playing the role of the orbital index, although this perspective does not appear particularly useful here.

read:

$$H_{AA'}^{(1nn)} = \begin{pmatrix} \Delta & t_\perp\gamma_1 & 0 & t_\parallel \\ t_\perp{\gamma_1}^* & -\Delta & t_\parallel & 0 \\ 0 & t_\parallel & \Delta & t_\perp{\gamma_1}^* \\ t_\parallel & 0 & t_\perp\gamma_1 & -\Delta \end{pmatrix}$$

where γ_1 has its usual definition:

$$\gamma_1(\mathbf{k}) = \sum_{\boldsymbol{\tau}} e^{i\mathbf{k}\cdot\boldsymbol{\tau}}$$

where the $\boldsymbol{\tau}$s are the first nearest neighbor Nitrogen to Boron vectors in layer 1. From there, the band energies are found:

$$E_{s_1,s_2}(\mathbf{k}) = s_1\sqrt{\Delta^2 + \Big(t_\parallel + s_2|t_\perp\gamma_1(\mathbf{k})|\Big)^2} \tag{5.9}$$

where $s_1, s_2 \in \{-1\,;1\}$ are signs: as expected, there are two conduction bands ($s_1 = +1$), and two valence bands ($s_1 = -1$).

Since $\gamma_1(\mathbf{K}) = 0$, the conduction and valence bands are twice degenerate at $\mathbf{K}$, and the transition energy between valence and conduction band at $\mathbf{K}$ is simply $E_\mathbf{K} = 2\sqrt{\Delta^2 + {t_\parallel}^2}$. However, contrary to the monolayer case, the direct electronic gap is typically not at $\mathbf{K}$, as can be seen easily from a plot of the bands. Still, the value of the gap can be readily obtained from the expression of the band energies. Indeed, up to a redefinition of s_2, we can replace $t_\parallel$ by $\left|t_\parallel\right|$ in the expression for $E_{s_1,s_2}(\mathbf{k})$ so that the upper valence and lower conduction bands both correspond to $s_2 = -1$. It is clear that the lowest direct transition energy is between these bands, so that we have to minimize:

$$\delta E(\mathbf{k}) = 2\sqrt{\Delta^2 + \Big(\left|t_\parallel\right| - |t_\perp\gamma_1(\mathbf{k})|\Big)^2}$$

which is clearly bounded from below by 2Δ. This bound is met if and only if there exists some $\mathbf{k}$ such that $|\gamma_1(\mathbf{k})| = \left|\frac{t_\parallel}{t_\perp}\right|$, which is guaranteed as long as $\left|\frac{t_\parallel}{t_\perp}\right| \leq 3$.[11] For physical values of $t_\perp$ and $t_\parallel$, this condition should always hold, so that within the first nearest neighbors approximation, the direct electronic gap is still:

$$E_g = 2\Delta$$

[11] Because γ_1 is continuous on the $\mathbf{\Gamma K}$ segment (which is a compact space), it follows from the intermediate value theorem that $|\gamma_1|$ takes every value between $|\gamma_1(\mathbf{\Gamma})| = 3$ and $|\gamma_1(\mathbf{K})| = 0$ on $\mathbf{\Gamma K}$. *A fortiori*, this also guarantees that the gap is realized on the triangle $\mathbf{\Gamma M K}$ where the bands are plotted. One such particular point where the gap is realized is given by $\mathbf{k}_g = \mathbf{K}\frac{3}{2\pi}\arccos\left(-\frac{1}{2} + \frac{1}{2}\left|\frac{t_\parallel}{t_\perp}\right|\right) \approx \mathbf{K}\Big(1 - \frac{\sqrt{3}}{2\pi}\left|\frac{t_\parallel}{t_\perp}\right|\Big)$.

In figure 5.2, we plot the tight-binding bands and transition energies, using parameters obtained from a fit on the *ab initio* exciton binding energies (same procedure as the monolayer, see next sections for details). The corresponding *GW* band structure computed by F. Paleari is also plotted for comparison.[38]

As we have already mentioned, this kind of fit on excitonic binding energies implicitly "sees" the transition energies rather than the bands. It produces a reasonable agreement in the neighborhood of **K** and in the **MK** region.[12] As in the monolayer, in addition to the π bands, σ and nearly free electron bands are visible in *ab initio* results, but they are likewise not expected to contribute much to the optical properties. We should point out that, since we only kept first nearest neighbors, the transition energies from the lowest valence band to the lowest conduction band and those from the highest valence band to the highest conduction band are found equal, so that the "middle" transition band is twice degenerate in tight-binding. This is not the case *ab initio*, where a small splitting can be seen. In tight-binding, the degeneracy may be lifted (away from **K**) by the inclusion of out-of-plane second nearest neighbors. However, the inclusion of in-plane second nearest neighbors alone, even though it breaks the electron-hole symmetry, is not enough to lift this degeneracy in the transition band structure.

5.2.2 Excitonic Hamiltonian

The excitonic Hamiltonian is the one of equations 5.6 and 5.7, for $N = 2$. It reads:

$$\langle \mathbf{R}_{\alpha,\beta} | \hat{H}_X | \mathbf{R}_{\alpha,\beta} \rangle = 2\Delta + 3t_\perp + \frac{t_\parallel^2}{\Delta} + V_{\alpha,\beta}(\mathbf{R})$$

$$\left\langle \mathbf{R}_{\alpha,\beta} \middle| \hat{H}_X \middle| \mathbf{R}'_{\alpha',\beta'} \right\rangle = \begin{cases} \frac{t_\perp^2}{\Delta} & \text{if } \mathbf{R} \text{ and } \mathbf{R}' \text{ are } 1n.n. \text{ with } \alpha = \alpha' \text{ and } \beta = \beta' \\ \frac{t_\perp t_\parallel}{\Delta} & \text{if } \mathbf{R} \text{ and } \mathbf{R}' \text{ are } 1n.n. \text{ with } (|\alpha' - \alpha| = 1) \veebar (|\beta' - \beta| = 1) \\ 0 & \text{otherwise} \end{cases} \tag{5.10}$$

We have $\mathcal{B}_{\alpha,\beta} = 2$ for all α, β, since there are only two layers, which are image by inversion of each other so that all coordination numbers are the same (equivalently, there are no specific surface effects because all layers are surface layers). Likewise, there are no second nearest layer hoppings because there are only two layers.

[12] It would be possible to fit the kinetic parameters directly on the band structure. It is then possible to get a better fit of the valence band at least, but this has the tendency to deteriorate the agreement with the *ab initio* transition energies.

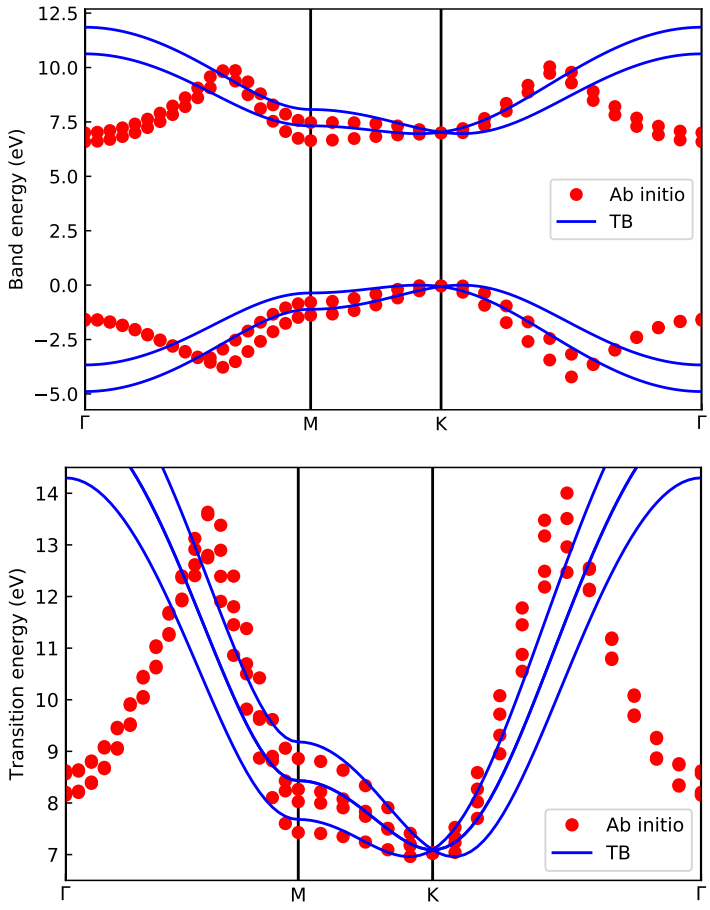

Figure 5.2: Band structure (top) and transition energies (bottom) for bilayer hBN in the AA' stacking. *Ab initio* data (red dots) is taken from a *GW* calculation by F. Paleari,[38] while tight-binding data (solid lines) corresponds to equation 5.9. Parameters used were $\Delta = 3.48$ eV, $t_\perp = -2.31$ eV and $t_\parallel = 0.685$ eV, obtained from the *ab initio* gap and a fit on the *ab initio* exciton binding energies. In the absence of second nearest neighbor out-of-plane hoppings, the transition energies from the lowest valence band to the lowest conduction band are the same as the ones between the upper valence band to the upper conduction band. For this reason, the "middle" tight-binding transition band is twice degenerate here.

The lattice of excitations, Λ, over which $\hat{H}_X$ is an effective tight-binding Hamiltonian, can be decomposed into four excitation sublattices, viz.:

$$\begin{aligned}\Lambda_{1,1} &= \mathcal{R} + \boldsymbol{\tau} \\ \Lambda_{2,2} &= \mathcal{R} - \boldsymbol{\tau} \\ \Lambda_{1,2} &= \mathcal{R} + \mathbf{d} \\ \Lambda_{2,1} &= \mathcal{R} - \mathbf{d}\end{aligned}$$

where $\boldsymbol{\tau}$ is any Nitrogen to Boron first nearest neighbor vector of layer 1. As a specificity of the $N = 2$ case, they are all disjoint. Note in particular that Λ is thus composed of *three* planes: $\Lambda_{1,1}$ and $\Lambda_{2,2}$ are in the $z = 0$ plane, while $\Lambda_{1,2}$ and $\Lambda_{2,1}$ are respectively in the $z = d$ and $z = -d$ planes. This lattice of excitations, along with the effective hoppings defined by $\hat{H}_0$, is depicted in figure 5.3.

By definition, sublattices of the form $\Lambda_{\alpha,\alpha}$ contain only *intra*layer transitions. We therefore call them in-plane (IP) sublattices, and excitons who are mainly composed of excitations from these sublattices are called in-plane excitons. Conversely, the $\Lambda_{\alpha,\beta}$ sublattices such that $\alpha \neq \beta$ correspond to *inter*layer transitions, which transfer charge from one layer to the other. We thus call these sublattices the interlayer (IL) sublattices, and the excitons mainly composed of these exciations are called interlayer excitons. Note that neither $\Lambda_{1,1}$ and $\Lambda_{2,2}$, nor $\Lambda_{1,2}$ and $\Lambda_{2,1}$ can interact directly with each other, as $\hat{H}_0$ contains no hoppings that connect them, and $\hat{U}$ is diagonal. Thus, the in-plane sublattices can only interact with each other through a second order process via the interlayer sublattices, and *vice versa*.

Because $N = 2$ is even, the system has the D_{3d} symmetry group, which includes inversion. The two in-plane (resp. interlayer) lattices are image of each other by inversion. This yields a constraint for the model potential:

$$\begin{aligned}\forall \mathbf{R} \in \Lambda_{1,1}, \quad V_{1,1}(\mathbf{R}) = V_{2,2}(-\mathbf{R}) \\ \forall \mathbf{R} \in \Lambda_{1,2}, \quad V_{1,2}(\mathbf{R}) = V_{2,1}(-\mathbf{R})\end{aligned}$$

i.e. $V_{1,1} = V_{2,2}$ and $V_{1,2} = V_{2,1}$ when seen as radial model functions.

5.2.3 Simple model for Davydov splitting

Among all electronic parameters, the weakest one is *a priori* the interlayer hopping, $t_\parallel$, or equivalently, out of all excitonic kinetic parameters, $T_\parallel$ is the weakest. Crucially, however, these parameters describe the coupling between the layers (from the electronic point of view) / the excitation sublattices

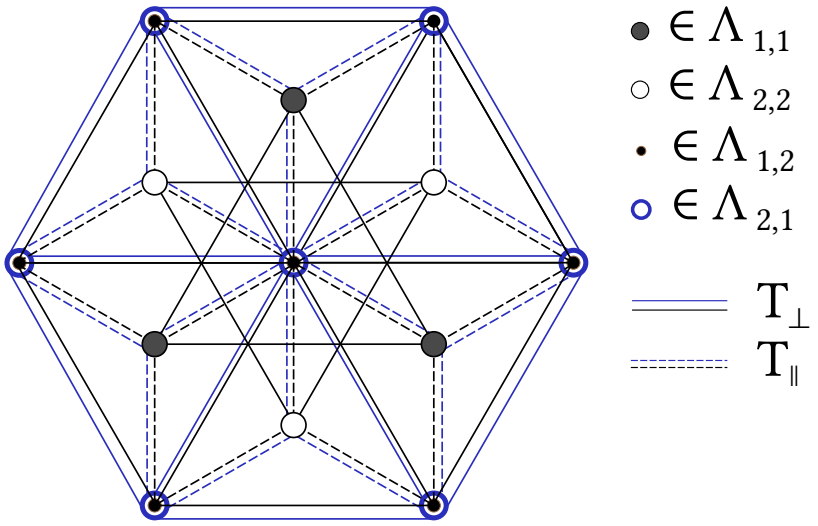

Figure 5.3: Lattice of excitations (with sublattices) and excitation hopping scheme for bilayer AA'. This is (up to completion by periodicity and addition of the potential, which we have not depicted here) the effective tight-binding problem associated to the excitonic Hamiltonian 5.10. Note that this is a top view; the system is composed of three planes: $\Lambda_{1,1}$ and $\Lambda_{2,2}$, the in-plane sublatices, lie in the $z = 0$ plane, as they correspond to in-plane excitations, while the interlayer sublattices $\Lambda_{1,2}$ and $\Lambda_{2,1}$ lie respectively in the $z = +d$ and $z = -d$ plane. Dots and circles correspond to excitation sites. Solid lines denote in-plane hoppings, of amplitude $T_\perp = \frac{t_\perp^2}{\Delta}$, which happen *within* a sublattice. On the other hand, dashed lines represent out-of-plane hoppings, of amplitude $T_\parallel = \frac{t_\perp t_\parallel}{\Delta}$, which connect different sublatices. Pictorially, they correspond to hoppings in which either the electron or the hole (but not both) "changes layers". Importantly, such hoppings only connect the interlayer sublattices to the in-plane sublattices: there is no (direct) connection between $\Lambda_{1,1}$ and $\Lambda_{2,2}$, nor between $\Lambda_{1,2}$ and $\Lambda_{2,1}$. Colors do not correspond to physical quantities and are used only to distinguish features which would otherwise be superimposed in top-view: for this reason, the sites of, and hoppings within, to and from sublattice $\Lambda_{2,1}$ have been colored in blue.

(from the excitonic point of view). We will show, in this section, that treating either as a perturbation yields a simple model for the Davydov splitting of the bilayer states.[13] Suppose, therefore, that $t_\parallel = 0$ (or $T_\parallel = 0$ while 2Δ and $T_\perp$ are kept fixed), and let $\hat{H}_\perp$ be the resulting excitonic Hamiltonian. Then, all sublattices decouple, i.e. $\hat{H}_\perp$ is block diagonal with respect to the sublattices. It is convenient (and possible), at this point, to define a basis $\mathcal{B}_0$ of $\hat{H}_\perp$ such that all its components have nonvanishing amplitudes on only one sublattice, and such that the eigenvectors for the $\Lambda_{2,2}$ and $\Lambda_{2,1}$ blocks are images by inversion of those of the $\Lambda_{1,1}$ and $\Lambda_{1,2}$ blocks respectively. Within this basis, we can speak in a well defined manner of the sublattice of a given eigenstate, and of its (strictly) in-plane (IP) or interlayer (IL) character.

We now aim to re-introduce $t_\parallel$ (or $T_\parallel$) as a perturbation of $\hat{H}_\perp$, and thus define the associated perturbing Hamiltonian $\hat{H}_\parallel = \hat{H}_X - \hat{H}_\perp$. Since each of the (decoupled) sublattices is its own tight-binding problem of C_{3v} (for the in-plane sublattices) or C_{6v} (for the interlayer sublattices, and thus *a fortiori* also C_{3v}) symmetry, the corresponding eigensubspaces are of dimension 2 for E-type states, and 1 for the others. Since sublattices come in inversion-equivalent pairs of two, the eigensubpaces of $\hat{H}_\perp$ are therefore of dimension 4 for E states and 2 for all others, barring accidental degeneracies.

We first consider the latter case. Let therefore $\mathcal{E}_\Psi = \{|\Psi_1\rangle, |\Psi_2\rangle\}$ be an eigensubspace of $\hat{H}_\perp$ with unperturbed energy E_Ψ, where $|\Psi_1\rangle$ and $|\Psi_2\rangle$ are extracted from $\mathcal{B}_0$ and therefore images of each other by inversion. Note that, by construction, $|\Psi_1\rangle$ and $|\Psi_2\rangle$ must both be of the same character (in-plane or interlayer). Second order degenerate perturbation theory allows us to build an effective Hamiltonian $\hat{H}_\Psi$ to express the effects of the perturbation $\hat{H}_\parallel$ in this basis:

$$\hat{H}_\Psi = E_\Psi \mathbb{1} + \frac{{t_\parallel}^2}{\Delta}\mathbb{1} + \begin{pmatrix} g_{1,1} & g_{1,2} \\ {g_{1,2}}^* & g_{2,2} \end{pmatrix}$$

where the second order terms are given by:

$$g_{i,j} = \sum_{\substack{|\mu\rangle \in \mathcal{B}_0 \\ E_\mu \neq E_\Psi}} \frac{\langle\Psi_i| \hat{H}_\parallel |\mu\rangle \langle\mu| \hat{H}_\parallel |\Psi_j\rangle}{E_\Psi - E_\mu} \tag{5.11}$$

Leveraging inversion symmetry, it can be shown that $g_{1,1} = g_{2,2}$ and that $g_{1,2} \in \mathbb{R}$, so introducing the notations $g_\Psi = g_{1,2}$ and $h_\Psi = g_{1,1} = g_{2,2}$, we are

[13] Which parametrization we choose is a matter of preference in interpretation here: both are equivalent, and the zeroth-order ($\hat{H}_\perp$) and the perturbating Hamiltonian ($\hat{H}_\parallel$) are the same in both cases, so it makes no practical difference. Were we taking further nearest neighbors into account, $\hat{H}_\perp$ would be chosen to contain the onsite energies and the in-plane hoppings (with out-of plane hoppigs set to zero), while $\hat{H}_\parallel = \hat{H}_X - \hat{H}_\perp$ would contain the out-of-plane hoppings.

left with:

$$\hat{H}_\Psi = \left(E_\Psi + \frac{{t_\perp}^2}{\Delta} + h_\Psi\right)\mathbb{1} + g_\Psi \begin{pmatrix} 0 & 1 \\ 1 & 0 \end{pmatrix}$$

from which it is clear that the states split into an even and an odd excitonic state, $|\Psi_\pm\rangle = (|\Psi_1\rangle \pm |\Psi_2\rangle)/\sqrt{2}$, with energies:

$$E_{\Psi,\pm} = E_\Psi + \frac{{t_\parallel}^2}{\Delta} + h_\Psi \pm g_\Psi \ ,$$

and this constitutes the Davydov splitting, with amplitude $s_\Psi = 2|g_\Psi|$. Note that by construction of $\mathcal{B}_0$, $|\Psi_+\rangle$ is even (*gerade*) with respect in inversion symmetry, while $|\Psi_-\rangle$ is odd (*ungerade*). Which one of the odd or the even state is lowest in energy depends on the sign of g_Ψ.

For zeroth-order states of E-type, $\mathcal{E}_\Psi$ is of dimension $2 \times 2 = 4$. In this case, we choose the corresponding eigenbasis such that the components on one of the sublattices are chiral, while the components on the other sublattice are their image by inversion. Because $\hat{H}_\parallel$ has the full symmetries of the system, and in particular the C_3 symmetry, it can only couple states of the same chirality (i.e. of the same irreducible *complex* repesentation of C_3), and therefore the corresponding 4×4 effective Hamiltonian obtained from perturbation theory is block diagonal with respect to chirality. These two "chiral blocks" are complex conjugates of one another, and so both chiral components have the same energy corrections. Possibly up to a change of basis (moving to a real basis), this lets us recover the same formalism as in the non-degenerate case. In-particular, our pair of E-type states splits into one even E_g exciton (twice degenerate) and one odd E_u exciton (twice degenerate). This will have rather important consequences in terms of the optical properties of the system, as group theoretical selection rules for the D_{3d} point group mandate that, for light polarized in-plane, only E_u states can be bright.

Because $\hat{H}_\parallel$ contains only out-of-plane hoppings, i.e. excitations between in-plane and interlayer excitations, the expression of the coupling matrix elements, g_Ψ, given in equation 5.11, shows that only interlayer states contribute to the splitting of in-plane states, and *vice versa*, as noted by Koskelo and coauthors.[83] In addition, only eigenstates of $\hat{H}_\perp$ of compatible symmetries can couple, i.e., since $\hat{H}_\parallel$ has the system's symmetry, excitons transforming according to the same representation of D_{3d}. Further, from the matrix elements of $\hat{H}_\parallel$, we have that $g_\Psi \propto \left(\frac{t_\perp t_\parallel}{\Delta}\right)^2$, so that the amplitude of the Davydov splitting scales as $t_\parallel^2$ in the perturbative regime. This, as well as the fact that the splitting is a second order phenomenon in $\hat{H}_\parallel$ can be traced back to the fact the hoppings in $\hat{H}_\parallel$ do not allow for the motion of both

the hole and the electron at the same time, or, equivalently, that in-plane (resp. interlayer) sublattices not directly connected to each other, but only indirectly through the interlayer (resp. in-plane) sublattices. Pictorially, to connect two states of the same character (in-plane or intelrayer) one must go through two "consecutive" hoppings: one for the electron, and one for the hole, and, in doing so, go through states of the opposite character.

Formally, if we limit the coupling described in equation 5.11 to neighboring states of energy E_ϕ, the amplitude of the splitting reads:

$$s_\Psi = 2\left|\frac{k_\Psi T_\parallel^2}{E_\Psi - E_\phi}\right|$$

where $k_\Psi \sim \frac{1}{T_\parallel^2}\langle\Psi_1|\hat{H}_\parallel^2|\Psi_2\rangle$ is a dimensionless quantity. The numerical diagonalization of $\hat{H}_X$ shows that, at least early in the excitonic series, E states exhibit a lower Davydov splitting than A states. It also shows that interlayer states of E symmetry do not occur until relatively high energies, while in-plane and interlayer A excitons both appear early and at comparable energies. Assuming k_Ψ to be roughly constant, this may give some qualitative understanding as to why, at least early in the excitonic series, the in-plane E states are less split than the A states.

We must close this section with a *caveat*: the description of the influence of the interlayer coupling and the resulting Davydov splitting that we have given here was obtained through perturbation theory. As such, it is expected to be valid only in the perturbative regime, which is to say if the perturbation remains small compared to the energy separation of $\mathcal{E}_\Psi$ and other unperturbed subspaces of the same symmetry and of opposite character, with which it may interact. These hypotheses are well satisfied for the lowest bound Davydov pair of the bilayer, for which this description is rather accurate. It remains reasonably valid for the first few states of the excitonic series, approximately up to the second peak (which are the states that we report in table 5.1). Further up, the energy separation between states becomes smaller, and in some cases the interlayer coupling appears to drive more complex behaviors. We will briefy discuss these phenomena in section 5.2.6.

5.2.4 Numerical diagonalization

To proceed further to a numerical calculation, we need to specify our model potentials, say $V_{1,1}$ and $V_{1,2}$. A simple choice is to take both as Rytova-Keldysh potential, but with two different polarizability radii: one for in-plane

exciations, and one for out-of-plane excitations. In other words, the "usual" Rytova-Keldysh potential being given by:

$$V_{RK}(R) = \frac{\pi e^2}{2r_0}\Big[H_0\Big(\frac{R}{r_0}\Big) - Y_0\Big(\frac{R}{r_0}\Big)\Big]$$

with $R = \|\mathbf{R}\|$, we introduce an in-plane (resp. interlayer) polarizability radius ρ_{IP} (resp. ρ_{IL}) such that:

$$V_{1,1}(R) = \frac{\pi e^2}{2\rho_{IP}}\left[H_0\left(\frac{R}{\rho_{IP}}\right) - Y_0\left(\frac{R}{\rho_{IP}}\right)\right]$$
$$V_{1,2}(R) = \frac{\pi e^2}{2\rho_{IL}}\left[H_0\left(\frac{R}{\rho_{IL}}\right) - Y_0\left(\frac{R}{\rho_{IL}}\right)\right]$$

This choice is, in some sense, arbitrary,[14] but it will suffice here to provide a reasonable description of the first few states of the excitonic series. With this, the excitonic Hamiltonian has been parametrized, and our next task is to estimate values for these parameters.

To this end, we employ the same strategy as in the monolayer case. We start by noting that 2Δ is nothing but the direct gap of the system, so we implicitly fix it to the *ab initio* value and shift our energy scale by -2Δ so that the eigenvalues of $\hat{H}_X$ are now the binding energies. The Hamiltonian has now effectively four parameters. We then have two kinetic parameters, which are effective hoppings: the hopping of excitations within a given sublattice, $T_\perp = \frac{t_\perp^2}{\Delta}$, and the hopping of excitations between different (connected) sublattices, $T_\parallel = \frac{t_\perp t_\parallel}{\Delta}$.[15] This latter quantity corresponds to the "motion" of a hole or an electron to a different layer. The potential parameters are simply ρ_{IP} and ρ_{IL}, as defined above. $\hat{H}_X$ now depends on four parameters, $T_\perp$, $T_\parallel$, ρ_{IP} and ρ_{IL}, which we adjust to reproduce the binding energies of the first eight *ab initio* excitons (not counting degeneracies). Best fit parameters are found to be:

$$T_\perp = 1.53 \text{ eV} \quad ; \quad T_\perp = 0.454 \text{ eV} \quad ; \quad \rho_{IP} = 12.3 \text{ Å} \quad ; \quad \rho_{IL} = 16.8 \text{ Å} \tag{5.12}$$

[14] Its long range potential asymptotics are problematic, since we would expect that, for excitons with a large Bohr radius, the entire bilayer would appear as a thin film, i.e. that for large R, both $V_{1,1}$ and $V_{1,2}$ would converge to a single Rytova-Keldysh potential, which is not the case here (although for very large R, both $V_{1,1}$ and $V_{1,2}$ *do* indeed converge to the unscreened Coulomb potential). In recent years, more sophisticated model potentials have been developped for Van der Waals multilayers; see e.g. [91, 74, 92, 93, 94]

[15] The quantity $\frac{t_\parallel^2}{\Delta}$ which appears in several places in the Hamiltonian is just $\frac{T_\parallel^2}{T_\perp}$, so it is not an extra parameter.

Using the set value of Δ, we can extract the values of the associated electronic parameters:

$$\Delta = 3.48 \text{ eV} \quad ; \quad t_\perp = 2.31 \text{ eV} \quad ; \quad t_\parallel = 0.685 \text{ eV} \tag{5.13}$$

which were used to compute the electronic and transition band structures depicted in figure 5.2, yielding reasonable agreement with the underlying GW calculation.

We report the *ab initio* and resulting tight-binding binding energies in table 5.1, as well as the symmetries of the states within the D_{3d} point group. The latter can be easily determined by accessing the phases of the tight-binding states, and for some states the same has been done *ab initio* to confirm the behavior of the states under inversion (which is not trivial to do by looking at the densities alone). It can be checked that all reported excitons do indeed come in Davydov pairs of even (*gerade*) and odd (*ungerade*) subspaces, with respect to the system's inversion symmetry. Numbering excitons according to ascending *ab initio* energy levels, these pairs are $(1, 2)$, $(3, 8)$, $(4, 6)$ and $(5, 7)$. Davydov pairs $(1, 2)$ and $(5, 7)$ are essentially in-plane, and correspond to the splitting of the first two monolayer excitons, respectively. The other reported pairs, however, are essentially interlayer states, and are therefore not obtained from the splitting of monolayer states. In this sense, they are "new": from the point of view of the model presented in section 5.2.3, they come from the splitting of unperturbed eigenstates of $\hat{H}_\perp$ which were purely interlayer, and therefore have no monolayer equivalent. This is in contrast to the previously discussed in-plane states which come from unperturbed in-plane states, whose sublattices, up to inversion, are equivalent to the monolayer lattice of excitations.[16]

As we have pointed out, because the system has inversion symmetry, only odd states can be bright, and, further, for in-plane polarized light, only states with the E symmetry can be bright. The only optically active states are therefore those that transform according to the E_u representation of D_{3d}. As a result, the lowest bound exciton is dark, and the main absorption peak comes from exciton 2, which is its Davydov partner, located about 30 meV above. For completeness, we note that these selection rules are modified when light is not polarized in-plane. In particular, when light is polarized parallel to the stacking axis (i.e. when the field is perpendicular to the layers), only states of A_{2u} symmetry can be bright. The first bright state in this case would therefore be state 4.

[16]Note, however, that the parameters of $\hat{H}_\perp$ differ from the monolayer parameters. Still, the similar geometry leads to similar excitonic states.

Exciton	1 (×2)	2 (×2)	3	4	5 (×2)	6	7 (×2)	8
Ab initio	−1.644	−1.614	−1.170	−1.162	−1.022	−1.000	−0.943	−0.899
Tight binding	−1.630	−1.612	−1.272	−1.220	−1.003	−0.891	−0.977	−0.895
Bright	no	yes	no	no	no	no	yes	no
Symmetry	E_g	E_u	A_{1g}	A_{1u}	E_g	A_{2g}	E_u	A_{2u}
Description	IP	IP	IL	IL	IP	IL	IP	IL

Table 5.1: First eight bilayer excitons (*ab initio* ordering). Listed are the *ab initio* and fitted tight-binding energies (all given in eV). The optical activities and symmetries (in the D_{3d} point group) of the states are also listed, as well as their description in terms of being in-plane (IP) or interlayer (IL).

Overall, the agreement of tight-binding with *ab initio* is fairly reasonable. The agreement in binding energies for the two in-plane pairs is rather good, and even though we are less accurate for interlayer states, we could still recover the *ab initio* binding energies within about 10%. This latter difficulty may originate from our use of a Rytova-Keldysh potential to model the interlayer potential. Indeed, the interlayer system is very inhomogenous, and has a finite thickness (of order d), which is not negligible compared to the characteristic radii of the first few interlayer states. Nevertheless, in both cases, the qualitative agreement with the *ab initio* wavefunctions is satisfying, as can be seen, e.g., in the example wavefunction provided in figure 5.5.

5.2.5 Analysis of the first bilayer states

Let us now briefly review the first AA' bilayer excitons, as reported in table 5.1. We discuss them by pairs, and separate the analysis of in-plane and interlayer pairs.

In-plane pairs

As we mentionned, the in-plane sublattices are of the form $\mathcal{R} \pm \boldsymbol{\tau}$, which, up to inversion, is the same geometry as the monolayer lattice of excitations, as can be seen in figure 5.3. The associated blocks of $\hat{H}_\perp$ are therefore effectively monolayer problems, up to a variation of the kinetic and potential parameters, which, according to the fitted parameters of equation 5.12, is mild. For the first few low energy in-plane excitons, we therefore expect pairs whose components on each sublattice are similar to the monolayer states, and this is indeed the case with pairs $(1, 2)$ and $(5, 7)$, which can be associated the first and second monolayer states.

We start with the pair $(1, 2)$. For illustration, panels (a) and (b) of figure 5.5 present respectively the wavefunctions two component states from excitons 1 and 2, both *ab initio* and in the tight-binding framework. This pair is descended from the (analogue of the) first monolayer exciton, which is twice degenerate and of E symmetry. As expected, the excitons of the pair $(1, 2)$ are also of E symmetry: exciton 1 is even, so E_g and therefore dark, while exciton 2 is odd, hence E_u and thus bright. Exciton 2 is therefore the first absorption peak of the AA' bilayer, and, like the first monolayer exciton, it dominates the absorption spectrum. The magnitude of the *ab initio* Davydov splitting for this pair comes out at about 30 meV, and from there we estimate the associated effective coupling at $g_\Psi \sim -15$ meV < 0. The tight-binding model moderately underestimates this splitting, and finds a magnitude of about 18 meV. Overall, this pair is relatively weakly split and, with a binding energy of around -1.6 eV, it is energetically well separated from the other excitons of the system, the first of which lies about 0.4 eV above. Overall, the pair is less bound than exciton 1 of the monolayer, from which it descends. This can be, in part, attibuted to the additional screening due to the presence of a second layer.

The case of the $(5, 7)$ pair is similar. Inspection of the excitonic wavefunctions suggests that it stems from the splitting of the second monolayer exciton, which likewise had E symmetry. Here, we thus have a pair of doubly degenerate excitons, with 5 being E_g (even, and thus dark) and 7 being E_u (odd, thus bright). The second peak in the bilayer absorption spectrum thus originates from exciton 7. The magnitude of the Davydov splitting is larger this time, at about 79 meV *ab initio*. Interestingly, we find again the even state at a lower energy than the odd state, so that the effective coupling $g_\Psi \approx -40$ meV < 0 is again negative.

Interlayer pairs

Interlayer pairs are, in some sense, "new" states, whose intensity lies mostly in the interlayer sublattices. In the AA' stacking, these sublattices are of the form $\mathcal{R} \pm \mathbf{c}$, and even discounting the vertical translation, do not have the same geometry as the monolayer lattice of excitations.[17] Loosely speaking, we thus expect a different "excitonic series" for the low energy interlayer excitons, and this is indeed what we observe.

[17] We could indeed see the interlayer blocks of $\hat{H}_\perp$ as independent $2D$ problems, on which the potentials are still radial: even then we obtain different problems. See figure 5.3. For completeness, we point out that the situation is different in, say, the AB stacking, where one of the interlayer sublattices *does* have the same geometry as the monolayer lattice of excitations.

The lowest bound interlayer exciton is exciton 3, which is part the $(3, 8)$ pair, which is depicted in panels (c) and (d) of figure 5.5. With an *ab initio* binding energy of -0.899 eV, state 8, with its A_{2u} symmetry, would be the first absorption peak for light polarized parallel to the stacking axis, lying about 0.72 eV above the lowest bound $(1, 2)$ pair, which contains the first bright exciton for in-plane polarized light (exciton 2). Remarkably, the $(3, 8)$ pair exhbits a very large Davydov splitting, of 271 meV. Again, the lowest bound state of the pair is even, so $g_\Psi < 0$.

The other interlayer pair reported in table 5.1, $(4, 6)$, exhibits a lower but comparatively still large Davydov splitting of 161 meV. Contrary to the other pairs of table 5.1, however, analysis of the tight-binding wavefunctions reveals that it is the odd state which is lower in energy, providing an example of a case where $g_\Psi > 0$.

To summarize, we provide in figure 5.4 a schematic representation of the splitting scheme for the states discussed above.

5.2.6 Optical properties and higher excited states

We now turn our attention to the optical properties of the AA' bilayer, i.e. the computation of its absorption spectrum, as well as its higher excited states. Before we begin, we must note that our simple tight-binding model, with *ad hoc* electron-hole potential, is not expected to be particularly precise when describing high energy states. Still, at least within the model description, interesting phenomena occur for states above the ones reported in table 5.1. We therefore briefly discuss them here, not quantitatively, but as a preliminary qualitative insight on the effects of interlayer coupling.

First, we need an expression for the optical matrix elements, i.e. a generalization of formula 3.6. The derivation is overall similar, so we simply state the result: for an arbitrary (direct) excitonic state $|\Phi\rangle = \sum_{\mathbf{R}_{\alpha,\beta}\in\Lambda} \Phi_{\mathbf{R}_{\alpha,\beta}} |\mathbf{R}_{\alpha,\beta}\rangle$, we have:

$$\langle\emptyset|\hat{\mathbf{p}}|\Phi\rangle = -\frac{m_e\sqrt{M}}{i\hbar} \sum_{\mathbf{R}_{\alpha,\beta}\in\Lambda} t_{\mathbf{R}_{\alpha,\beta}} \Phi_{\mathbf{R}_{\alpha,\beta}} \mathbf{R} \tag{5.14}$$

where the $t_{\mathbf{R}_{\alpha,\beta}} = \left\langle A_\alpha, \mathbf{m}^0_{N,\alpha} \middle| \hat{H}^{(el)}_0 \middle| B_\beta, \mathbf{m}^0_{N,\alpha} + \mathbf{R} \right\rangle$ are electronic hoppings, i.e. here $t_\perp$ or $t_\parallel$ if $\mathbf{R}$ is (respectively) an in-plane or interlayer Nitrogen to Boron nearest neighbor vector (in the crystal lattice), and zero otherwise. Indirect states are dark.

An important consequence of this formula in the first nearest neighbors approximation is that, for light polarized in-plane, only exitations in the in-plane sublattices can contribute to a state's oscillator strength. This is because the only out-of-plane excitations for which $t_{\mathbf{R}_{\alpha,\beta}} \neq 0$ are vertical,

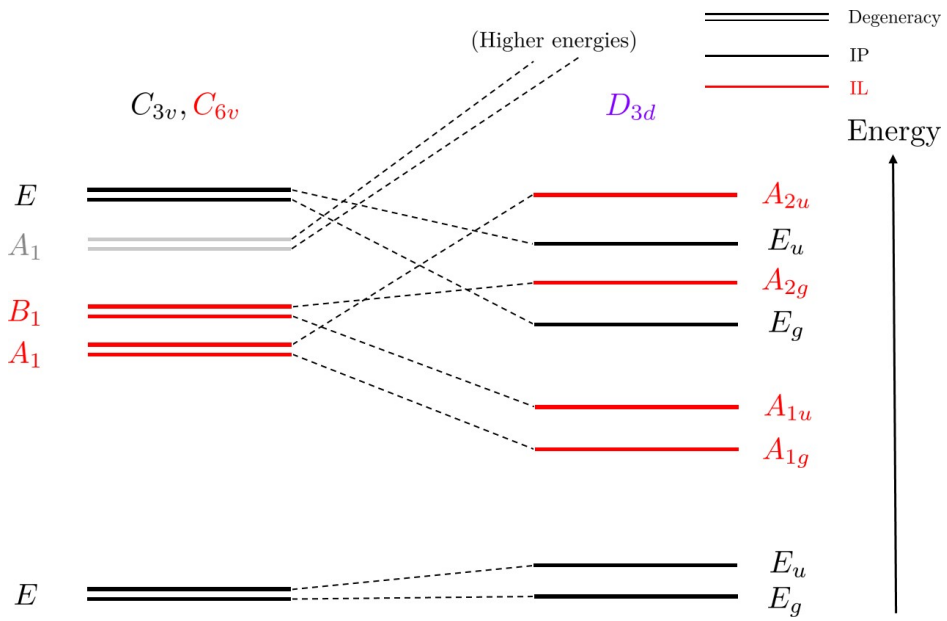

Figure 5.4: Qualitative splitting scheme for the hBN AA' bilayer for the excitons in table 5.1, following the scheme described in section 5.2.3. Left: excitons without interlayer couplings (eigenstates of $\hat{H}_\perp$). Right: bilayer excitonic states, in *ab initio* order. The eigenstates of $\hat{H}_\perp$ were computed using the tight-binding model with the interlayer coupling $t_\parallel$ set to zero, but other parameters set by equations 5.12 and 5.13. Eigenstates of $\hat{H}_\perp$ have been labeled according to the symmetry groups of the intra- and interlayer sublattices (resp. C_{3v} and C_{6v}), while the excitons of the full system have been accordingly classified according to the representatiosn of the D_{3d} group. For clarity, states transforming according to the E, E_g or E_u representations have been represented as non-degenerate. States depicted in black (resp. red) are of in-plane (resp. interlayer) character. The states depicted in grey do not appear in table 5.1: in $\hat{H}_\perp$ they correspond to the first A_1 monolayer state, but the full interlayer coupling brings them to higher energies.

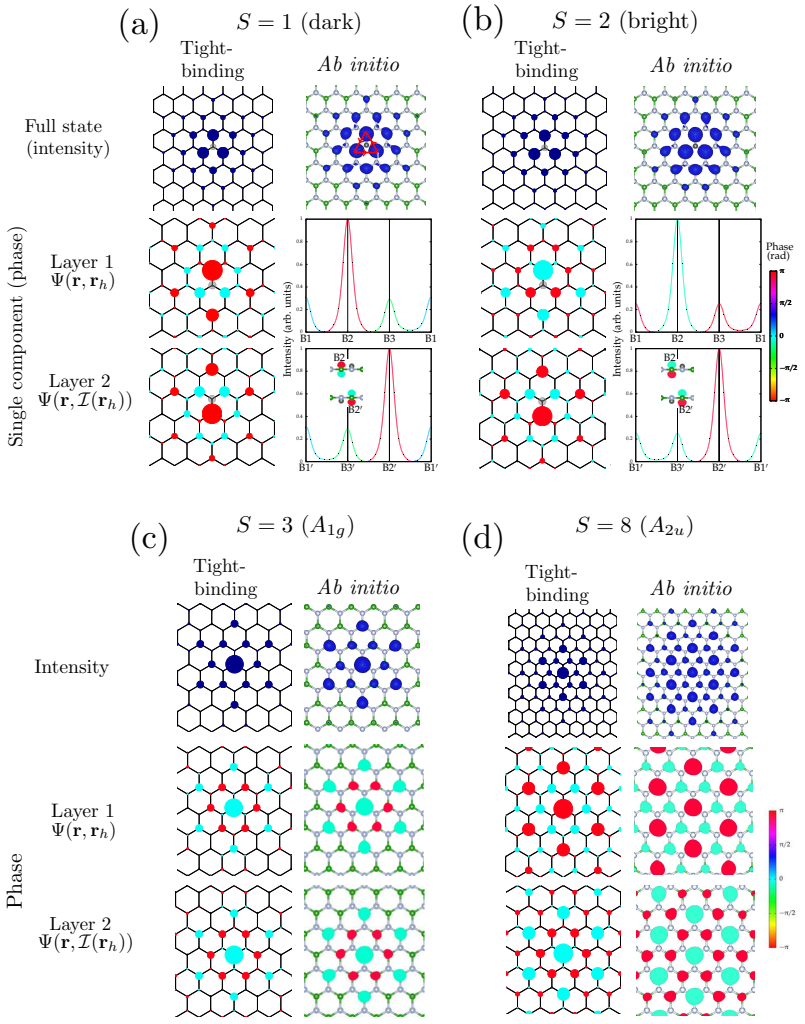

Figure 5.5: Figure reproduced from [38]. *Ab initio* results by F. Paleari. The wavefunctions $\Psi(\mathbf{r}, \mathbf{r_h})$ have been represented in the "fixed hole" representation. Here, $\mathbf{r}$ corresponds to the electron coordinate and $\mathbf{r}_h$ corresponds to to the fixed hole coordinate, which has been set on a Nitrogen site. $\mathcal{I}(\mathbf{r}_h)$ corresponds to its image by inversion. For consistency, tight-binding wavefunctions have been likewise projected, including first-order corrections to the electron and hole states; the gray disk depicting the position of the hole. Details of the *ab initio* calculations and representations can be found in [38]. Panels (a) and (b) depict the $(1, 2)$ pair. Since these states have most of their intensity in-plane, we only show the electronic amplitudes in the same layers as the hole (the equivalent in the full TB description would be only showing the IP sublattices). Panels (c) and (d) depicts components of excitons 1 and 2. Since these states have most of their intensity out-of-plane, we only show the electronic amplitudes in the layer without the hole (corresponding to only showing the IL sublattices).

i.e. along $\mathbf{e}_z$ and therefore orthogonal to any in-plane polarization vector: they are the ones that correspond to the first nearest neighbor out-of-plane electronic hoppings. We therefore expect that, in general, for a state to contribute a significant peak in the absorption spectrum for in-plane polarized light, it should have significant in-plane intensity on the in-plane sublattices.

Equipped with equation 5.14, we can now compute the oscillator strength of the bilayer excitons, as well as its absorption spectrum. One of the interests of having a (computationally efficient) tight-binding model at our disposal, however, is that we can vary its parameters, in order to gain insight on their effects. Therefore, we will generalize the idea of section 5.2.3, where we had seen that the variations of $t_\parallel$ could be seen as the main drive of the evolution from the monolayer to the bilayer, and compute the excitonic states, their oscillator strength and the resulting spectra for a range of values of $t_\parallel$, from 0 to its fitted value, $t_\parallel^{opt.}$.

The corresponding spectra are displayed in figure 5.6. As we have already discussed in section 5.2.3, when $t_\parallel = 0$, the sublattices decouple, and the problem of the in-plane sublattices is formally similar to the monolayer problem, up to a moderate variation of the parameters. Adding to this that, at $t_\parallel = 0$, interlayer states are purely interlayer, and therefore do not contribute to absorption within our approximations, the spectrum for $t_\parallel = 0$ is therefore analogous to the monolayer spectrum. Indeed, we can recognize its first three peaks, which we have previously classified as the $1s$, $2p$ and $2s$ states.

The model evolution happening in the region of the third monolayer peak is particularly interesting: following the peaks as the interlayer coupling is increased, we see that the peak that was initially associated to the monolayer $2s$ state decays in intensity, while another "new" peak rises next to it. The situation can be clarified by examining the evolution of the excitonic states while $t_\parallel$ is varied. To this end, we depict in figure 5.7 the evolution of the excitonic binding energies, along with the oscillator strength associated to their subspaces. Let us now provide a tentative explanation. It can be seen that this "new" peak comes from what was originally a degenerate set of dark states at a binding energy of about -0.7 eV. Careful analysis of the corresponding excitonic wavefunctions shows that this is a group of four excitons of E symmetry (so eight states), which subsequently split into two Davydov pairs. One of these excitons has the correct symmetries to couple with a "bare" ($t_\parallel = 0$) bright in-plane state, and as a result the "bare" in-plane exciton and this "bare" interlayer exciton mix. The initially interlayer exciton therefore acquires intensity in the in-plane sublattices, which, seeing as it has the right symmetries, allows it to obtain a non-zero oscillator strength according to equation 5.14. Conversely, the initially "bare" in-plane state ac-

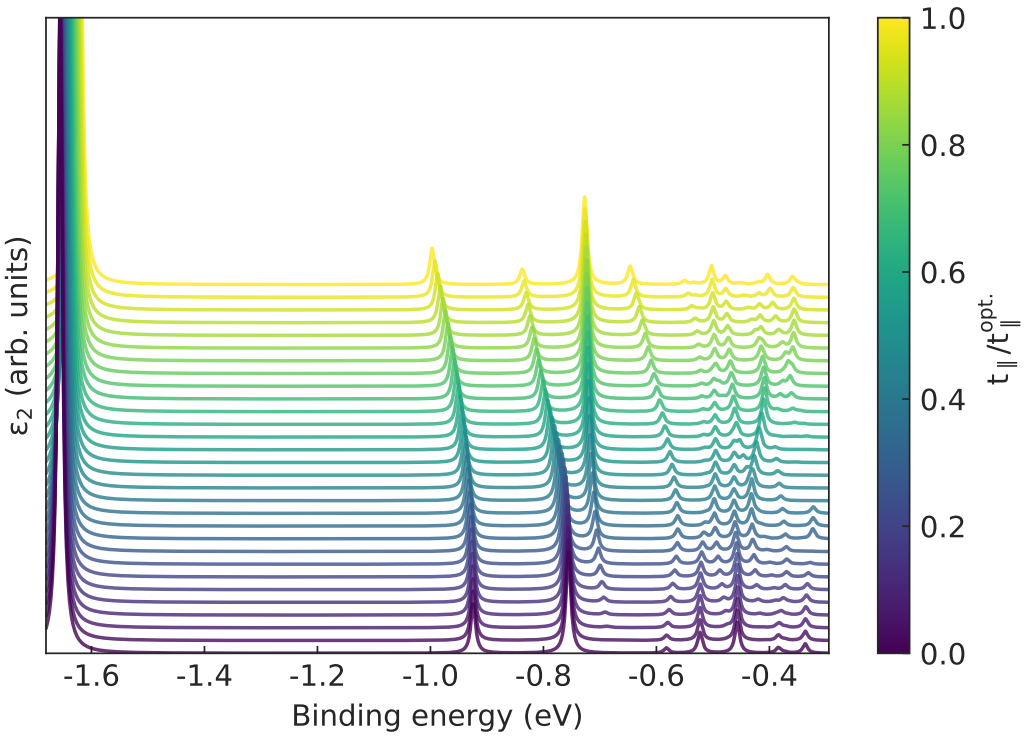

Figure 5.6: Evolution of the absorption spectrum of hBN AA' bilayer when the interlayer coupling $t_\parallel$ is varied from 0 (monolayer like) to its fitted value of $t_\parallel^{opt.} = 0.685$ eV. Other parameters are kept to their fitted values, as given in equations 5.12 and 5.13. We used a lorentzian broadening of 5 meV, and have cut viewing range below the maximum of the first peak to better display the more complex evolution of the subsequent ones. All spectra were normalized with respect to their highest peak, and their zero lines slightly displaced for clarity. Note that $t_\parallel$ is increased as one goes *up* in the figure, so that the "true" bilayer spectrum is the one at the "top". It can be compared with the *ab initio* spectrum presented in the $N = 2$ panel of figure 5.8. The quantitative agreement does not appear to be very good, but we are here more after qualitative insight (see text).

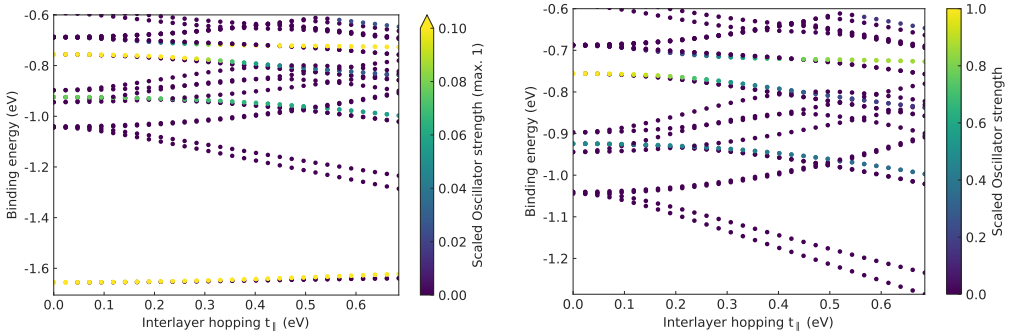

Figure 5.7: Evolution of the binding energies of the excitons of hBN AA' bilayer and their ocsilator strengths when the interlayer coupling $t_\parallel$ is varied from 0 (monolayer like) to its fitted value of $t_\parallel^{opt.} = 0.685$ eV. Other parameters are kept to their fitted values, as given in equations 5.12 and 5.13. Left: all excitons up to a binding energy of -0.6eV; the oscillator strength scale has been compressed for clarity: without this, the brightness of the exciton 2 overwhelms the scale. Right: same plot, but without excitons 1 and 2. Oscillator strength have been scaled to the brightest peak. For the low energy states, compare with the schematic depiction of figure 5.4.

quires intensity in the interlayer sublattices at the cost of some of its in-plane intensity, and therefore loses oscillator strength by the same mechanism.

The magnitude of the change in oscillator strength, as well as the analysis of the excitonic wavefunctions shows that this is not a small perturbative effect. At these energies, "bare" intra- and interlayer excitons appear to couple strongly. It is likely that this phenomenon is responsible for the complexity of the spectra of multilayer (and bulk) hBN above the low energy peaks: the observed peaks cannot be trivially traced back to a monolayer peak. Instead, they arise from excitons with a mixed intra- and interlayer character, which come about through the coupling of bare bright intralayer excitons with the "new" bare interlayer states, as we have describe above.

5.3 General multilayers

We now come to the general case, with particular interest on the situation where $N \geq 3$, as we expect surface effects. The excitonic tight-binding Hamiltonian is theoretically known for arbitrary N, although the determination of the direct electron-hole potential in that case is not trivial.

We note, however, that the Davydov multiplet associated to the lowest bound monolayer exciton is expected to account for the dominant structure

in the absorption spectrum. It is therefore natural, at this point, to focus our study on this Davydov multiplet. To this end, we shall extend the perturbative model for the Davydov splitting developed in section 5.2.3. Because the first Davydov multiplet is expected to remain well separated in energy from other excitons, we expect our perturbative treatment to remain qualitatively accurate.

5.3.1 Introduction and *ab initio* results

By way of introduction to the discussion of general multilayers, we display some *ab initio* results from F. Paleari. In figure 5.8, the absorption spectra of N-layers are shown for $N = 1, 2, 3$ and 5, along with a qualitative scheme of the splitting of the Davydov multiplet associated to the first monolayer exciton. This Davydov multiplet (N-uplet, more precisely) gives rise to the main structure in the absorption spectrum.

The situation for $N = 1$ was the object of chapter 4. When moving to $N = 2$, we have seen in section 5.2.3 that the first exciton of the monolayer undergoes a Davydov splitting into a bonding and an antibonding pair (respectively even and odd with respect to inversion) in this order, whose components are respectively dark and bright. The situation becomes more complex for $N = 3$ and $N = 5$. There, we still observe an alternance of bright and dark peaks, but they do not split "symmetrically" anymore. It appears that the N-uplet in both cases displays two structures: two excitons at low energy, and $N-2$ at high energies. As the pentalayer exemple shows, these two structures are rather well separated in energy.

From our earlier discussions, we do expect surface effects in multilayers for $N > 2$: we had seen that excitations involving only sites on the surface layers had a kinetic energy lower than the ones involving only inner sites, by about 100 meV. This strongly hints at the fact that the two substructures we are observing arise because of surface effects. The goal of this section is to show that this is indeed the case, and to provide a generalization of the model discussed in 5.2.3 that accounts for such effects. We will then use this model to investigate the optical activity of the resulting Davydov N-uplet, and how it evolves with the number of layers.

5.3.2 Linear chain effective Hamiltonian

As in section 5.2.3, we wish to construct an effective Hamiltonian using degenerate perturbation theory. It thus seems natural to define a Hamiltonian $\hat{H}_\perp$ from the full tight-binding excitonic hamiltonian $\hat{H}_X$ by setting the interlayer hopping $t_\parallel$ to zero and to construct an eigenbasis of $\hat{H}_\perp$ with the

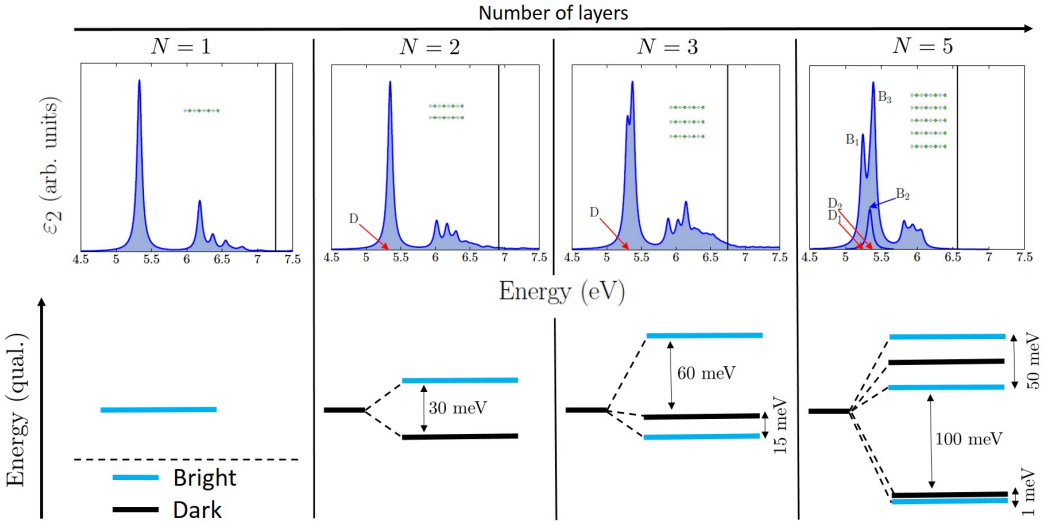

Figure 5.8: Top panels adapted from [38]. *Ab initio* results by F. Paleari; computational details available in [38]. Top: *ab initio* spectra for monolayer ($N = 1$), bilayer ($N = 2$), trilayer ($N = 3$) and pentalayer ($N = 5$). The black vertical line indicates the electronic gap. Dark states in the first Davydov N-uplet have been indicated by D. In the pentalayer, bright states have also been labeled. There, the second bright state (B_2) is not very bright, and the corresponding peak has been overlayed onto the main spectra for clarity. Bottom: qualitative depiction of the Davydov splitting of the first monolayer exciton into the corresponding Davydov N-uplet. Energies are not to scale, but the orders of magnitude of the main splittings have been reported.

defining properties of the basis $\mathcal{B}_0$ which we used in the bilayer case.

There is, however, a crucial difference between the $N = 2$ (bilayer) case and the general case. Indeed, not all layers are related by symmetry anymore, and therefore, they are no longer equivalent. In excitonic language, the blocks of $\hat{H}_\perp$ that correspond to *geometrically* equivalent sublattices are not necessarily identical up to symmetry anymore. There are two physical reasons for this. First, as we have already pointed out in section 5.1.3, excitations involving sites on the surface ($i = 1$ or N) layers have a lower kinetic / single particle contribution to their effective on-site energies when compared to excitations involving only the inner layers ($i \in [\![2, N-1]\!]$). This effect is proportional to $t_\parallel^2$, and can be seen in $\hat{H}_X$ through the variations of $\mathcal{B}(\alpha, \beta)$ (equations 5.6 and 5.8). It is thus contained in $\hat{H}_\parallel = \hat{H}_X - \hat{H}_\perp$. Secondly, we expect excitations involving sites on the outer layers to be subjected to a (gradually) weaker screening of the direct electron-hole interaction than those involving sites on the inner layers. Consequently, excitations involving outer sites are expected to be more bound, which again lowers their effective on-site energies. Algebraically, this effect manifests itself through variations of $V_{\alpha,\beta}$, and is therefore contained in the direct electron-hole interaction part of the hamiltonian, $\hat{U}$, which is part of $\hat{H}_\perp$. Importantly, both effects go in the same direction: they lower the effective on-site energies of excitations composed of sites on the outer layers compared to those involving sites on the inner layers: they are thus expected to drive surface effects.

Formally, we take our zeroth-order Hamiltonian to be a modified version $\bar{H}_\perp$ of $\hat{H}_\perp$ such that all screening variations have been averaged out.[18] Pictorially, this zeroth-order hamiltonian $\bar{H}_\perp$ describes the problem of N identical hBN layers where the electrons are forbidden to hop between layers. We thus construct an eigenbasis $\mathcal{B}_0$ of $\bar{H}_\perp$ with analogous properties to the one constructed in the $N = 2$ case.[19] In particular, the ground state eigensubspace of $\bar{H}_\perp$ is spanned by N copies of the analogue of the lowest bound monolayer exciton. Using the same technique as in the $N = 2$ case, we treat these copies as effectively non-degenerate states $|1\rangle, |2\rangle, \ldots, |N\rangle$ such that $|i\rangle$ corresponds to the effective copy on the i^{th} layer (in excitonic language: in the $\Lambda_{i,i}$ excitation sublattice). Using second order degenerate perturbation theory in the subspace spanned by $\{|i\rangle\}_{i\in[\![1,N]\!]}$, we build an effective Hamiltonian $\hat{H}_f$ to describe its splitting. A detailed derivation of this effective hamiltonian from the tight-binding excitonic Hamiltonian $\hat{H}_X$ through the steps outlined above is given in appendix E of [38]. Neglecting second nearest

[18] We average the functions $V_{\alpha,\beta}$ over the (α, β) pairs of geometrically equivalent $\Lambda_{(\alpha,\beta)}$.

[19] Which is to say that states on geometrically equivalent sublattices are copies or images by inversion of each other, accordingly.

planes hoppings and assuming screening variations are limited to the surface layers, we find, up to a shift in the global energy scale:

$$\hat{H}_f = -|g| \left[\sum_{\langle i,j \rangle} |i\rangle\langle j| + X(|1\rangle\langle 1| + |N\rangle\langle N|) \right] \tag{5.15}$$

where the sum is taken over neighboring layers. The quantity g is analogous to g_Ψ in section 5.2.3, and describes the strength of the coupling between states of neighboring layers. Based on *ab initio* results for $N = 2$, 3, 5 and $+\infty$ (bulk), we have taken it here negative. X is a dimensionless quantity characterizing the surface effects described above, and corresponds to the energy difference between the "bare" (uncoupled, i.e. $g = 0$) inner and surface excitons divided by the interlayer coupling energy. Expressions for g and X in terms of unperturbed eigenstates of $\bar{H}_\perp$ can be found in [38]. We only note here that g, like its bilayer equivalent, describes the coupling of "bare" in-plane excitons though "bare" interlayer states. Since the electron-hole potential is diagonal in the basis of elementary excitations, it does not induce a coupling between states on different sublattices. X accounts for potential effects as well as surface effects originating from the kinetic Hamiltonian.

Independently of its microscopic origins, $\hat{H}_f$ effectively describes the tight-binding problem of a linear chain with boundary effects: each layer of the multilayer can be seen as a chain site, while the "copies" of the monolayer excitons are the corresponding orbitals. This Hamiltonian can be diagonalized using standard methods, and a detailed solution can be found in [95], including asymmetric boundary conditions. The eigenvalues are given by:

$$E_n = -2|g| \cos(k_n)$$

where the allowed wavenumbers k_n are determined by the boundary conditions. In the case of an ideal linear chain ($X = 0$), they would be $k_n = n\pi/(N+1)$ for $n \in [\![1, N]\!]$. Here, $X \neq 0$ *a priori*, and they are determined implicitly from the relation:

$$(\cos(k) - p(X)) \sin(Nk) = r(X) \sin(k) \cos(Nk) \tag{5.16}$$

with:

$$p(X) = \frac{2X}{X^2+1} \quad ; \quad r(X) = \frac{X^2-1}{X^2+1}$$

It can be shown that, for values of X larger than a certain threshold (specifically $X \geq (N+1)/(N-1)$), equation 5.16 admits $N-2$ real solutions in $[0, \pi[$ and two purely imaginary ones, which correspond to surface states, the

lowest one of which is even with respect to the $1D$ inversion symmetry of the chain, while the next is odd.[20]

This behavior can be easily seen if one considers the regime $X \gg 1$. In this case, at zeroth order, the 2 surface layers are decoupled from the $N-2$ inner layers. This approximation is relevant because *ab initio* results suggest that this might indeed be the case for $N > 3$. In this case, we have two degenerate surface states with energy $-|g|X$, and the inner layers behave as an ideal ($X = 0$) linear chain of $N-2$ sites with eigenenergies $E_n = -2|g|\cos\left(\frac{n\pi}{N-1}\right)$ and eigenstates which are, overall, delocalized over the $N-2$ coupled layers.

5.3.3 Inner and surface states

At this point, the coupling between inner and surface layers can be re-introduced as a perturbation.

Inner states

The situation for the inner states is rather straightforward. Going to first order in $1/X$, we can obtain an effective hamiltonian describing the inner states:

$$\hat{H}_{inner} = -|g|\left[\sum_{\langle i,j\rangle} |i\rangle\langle j| - \frac{1}{X}(|1\rangle\langle 1| + |N\rangle\langle N|)\right]$$

which has the same structure as $\hat{H}_f$, but with $X \leftarrow -\frac{1}{X}$. This is, however a crucial difference, because, at large X, $\hat{H}_{inner}$ therefore describes a linear chain with *weak* border effects, which only slightly displace the energy levels and modify the states, but are not expected to bring about qualitative changes.

Surface states

Surface states are more interesting. Since we have only kept "first nearest layers" interactions in $\hat{H}_f$, the two zeroth-order surface states $|1\rangle$ and $|N\rangle$ are not coupled by second order perturbation theory as soon as $N > 3$: we simply obtain a rigid energy shift of their (degenerate) energies, which lower slightly to become $-|g|(X + 1/X)$. However, *ab initio* calculations do show a splitting of the two surface states, which we can understand as $|1\rangle$ and $|N\rangle$ interacting through the $N-2$ inner states. Instead of going to higher order perturbation theory, we simply introduce an effective coupling γ between

[20] The exact expression of the associated eigenstates can be found in [95].

the two surface states as well as an effective on-site energy E_s, yielding an effective Hamiltonian in the subspace $\{|1\rangle, |N\rangle\}$:

$$\hat{H}_{surface} = -|g|[E_s + \gamma(|1\rangle\langle N| + |N\rangle\langle 1|)]$$

which is the general form of a two level system, and describes a splitting into an even and an odd surface state:

$$\left|\Psi^s_{\pm}\right\rangle = \frac{1}{\sqrt{2}}(|1\rangle \pm |N\rangle) \quad ; \quad E_s = -|g|(E_s \pm \gamma)$$

with a splitting width of $2|g|\gamma$. We can estimate $E_s = -|g|(X + 1/X)$ from above, and an asymptotic study of equation 5.16 yields $\gamma \approx 1/X^{N-2}$. As expected, the lowest energy state is even, and the other (higher) one is odd. The splitting between them, as expected, is predicted to be very weak and decay rapidly with the number of layers.

5.3.4 Optical activities in the lowest bound Davydov multiplet

We now turn to the problem of estimating the optical activity of the components of a Davydov multiplet.

Theory and selection rules

Let us first notice that the linear chain model of equation 5.16 exhibits $1D$ inversion symmetry. This symmetry corresponds with the mirror (N odd) or inversion (N even) symmetry of the multilayer crystal.[21] Within the chain model we can write a multiplet eigenstate $|\Psi\rangle$ as:

$$|\Psi\rangle = \sum_{i=1}^{N} A_i |i\rangle$$

Because the typical exciton energy is of the order of the gap, which is much larger than the Davydov splitting, comparing the oscillator strength of the states in a multiplet essentially amounts to comparing the magnitude of their momentum matrix elements, i.e. the quantities $|\langle\emptyset|\mathbf{e}\cdot\hat{\mathbf{p}}|\Psi\rangle|^2$, where $|\emptyset\rangle$ is the vacuum state and $\mathbf{e}$ is the polarization vector of the incoming light. We thus have:

$$\langle\emptyset|\hat{\mathbf{p}}|\Psi\rangle = \sum_{i=1}^{N} A_i \langle\emptyset|\hat{\mathbf{p}}|i\rangle$$

[21] This immediately provides a selection rule for even N: in that case, only odd states can be dark.

Leaving us to examine the $\langle\emptyset|\hat{\mathbf{p}}|i\rangle$. Recall that, for an arbitrary (direct) excitonic state $|\Phi\rangle = \sum_{\mathbf{R}_{\alpha,\beta}\in\Lambda} \Phi_{\mathbf{R}_{\alpha,\beta}} |\mathbf{R}_{\alpha,\beta}\rangle$, we have:

$$\langle\emptyset|\hat{\mathbf{p}}|\Phi\rangle = -\frac{m_e\sqrt{M}}{i\hbar} \sum_{\mathbf{R}_{\alpha,\beta}\in\Lambda} t_{\mathbf{R}_{\alpha,\beta}} \Phi_{\mathbf{R}_{\alpha,\beta}} \mathbf{R}$$

where the $t_{\mathbf{R}_{\alpha,\beta}} = \left\langle A_\alpha, \mathbf{m}^0_{N,\alpha} \middle| \hat{H}_0^{(el)} \middle| B_\beta, \mathbf{m}^0_{N,\alpha} + \mathbf{R} \right\rangle$ are electronic hoppings, i.e. here $t_\perp$ or $t_\parallel$ if $\mathbf{R}$ is (respectively) an in-plane or interlayer Nitrogen to Boron nearest neighbor vector (in the crystal lattice), and zero otherwise. From there, leveraging the geometry of the lattice of excitations as well as the definition of the basis $\{|i\rangle\}_{i\in[\![1,N]\!]}$, it can be seen that:

$$\forall i \in [\![1, N-1]\!], \quad \langle\emptyset|\hat{\mathbf{p}}|i+1\rangle = -\langle\emptyset|\hat{\mathbf{p}}|i\rangle \tag{5.17}$$

which can be understood pictorially as follows: because in the AA' stacking, two consecutive layers are "heads to tails", so are the wavefunction dipoles of the copies of the in-plane "monolayer" excitons they support. This leads to the convenient expression:

$$\langle\emptyset|\hat{\mathbf{p}}|\Psi\rangle = -\mathbf{d}_1 \sum_{i=1}^{N} (-1)^i A_i \tag{5.18}$$

where $\mathbf{d}_1 = \langle\emptyset|\hat{\mathbf{p}}|1\rangle$ is in-plane. If we introduce the auxiliary vector $|z\rangle = -\sum_{i=1}^{N} (-1)^N |i\rangle$, the above can be rewritten very compactly: $\langle\emptyset|\hat{\mathbf{p}}|\Psi\rangle = \mathbf{d_1} \langle z|\Psi\rangle$.

We can go further. Because the chain has inversion symmetry, our eigenstate $|\Psi\rangle$ of $\hat{H}_f$ can be chosen to have a definite parity with respect to this symmetry, i.e. such that there exists $s_\Psi = \pm 1$ such that for all $i \in [\![1, N]\!]$, $A_{N-i+1} = s_\Psi A_i$. Inserting this constraint into equation 5.18, it can be checked that:

$$\langle\emptyset|\hat{\mathbf{p}}|\Psi\rangle = -\frac{1 - s_\Psi(-1)^N}{2} \mathbf{d}_1 \sum_{i=1}^{N} (-1)^i A_i$$

where the extra factor of $\left[1 - s_\Psi(-1)^N\right]/2$ expresses a selection rule for multiplets of in-plane states:

- if N is even, the even ($s_\Psi = +1$) states are dark.
- if N is odd, the odd ($s_\Psi = -1$) states are dark.

which, as announced, depends on the parity of the number of layers.

With this, we can go back to our initial goal of comparing the oscillator strengths of the different multiplet states. As we have already pointed out,

the relevant quantities are the $|\langle\emptyset|\hat{\mathbf{p}}|\Psi\rangle|^2$, which, according to the above, evaluate to $|\mathbf{e}\cdot\mathbf{d}_1|^2|\langle z|\Psi\rangle|^2$. To make comparisons meaningful, we need to compute the total optical activity of the multiplet as a reference, i.e.:

$$\mathcal{N}^2 \approx \sum_{|\Psi\rangle\in\mathcal{M}} |\langle\emptyset|\mathbf{e}\cdot\hat{\mathbf{p}}|\Psi\rangle|^2 = |\mathbf{e}\cdot\mathbf{d}_1|^2 \underbrace{\sum_{|\Psi\rangle\in\mathcal{M}} |\langle z|\Psi\rangle|^2}_{=\||z\rangle\|^2=N}$$

where $\mathcal{M}$ is an orthnormal eigenbasis of $\hat{H}_f$. The latter sum is conveniently evaluated using the auxiliary vector $|z\rangle$: because we have taken $\mathcal{M}$ orthnormal, it is just $\||z\rangle\|^2 = N$.[22] Discarding factors that are constant across the multiplet, we are thus left with the study of the quantities:

$$f_\Psi = \frac{|\langle z|\Psi\rangle|^2}{N} = \frac{1}{N}\left|\sum_{i=1}^{N}(-1)^i A_i\right|^2 \tag{5.19}$$

which are both (approximately) proportional to the oscillator strength of their associated state $|\Psi\rangle$ and sum to one over the multiplet: $\sum_{|\Psi\rangle\in\mathcal{M}} f_\Psi = 1$.

The object of the following sections is to explicitly compute the f_Ψ in the limit of strong border effects ($X \gg 1$).

Surface states

In this limit, the surface states are the lowest bound states, lying at an energy of about $-|g|X$. Their case is rather straightforward: there are only two of them, one bright, one dark. Since the lowest bound state is always even with respect to the chain inversion, it is bright if N is even, otherwise it is the odd surface state above it which is bright. In either case, the bright state has an effective oscillator strength of:

$$f_{surf} = \frac{2}{N}$$

This is interesting in itself. Indeed, for large X, the surface states form a low energy subspace that is well seperated from the "high" energy subspace corresponding to the inner states, and so by the sum rule on the f_Ψ, the intensity of the peak due to the surface states will decrease approximately as the inverse of the number of layers with respect to the collective intensity of the peaks due to the inner states within the multiplet. We will come back to this idea once we have examined the optical activty of the inner states.

[22] This result is parameter independant: pictorially, each of the N layers contributes one unit of oscillator strength to the system, which the different splitting effects then redistribute between the multiplet states.

Inner states

The case of the inner states requires slightly more calculations. Taking the limit $X \gg 1$, we can treat the inner layers as an ideal (finite) linear chain of $N-2$ sites, completely decoupled from the surface layers. In this case, we find the usual eigenenergies and eigenstates, which we can label with $m \in [\![1, N-2]\!]$:

$$E_m = -2|g| \cos\left(\frac{m\pi}{N-1}\right) \quad ; \quad A_i = \sqrt{\frac{2}{N-1}} \sin\left(\frac{im\pi}{N-1}\right) \tag{5.20}$$

while effective oscillator strengths are given by:

$$f_{\Psi_m} = \frac{1+(-1)^{N+m}}{N(N-1)} \tan^2\left(\frac{m\pi}{2(N-1)}\right)$$

We thus find that odd and even states alternate in such a way that if m is odd, then $|\Psi_m\rangle$ is even and *vice versa*, and therefore bright or dark in accordance with the selection rules presented above.

The energies of the peaks appear at the energies E_m for values of m corresponding to bright states. Further, the inner states and their associated peaks are concentrated in the energy interval $\left[-2|g| \cos\left(\frac{\pi}{N-1}\right), 2|g| \cos\left(\frac{\pi}{N-1}\right)\right]$, so that when X is large enough, they are well separated from the surface states and their peak. Because f_{Ψ_m} is a sharply increasing function of m and E_m also increases with m, we expect to see a series of increasingly bright states as we go up in energy. The last bright state, say $|\Psi_{m^*}\rangle$ is therefore expected to dominate this part of the absorption spectrum while previous inner states effectively provide a fine-structured "shoulder" to its "left". In fact, it is always the highest energy state of the multiplet, corresponding to $m^* = N-2$.

We should mention at this point that there is a physical reason for us to expect the oscillator strength of inner states to increase as energy increases. Indeed, looking at equations 5.17 and 5.18, we know that the wavefunction dipoles of the "monolayer" excitons, the $\mathbf{d}_i = \langle\emptyset|\hat{\mathbf{p}}|i\rangle$ on two consecutive layers are opposite from one another, because of the AA' geometry. For a state to have a high oscillator strength, the preferred situation is for the contributions of each layer to the total dipole ($\langle\emptyset|\hat{\mathbf{p}}|\Psi\rangle$), the $A_i\mathbf{d}_i$, to all be in phase. But since the $\mathbf{d}_i$ are exactly anti-aligned, this happens only if the amplitudes on the layers, the A_i, are likewise. In other words, the brightest states are the most antibonding ones, which (in an ideal chain) are the highest in energy since the interlayer coupling, g, is negative.

Discussion and optical estimation of the number of layers

The predicted absorption spectra corresponding to the lowest bound Davydov mutiplet within the linear chain model are depicted for various values of N in figure 5.9. The two structures, one due to the surface states, and one due to the inner states, are clearly visible.

For large but finite N, it can be shown that:

$$f_{\Psi_{m^*}} \approx \frac{8}{\pi^2}\frac{N-1}{N}$$

so that a fraction of about $\frac{8}{\pi^2} \sim 81\%$ of the total oscillator strength of the multiplet is due to the brightest inner state. In the bulk limit, which corresponds to $N \to +\infty$, the energy of this state tends towards $2|g|$ and more and more bright states appear arbitrarily close to this energy. These states will contribute the missing $\sim 19\%$ to form a single bright peak with all of the oscillator strength of the multiplet, as expected in the spectrum of bulk hBN. On the other hand, the effective oscillator strength of the bright surface state decays quickly with the number of layers, as $f_{surf} = \frac{2}{N}$, while the total oscillator strength of the inner states takes up the remaining $\Sigma_m f_{\Psi_m} = \frac{N-2}{N}$.

These dependencies of the predicted spectrum on the number of layers opens an interesting avenue of investigation. Indeed, we can think of reversing the problem, and asking if we can estimate the number of layers from the knowledge of the absorption spectrum. The most straightforward way to do so is by comparing the inner features with the surface peak. Using the results obtained above, if we consider all the inner peaks as one composition peak of strength $f_{inner} = \Sigma_m f_{\Psi_m}$, then the ratio of intensities between this peak and the surface state peak satisfies:

$$N \approx 2\left(\frac{f_{inner}}{f_{surf}} + 1\right) \tag{5.21}$$

If we compare instead intensity of the surface peak with the intensity of the brightest inner peak Ψ_{m^*}, we have:

$$\frac{f_{\Psi_{m^*}}}{f_{surf}} = \frac{1}{N-1}\cot^2\left(\frac{\pi}{2(N-1)}\right) \tag{5.22}$$

which can be solved for N if the ratio of intensities $\frac{f_{\Psi_{m^*}}}{f_{surf}}$ is known. In the large N limit, this equation can be simplified to:

$$N \approx \frac{\pi^2}{4}\frac{f_{\Psi_{m^*}}}{f_{surf}} + 1 \tag{5.23}$$

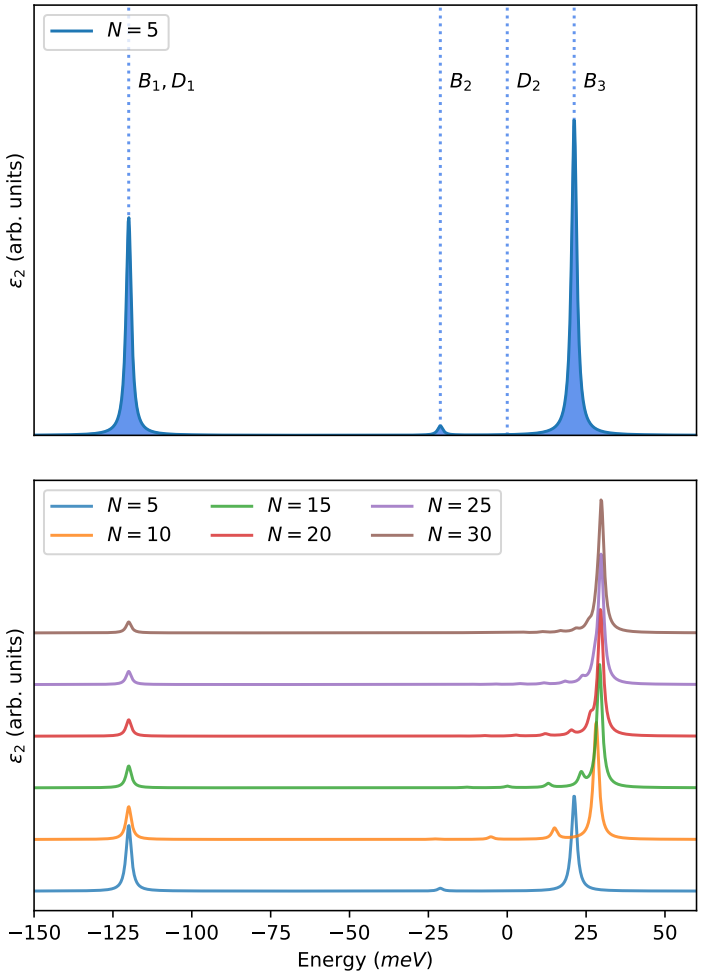

Figure 5.9: Absorption spectra corresponding to the lowest bound Davydov multiplet, computed using the linear chain model in the large X limit. For concreteness, we have taken the parameters $|g| = 15$ meV and $X = 8 \gg 1$, although the qualitative features of the spectrum are largely independent ($|g|$ simply sets the energy scale, while X sets the energy position of the surface states). Top: spectrum for the pentalayer ($N = 5$), with dotted lines indictating the positions of the bright (B) and dark (D) states. Labels are the same as in figure 5.8. Bottom: spectra for various values of the number of layers N. A lorentzian broadening of 1 meV was used. In the bottom panel, the spectra were normalized such that the total oscillator strength of the multiplet is unity ($\sum_{|\Psi\rangle \in \mathcal{M}} f_\Psi = 1$), independently of N. For clarity the zeros of the spectra were shifted for the different values of N. The zero of energies is implicitly set for each spectrum, and corresponds to the zero of energies for $\hat{H}_f$, i.e. the energy of the unperturbed multiplet, before splitting. Notice how, as N is increased, the surface peak decreases in intensity relative to the main inner peak.

Using equation 5.21 with the *ab initio* oscillator strengths for the pentalayer ($N = 5$), we estimate $N \approx 5.6$. Equation 5.22, which only considers the brightest inner peak, leads to $N \approx 5.0$, while its large N approximation, equation 5.23, yields $N \approx 4.6$. Overall, the estimates are rather good, especially when only the main inner peak is used instead of the full inner structure. This can be traced back to the fact that the intensities of the lower energy inner peaks are no so well reproduced by the linear chain model (they tend to be underestimated).

5.3.5 Comparison with *ab initio* results and representation of multiplet states

At this point, we have to verify, more generally, if the approximations we have made in the preceding sections are in fact justified, and if they provide at least a reasonable qualitative description of the *ab initio* results. Likewise, even though its qualitative results do not depend too much on them, it is useful to estimate the parameters involved in the linear chain model, g and X, in order to understand how they vary with the number of layers. At least three quantities can be fruitfully compared with *ab initio*: the energies of the multiplet, the multiplet states, and the resulting absorption spectra.

A direct manner to estimate the parameters of the linear chain hamiltonian $\hat{H}_f$ is to adjust its eigenenergies on those of the Davydov multiplet obtained *ab initio*. Likewise, the absorption spectra may be compared directly. The situation for the states is more complex, and is the object of the following section.

Representation of the multiplet states

The representation of the *ab initio* states is not so trivial, because of the difficulties we mentioned in section 5.1.4: we cannot simply fix the position of the hole on an arbitrary Nitrogen atom, because they are no longer all translationally equivalent. A possible representation is suggested by the linear chain model. Indeed, since we expect our states to be of the form:

$$|\Psi\rangle = \sum_{i=1}^{N} A_i \, |i\rangle$$

i.e. linear combinations of intralayer states, it follows that if we fix the hole on a Nitrogen atom in a given layer, say i, we should essentially see a fixed hole representation of the associated "monolayer" state multiplied by the corresponding amplitude $A_i \, |i\rangle$, up to phases. Letting $\Psi(\mathbf{r}_h, \mathbf{r}_e)$ be the

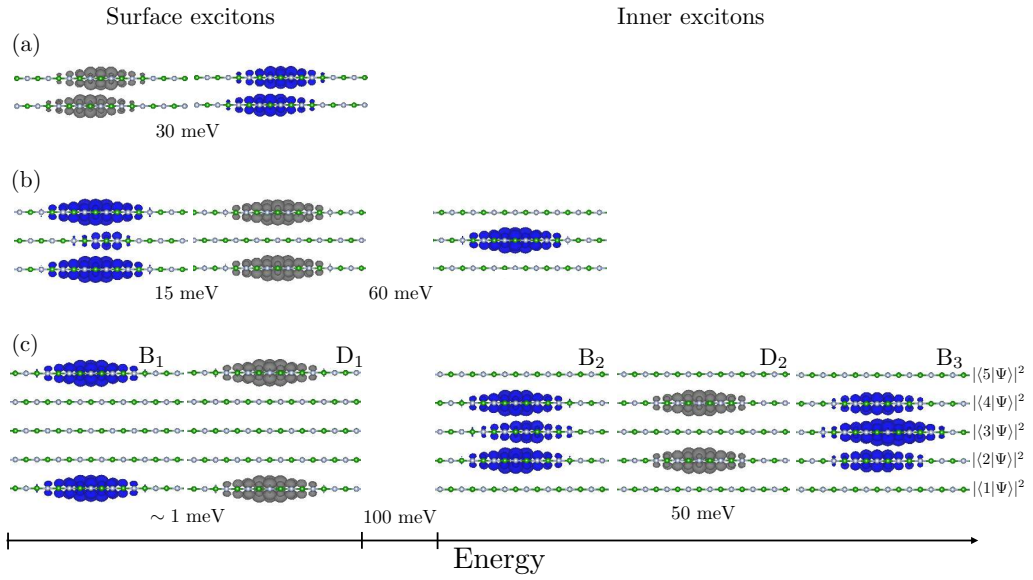

Figure 5.10: Figure reproduced from [38]. *Ab initio* calculations by F. Paleari. Representations (see text) of the *ab initio* exciton densities of the lowest bound Davydov multiplets for the bilayer (a), trilayer (b) and pentalayer (c). Dark excitons have been depicted in gray and bright excitons in blue. The excitons are represented in order of ascending energy, from left to right, and the amplitudes of some of the relevant splittings have been reported (the energy axis is not to scale). Compare with figures 5.8 and 5.11. For the pentalayer, bright (B) and dark (D) states have been labeled in accordance with figure 5.8.

position representation of the excitonic state under study, and $\left\{\mathbf{r}_h^{(i)}\right\}_{i\in[\![1,N]\!]}$ be a collection a chosen hole positions in each layer, this suggests that a good *representation* of the density of the state on the $3D$ crystal geometry is given by the quantity $\sum_{i=1}^{N}\left|\Psi\left(\mathbf{r}_h^{(i)},\mathbf{r}\right)\right|^2$. In this representation, if the linear chain model was exact, we would expect on each of the layers a copy of the fixed hole density of the effective monolayer exciton multiplied by the corresponding layer weight $|A_i|^2$. This representation is depicted in figure 5.10. While the visual representation is telling, it would be of interest to have a more quantitative comparison. One way to obtain it is to compute, *ab initio*, the volume integral of $\left|\Psi\left(\mathbf{r}_h^{(i)},\mathbf{r}\right)\right|^2$, which, again, if the linear chain model was exact, would correspond to $|A_i|^2$. This is done for the pentalayer in figure 5.11.

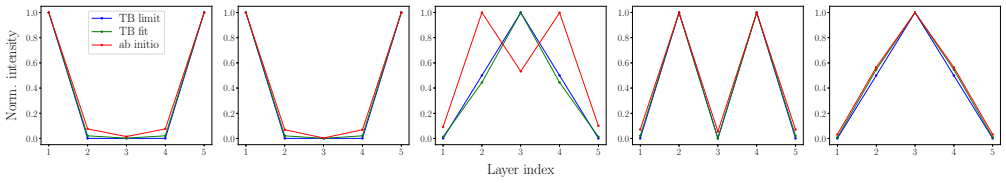

Figure 5.11: Figure reproduced from [38]. *Ab initio* calculations by F. Paleari. Comparison of the excitonic weights $|A_i|^2$ on each layer ($i = 1, \ldots, 5$) for the lowest bound N-uplet of the pentalayer, computed by different methods. Each panel corresponds to an excitonic state, and the panels are arranged from left to right in order of ascending energies. Compare with the visual representation of figure 5.10. Blue dots ("TB limit") correspond to the $|A_i|^2$ computed within the linear chain model in the limit of large X. Green dots ("TB limit") correspond to the $|A_i|^2$ computed within the linear chain model by diagonalization of $\hat{H}_f$ with the fitted value of $X = 7.1$. Red dots ("ab initio") correspond to the volume integrals of the $\left|\Psi\left(\mathbf{r}_h^{(i)}, \mathbf{r}\right)\right|^2$, as explained in the text. Lines are there only as a guide to the eye. We note that, as far as the linear chain model is concerned, we are clearly in the $X \gg 1$ limit. Agreement between *ab initio* and tight-binding (TB) data is overall satisfying, with the notable exception of the third exciton, whose oscillator strength is also (consequently) poorly reproduced in the linear chain model.

Discussion

The case of the bilayer effectively reduces to the model discussed in section 5.2.3 for the lowest bound pair, and we consequently find $g_{2L} = -15$ meV. The value of X is just a rigid shift (again, there are *only* surface layers in a bilayer), and is therefore neither directly accessible (it would require knowledge of the "bare" *ab initio* energies), nor immediately pertinent here.

As expected, the case $N = 3$, the trilayer, is the first one to display border effects. This can be seen from the asymmetry of the Davydov splitting. Indeed, let E_1, E_2 and E_3 be the triplet's energies in ascending order, and $r_{i,j} = E_j - E_i$ denote the associated splittings. The ratio $r_{3,2}/r_{2,1}$ of the "lower" and "upper" splittings is then a relevant quantity here, because it depends only on X and not g, and consequently characterizes the boundary effects.[23] Indeed, in the case where $X = 0$, $\hat{H}_f$ simply describes an ideal linear chain, and we would expect a symmetric splitting: $r_{3,2}/r_{2,1} = 1$. Instead, we observe $r_{3,2}/r_{2,1} = 4$ in the *ab initio* simulations. This corresponds to a value of $X_{3L} \approx 2$, which is not yet in the high X limit. Nevertheless, the asymmetry of the Davydov splitting is explained, and the results of our analysis which do not directly depend on $X \gg 1$ apply. In particular, the two lowest bound excitons the the trilayer still have a markedly higher intensity on the surface layers than on the central layer (although for the secodn state, this is actually mandated by symmetry). The states alternate between bright and dark (respectively even and odd) with the first state being bright, as expected from the one-dimensional model with N odd. The case of the second exciton is in fact very interesting. It is odd with respect to the inversion symmetry of the chain, i.e. here odd with respect to the mirror symmetry about the central layer. As a result, we expect no (or very little) in-plane intensity on the central layer for this exciton, and this is indeed what is observed *ab initio*. This means that, if one were to fix the hole on a Nitrogen atom in the central layer - *a priori* the most symmetric position -, one would see at most diffuse interlayer components which are not at all representative of the exciton as a whole. This is an illustration of the difficulty we discussed in section 5.1.4: for $N \geq 2$, not all (Nitrogen site) hole positions are equivalent, and it is necessary to consider a full set of non-equivalent ones in order to obtain an accurate representation of an excitonic state. Lastly, we obtain a value of $g_{3L} = -22$ meV for the interlayer interaction parameter in the trilayer.

A direct fit on the energies of the pentalayer multiplet provide the values $g_{5L} = -17$ meV and $X \approx 7.1$, which is indeed in the large X limit, as is confirmed by the analysis of the tight-binding states in figure 5.11. Energy-

[23] Of course, it is not the only such quantity.

wise, the separation between inner and surface excitons is very clear in the *ab initio* simulations: the two structures are separated by about 100 meV, which could likely be resolved by precise spectroscopic measurements. Indirectly, we have already discussed the multiplet absorption spectrum in the previous section when we estimated the number of layers from it. A direct comparison should be made between figure 5.8, which presents the *ab initio* spectrum, and the tight-binding estimate of figure 5.9. Again, we find alternating bright and dark (resp. even and odd) states starting with a bright exciton first, which is in agreement with the one-dimensional model for N odd. While, as we have seen before, the ratio of the brightest inner peak to the surface peak is very well reproduced by the linear chain model, the agreement is not so good for the second bright exciton (the first inner exciton), whose density is strongly underestimated. This can likely be traced back to the state itself: as can be seen in figure 5.11, exciton 3 is not so well reproduced by the linear chain model. A probable cause of this lies in the simplifying assumptions we made in deriving this model, and in particular the assumption that all boundary variations were limited to the surfaces (including the variations in screening). The influence of second nearest plane hoppings, that we have neglected, may also have provided a correction for this state. Still, considering the simplicity of the model, the overall agreement is rather satisfying.

Finally, we spare a word for the situation in bulk, which corresponds to the $N = +\infty$ limit we have briefly touched upon in section 5.3.4. In this case, there are also no surfaces, and the effective hamiltonian becomes that of an inifinite ideal linear chain of layers:

$$\hat{H}_f^{(\infty)} = -|g| \sum_{\langle i,j \rangle} |i\rangle\langle j|$$

whose eigenvalues and eigenvectors can be indexed by a wavenumber $k \in]-\pi, \pi]$, and are known to be:

$$E(k) = -2|g| \cos(k) \quad ; \quad |k\rangle = \frac{1}{\sqrt{N}} \sum_{n=-\infty}^{+\infty} e^{ikn} |n\rangle$$

Since the "true" periodicity of AA' bulk hBN in the stacking direction is two layers, this exciton band structure must be folded in two, in accordance with a two-layer unit cell. We then recover two direct states:

$$E(0) = -2|g| \quad ; \quad |0\rangle = \frac{1}{\sqrt{N}} \sum_{n=-\infty}^{+\infty} |n\rangle$$

$$E(\pi) = 2|g| \quad ; \quad |k\rangle = \frac{1}{\sqrt{N}} \sum_{n=-\infty}^{+\infty} (-1)^n |n\rangle$$

which are respectively even and odd with respect to inversion. It follows (but this is easily checked by computing the associated oscillator strengths) that the lowest bound exciton is dark, while the second is bright.[24] We thus recover the known Davydov pair of bulk hBN.[83] The amplitude of the splitting is then given by $s_\Psi = 4|g|$. Assuming g roughly constant, this is twice the bilayer value, and we thus expect $s_\Psi \approx 60$ meV, which is indeed in good agreement with the *ab initio* value of 58 meV. We thus find $g_\infty \approx -15$ meV as well for the bulk.

[24] All other excitons in this band structure are indirect and dark.

Chapter 6

Bulk hBN

For completeness, we now briefly discuss the case of bulk hBN in the AA' stacking, which corresponds to the limit of an infinite number of layers. We start by establishing the excitonic tight-binding model for bulk, as it can be found in [48].

6.1 Electronic structure and relevant lattices

6.1.1 Notations

We consider bulk hBN, in its AA' stacking. It has a periodicity of two layers in the vertical direction. Its unit cell contains four atoms spread over two layers, each of which contains one Nitrogen and one Boron atom.

To fix notations, let us denote by $\mathcal{R}$ the underlying Bravais lattice of the system, which is now hexagonal. We denote by $\mathbf{n}^0_{\mu,\alpha}$ the position of the unit cell atoms, where μ runs over the atomic types ($\mu = B$ or N) and α is the layer index ($\alpha = 1$ or 2), and introduce the sublattices $\Lambda_{\mu,\alpha}$ as:

$$\Lambda_{\mu,\alpha} = \mathbf{n}^0_{\mu,\alpha} + \mathcal{R}$$

so that the sites in $\Lambda_{\mu,\alpha}$ are exactly those which are translationnally equivalent to the unit cell site $\mathbf{n}^0_{\mu,\alpha}$, and the set of sites of the full crystal lattice are given by $\cup_{\mu,\alpha}\Lambda_{\mu,\alpha}$. We shall denote by a and c the in-plane and out-of-plane lattice parameters of the hexagonal lattice $\mathcal{R}$. The in-plane nearest neighbor $B-N$ distance is then $\tau = a/\sqrt{3}$ while the out-of plane nearest neighbor $B-N$ distance is $d = c/2$, which is the interplane distance. Calling $\mathbf{e}_z$ a unit vector along the stacking axis, arbitrarily oriented from a layer of type 1 to a layer of type 2, we define $\mathbf{d} = d\mathbf{e}_z$ and $\mathbf{c} = c\mathbf{e}_z$.

As usual, we restrict ourselves to the p_z orbitals, which are responsible for most of the low energy optical properties of the system. We thus denote

by $|B, \mathbf{n}\rangle$ and $|N, \mathbf{m}\rangle$ these localized boron and nitrogen p_z atomic orbitals, where $\mathbf{n} \in \cup_\alpha \Lambda_{B,\alpha}$ and $\mathbf{m} \in \cup_\alpha \Lambda_{N,\alpha}$ denote the atomic coordinates. From this basis of localized atomic orbitals, that we assume orthonormal, we define the associated tight-binding basis functions:

$$|\mu_\alpha, \mathbf{k}\rangle = \frac{1}{\sqrt{N}} \sum_{\mathbf{n} \in \Lambda_{\mu,\alpha}} e^{-\mathbf{k}\cdot\mathbf{n}} |\mu, \mathbf{n}\rangle$$

where N is now again the number of unit cells in the system.

6.1.2 Electronic hamiltonian

Per our usual strategy, we describe the electronic structure of the system using a tight-binding hamiltonian $\hat{H}_0^{(el)}$ up to second nearest nieghbours in and out of plane, which, in the basis of localized atomic orbitals, is given by:

$$\langle B, \mathbf{n}|\hat{H}_0^{(el)}|B, \mathbf{n}'\rangle = \begin{cases} \Delta & \text{if } \mathbf{n} = \mathbf{n}' \\ t_\perp^{BB} & \text{if } \mathbf{n} \text{ and } \mathbf{n}' \text{ are 2n.n. in plane} \\ t_\parallel^{BB} & \text{if } \mathbf{n} \text{ and } \mathbf{n}' \text{ are 2n.n. out of plane} \\ 0 & \text{else} \end{cases}$$

$$\langle N, \mathbf{m}|\hat{H}_0^{(el)}|N, \mathbf{m}'\rangle = \begin{cases} -\Delta & \text{if } \mathbf{m} = \mathbf{m}' \\ t_\perp^{NN} & \text{if } \mathbf{m} \text{ and } \mathbf{m}' \text{ are 2n.n. in plane} \\ t_\parallel^{NN} & \text{if } \mathbf{m} \text{ and } \mathbf{m}' \text{ are 2n.n. out of plane} \\ 0 & \text{else} \end{cases}$$

$$\langle B, \mathbf{n}|\hat{H}_0^{(el)}|N, \mathbf{m}\rangle = \begin{cases} t_\perp & \text{if } \mathbf{n} \text{ and } \mathbf{m} \text{ are 1n.n. in plane} \\ t_\parallel & \text{if } \mathbf{n} \text{ and } \mathbf{m} \text{ are 1n.n. out of plane} \\ 0 & \text{else} \end{cases}$$

where $\Delta, t_\perp, t_\parallel, t_\perp^{NN}, t_\parallel^{NN}, t_\perp^{BB}$ and $t_\parallel^{BB}$ are the kinetic parameters.

This hamiltonian is block diagonal in the basis of the tight-binding basis functions, and leads to the integral transfer matrix:

$$H(\mathbf{k}) = \begin{pmatrix} \Delta + t_\perp^{BB}\gamma_2(\mathbf{k}) & t_\perp\gamma_1(\mathbf{k}) & t_\parallel^{BB}\gamma_c(\mathbf{k}) & t_\parallel h_1(\mathbf{k}) \\ t_\perp\gamma_1(\mathbf{k})^* & -\Delta + t_\perp^{NN}\gamma_2(\mathbf{k}) & t_\parallel h_1(\mathbf{k}) & t_\parallel^{NN}\gamma_c(\mathbf{k})^* \\ t_\parallel^{BB}\gamma_c(\mathbf{k})^* & t_\parallel h_1(\mathbf{k}) & \Delta + t_\perp^{BB}\gamma_2(\mathbf{k}) & \Delta + t_\perp\gamma_1(\mathbf{k})^* \\ t_\parallel h_1(\mathbf{k}) & t_\parallel^{NN}\gamma_c(\mathbf{k}) & t_\perp\gamma_1(\mathbf{k}) & -\Delta + t_\perp^{NN}\gamma_2(\mathbf{k}) \end{pmatrix}$$

in the basis $\{|B_1, \mathbf{k}\rangle, |N_1, \mathbf{k}\rangle, |B_2, \mathbf{k}\rangle, |N_2, \mathbf{k}\rangle\}$, where:

$$\begin{aligned}\gamma_1(\mathbf{k}) &= \sum_{\boldsymbol{\tau}} e^{i\mathbf{k}\cdot\boldsymbol{\tau}} \\ \gamma_2(\mathbf{k}) &= |\gamma_1(\mathbf{k})|^2 - 3 \\ h_1(\mathbf{k}) &= 2\cos(\mathbf{k}\cdot\mathbf{d}) \\ \gamma_c(\mathbf{k}) &= \gamma_1(\mathbf{k})h_1(\mathbf{k})\end{aligned}$$

where the $\boldsymbol{\tau}$ are the in-plane first nearest neighbors nitrogen to boron vectors in planes of type 1. Here, γ_1 and γ_2 correspond respectively to the geometric terms for the first and second nearest neighbours *in* plane, while h_1 and γ_c correspond respectively to the geometric terms for the first and second nearest neighbours *out of* plane. It is interesting to note that, since the $\boldsymbol{\tau}$ are in plane, γ_1 and γ_2 depend only on the in-plane component of $\mathbf{k}$, say $\mathbf{k}_\perp$, while, since $\mathbf{d}$ is along the stacking axis, h_1 depends only on the out of plane component of $\mathbf{k}$, say $\mathbf{k}_\parallel$. Finally, $\gamma_c = \gamma_1 h_1$, so here the dependance in $\mathbf{k}_\perp$ and $\mathbf{k}_\parallel$ factorizes. For completeness, it should be noted that the AA' bilayer is described by an integral transfer matrix of the same form, obtained from the one above by the substitution $h_1 \leftarrow 1$.[1]

We now proceed with our usual approximations by considering the decomposition electronic of the hamiltonian:

$$\hat{H}_0^{(el)} = \hat{\Delta} + \hat{V}$$

where we define $\hat{\Delta}$ as $\hat{H}_0^{(el)}$ with all hoppings (every parameter except Δ) set to 0, and, consequently, $\hat{V} = \hat{H}_0^{(el)} - \hat{\Delta}$ is likewise $\hat{H}_0^{(el)}$ with Δ set to 0. As a reminder, $\hat{\Delta}$ has two eigensubspaces: one at low energy, $-\Delta$, spanned by all the nitrogen atomic orbitals, and one at high energy, $+\Delta$, spanned by all the boron atomic orbitals. We treat $\hat{V}$ as a perturbation, and perform degenerate perturbation theory in both subspaces to obtain two separate effective hamiltonians for the low and high energy eigenstates of $\hat{H}_0^{(el)}$, which are by definition the valence and conduction bands. Consequently, we call the low energy effective hamiltonian $\hat{H}_h$ (h for "holes") and the high energy one $\hat{H}_e$ (e for "electrons"), and compute them up to second order in $\hat{V}$. Two basis are of interest to express their matrix elements: the basis of localized atomic orbitals, and the basis of the tight-binding basis functions.

[1] It can be compared with the integral transfer matrices found in section 5.2.1, although there we had kept to first nearest neighbors, while here we have retained second nearest neighbors both in and out of plane.

In the basis of localized atomic orbitals, we find:

$$\langle B,\mathbf{n}|\hat{H}_e|B,\mathbf{n}'\rangle = \begin{cases} \Delta + 3\frac{t_\perp^2}{2\Delta} + 2\frac{t_\parallel^2}{2\Delta} & \text{if } \mathbf{n}=\mathbf{n}' \\ \frac{t_\perp^2}{2\Delta} + t_\perp^{BB} & \text{if } \mathbf{n} \text{ and } \mathbf{n}' \text{ are in-plane 1n.n. in } \Lambda_B \\ \frac{t_\perp t_\parallel}{\Delta} + t_\parallel^{BB} & \text{if } \mathbf{n} \text{ and } \mathbf{n}' \text{ are out of plane 1n.n. in } \Lambda_B \\ \frac{t_\parallel^2}{2\Delta} & \text{if } \mathbf{n}'-\mathbf{n} = \pm 2\mathbf{d} \\ 0 & \text{else} \end{cases}$$

$$-\langle N,\mathbf{m}|\hat{H}_h|N,\mathbf{m}'\rangle = \begin{cases} \Delta + 3\frac{t_\perp^2}{2\Delta} + 2\frac{t_\parallel^2}{2\Delta} & \text{if } \mathbf{m}=\mathbf{m}' \\ \frac{t_\perp^2}{2\Delta} - t_\perp^{NN} & \text{if } \mathbf{m} \text{ and } \mathbf{m}' \text{ are in-plane 1n.n. in } \Lambda_N \\ \frac{t_\perp t_\parallel}{\Delta} - t_\parallel^{NN} & \text{if } \mathbf{m} \text{ and } \mathbf{m}' \text{ are out of plane 1n.n. in } \Lambda_N \\ \frac{t_\parallel^2}{2\Delta} & \text{if } \mathbf{m}'-\mathbf{m} = \pm 2\mathbf{d} \\ 0 & \text{else} \end{cases}$$

Notice the $-$ sign in front of $\langle N,\mathbf{m}|\hat{H}_h|N,\mathbf{m}'\rangle$. We can comment a bit on these effective Hamiltonians. First, we note that both are effective first nearest neighbours tight-binding hamiltonians in their subspaces, except for a hopping term in $t_\parallel^2$ that connects second neighboring planes, as in the multilayer case. This term, which perturbatively "comes" from a vertical hopping from (say) B to N and then to B, is relatively small. It is neglected in the excitonic hamiltonian in [48]. Like in the chain and monolayer cases, we started with a second nearest neighbour hamiltonian, and now have only effective first nearest neighbours apart from these terms. This is again because second nearest neighbours, by definition in our lattice, connect atoms of the same type, and therefore are effectively first nearest neighbours within their subspaces. Still, second nearest neighbour interactions in the crystal break the electron-hole symmetry, even if $t_\perp^{NN} = t_\perp^{BB}$ and $t_\parallel^{NN} = t_\parallel^{BB}$.

We can, likewise, express these effective hamiltonians in the basis of tight-binding basis functions where they are block-diagonal, either by reconstructing them from the expression of the effective hamiltonians above, or by doing perturbation theory on the full integral transfer matrix above. Both ways are equivalent, and we find the following integral transfer matrices:

$$H_e(\mathbf{k}) = \left[\Delta + \frac{t_\perp^2}{2\Delta}|\gamma_1(\mathbf{k})|^2 + t_\perp^{BB}\gamma_2(\mathbf{k}) + \frac{t_\parallel^2}{2\Delta}|h_1(\mathbf{k})|^2\right] I_2 + \left[\frac{t_\perp t_\parallel}{\Delta} + t_\parallel^{BB}\right] \begin{pmatrix} 0 & \gamma_c(\mathbf{k}) \\ \gamma_c(\mathbf{k})^* & 0 \end{pmatrix}$$

in the basis $\{|B_1, \mathbf{k}\rangle, |B_2, \mathbf{k}\rangle\}$ for the electron bands, and:

$$H_h(\mathbf{k}) = -\left[\Delta + \frac{t_\perp^2}{2\Delta}|\gamma_1(\mathbf{k})|^2 - t_\perp^{NN}\gamma_2(\mathbf{k}) + \frac{t_\parallel^2}{2\Delta}|h_1(\mathbf{k})|^2\right] I_2 \\ - \left[\frac{t_\perp t_\parallel}{\Delta} - t_\parallel^{NN}\right] \begin{pmatrix} 0 & \gamma_c(\mathbf{k})^* \\ \gamma_c(\mathbf{k}) & 0 \end{pmatrix}$$

in the basis $\{|N_1, \mathbf{k}\rangle, |N_2, \mathbf{k}\rangle\}$ for the hole bands. Here, I_2 stands for the identity matrix in dimension 2. Both have a similar structure, up to hermitian conjugation, and differ essentially by the values of their parameters. In this approximation, the conduction and valence band energies are respectively given by:

$$E_{c,\pm}(\mathbf{k}) = \Delta + \frac{t_\perp^2}{2\Delta}|\gamma_1(\mathbf{k})|^2 + t_\perp^{BB}\gamma_2(\mathbf{k}) + \frac{t_\parallel^2}{2\Delta}|h_1(\mathbf{k})|^2 \pm \left|\frac{t_\perp t_\parallel}{\Delta} + t_\parallel^{BB}\right||\gamma_c(\mathbf{k})|$$

$$E_{v,\pm}(\mathbf{k}) = -\left[\Delta + \frac{t_\perp^2}{2\Delta}|\gamma_1(\mathbf{k})|^2 - t_\perp^{NN}\gamma_2(\mathbf{k}) + \frac{t_\parallel^2}{2\Delta}|h_1(\mathbf{k})|^2\right] \pm \left|\frac{t_\perp t_\parallel}{\Delta} - t_\parallel^{NN}\right||\gamma_c(\mathbf{k})|$$

where in the $\pm$, the $-$ sign corresponds to the lowest energy band of a subspace, in keeping with usual convention of attributing band index by order of energy. Figure 6.1 provides a visualization of the bands at these different levels of approximation, with parameters taken from a fit of the "exact" tight-binding bands energie (obtained from $H(\mathbf{k})$) to a GW calculation by F. Paleari.[2]

Within these approximations, the band states, away from zeros of γ_c, are likewise given by:

$$|\Phi_{\mu,\pm}(\mathbf{k})\rangle = \frac{\alpha_{\mu,\pm}(\mathbf{k})}{\sqrt{2}}\left[|\mu_1, \mathbf{k}\rangle \pm \frac{c_\mu(\mathbf{k})^*}{|c_\mu(\mathbf{k})|}|\mu_2, \mathbf{k}\rangle\right] \tag{6.1}$$

where $\alpha_{\mu,\pm}(\mathbf{k})$ is such that $|\alpha_{\mu,\pm}(\mathbf{k})| = 1$ and:

$$c_c(\mathbf{k}) = \left[\frac{t_\perp t_\parallel}{\Delta} + t_\parallel^{BB}\right]\gamma_c(\mathbf{k})$$
$$c_v(\mathbf{k}) = -\left[\frac{t_\perp t_\parallel}{\Delta} - t_\parallel^{NN}\right]\gamma_c(\mathbf{k})^*$$

Crucially for our purposes here, there are no other restrictions on $\alpha_{\mu,\pm}(\mathbf{k})$ that the ones given above. In particular, in the case of a numerical diagonalization of the effective hamiltonians, it depends on the particular numerical

[2]Best fit parameters for this particular band structure are found to be $\Delta = 3.226$ eV, $t_\perp = -2.01$ eV, $t_\parallel = 0.638$ eV, $t_\perp^{BB} = -0.41$ eV, $t_\perp^{NN} = -0.4$ eV, $t_\parallel^{BB} = -0.0.054$ eV, $t_\perp^{BB} = -0.05$ eV.

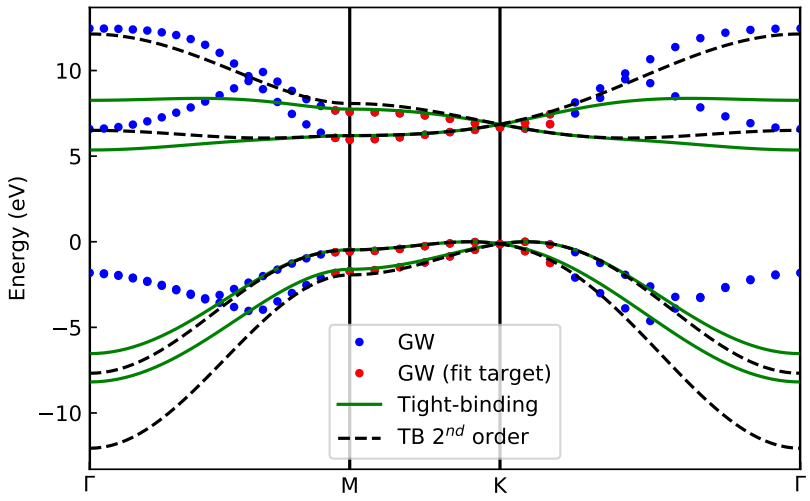

Figure 6.1: Band structure of bulk hBN in the AA' stacking in the $\mathbf{k}_\parallel = \mathbf{0}$ plane. Dots correspond to the *ab initio* GW results by F. Paleari, with the points being used to fit the tight-binding parameters highlighted in red: here, the fit is essentially done along the **MK** line. The solid line depicts the "exact" tight-binding bands computed from $H(\mathbf{k})$, which are fitted to the *ab initio* data, while dashed lines correspond to the approximate bands computed from $H_h(\mathbf{k})$ and $H_e(\mathbf{k})$ with the same parameters.

algorithm. Of course, this affects only the phase of the individual band states, since the modulus of $\alpha_{\mu,\pm}(\mathbf{k})$ is fixed to 1. Further sources of discontinuities in the band states arise from the zeroes of γ_c. At these points, the coupling between the planes effectively vanishes, and the bands are degenerate. In particular, lines of the form $\mathbf{K}+s\mathbf{c}$ and $\mathbf{K}'+s\mathbf{c}$ for $s \in \mathbb{R}$ are 1D singularities in the Brillouin zone in this sense: the phase of γ_c rotates by 2π as $\mathbf{k}$ describes an infinitesimal circle around such a line[3], so that there is no way to make the band states continuous on the full Brillouin zone. Nevertheless, if we choose $\alpha_{\mu,\pm}(\mathbf{k})$ continuous, the continuity of the band states will be ensured, except on the lines and planes mentionned above where the bands are degenerate. The obvious choice is to take $\alpha_{\mu,\pm}(\mathbf{k}) = 1$, but this will particularize one of the real-space planes. We shall come back to this discussion later, but to make further discussions general and independent on our specific choice of parameters and number of nearest neighbours, as well as to lighten notations as we move on to excitonic problems, we will from here on write down the

[3]Except on the horizontal edges of the Brillouin zone, where γ_c vanishes identically.

(approximate) band states as:

$$|\Phi_c(\mathbf{k})\rangle = \sum_\beta b^c_\beta(\mathbf{k})\,|B_\beta, \mathbf{k}\rangle$$
$$|\Phi_v(\mathbf{k})\rangle = \sum_\alpha a^v_\beta(\mathbf{k})\,|N_\alpha, \mathbf{k}\rangle$$

where v and c are valence and conduction band indices, taking on the values 0 for the lowest band ($-$ above) and 1 for the highest ($+$ above).

6.2 Excitonic hamiltonian

6.2.1 The basis of localized pairs

With the single particle band structure described by $\hat{H}_0^{(el)} \approx \hat{H}_h \oplus \hat{H}_e$, we move to excitonic states. As per our usual strategy, we write transition space as a tensor product between the low (holes) and high (electrons) energy spaces described earlier:

$$\mathcal{H} \approx \mathcal{H}_h \otimes \mathcal{H}_e$$

and describe the non interacting electron-hole pairs by the kinetic hamiltonian:

$$\hat{H}_0 \approx \hat{H}_h \otimes \mathbb{1}_e - \mathbb{1}_h \otimes \hat{H}_e$$

where $\mathbb{1}_h$ (resp. $\mathbb{1}_e$) is the identity on $\mathcal{H}_h$ (resp. $\mathcal{H}_e$). The space of transitions is then spanned by the localized pair states:

$$|\mathbf{m}, \mathbf{n}\rangle = |N, \mathbf{m}\rangle \otimes |B, \mathbf{n}\rangle$$

each of which represents a localized electron-hole pair, where the hole and the electron are separated by the vector $\mathbf{R} = \mathbf{n} - \mathbf{m}$. The kinetic hamiltonian $\hat{H}_0$ is then a six-dimensional tight-binding hamiltonian in this basis. The direct electron-hole interaction is treated as usual, and we have:

$$\langle \mathbf{m}, \mathbf{n}|\hat{U}|\mathbf{m}', \mathbf{n}'\rangle \approx \delta_{\mathbf{m},\mathbf{m}'}\delta_{\mathbf{n},\mathbf{n}'}W(\mathbf{m}, \mathbf{n})$$

where we will use a model potential $V(\mathbf{R})$ to approximate W.

6.2.2 Elementary excitations

Having established the matrix elements of the kinetic Hamiltonian $\hat{H}_0$ and the direct electron-hole interaction $\hat{U}$ in the basis of pairs (we will, once again, neglect exchange), we now wish to move to a basis of elementary excitations.

Because we have an interest in the expression of excitonic states in reciprocal space, it is fruitful here to establish this basis by generalizing the "Fourier transform" point of view on elementary excitations discussed in section 3.2.2. We start by noting that a given transition from valence band v at wavevector $\mathbf{k}$ to conduction band c at wavevector $\mathbf{k}+\mathbf{Q}$ can be written as:

$$\begin{aligned}|v\mathbf{k}, c(\mathbf{k}+\mathbf{Q})\rangle &= |v\mathbf{k}\rangle \otimes |c(\mathbf{k}+\mathbf{Q})\rangle \\ &= \frac{1}{\sqrt{N}} \sum_{\alpha} \sum_{\mathbf{m}\in\Lambda_{N,\alpha}} a_{\alpha}^{v}(\mathbf{k})^{*} e^{i\mathbf{k}\cdot\mathbf{m}} |N, \mathbf{m}\rangle \\ &\qquad \otimes \frac{1}{\sqrt{N}} \sum_{\beta} \sum_{\mathbf{n}\in\Lambda_{B,\beta}} b_{\beta}^{c}(\mathbf{k}+\mathbf{Q}) e^{-i(\mathbf{k}+\mathbf{Q})\cdot\mathbf{n}} |B, \mathbf{n}\rangle \\ &= \frac{1}{N} \sum_{\alpha,\beta} a_{\alpha}^{v}(\mathbf{k})^{*} b_{\beta}^{c}(\mathbf{k}+\mathbf{Q}) \sum_{\substack{\mathbf{m}\in\Lambda_{N,\alpha} \\ \mathbf{n}\in\Lambda_{B,\beta}}} e^{-i\mathbf{Q}\cdot\mathbf{n}} e^{-i\mathbf{k}\cdot(\mathbf{n}-\mathbf{m})} |\mathbf{m}, \mathbf{n}\rangle\end{aligned}$$

where we have defined $|\mathbf{m}, \mathbf{n}\rangle = |N, \mathbf{m}\rangle \otimes |B, \mathbf{n}\rangle$. We now move to relative coordinates by changing variables from $\mathbf{m}, \mathbf{n}$ to $\mathbf{m}, \mathbf{R}$. For a given (α, β) pair and $\mathbf{m} \in \Lambda_{N,\alpha}$, the set of $\mathbf{R}$ to be summed upon is *a priori* $\Lambda_{\alpha,\beta}(\mathbf{m}) = \Lambda_{B,\beta} - \mathbf{m}$, but because the crystal is translationally invariant, $\Lambda_{\alpha,\beta}(\mathbf{m})$ is the same for any $\mathbf{m} \in \Lambda_{N,\alpha}$. This naturally lets us define the *excitation sublattices*, like we did for multilayers:

$$\Lambda_{\alpha,\beta} = \Lambda_{B,\beta} - \mathbf{m}_{N,\alpha}^{0} = \mathcal{R} + \left(\mathbf{n}_{B,\beta}^{0} - \mathbf{m}_{N,\alpha}^{0}\right)$$

which are here the sets of all possible hole-electron vectors from a hole in a layer of "type" α to an electron in a layer of "type" β. With this, we can permute the sums above, and obtain:

$$|v\mathbf{k}, c(\mathbf{k}+\mathbf{Q})\rangle = \sum_{\alpha,\beta} \sum_{\mathbf{R}\in\Lambda_{\alpha,\beta}} \frac{1}{\sqrt{N}} a_{\alpha}^{v}(\mathbf{k})^{*} b_{\beta}^{c}(\mathbf{k}+\mathbf{Q}) e^{-i(\mathbf{k}+\mathbf{Q})\cdot\mathbf{R}} \underbrace{\frac{1}{\sqrt{N}} \sum_{\mathbf{m}\in\Lambda_{N,\alpha}} e^{-i\mathbf{Q}\cdot\mathbf{m}} |\mathbf{m}, \mathbf{m}+\mathbf{R}\rangle}_{|\mathbf{R}_{\alpha,\beta},\mathbf{Q}\rangle}$$

Where we have defined the states $|\mathbf{R}_{\alpha,\beta}, \mathbf{Q}\rangle$, which are as usual tight-binding basis functions over the localized electron hole pairs. Inserting now this expression in the transition basis expression of an indirect excitonic state with center of mass momentum $\mathbf{Q}$:

$$|\Psi_{\mathbf{Q}}\rangle = \sum_{\mathbf{k}} \sum_{v,c} \Psi_{v\mathbf{k},c(\mathbf{k}+\mathbf{Q})} |v\mathbf{k}, c(\mathbf{k}+\mathbf{Q})\rangle \tag{6.2}$$

and permuting the sums, we have:

$$
\begin{aligned}
|\Psi_{\mathbf{Q}}\rangle &= \sum_{\alpha,\beta} \sum_{\mathbf{R}\in\Lambda_{\alpha,\beta}} \underbrace{\frac{1}{\sqrt{N}} \sum_{\mathbf{k}} \sum_{v,c} \Psi_{v\mathbf{k},c(\mathbf{k}+\mathbf{Q})} a^v_\alpha(\mathbf{k})^* b^c_\beta(\mathbf{k}+\mathbf{Q}) e^{-i(\mathbf{k}+\mathbf{Q})\cdot\mathbf{R}}}_{\Psi_{\mathbf{R}_{\alpha,\beta},\mathbf{Q}}} |\mathbf{R}_{\alpha,\beta},\mathbf{Q}\rangle \\
&= \sum_{\alpha,\beta} \sum_{\mathbf{R}\in\Lambda_{\alpha,\beta}} \Psi_{\mathbf{R}_{\alpha,\beta},\mathbf{Q}} |\mathbf{R}_{\alpha,\beta},\mathbf{Q}\rangle
\end{aligned}
$$

so that we have obtained our elementary excitation states $|\mathbf{R}_{\alpha,\beta},\mathbf{Q}\rangle$. In doing so, we have also obtained the conversion formulas between the excitonic weights in reciprocal / band space and their analogues in elementary excitation space:

$$\Psi_{\mathbf{R}_{\alpha,\beta},\mathbf{Q}} = \frac{1}{\sqrt{N}} \sum_{\mathbf{k}} \sum_{v,c} \Psi_{v\mathbf{k},c(\mathbf{k}+\mathbf{Q})} a^v_\alpha(\mathbf{k})^* b^c_\beta(\mathbf{k}+\mathbf{Q}) e^{-i(\mathbf{k}+\mathbf{Q})\cdot\mathbf{R}} \tag{6.3}$$

$$\Psi_{v\mathbf{k},c(\mathbf{k}+\mathbf{Q})} = \frac{1}{\sqrt{N}} \sum_{\alpha,\beta} a^v_\alpha(\mathbf{k}) b^c_\beta(\mathbf{k}+\mathbf{Q})^* \sum_{\mathbf{R}\in\Lambda_{\alpha,\beta}} \Psi_{\mathbf{R}_{\alpha,\beta},\mathbf{Q}} e^{i(\mathbf{k}+\mathbf{Q})\cdot\mathbf{R}} \tag{6.4}$$

6.2.3 Hamiltonian

Having now obtained the desired hybrid basis, where the relative coordinate is treated in direct space, while the center of mass motion is treated in reciprocal space, we proceed to rewrite the Bethe-Salpeter Hamiltonian in this new basis. Again, the process is relatively straightforward, since we already know the matrix elements of $\hat{H}_X$ in the basis of localized pairs, and know the expressions of the $|\mathbf{R}_{\alpha,\beta},\mathbf{Q}\rangle$ in terms of the localized pairs.

Kinetic hamiltonian

The free transition / kinetic hamiltonian, $\hat{H}_0$, becomes itself an effective tight-binding hamiltonian on the lattice Λ of the $\mathbf{R}_{\alpha,\beta}$. It preserves $\mathbf{Q}$ and

its matrix elements are given by:

$$\langle \mathbf{R}_{\alpha,\beta}, \mathbf{Q}|\hat{H}_0|\mathbf{R}_{\alpha,\beta}, \mathbf{Q}\rangle = 2\Delta + 3\frac{t_\perp^2}{\Delta} + 2\frac{t_\parallel^2}{\Delta}$$

$$\left\langle \mathbf{R}_{\alpha,\beta}, \mathbf{Q}\middle|\hat{H}_0\middle|\mathbf{R}'_{\alpha,\beta}, \mathbf{Q}\right\rangle = \begin{cases} \left[\frac{t_\perp^2}{2\Delta} + t_\perp^{BB}\right] + \left[\frac{t_\perp^2}{2\Delta} - t_\perp^{NN}\right] e^{i\mathbf{Q}\cdot(\mathbf{R}'-\mathbf{R})} & \text{if } \mathbf{R}, \mathbf{R}' \text{ are 1n.n. in plane} \\ \frac{t_\parallel^2}{2\Delta}\left(1 + e^{i\mathbf{Q}\cdot(\mathbf{R}'-\mathbf{R})}\right) & \text{if } \mathbf{R}' - \mathbf{R} = \pm 2\mathbf{d} \end{cases}$$

$$\left\langle \mathbf{R}_{1,1}, \mathbf{Q}\middle|\hat{H}_0\middle|\mathbf{R}'_{1,2}, \mathbf{Q}\right\rangle = \left[\frac{t_\perp t_\parallel}{2\Delta} + t_\parallel^{BB}\right] \quad \text{if } \mathbf{R}, \mathbf{R}' \text{ are 1n.n. out of plane}$$

$$\left\langle \mathbf{R}_{1,1}, \mathbf{Q}\middle|\hat{H}_0\middle|\mathbf{R}'_{2,1}, \mathbf{Q}\right\rangle = \left[\frac{t_\perp t_\parallel}{2\Delta} - t_\parallel^{NN}\right] e^{i\mathbf{Q}\cdot(\mathbf{R}'-\mathbf{R})} \quad \text{if } \mathbf{R}, \mathbf{R}' \text{ are 1n.n. out of plane}$$

$$\left\langle \mathbf{R}_{2,2}, \mathbf{Q}\middle|\hat{H}_0\middle|\mathbf{R}'_{1,2}, \mathbf{Q}\right\rangle = \left[\frac{t_\perp t_\parallel}{2\Delta} - t_\parallel^{NN}\right] e^{i\mathbf{Q}\cdot(\mathbf{R}'-\mathbf{R})} \quad \text{if } \mathbf{R}, \mathbf{R}' \text{ are 1n.n. out of plane}$$

$$\left\langle \mathbf{R}_{1,1}, \mathbf{Q}\middle|\hat{H}_0\middle|\mathbf{R}'_{2,1}, \mathbf{Q}\right\rangle = \left[\frac{t_\perp t_\parallel}{2\Delta} + t_\parallel^{BB}\right] \quad \text{if } \mathbf{R}, \mathbf{R}' \text{ are 1n.n. out of plane}$$

and their complex conjugates. They are 0 in all other cases, notably if $\mathbf{Q} \neq \mathbf{Q}'$. We thus have, as usual, one effective hamiltonian $H_X(\mathbf{Q})$ per value of $\mathbf{Q}$, which appears as a tight-binding hamiltonian on the lattice of excitations $\Lambda = \bigcup_{\alpha,\beta\in[\![1,2]\!]} \{\mathbf{R}_{\alpha,\beta} \quad / \quad \mathbf{R} \in \Lambda_{\alpha,\beta}\}$.

It is interesting to point out, here, that out-of-plane second-nearest neighbors play a special role compared to their in-plane equivalents. Because hoppings within the same sublattice in Λ combine contributions from both the hole and the electron, compensation effects can occur, which decrease the influence of in-plane second nearest neighbors at $\mathbf{Q} = \mathbf{0}$, as we have discussed previously. However, no such compensation can occur for out of plane hoppings, because changing sublattices can only be done by having the electron *or* the hole hop between layers, not both at the same time.

It is also worth noting that the excitation sublattices, the $\Lambda_{\alpha,\beta}$, are hexagonal lattices in the bulk case, and therefore unlike in the (finite) multilayer description, the $\Lambda_{\alpha,\alpha}$ do not contain *only* in-plane excitations anymore. They are still the only excitation sublattices which have excitation sites in the $z = 0$ plane, so the only ones to *contain* in-plane excitations, but they also contain excitations between second nearest planes, fourth nearest planes, etc.: they contain excitations between planes of the same "kind", i.e. that are connected by a lattice translation. The $\Lambda_{\alpha,\beta}$ with $\alpha \neq \beta$ contain the other excitations, i.e. those between first-neighbor planes, third neighbor planes, etc.

Direct electron-hole interaction

The direct electron-hole interaction, which depends only on $\mathbf{R}_{\alpha,\beta}$ and preserves $\mathbf{Q}$ has a particularly simple expression:

$$\left\langle \mathbf{R}_{\alpha,\beta}, \mathbf{Q} \middle| \hat{U} \middle| \mathbf{R}'_{\alpha',\beta'}, \mathbf{Q}' \right\rangle = \delta_{\mathbf{R},\mathbf{R}'}\delta_{\mathbf{Q},\mathbf{Q}'}\delta_{\alpha,\alpha'}\delta_{\beta,\beta'}V_{\alpha,\beta}(R)$$

where $V_{\alpha,\beta}(R)$ is an appropriate model potential as described in the basis of localized pairs.

To perform practical calculations, we still need to specify a model for the potential, i.e. a function $V_{\alpha,\beta}(R)$.

Since we are dealing with a bulk system, a simple model which can be used to provide qualitative trends is a screened Coulomb potential, where the in-plane / out of plane anisotropy is represented by different dielectric constants $\epsilon_\perp$ and $\epsilon_\parallel$:

$$V_{\alpha,\beta}(\mathbf{R}) = \begin{cases} -\frac{e^2}{\epsilon_\perp R} & \text{if } \alpha = \beta \\ -\frac{e^2}{\epsilon_\parallel R} & \text{if } \alpha \neq \beta \text{ and } \mathbf{R}\cdot\mathbf{d} = \pm 1 \\ 0 & \text{else} \end{cases}$$

i.e. we have a Coulomb interaction screened by $\epsilon_\perp$ for in-plane pairs, while out of plane pairs in neighboring planes are screened by $\epsilon_\parallel$. Interactions between pairs separated by one plane or more (i.e. such that $|\mathbf{R}\cdot\mathbf{d}| \geq 2$) are neglected due to the screening from the atomic planes between them. Both $\epsilon_\perp$ and $\epsilon_\parallel$ are additional potential parameters of the model. In particular, excitations between second neighboring planes and up are considered unbound with such a model.

To perform more accurate calculations, a more sophisticated model potential would probably be needed.[91, 74, 92] In particular, it is desirable to have a model which is able to describe the direct interaction for excitations involving pairs spread over more than first nearest layers would be useful to describe higher energy excitons, which are likely to be spread in the stacking direction; as well a reducing to the monolayer limit in the case of less extended excitons. To this end, we take a model potential for bulk where each layer is described as a purely two-dimensional dielectric sheet with polarizability radius r_0, and solve the corresponding Poisson equation for this system using the methods introduced by Cudazzo and coauthors in [61].[4]

[4]We must however note that, in the context of multilayers, while the strict two-dimensional limit we adopt here does reproduce some expected behaviors of multilayer potentials and provides a simple functional form to be fitted, it is known to underestimate the overall screening. See [74] for details.

In this macroscopic framework, where the model system has cylinder symmetry, V does not explicitly depend on α and β, but rather on $m = \mathbf{R}\cdot\mathbf{d}$. It is useful to decompose $\mathbf{R}$ into cylinder coordinates:

$$\mathbf{R} = \boldsymbol{\rho} + m\mathbf{c}$$

and the problem becomes effectively that of computing the V_m as functions of $\boldsymbol{\rho}$. It can be shown in that case that:

$$\tilde{V}_m(\mathbf{q}) = -\frac{e^2}{q}\int_{-\pi}^{\pi} \frac{e^{-ikm} f(k)}{1 + r_0 q f(k)} dk$$

for $m \in \mathbb{N}$, where $\mathbf{q}$ is conjugate to $\boldsymbol{\rho}$ and:

$$f(k) = \frac{e^{-qh}}{e^{ik} - e^{-qh}} + \frac{1}{1 - e^{ik}e^{-qh}}$$

The real space potential is then obtained by inverse Fourier transform:

$$V_m(\rho) = \frac{1}{2\pi}\int \tilde{V}_m(\mathbf{q}) J_0(q\rho) q dq$$

A numerical evaluation is provided in figure 6.3.

6.3 Direct exciton series

In the same way as it was done for the bilayer, the model can be used to compute the direct excitonic series for bulk hBN. We present here preliminary results on this topic. Many works[23, 96, 97, 98, 99] exist on the topic, although often with focus on the first excitonic peak.

6.3.1 *Ab initio* results

Let us start this section by discussing some *ab initio* results on absorption in AA' bulk hBN. The calculations in question have been performed by S. Reichardt, using DTF + Scissor shift for the bands, on top of which the Bethe-Salpeter equation was solved.[100] In-plane and interlayer lattice parameters were taken to be $a = 2.478$ Å and $c = 6.453$ Å.

We present the system's absorption spectrum in figure 6.2, along with the corresponding bright states. The first eigenergies are reported in table 6.1, along with their bright/dark character. Since bulk hBN is obtained by the repetition of a unit cell composed of two layers in the AA' stacking, we expect some similarities with the situation in the bilayer, despite the increased

screening. This is indeed the case: while bulk excitons are significantly less bound than their bilayer counterparts, because of the additional screening induced by the additional layers, the "low energy" excitons of bulk bear a strong similarity to their bilayer counterparts. This is possibly due to the fact that, in both cases, these excitons are the smallest in radius, and are therefore strongly affected - and therefore constrained - by the lattice symmetries of the system. Higher excitons tend to be larger, and therefore more sensitive to the variations of the potential, in addition to the fact that they can involve excitations between planes that are not nearest neighbors, which is impossible in the bilayer (in which there are only two planes).

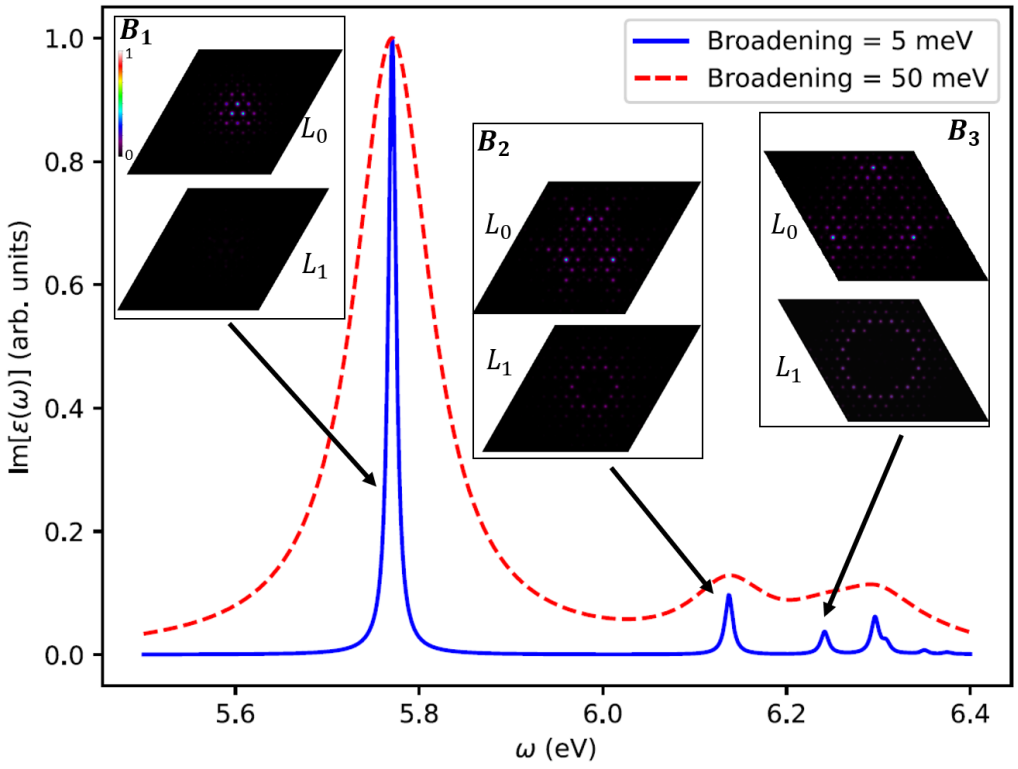

Figure 6.2: Low energy *ab initio* absorption spectrum for bulk hBN in the AA' stacking. The system's direct gap is at an energy of 6.4965 eV. Insets: densities of the first three bright excitons (B_1, B_2 and B_3 respectively). The densities are depicted in the fixed hole representation *via* an in-plane cut: L_0 corresponds to the layer where the hole was placed, L_1 is the layer immediately above. Some of these states also have low intensity of further layers ($L_i,\ i \geq 2$), we do not depict it here here. *Ab initio* calculations by S. Reichardt.

Exciton	1 (×2)	2 (×2)	3	4	5 (×2)	6	7 (×2)	8
Ab initio	−0.81	−0.726	−0.546	−0.461	−0.435	−0.368	−0.359	−0.358
Bright	no	yes	no	no	no	no	yes	no

Table 6.1: *Ab initio* binding energies (in eV), degeneracies and optical activities of the first eight bulk excitons. Calculations by S. Reichardt.

Analysis of the states displayed in table 6.1 show that they occur in Davydov pairs. Again, this is due to the fact that each unit cell contains two inequivalent layers. The lowest bound Davydov pair is well understood from the simple model for Davydov splitting discussed in chapter 5, whose consequences in bulk have been discussed in section 5.3.5. The lowest bound exciton is its even component, which is dark, while the second exciton is its odd component, which is bright and constitutes the first peak.

The next two bright states appear more peculiar: they are dominated by three in-plane excitations, and assume a triangular shape which does not appear directly reminiscent of a monolayer state. Interestingly, however, their closeness in energy suggests that exciton 7, to which the second bright peak is associated, is the Davydov partner of exciton 5, whose density appears different.[5] We will come back to this and discuss the origin of this state with the tools of the tight-binding formalism.

6.3.2 Tight-binding analysis

Optical activity and remarks on symmetries

Bulk hBN has the symmetries of the D_{6h} point group. Notable symmetries included in D_{6h} are the inversion symmetry, which provides the usual selection rule (only excitons transforming according to an *ungerade* representation can be bright), as well as a horizontal mirror symmetry, σ_h. Group theoretical considerations yield that only states transforming according to the E_{1u} representation may be bright for in-plane polarized light.[6]

In the tight-binding formalism, this latter symmetry manifests itself as a mirror symmetry about the $z = 0$ plane. This has interesting consequences: it means that states that are odd under σ_h cannot have any intensity on the excitations of Λ which are in the $z = 0$ plane, i.e. all the in-plane excita-

[5] A difference between the two states of this pair is, in fact, also visible in the case of the bilayer.

[6] E_{1u} is a two-dimensional representation which has character -2 for inversion and 2 for σ_h: its excitons are thus "odd" under inversion and "even" under the horizontal mirror.

tions. Such states are therefore expected to have no in-plane components, i.e. to be purely interlayer.[7] Such excitons have been noted by Aggoune and coauthors.[98]

Within the tight-binding approximations the optical matrix elements are given by the usual expression. For a direct excitonic state:

$$|\Phi\rangle = \sum_{\mathbf{R}_{\alpha,\beta}\in\Lambda} \Phi_{\mathbf{R}_{\alpha,\beta}} |\mathbf{R}_{\alpha,\beta}\rangle$$

we have:

$$\langle\emptyset|\hat{\mathbf{p}}|\Phi\rangle = -\frac{m_e\sqrt{N}}{i\hbar} \sum_{\mathbf{R}_{\alpha,\beta}\in\Lambda} t_{\mathbf{R}_{\alpha,\beta}} \Phi_{\mathbf{R}_{\alpha,\beta}} \mathbf{R}$$

where the $t_{\mathbf{R}_{\alpha,\beta}} = \left\langle A_\alpha, \mathbf{m}^0_{N,\alpha} \middle| \hat{H}_0^{(el)} \middle| B_\beta, \mathbf{m}^0_{N,\alpha} + \mathbf{R} \right\rangle$ are electronic hoppings, which are here again $t_\perp$ or $t_\parallel$ if $\mathbf{R}$ is (respectively) an in-plane or interlayer Nitrogen to Boron nearest-neighbor vector (in the crystal lattice), and zero otherwise. The conclusions are analogous to those given in the bilayer case in section 5.2.6: for an exciton to be bright in this framework, it must have some intensity in-plane. We thus recover the group theoretical requirement that only E_{1u} excitons may be bright for in-plane polarized light: other E representations are either *gerade* (so forbidden by inversion) or odd under σ_h, which forbids in-plane excitations.

The remarks above suggest that in an E Davydov pair with a mostly in-plane character the bright component must be E_{1u}, while the dark component must be E_{2g} (the only E representation which is even both under inversion and under σ_h, the latter being necessary to have intensity in-plane).

Numerical results

To proceed with a numerical diagonalisation of $\hat{H}_X$ at $\mathbf{Q} = \mathbf{0}$, we make, for simplicity, the first-nearest neighbors approximation, leaving us with three effective parameters: $T_\perp = \frac{t_\perp^2}{\Delta}$, $T_\parallel = \frac{t_\perp t_\parallel}{\Delta}$ and r_0, 2Δ being fixed to the value of the *ab initio* gap. We take the effective potential up to $m = 3$. We adjust these parameters on the *ab initio* binding energies reported in table 6.1. We thus estimate the following effective parameters:

$$2\Delta = 6.5 \text{ eV} \quad ; \quad T_\perp = 1.47 \text{ eV} \quad ; \quad T_\parallel = 0.548 \text{ eV} \quad ; \quad r_0 = 16.2 \text{ Å}.$$

[7] In fact, a similar situation manifests itself in the bilayer case if one keeps to the first-nearest neighbors approximation. In this case, the excitonic tight-binding problem exhibits a D_{6h} symmetry, even though the crystal itself does not.

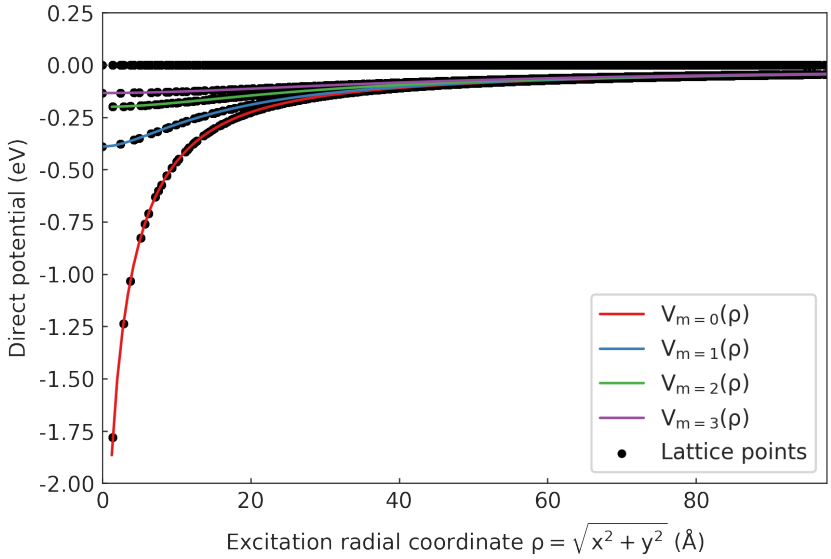

Figure 6.3: Effective bulk potential for up to third nearest planes excitations. The set of lattice points with $V = 0$ corresponds to excitations with $m > 3$, which are here kept unbound.

These parameters provide a reasonable agreement for the binding energies. The corresponding band structure agreement is moderate at best, but this is sufficient for the purpose of the preliminary results presented here.

The effective potential, in real space, is depicted in figure 6.3. Like in section 5.2.6, we do not necessarily expect the model to be very accurate above the level of the second bright peak, at least with this parametrization. We depict in figure 6.4 the variations of its optical spectrum as a function of $t_{\parallel}$, and well as the corresponding binding energy / oscillator strength diagram. Overall, the situation is analogous to that of the bilayer: it is the interaction of in-plane bright monolayer state at $t_{\parallel} = 0^+$ with purely interlayer states of symmetry E_{1u} at $t_{\parallel} = 0^+$ that give rise to the additional peaks in the bulk structure compared to the "bare" monolayer.

From the point of view of excitonic wavefunctions, the strongly "triangular" exciton 7 ("B_1") is well reproduced in tight-binding. Its Davydov partner is now rather clearly exciton 5, which interestingly does not have this sharp triangular features: instead, it is much more similar to the corresponding monolayer exciton (exciton 2). This is depicted in figure 6.5 using tight-binding wavefunctions. A similar phenomenon seems to occur within the (E_{2g}, E_{1u}) dark/bright Davydov pairs corresponding to higher peaks, but their detailed analysis is outside of the scope of this work.

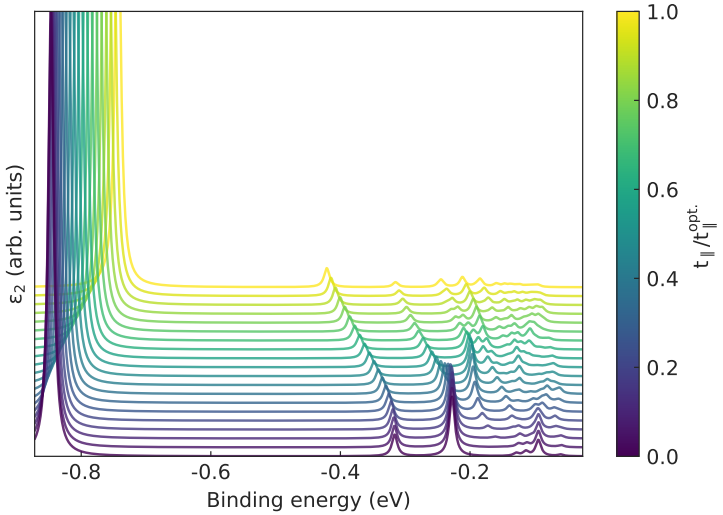

Figure 6.4: Sample evolution of the tight-binding absorption spectrum for bulk hBN in the AA' stacking with the variations of $t_{\parallel}$. The system's direct gap is at an energy of 6.4965 eV. This behavior of the spectrum after the first two peaks depends rather significantly on the exact parameters (kinetic and potential), so the evolution presented here is qualitative.

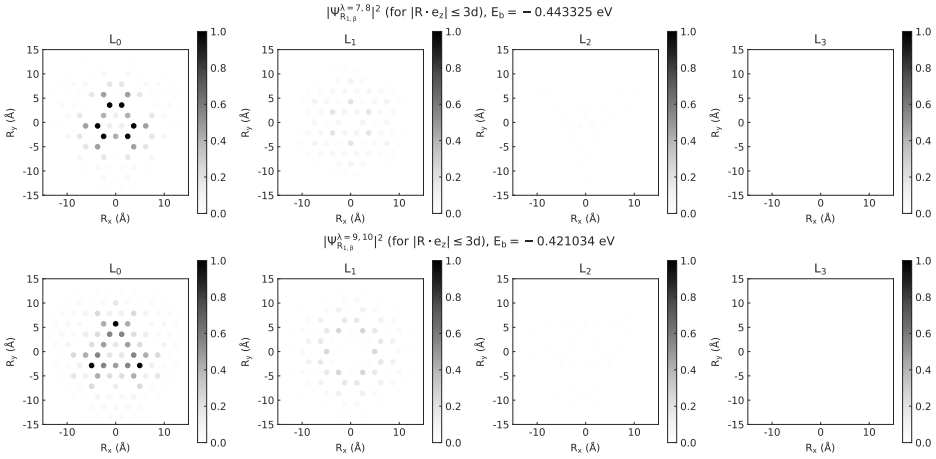

Figure 6.5: Tight-binding densities for exciton 5 (top) and 7 (bottom). The representation is analogue to the *ab initio* depiction of figure 6.2; the E_b are the tight-binding binding energies, and the λ indicate the indices of the constituent states, in tight-binding order. Excitons (5,7) form a Davydov pair, with exciton 5 being of symmetry E_{2g} and thus dark, while its partner exciton 7 has E_{1u} symmetry and is thus bright: it is responsible for teh second peak in the bulk absorption spectrum.

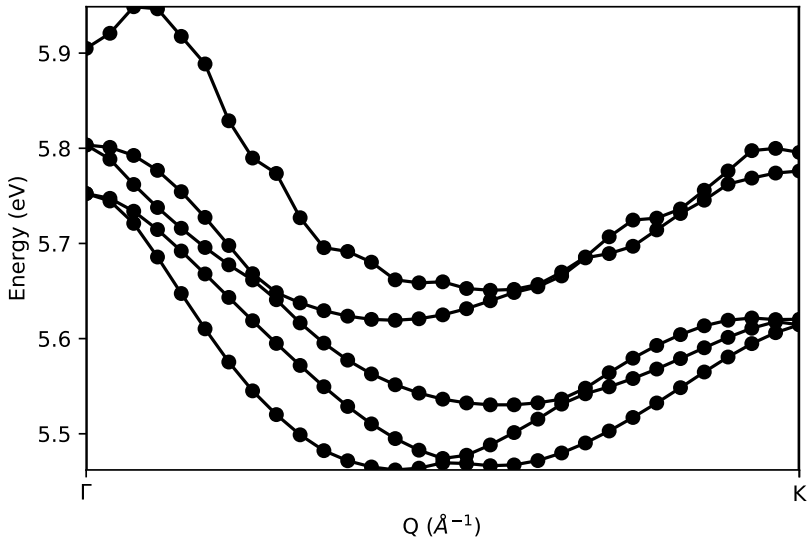

Figure 6.6: Sample exciton band structure of bulk hBN in the AA' stacking along the **ΓK** line of the excitonic Brillouin zone, computed by diagonalization of $\hat{H}_X$. Kinetic parameters are taken from a fit of the bands as given in figure 6.1, while potential parameters are manually adjusted such that the dispersion roughly describes the double minimum structure near $\frac{1}{2}\mathbf{\Gamma K}$; we have here taken the simple Coulomb potential with $\epsilon_\perp = 6$ and $\epsilon_\parallel = 6.8$. Second nearest plane hoppings in $t_\parallel^2$ are neglected. Solid dots correspond to the calculated points, lines are a guide to the eye. At each $\mathbf{Q}$-point, only the first five lowest energy sates are depicted.

6.4 Exciton dispersion

This section only presents sample results. See [48] for a more complete discussion.

6.4.1 Exciton band structure

We can diagonalize the excitonic hamiltonian $\hat{H}(\mathbf{Q})$ for each value of $\mathbf{Q}$ to obtain a dispersion relation for the excitons. A sample dispersion is presented in figure 6.6.

The dispersion here is presented along the **ΓK** line, which is the region which is known to host the system's indirect excitonic gap.[37] The influence of the various parameters on the dispersion has been discussed in detail in [48]. Here, we have manually adjusted the potential parameters to qualitatively reproduce the double minima structure around $\frac{1}{2}\mathbf{\Gamma K}$. The rest of the

exciton dispersion with these parameters is not in very good agreement with the calculated *ab initio* dispersion.[48]

We can likewise extract the excitonic states from the diagonalization of the above hamiltonian, both in real and in reciprocal space. In the latter case, in particular, they may be useful as ingredients for the study of indirect phenomena.[8] To illustrate this ability, we briefly discuss the lowest bound direct exciton, at excitonic $\mathbf{\Gamma}$. This exciton presents the additional difficulty of being twice degenerate; more precisely, it transforms as the E_{2g} representation of the D_{6h} point group. We must thus choose a basis to meaningfully discuss this state. A natural choice, which is well adapted to study in reciprocal space, is a chiral basis. A practical way to construct it from a numerical diagonalization has been discussed in section 4.4.2, and so we assume here that we have such a basis, say $\left\{\Psi^{\lambda=1}, \Psi^{\lambda=2}\right\}$.

We can obtain the reciprocal space amplitudes, the $\Psi_{v\mathbf{k},c(\mathbf{k}+\mathbf{Q})}$, from the knowledge of the $\Psi_{\mathbf{R}_{\alpha,\beta},\mathbf{Q}}$ that are computed from the diagonalization of $\hat{H}_X(\Gamma)$. This can be done via the change of basis formula 6.4, which can be rewritten as:

$$\Psi_{v\mathbf{k},c(\mathbf{k}+\mathbf{Q})} = \sum_{\alpha,\beta} a^v_\alpha(\mathbf{k}) b^c_\beta(\mathbf{k}+\mathbf{Q})^* \underbrace{\frac{1}{\sqrt{N}} \sum_{\mathbf{R}\in\mathbf{\Lambda_{\alpha,\beta}}} \Psi_{\mathbf{R}_{\alpha,\beta},\mathbf{Q}} e^{i(\mathbf{k}+\mathbf{Q})\cdot\mathbf{R}}}_{\Gamma_{\alpha,\beta}(\mathbf{k},\mathbf{Q})}$$

Here, the $\Gamma_{\alpha,\beta}(\mathbf{k},\mathbf{Q})$ are simply Fourier transforms over the sublattices $\Lambda_{\alpha,\beta}$, and do not depend on the choice of phases of the band states. However, the product $a^v_\alpha(\mathbf{k}) b^c_\beta(\mathbf{k}+\mathbf{Q})^*$ does depend on the choice of band states, and, as discussed in section 6.1.2 needs not even be continuous.

Before discussing the details of $\Psi_{v\mathbf{k},c\mathbf{k}}$, let us first look at $|\Psi_{v\mathbf{k},c\mathbf{k}}|^2$. A cut along the **ΓMK** and **ALH** planes is depicted in figure 6.7 for $\left|\Psi^{\lambda=1}\right\rangle$. Let us first discuss the situation in the former. There, we find that most of the density comes from transitions from the highest valence band ($v = 1$), to the lowest conduction band ($c = 0$), as expected energetically. Similarly, most of the intensity is located around the high symmetry **K** and **K′** points, although for ($v = 1, c = 0$) transitions, the intensity *at* these points is quite low. This is not surprising, since, as can be seen from figure 6.1, these points are actually local maxima for the ($v = 1, c = 0$) transition energies. The direct minima are instead located around these points, and are consistent with the regions of highest densities of $\left|\Psi^{\lambda=1}{}_{(v=1)\mathbf{k},(c=0)\mathbf{k}}\right|^2$. The situation is more symmetric in the **ALH** plane: this can be understood from the fact that $\gamma_c = 0$ on this

[8] We note that an *ab initio* calculation of the reciprocal space densties of the first four bright excitons may be found in [99].

plane, and so the interplane couplings vanish, leading to a degenracy of the bands in this region.

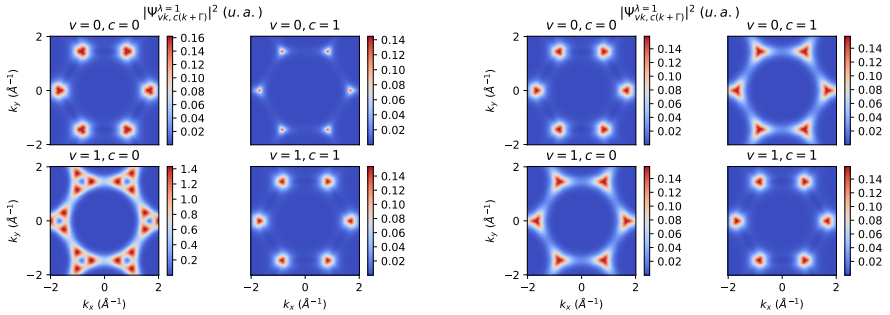

Figure 6.7: Cuts of the reciprocal space densities $\left|\Psi^{\lambda=1}_{v\mathbf{k},c\mathbf{k}}\right|^2$ densities for the polarized state $\left|\Psi^{\lambda=1}\right\rangle$ of the twice degenerate lowest bound subspace at $\mathbf{Q} = \Gamma$ along the **ΓMK** (left) and **ALH** (right) planes. Note that each component has its own colorbar. Note also that this is only the density for one component of the lowest bound excton (which is a twice degenerate subspace).

To gain further insight, we can consider a simple model, by studying the real space amplitudes $\Psi_{\mathbf{R}_{\alpha,\beta},\mathbf{Q}}$. We assume that the interlayer hoppings are negligible (which is a strong approximation),[9] and we concern ourselves only with states of the lowest bound Davydov pair. These states are mostly in-plane, i.e. most of their intensity is on excitations in the $z = 0$ plane. *A fortiori*, their components on the $\Lambda_{\alpha,\beta}$ sublattices such that $\alpha \neq \beta$ should be negligible. Choosing a basis with definite parity $\pm$ under inversion, we thus have:

$$\begin{aligned} |\Psi_\pm\rangle &\approx |\Psi_{11}\rangle \pm |\Psi_{22}\rangle \\ &\approx |\Psi_{11}\rangle \pm \hat{I}\,|\Psi_{11}\rangle \end{aligned}$$

where $\hat{I}$ is the inversion operator, and we have defined:

$$\Psi_{\alpha,\beta} = \left(\sum_{\mathbf{R}\in\Lambda_{\alpha,\beta}} |\mathbf{R}_{\alpha,\beta}\rangle\langle\mathbf{R}_{\alpha,\beta}|\right)|\Psi\rangle$$

[9]The comparaison with the direct calculation will hint at the fact that this approximattion (or possibly one of the following) is actually not very good, because it would yield the same densities on each (v, c) components. It becomes exact if the out of plane hoppings tend to zero, in which case the bands become degenerate. Still, it appears to be be in reasonable agreement with observed phase patterns.

the projection of $|\Psi\rangle$ on the sublattice $\Lambda_{\alpha,\beta}$. It follows that:

$$\Psi_{v\mathbf{k},c\mathbf{k}} \approx a_1^v(\mathbf{k})b_1^c(\mathbf{k})^*\Gamma_{11}(\mathbf{k},\mathbf{0}) \pm a_2^v(\mathbf{k})b_2^c(\mathbf{k})^*\Gamma_{11}(-\mathbf{k},\mathbf{0})$$

Recalling now the definition of $\Gamma_{11}(\mathbf{k},\mathbf{0})$, we note that it is the Fourier transform of $|\Psi_{11}\rangle$, which is in-plane and therefore should be similar to the $\mathbf{k}$-space representation of the chiral $1s$ states of the single layer: mostly localized around the three (say) $\mathbf{K}$ points, of constant phase around them, and with phase rotating by $\frac{2\pi}{3}$ when going from one $\mathbf{K}$ point to the next. $\Gamma_{11}(-\mathbf{k},\mathbf{0})$ is hence expected to exhibit the same behavior, but with the $\mathbf{K}'$ points instead. In particular, the overlap between the two terms is expected to be limited.

To proceed further, we need to make a choice of phase for the band states. In fact, to be able analyse the $\Psi_{v\mathbf{k},c\mathbf{k}}$, it is helpful to control the definition of the band states.[10] To this end, we can use the analytical expressions given by equation 6.1 and make the simplest choice for their phases by setting $\alpha_{\mu,\pm}(\mathbf{k}) = 1$.[11] We represent the result for our example state with this choice in figure 6.8.

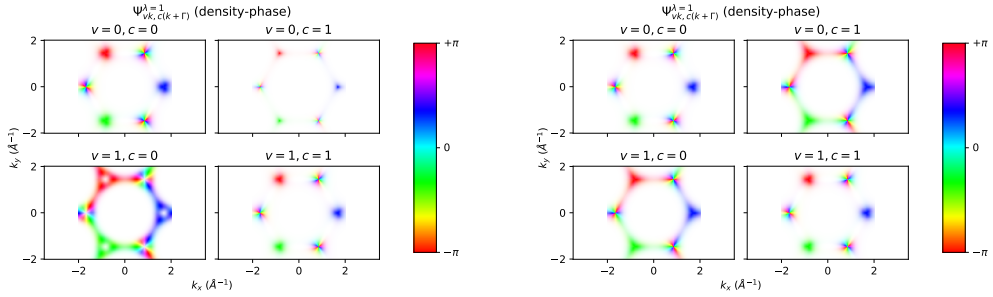

Figure 6.8: Cuts of the reciprocal space amplitudes $\Psi^{\lambda=1}_{v\mathbf{k},c\mathbf{k}}$ for the chiral state $\left|\Psi^{\lambda=1}\right\rangle$ of the twice degenerate lowest bound subspace at $\mathbf{Q} = \Gamma$ along the $\mathbf{\Gamma MK}$ (left) and $\mathbf{ALH}$ (right) planes. Density-phase representation.

In this case, the product $a_1^v(\mathbf{k})b_1^c(\mathbf{k})^*$ is constant, so the vicinity of the $\mathbf{K}$ points should (and does) display the phase pattern expected from Γ_{11} alone. The situation at the $\mathbf{K}'$ points, whose phase pattern is essentially dependent on $a_2^v(\mathbf{k})b_2^c(\mathbf{k})^*\Gamma_{11}(-\mathbf{k},\mathbf{0})$ is slightly more complex: we see that the phase still rotates by $\frac{2\pi}{3}$ under a C_3 rotation, but now locally winds twice around each $\mathbf{K}'$ point. The behavior under C_3 rotations clearly stems from the $\Gamma_{11}(-\mathbf{k},\mathbf{0})$

[10] This is difficult to do if one only has access to the band states numerically, where the phases of the band prefactors are essentially random. We have here the advantage of having analytical expressions.

[11] While this is possibly the simplest choice, its disadvantage is that is breaks the system's symmetry by particularizing a plane.

term, which otherwise only contributes a locally constant phase around the $\mathbf{K}'$ points. The "local" phase pattern can thus be ascribed to the terms coming from the band states: $a_2^v(\mathbf{k})b_2^c(\mathbf{k})^*$. These depend on v and c, but from equation 6.1 this dependence is of the form:

$$a_2^v(\mathbf{k})b_2^c(\mathbf{k})^* = \frac{1}{2}\varepsilon_{v,c}\Big(e^{-i\phi(k)}\Big)^2$$

where $\varepsilon_{v,c}$ is a sign, i.e. only takes the values ± 1, and is such that $\varepsilon_{v,c}$ is of one sign if $v = c$ and the other if $v \neq c$,[12] and $\phi(k) = \arg[\gamma_c(\mathbf{k})]$. As a result, $a_2^v(\mathbf{k})b_2^c(\mathbf{k})^*$ has a phase that locally winds twice around the $\mathbf{K}'$ points, as observed in figure 6.8. We can further observe that this local pattern is rotated by π when passing from a component with $v = c$ to a component where $v \neq c$: this stems precisely from the change in the sign of $\varepsilon_{v,c}$.

[12] Which one is positive and which one is negative depends on the values of the kinetic parameters.

Chapter 7

Conclusion

7.1 Results

Throughout this work, we have sought to study the influence of lattice geometry and symmetries on the excitonic effects of hexagonal Boron Nitride, as a prototypical $2D$ system with pronounced excitons. To this end, we have shown that, in BN-like systems, it is possible to approximately map the Bethe-Salpeter equation onto the problem of a particle moving on an effective lattice of excitations under the influence of an external field. This tool presents two main advantages: it is semi-analytical, and therefore computationally very cheap, and at the same time preserves the crystal geometry, thus allowing for the aforementioned study of lattice effects and an efficient identification of symmetries. We have endeavored to adjust its parameters to state of the art *ab initio* calculations from collaborators and shown that both methods are complementary tools of investigation.

Using this model, we have presented a detailed investigation of the excitonic series for single-layer hBN. We have studied both the limits of strong and weak electron-hole interactions. In doing so, we have classified the states according to the symmetries of the crystal lattice, clarified the relevant optical selection rules and obtained estimates of the associated oscillator strengths. We have provided a connection between this tight-binding description and the envelope function description of the Wannier model. In particular, we have highlighted the information that is carried by the phase of the excitonic wavefunctions, both in real space and in reciprocal space, provided the basis transition states are chosen carefully. We have shown that the excitons of hBN are neither quite hydrogenoïd Wannier excitons, nor atomically localized Frenkel excitons: instead, they are strongly bound excitons, which are extended, yet strongly feel the influence of the crystal lattice and the

interaction between the $\mathbf{K}$ and $\mathbf{K}'$ minima. This is particularly visible in the splitting of the hydrogenoïd $2p$ subspace, which, along with its associated optical peak, strongly depends on the strength of the electron-hole interaction and actually vanishes in the weak coupling limit.

This model naturally extends to the study of indirect states: the effective lattice of excitations remains the same, but the hoppings and electron-hole interactions become dependent on the exciton center of mass momentum $\mathbf{Q}$. In this work, we have reported and studied the excitonic band structure of single layer hBN, while the study of bulk hBN in the AA', AB and ABC can be found in [48] with the same model.

We have then extended this model to study the problem of several coupled hBN layers. We highlighted the role of couplings between intra- and inter-layer excitions, atomic coordination numbers and screening variations in the evolution of the absorption spectra of hBN multilayers. We have reported the excitonic series for the AA' bilayer, and studied its evolution as a function of the interlayer coupling. For higher numbers of layers, we have provided a simple one dimensional, almost parameter free model for the splitting of the main peak, by considering the multilayer as a linear chain of layers, where each layer can accommodate a copy of the lowest bound monolayer exciton. Notably, we have demonstrated that this peak splits into two energetically separated substructures: one composed of "inner" excitons, which are localized in the inner layers, and one composed of surface excitons, which are localized on the surface layers. Further, we have shown that the lowest bound excitons in multilayers are expected to be localized on the surfaces of the multilayers and that these excitons can be optically active.

There as well, we have given particular attention to the representation of excitonic states and their symmetries. This is particularly relevant in multilayers because there, not all nitrogen sites are equivalent choices of hole positions. The representation of multilayer states by the standard *ab initio* practice of fixing the position of the hole is therefore challenging, and the "most symmetric" choice of hole position is not necessarily the most judicious choice. Within the tight-binding model, the lattice of excitations provides a representation that naturally preserves all the symmetries of the excitonic wavefunction, and therefore avoids this issue. The linear chain model also provides insight as to which hole positions are associated to relevant transitions for a given state.

For completeness, we have also presented the excitonic tight-binding model in the case of bulk hBN in the AA' stacking. We briefly reported on its absorption spectrum in comparison with *ab initio* results, and provided a short discussion on the dispersion of the excitonic states along with the associated computation of reciprocal space excitonic amplitudes.

7.2 Outlook

In the present work, we have mostly remained at the level of defect-free samples and frozen atoms. Recent works[33, 34, 35, 36, 37] have shown that phonon assisted indirect phenomena play a crucial role in the optical properties of hBN, at least in emission spectroscopies. Further, the development of ultrafast spectroscopy techniques has led to a strong interest in the diffusion of excitons, through phononic channels or through the influence of defects.[101, 102, 103] In fact, the scattering of excitons off material defects may also play a role in their relaxation and recombination in emission spectroscopies.

Going forward, the direct space techniques that we have described in this work are in fact well suited for the study of these problems. Let us start with indirect effects in pristine systems. As we have already mentioned, recently developed diagrammatic methods,[78] that include dynamical exciton-phonon effects can require knowledge of indirect excitonic states and binding energies on a very fine mesh of $\mathbf{Q}$ points (center of mass momenta). This is a delicate task *ab initio*, but tight-binding methods, once adjusted on a coarse *ab initio* grid, can overcome this computational barrier. The inclusion of electron-phonon coupling, either directly in the excitonic tight-binding model, or through an external calculation, may then provide access to the sought after results.

The inclusion of defects, is, in a sense, the other side of the same coin. In a non-pristine system, the exciton center of mass momentum, $\mathbf{Q}$, is no longer a good quantum number. Indeed, in this situation, the system loses its translational invariance, and the description through the lattice of excitations becomes less straightforward. However, the description through the lattice of pairs remains available: we can still represent a system with defects, at the price of doubling the crystal dimension. With effective tight-binding methods, this is not as daunting a task as it may seem. Indeed, for tight-binding hamiltonians, efficient methods are known which scale linearly with the number of sites.[104] Our mapping of the Bethe-Salpeter equation on the lattice of pairs therefore allows for the efficient investigation of exciton diffusion with a quadratic scaling in the number of crystal atoms.

Be it in pristine or non pristine systems, the capacity of the tight-binding model to preserve the system's geometry opens interesting avenues of investigation when it comes to exciton diffusion. The study of multilayers or semi-infinite stackings, with their surface states, appears particularly relevant.

Lastly, multilayer systems of $2D$ materials in general hold great promise,[105] as do interlayer excitons[106] in such systems. Our studies of the influence

of layer interactions on excitonic properties could be adapted to other two-dimensional materials, such as transition metal dichalcogenides. Indeed, even though the single-layer excitons in these materials are better described by a continuum picture, the problem of interlayer coupling can be approached by tight-binding methods. Thus, much of our analysis on Davydov splitting, interlayer and surface excitons could be carried over from hBN to other layered materials.

Bibliography

[1] N. Bohr, "On the constitution of atoms and molecules, Part I," *The London, Edinburgh, and Dublin Philosophical Magazine and Journal of Science*, vol. 26, no. 151, pp. 1–25, 1913.

[2] N. Bohr, "On the constitution of atoms and molecules, Part II.- Systems containing only a single nucleus," *The London, Edinburgh, and Dublin Philosophical Magazine and Journal of Science*, vol. 26, no. 153, pp. 476–502, 1913.

[3] F. Paleari, *First-principles approaches to the description of indirect absorption and luminescence spectroscopy: exciton-phonon coupling in hexagonal boron nitride*. PhD thesis, University of Luxembourg, Luxembourg, 2019.

[4] A. K. Geim, "Graphene prehistory," *Physica Scripta*, vol. T146, p. 014003, jan 2012.

[5] K. S. Novoselov, A. K. Geim, S. V. Morozov, D. Jiang, Y. Zhang, S. V. Dubonos, I. V. Grigorieva, and A. A. Firsov, "Electric field effect in atomically thin carbon films," *Science*, vol. 306, no. 5696, pp. 666–669, 2004.

[6] A. H. Castro Neto, F. Guinea, N. M. R. Peres, K. S. Novoselov, and A. K. Geim, "The electronic properties of graphene," *Rev. Mod. Phys.*, vol. 81, pp. 109–162, Jan 2009.

[7] NobelPrize.org. Nobel Media AB, "The Nobel Prize in Physics 2010." https://www.nobelprize.org/prizes/physics/2010/summary/, 2020. Accessed 2020-11-05.

[8] A. Castellanos-Gomez, "Why all the fuss about 2D semiconductors?," *Nature Photonics*, vol. 10, pp. 202–204, Apr. 2016.

[9] X. Ling, H. Wang, S. Huang, F. Xia, and M. S. Dresselhaus, "The renaissance of black phosphorus," *Proceedings of the National Academy of Sciences*, vol. 112, no. 15, pp. 4523–4530, 2015.

[10] P. Vogt, P. De Padova, C. Quaresima, J. Avila, E. Frantzeskakis, M. C. Asensio, A. Resta, B. Ealet, and G. Le Lay, "Silicene: Compelling experimental evidence for graphenelike two-dimensional silicon," *Phys. Rev. Lett.*, vol. 108, p. 155501, Apr 2012.

[11] M. Xu, T. Liang, M. Shi, and H. Chen, "Graphene-like two-dimensional materials," *Chemical reviews*, vol. 113, no. 5, pp. 3766–3798, 2013.

[12] K. Watanabe, T. Taniguchi, and H. Kanda, "Direct-bandgap properties and evidence for ultraviolet lasing of hexagonal boron nitride single crystal," *Nature materials*, vol. 3, no. 6, pp. 404–409, 2004.

[13] Y. Kubota, K. Watanabe, O. Tsuda, and T. Taniguchi, "Deep ultraviolet light-emitting hexagonal boron nitride synthesized at atmospheric pressure," *Science*, vol. 317, no. 5840, pp. 932–934, 2007.

[14] J. D. Caldwell, I. Aharonovich, G. Cassabois, J. H. Edgar, B. Gil, and D. Basov, "Photonics with hexagonal boron nitride," *Nature Reviews Materials*, vol. 4, no. 8, pp. 552–567, 2019.

[15] Y. Toyozawa, *Optical Processes in Solids*. Cambridge University Press, 2003.

[16] P. Y. Yu and M. Cardona, *Fundamentals of Semiconductors*. Springer, 2010.

[17] G. H. Wannier, "The structure of electronic excitation levels in insulating crystals," *Phys. Rev.*, vol. 52, pp. 191–197, Aug 1937.

[18] B. Zaslow and M. E. Zandler, "Two-dimensional analog to the hydrogen atom," *American Journal of Physics*, vol. 35, no. 12, pp. 1118–1119, 1967.

[19] N. S. Rytova, "The screened potential of a point charge in a thin film," *Moscow University Physics Bulletin*, vol. 3, no. 3, p. 18, 1967.

[20] L. V. Keldysh, "Coulomb interaction in thin semiconductor and semimetal films," *JETP Lett.*, vol. 29, p. 658, June 1979.

[21] T. C. Berkelbach, M. S. Hybertsen, and D. R. Reichman, "Theory of neutral and charged excitons in monolayer transition metal dichalcogenides," *Phys. Rev. B*, vol. 88, p. 045318, Jul 2013.

[22] A. Chernikov, T. C. Berkelbach, H. M. Hill, A. Rigosi, Y. Li, O. B. Aslan, D. R. Reichman, M. S. Hybertsen, and T. F. Heinz, "Exciton binding energy and nonhydrogenic Rydberg series in monolayer WS_2," *Phys. Rev. Lett.*, vol. 113, p. 076802, Aug 2014.

[23] B. Arnaud, S. Lebègue, P. Rabiller, and M. Alouani, "Huge excitonic effects in layered hexagonal boron nitride," *Phys. Rev. Lett.*, vol. 96, p. 026402, Jan 2006.

[24] L. Wirtz, A. Marini, M. Grüning, C. Attaccalite, G. Kresse, and A. Rubio, "Comment on "huge excitonic effects in layered hexagonal boron nitride"," *Phys. Rev. Lett.*, vol. 100, p. 189701, May 2008.

[25] B. Arnaud, S. Lebègue, P. Rabiller, and M. Alouani, "Arnaud, Lebègue, Rabiller, and Alouani Reply:," *Phys. Rev. Lett.*, vol. 100, p. 189702, May 2008.

[26] E. E. Salpeter and H. A. Bethe, "A relativistic equation for bound-state problems," *Phys. Rev.*, vol. 84, pp. 1232–1242, Dec 1951.

[27] W. Hanke and L. J. Sham, "Many-particle effects in the optical spectrum of a semiconductor," *Phys. Rev. B*, vol. 21, pp. 4656–4673, May 1980.

[28] G. Strinati, "Application of the green's functions method to the study of the optical properties of semiconductors," *La Rivista del Nuovo Cimento (1978-1999)*, vol. 11, no. 12, pp. 1–86, 1988.

[29] S. Albrecht, *Optical absorption spectra of semiconductors and insulators: ab initio calculation of many-body effects*. PhD thesis, 1999.

[30] M. Rohlfing and S. G. Louie, "Electron-hole excitations and optical spectra from first principles," *Phys. Rev. B*, vol. 62, pp. 4927–4944, Aug 2000.

[31] G. Onida, L. Reining, and A. Rubio, "Electronic excitations: density-functional versus many-body green's-function approaches," *Rev. Mod. Phys.*, vol. 74, pp. 601–659, Jun 2002.

[32] F. Bechstedt, *Many-Body Approach to Electronic Excitations*. Springer, 2016.

[33] G. Cassabois, P. Valvin, and B. Gil, "Hexagonal boron nitride is an indirect bandgap semiconductor," *Nature Photonics*, vol. 10, no. 4, pp. 262–266, 2016.

[34] T. Q. P. Vuong, G. Cassabois, P. Valvin, V. Jacques, R. Cuscó, L. Artús, and B. Gil, "Overtones of interlayer shear modes in the phonon-assisted emission spectrum of hexagonal boron nitride," *Phys. Rev. B*, vol. 95, p. 045207, Jan 2017.

[35] L. Schué, L. Sponza, A. Plaud, H. Bensalah, K. Watanabe, T. Taniguchi, F. Ducastelle, A. Loiseau, and J. Barjon, "Bright luminescence from indirect and strongly bound excitons in h-BN," *Phys. Rev. Lett.*, vol. 122, p. 067401, Feb 2019.

[36] E. Cannuccia, B. Monserrat, and C. Attaccalite, "Theory of phonon-assisted luminescence in solids: Application to hexagonal boron nitride," *Phys. Rev. B*, vol. 99, p. 081109, Feb 2019.

[37] F. Paleari, H. P. C. Miranda, A. Molina-Sánchez, and L. Wirtz, "Exciton-phonon coupling in the ultraviolet absorption and emission spectra of bulk hexagonal boron nitride," *Phys. Rev. Lett.*, vol. 122, p. 187401, May 2019.

[38] F. Paleari, T. Galvani, H. Amara, F. Ducastelle, A. Molina-Sánchez, and L. Wirtz, "Excitons in few-layer hexagonal boron nitride: Davydov splitting and surface localization," *2D Materials*, vol. 5, p. 045017, aug 2018.

[39] R. Saito, G. Dresselhaus, and M. Dresselhaus, *Physical Properties of Carbon Nanotubes*. Imperial College Press, 1998.

[40] C. J. Delerue and M. Lannoo, *Nanostructures: Theory and Modeling*. Springer, 2004.

[41] S. H. Simon, *The Oxford solid state basics*. OUP Oxford, 2013.

[42] L. J. Sham and T. M. Rice, "Many-particle derivation of the effective-mass equation for the wannier exciton," *Phys. Rev.*, vol. 144, pp. 708–714, Apr 1966.

[43] S. Latini, *Excitons in van der Waals Heterostructures: A theoretical study*. PhD thesis, 2016.

[44] C. Delerue, M. Lannoo, and G. Allan, "Excitonic and quasiparticle gaps in si nanocrystals," *Phys. Rev. Lett.*, vol. 84, pp. 2457–2460, Mar 2000.

[45] C. Delerue, M. Lannoo, and G. Allan, "Erratum: Excitonic and quasiparticle gaps in si nanocrystals [phys. rev. lett. 84, 2457 (2000)]," *Phys. Rev. Lett.*, vol. 89, p. 249901, Nov 2002.

[46] F. Ducastelle. Personal communication, 2015.

[47] T. Galvani, F. Paleari, H. P. C. Miranda, A. Molina-Sánchez, L. Wirtz, S. Latil, H. Amara, and F. Ducastelle, "Excitons in boron nitride single layer," *Phys. Rev. B*, vol. 94, p. 125303, Sep 2016.

[48] L. Sponza, H. Amara, C. Attaccalite, S. Latil, T. Galvani, F. Paleari, L. Wirtz, and F. Ducastelle, "Direct and indirect excitons in boron nitride polymorphs: A story of atomic configuration and electronic correlation," *Phys. Rev. B*, vol. 98, p. 125206, Sep 2018.

[49] R. Fei, G. Luo, Y. Wang, Z. Gao, S. Nagase, D. Yu, and J. Lu, "Enhanced many-body effects in one-dimensional linear atomic chains," *physica status solidi (b)*, vol. 250, no. 8, pp. 1636–1643, 2013.

[50] D. Gunlycke and F. Tseng, "Triangular lattice exciton model," *Phys. Chem. Chem. Phys.*, vol. 18, pp. 8579–8586, 2016.

[51] C. Attaccalite, M. Grüning, H. Amara, S. Latil, and F. Ducastelle, "Two-photon absorption in two-dimensional materials: The case of hexagonal boron nitride," *Physical Review B*, vol. 98, no. 16, p. 165126, 2018.

[52] D. Moldovan, M. Anđelković, and F. Peeters, "pybinding v0.9.5: a Python package for tight-binding calculations," Aug. 2020.

[53] R. Loudon, "One-dimensional hydrogen atom," *Proc. R. Soc. A.*, vol. 472, p. 20150534, 2016.

[54] S. V. Gaponenko and H. V. Demir, *Applied Nanophotonics*. Cambridge University Press, 2018.

[55] A. Tan and M. E. Edwards, "Elecrostatics and dimensions of space," *Georgia Journal of Science*, vol. 68, p. 8, 2010.

[56] R. J. Elliott, "Intensity of optical absorption by excitons," *Phys. Rev.*, vol. 108, pp. 1384–1389, Dec 1957.

[57] P. Atkins, P.W. Atkins, and J. de Paula, *Atkins' Physical Chemistry*. OUP Oxford, 2014.

[58] R. M. Ribeiro and N. M. R. Peres, "Stability of boron nitride bilayers: Ground-state energies, interlayer distances, and tight-binding description," *Phys. Rev. B*, vol. 83, p. 235312, Jun 2011.

[59] X. Blase, A. Rubio, S. G. Louie, and M. L. Cohen, "Quasiparticle band structure of bulk hexagonal boron nitride and related systems," *Phys. Rev. B*, vol. 51, pp. 6868–6875, Mar 1995.

[60] L. Wirtz and A. Rubio, "Optical and vibrational properties of boron nitride nanotubes," in *BCN nanotubes and related nanostructures* (Y. K. Yap, ed.), vol. 6, ch. 5, Springer Science & Business Media, 2009.

[61] P. Cudazzo, I. V. Tokatly, and A. Rubio, "Dielectric screening in two-dimensional insulators: Implications for excitonic and impurity states in graphane," *Phys. Rev. B*, vol. 84, p. 085406, Aug 2011.

[62] D. Y. Qiu, T. Cao, and S. G. Louie, "Nonanalyticity, valley quantum phases, and lightlike exciton dispersion in monolayer transition metal dichalcogenides: Theory and first-principles calculations," *Phys. Rev. Lett.*, vol. 115, p. 176801, Oct 2015.

[63] P. Cudazzo, L. Sponza, C. Giorgetti, L. Reining, F. Sottile, and M. Gatti, "Exciton band structure in two-dimensional materials," *Phys. Rev. Lett.*, vol. 116, p. 066803, Feb 2016.

[64] F. Wu, F. Qu, and A. H. MacDonald, "Exciton band structure of monolayer MoS_2," *Phys. Rev. B*, vol. 91, p. 075310, Feb 2015.

[65] J. C. G. Henriques, G. B. Ventura, C. D. M. Fernandes, and N. M. R. Peres, "Optical absorption of single-layer hexagonal boron nitride in the ultraviolet," *Journal of Physics: Condensed Matter*, vol. 32, p. 025304, oct 2019.

[66] Z. Rukelj and V. Despoja, "Estimation of the single-particle band gap and exciton binding energy in two dimensional insulators: a modified G_0W_0-BSE method approach," *New Journal of Physics*, vol. 22, p. 063052, jun 2020.

[67] M. Bander and C. Itzykson, "Group theory and the hydrogen atom (i)," *Rev. Mod. Phys.*, vol. 38, pp. 330–345, Apr. 1966.

[68] T. Olsen, S. Latini, F. Rasmussen, and K. S. Thygesen, "Simple screened hydrogen model of excitons in two-dimensional materials," *Phys. Rev. Lett.*, vol. 116, p. 056401, Feb 2016.

[69] O. Pulci, M. Marsili, V. Garbuio, P. Gori, I. Kupchak, and F. Bechstedt, "Excitons in two-dimensional sheets with honeycomb symmetry," *physica status solidi (b)*, vol. 252, no. 1, pp. 72–77, 2015.

[70] "Jens" (https://mathematica.stackexchange.com/users/245/jens), "Ndeigensystem returns incorrect eigenvalues for 2d coulomb problem, eigenfunctions contain discontinuity." Mathematica Stack Exchange. https://mathematica.stackexchange.com/q/113906 (version: 2021-01-02).

[71] M. Hamermesh, *Group Theory and Its Application to Physical Problems*, ch. 4, p. 126. Addison-Wesley, 1964.

[72] F. Paleari. Personal communication, 2018.

[73] J. Serrano, A. Bosak, R. Arenal, M. Krisch, K. Watanabe, T. Taniguchi, H. Kanda, A. Rubio, and L. Wirtz, "Vibrational properties of hexagonal boron nitride: Inelastic x-ray scattering and ab initio calculations," *Phys. Rev. Lett.*, vol. 98, p. 095503, Mar 2007.

[74] S. Latini, T. Olsen, and K. S. Thygesen, "Excitons in van der waals heterostructures: The important role of dielectric screening," *Physical Review B*, vol. 92, no. 24, p. 245123, 2015.

[75] D. Y. Qiu, F. H. da Jornada, and S. G. Louie, "Screening and many-body effects in two-dimensional crystals: Monolayer mos_2," *Phys. Rev. B*, vol. 93, p. 235435, Jun 2016.

[76] M. L. Trolle, T. G. Pedersen, and V. Véniard, "Model dielectric function for 2d semiconductors including substrate screening," *Scientific reports*, vol. 7, p. 39844, 2017.

[77] G. Arfken, H. Weber, and F. Harris, *Mathematical Methods for Physicists: A Comprehensive Guide*, ch. 14, p. 655. Elsevier Science, 2013.

[78] P. Cudazzo, "First-principles description of the exciton-phonon interaction: A cumulant approach," *Phys. Rev. B*, vol. 102, p. 045136, Jul 2020.

[79] Z. Liu, F. Liu, and Y.-S. Wu, "Exotic electronic states in the world of flat bands: From theory to material," *Chinese Physics B*, vol. 23, p. 077308, Jul 2014.

[80] W. Zhao, Z. Ghorannevis, L. Chu, M. Toh, C. Kloc, P.-H. Tan, and G. Eda, "Evolution of electronic structure in atomically thin sheets of WS_2 and WSe_2," *ACS Nano*, vol. 7, no. 1, pp. 791–797, 2013. PMID: 23256505.

[81] A. Pierret, J. Loayza, B. Berini, A. Betz, B. Plaçais, F. Ducastelle, J. Barjon, and A. Loiseau, "Excitonic recombinations in $h-$BN: From bulk to exfoliated layers," *Phys. Rev. B*, vol. 89, p. 035414, Jan 2014.

[82] L. Schué, B. Berini, A. C. Betz, B. Plaçais, F. Ducastelle, J. Barjon, and A. Loiseau, "Dimensionality effects on the luminescence properties of hbn," *Nanoscale*, vol. 8, no. 13, pp. 6986–6993, 2016.

[83] J. Koskelo, G. Fugallo, M. Hakala, M. Gatti, F. Sottile, and P. Cudazzo, "Excitons in van der waals materials: From monolayer to bulk hexagonal boron nitride," *Phys. Rev. B*, vol. 95, p. 035125, Jan 2017.

[84] A. Davydov, *Theory of molecular excitons*. MCGraw-Hill, 1969.

[85] P. Dawson, "Dipole dipole interactions and davydov splitting in crystals," *Journal of Physics and Chemistry of Solids*, vol. 36, no. 12, pp. 1401 – 1403, 1975.

[86] X. Luo, Y. Zhao, J. Zhang, Q. Xiong, and S. Y. Quek, "Anomalous frequency trends in MoS_2 thin films attributed to surface effects," *Phys. Rev. B*, vol. 88, p. 075320, Aug 2013.

[87] M. Staiger, R. Gillen, N. Scheuschner, O. Ochedowski, F. Kampmann, M. Schleberger, C. Thomsen, and J. Maultzsch, "Splitting of monolayer out-of-plane $A_1^{'}$ raman mode in few-layer WS_2," *Phys. Rev. B*, vol. 91, p. 195419, May 2015.

[88] H. P. Miranda, S. Reichardt, G. Froehlicher, A. Molina-Sánchez, S. Berciaud, and L. Wirtz, "Quantum interference effects in resonant raman spectroscopy of single-and triple-layer mote2 from first-principles," *Nano Letters*, vol. 17, no. 4, pp. 2381–2388, 2017.

[89] C.-J. Kim, L. Brown, M. W. Graham, R. Hovden, R. W. Havener, P. L. McEuen, D. A. Muller, and J. Park, "Stacking order dependent second harmonic generation and topological defects in h-bn bilayers," *Nano letters*, vol. 13, no. 11, pp. 5660–5665, 2013.

[90] M. Chubarov, H. Pedersen, H. Högberg, J. Jensen, and A. Henry, "Growth of high quality epitaxial rhombohedral boron nitride," *Crystal growth & design*, vol. 12, no. 6, pp. 3215–3220, 2012.

[91] K. Andersen, S. Latini, and K. S. Thygesen, "Dielectric genome of van der waals heterostructures," *Nano letters*, vol. 15, no. 7, pp. 4616–4621, 2015.

[92] K. S. Thygesen, "Calculating excitons, plasmons, and quasiparticles in 2d materials and van der waals heterostructures," *2D Materials*, vol. 4, no. 2, p. 022004, 2017.

[93] L. S. R. Cavalcante, A. Chaves, B. Van Duppen, F. M. Peeters, and D. R. Reichman, "Electrostatics of electron-hole interactions in van der waals heterostructures," *Phys. Rev. B*, vol. 97, p. 125427, Mar 2018.

[94] H. C. Kamban and T. G. Pedersen, "Interlayer excitons in van der waals heterostructures: Binding energy, stark shift, and field-induced dissociation," *Scientific reports*, vol. 10, no. 1, pp. 1–10, 2020.

[95] H. Puszkarski, "Eigenvalue problem of a finite monoatomic linear chain with asymmetrical boundary conditions; surface states," *Surface Science*, vol. 34, no. 1, pp. 125 – 135, 1973.

[96] L. Wirtz, A. Marini, M. Grüning, C. Attaccalite, G. Kresse, and A. Rubio, "Comment on "huge excitonic effects in layered hexagonal boron nitride"," *Physical review letters*, vol. 100, no. 18, p. 189701, 2008.

[97] R. Bourrellier, M. Amato, L. H. Galvaão Tizei, C. Giorgetti, A. Gloter, M. I. Heggie, K. March, O. Stephan, L. Reining, M. Kociak, *et al.*, "Nanometric resolved luminescence in h-bn flakes: excitons and stacking order," *ACS photonics*, vol. 1, no. 9, pp. 857–862, 2014.

[98] W. Aggoune, C. Cocchi, D. Nabok, K. Rezouali, M. A. Belkhir, and C. Draxl, "Dimensionality of excitons in stacked van der waals materials: The example of hexagonal boron nitride," *Phys. Rev. B*, vol. 97, p. 241114, Jun 2018.

[99] S. Reichardt and L. Wirtz, "Nonadiabatic exciton-phonon coupling in raman spectroscopy of layered materials," *Science advances*, vol. 6, no. 32, p. eabb5915, 2020.

[100] S. Reichardt. Personal communication, 2020.

[101] R. Perea-Causin, S. Brem, R. Rosati, R. Jago, M. Kulig, J. D. Ziegler, J. Zipfel, A. Chernikov, and E. Malic, "Exciton propagation and halo formation in two-dimensional materials," *Nano Letters*, vol. 19, no. 10, pp. 7317–7323, 2019.

[102] J. Zipfel, M. Kulig, R. Perea-Causín, S. Brem, J. D. Ziegler, R. Rosati, T. Taniguchi, K. Watanabe, M. M. Glazov, E. Malic, and A. Chernikov, "Exciton diffusion in monolayer semiconductors with suppressed disorder," *Phys. Rev. B*, vol. 101, p. 115430, Mar 2020.

[103] R. Rosati, R. Perea-Causín, S. Brem, and E. Malic, "Negative effective excitonic diffusion in monolayer transition metal dichalcogenides," *Nanoscale*, vol. 12, no. 1, pp. 356–363, 2020.

[104] Z. Fan, J. H. Garcia, A. W. Cummings, J. E. Barrios-Vargas, M. Panhans, A. Harju, F. Ortmann, and S. Roche, "Linear scaling quantum transport methodologies," *arXiv preprint arXiv:1811.07387*, 2018.

[105] A. K. Geim and I. V. Grigorieva, "Van der waals heterostructures," *Nature*, vol. 499, no. 7459, pp. 419–425, 2013.

[106] E. Torun, H. P. C. Miranda, A. Molina-Sánchez, and L. Wirtz, "Interlayer and intralayer excitons in MoS_2/WS_2 and $MoSe_2/WSe_2$ heterobilayers," *Phys. Rev. B*, vol. 97, p. 245427, Jun 2018.

List of publications

1. **T. Galvani**, F. Paleari, H. Miranda, A. Molina-Sànchez, L. Wirtz, S. Latil, H. Amara and F. Ducastelle, "Excitons in boron nitride single layer", *Phys. Rev. B*, vol. 94, p. 125303, Sep 2016.

2. L. Sponza, H. Amara, C. Attaccalite, S. Latil, **T. Galvani**, F. Paleari, L. Wirtz and F. Ducastelle, "Direct and indirect excitons in boron nitride polymorphs: A story of atomic configuration and electronic correlation", *Phys. Rev. B*, vol. 98, p. 125206, Sep 2018.

3. F. Paleari, **T. Galvani**, H. Amara, F. Ducastelle, A. Molina–Sánchez, and L. Wirtz, "Excitons in few–layer hexagonal boron nitride: Davydov splitting and surface localization", *2D Materials*, vol. 5, p. 045017, Aug 2018.

4. C. Spindler, **T. Galvani**, L. Wirtz, G. Rey, S. Siebentritt, "Excitation-intensity dependence of shallow and deep-level photoluminescence transitions in semiconductors", *Journal of Applied Physics*, vol. 126, no. 17, p. 175703, 2019.[1]

[1]This publication is not discussed in the present thesis.

Acknowledgments

It goes almost without saying that the results presented therein, as a significant amount of research nowadays, are the fruits of a collaborative effort. I would therefore like to acknowledge, in no particular order, those who have helped shape this work.

Hakim Amara, for his availability, his help with the computational and theoretical aspects of the excitonic tight-binding model and his academic advice and support in general. Sylvain Latil, for kindly providing his tight-binding code, which was used for much of the numerical calculations in this work. Lorenzo Sponza and Claudio Attaccalite, for helpful discussions, and their work on exciton dispersion in hBN, notably in terms of *ab initio* simulations. Annick Loiseau, Julien Barjon and Léonard Schue, for fruitful discussions on the experimental aspects of hBN spectroscopy, particularly in multilayers and bulk, as well as exciton diffusion in these systems. I would like to thank Annick Loiseau in particular, for the opportunities she has offered me. More generally, I am grateful to the community of the Laboratoire d'Étude des Microstructures (LEM), where I had the opportunity to make several collaborative visits, which always led to very fruitful discussions.

I would also like to thank Henrique P. C. Miranda, for his direct help with early computational issues, and for the tools he developed to enable *ab initio* calculations. Alejandro Molina-Sánchez, who provided the initial *ab initio* data for single layer hBN which allowed this work to be started and for his helpful collaboration. Sven Reichardt, for fruitful discussions about mathematics, quantum mechanics and the teaching thereof, as well as recent collaboration on the topic of bulk hBN. Engin Torun, for fruitful discussions and collaborative work on transition metal dichalcogenides and their (hetero)bilayers. Pierluigi Cudazzo, who shared his knowledge of analytical methods pertaining to exciton physics and electron-hole interactions, and provided helpful suggestions for ways to extend the use of the excitonic tight-binding model, notably with regards to indirect phenomena. I am likewise grateful to the members, past and present, of the Theoretical Solid State Physics research group, for many helpful discussions. It has been a pleasure

to work with them.

I also extend my thanks to Laure Galopin, for artistic support with some of the figures in this work and help in proofreading the manuscript.

I can hardly overstate what I owe to François Ducastelle, who, in many ways, has effectively acted as a mentor. He is at the origin of what we have called here the excitonic tight-binding model. His initial and continued developments of it have directly led to this work, which has greatly benefited from his theoretical insights.

I must reserve, as well, particular thanks for Fulvio Paleari, who was, for a significant length of time, a fellow PhD student at the University of Luxembourg, and strongly collaborated to this work, notably through numerous discussions on excitons and hBN, and his expertise in the field of *ab initio* calculations. As mentioned several times, he is the originator of most of the *ab initio* simulations discussed here.

Finally, I would like to express my heartfelt thanks to my supervisor, Ludger Wirtz. I am extremely grateful for his continued support over the years, his precious help, as well as his teachings, relevant advice and directions.